

The role of IGFR-L1 in Insulin Signalling of Pancreatic β -cells and Hormone-dependent Cancers

Katharina Wißmiller

Vollständiger Abdruck der von der Fakultät für Medizin der Technischen Universität München zur Erlangung des akademischen Grades eines

Doktors der Naturwissenschaften

genehmigten Dissertation.

Vorsitzende/-r: Prof. Dr. Roland M. Schmid

Prüfende/-r der Dissertation:

1. Prof. Dr. Heiko Lickert
2. Prof. Dr. Hans-Jürgen Wester

Die Dissertation wurde am 19.11.2020 bei der Technischen Universität München eingereicht und durch die Fakultät für Medizin der Technischen Universität München am 13.04.2021 angenommen.

Table of Contents

I List of Abbreviations.....	1
II Summary.....	3
1 Introduction.....	4
1.1 Mechanisms and Therapy of Diabetes.....	4
1.1.1 Pancreatic β -cells in Diabetes.....	4
1.1.2 The Insulin/IGF1 Signalling Pathway.....	5
1.1.3 Intracellular Trafficking of Receptor Tyrosine Kinases.....	9
1.1.4 Diabetes Treatment.....	12
1.1.5 Therapeutic Antibodies in Diabetes Therapy.....	13
1.1.6 Estrogen and Androgen Signalling in Diabetes.....	14
1.1.7 Link between Diabetes and Hormone-dependent Cancers.....	16
1.2 Proliferative Signalling in Prostate Cancer.....	18
1.2.1 Prostate Anatomy.....	18
1.2.2 Androgen Signalling in Prostate Cancer.....	19
1.2.3 Androgen-independent Prostate Cancer.....	20
1.2.4 Cell line Models of Prostate Cancer.....	23
1.2.5 Targeting Prostate Cancer via PI3K/Akt.....	23
1.2.6 Therapeutic Antibodies in Cancer.....	24
1.3 Identification of IGFR-L1.....	26
1.4 Scope of the Project.....	27
2 Results.....	28
2.1 Establishment of IGFR-L1 antibodies.....	28
2.1.1 Antibody Screening.....	28
2.1.2 Impact of IGFR-L1 Antibodies on Proliferation.....	36
2.2 Endocytosis and Intracellular Trafficking of IGFR-L1 in β -cells.....	38
2.2.1 Tool Generation.....	38
2.2.2 Analysing the Trafficking Dynamics of IGFR-L1 in Live Cells.....	41
2.2.3 Influence of IGFR-L1 on IR Trafficking.....	48
2.2.4 Clathrin-mediated Endocytosis of IGFR-L1.....	52
2.2.5 Insulin Uptake.....	54
2.3 The Role of IGFR-L1 in Cancer.....	62

2.3.1 IGFR-L1 expression in Benign Tissue	62
2.3.2 IGFR-L1 in Human Prostate Cancer	67
2.3.3 Cell line Generation for Analysis of IGFR-L1 in Cancer	71
2.3.4 IGFR-L1 in Prostate Cancer Cells	74
2.3.5 Potential Regulation of IGFR-L1 via Reproductive Hormone Signalling	77
2.3.6 Insulin/IGF1 Signalling in Prostate Cancer Cells	80
2.3.7 Biodistribution of IGFR-L1 Antibody	84
3 Discussion	87
3.1 Endocytosis and Intracellular Trafficking of IGFR-L1.....	87
3.1.1 Endocytosis Pathways of IGFR-L1.....	87
3.1.2 Regulation of Insulin/IGF1 signalling.....	89
3.1.3 Model of IGFR-L1 Trafficking.....	91
3.2 The Role of IGFR-L1 in Cancer	93
3.2.1 IGFR-L1 in Benign Tissues	93
3.2.2 Expression of IGFR-L1 in Cancer	94
3.2.3 Cell line Development for Cancer Research.....	95
3.2.4 Regulation of IGFR-L1.....	96
3.2.5 Function of IGFR-L1 in Prostate Cancer	98
3.2.6 Biodistribution.....	101
3.3 Targeting IGFR-L1 using Antibodies	102
3.4 Conclusion	104
4 Materials and Methods	105
4.1 Methods	105
4.1 Animal Breeding	105
4.2 Cell Culture	105
4.3 Molecular Cloning	105
4.4 IGFR-L1-Venus and IGFR-L1-AP2*-Venus Cloning strategy.....	106
4.5 Transfection.....	106
4.6 Fluorescence-Activated Cell Sorting (FACS)	107
4.7 Live Imaging.....	107
4.8 CRISPR/Cas9 Knockout	107
4.9 Antibody Generation.....	108
4.10 Immunohistochemistry	108
4.11 Western Blot.....	109

4.12 Co-immunoprecipitation	109
4.13 Proliferation Assay	110
4.14 Endocytosis Assay in LNCaP	110
4.15 Insulin Uptake Assay in Min6	111
4.16 Migration Assay	111
4.17 Image Processing in ImageJ.....	111
4.18 Statistics	113
4.19 Bioinformatic Analyses	114
4.2 Materials.....	115
4.2.1 General Lab ware	115
4.2.2 Cell Culture	116
4.2.3 Molecular Cloning	119
4.2.4 Immunohistochemistry and Imaging	122
4.2.5 Western Blot.....	123
4.2.6 Antibodies	125
5 References	127
III List of Figures	139
IV List of Tables	140
V Acknowledgements.....	141
VI List of Publications	143

I List of Abbreviations

Ab	Antibody
AIPC	Androgen-independent prostate cancer
AMPK	Adenosine monophosphate-activated protein kinase
AR	Androgen receptor
ARE	Androgen response element
CK	Cytokeratin
DAPI	4',6-diamidino-2-phenylindole
DHEA	Dehydroepiandrosterone
DHT	5 α -dihydrotestosterone
E2	17 β -estradiol
eBFP	Enhanced blue fluorescent protein
EdU	5-Ethynyl-2'-deoxyuridine
EEA1	Early endosome antigen 1
EGF	Epidermal growth factor
eGFP	Enhanced green fluorescent protein
EGFR	Epidermal growth factor receptor
EIG121	Estrogen-inducible gene 121 (alternate for IGFR-L1)
ER- α / β	Estrogen receptor alpha / beta
ERE	Estrogen response element
ESCRT	Endosomal sorting complexes required for transport
Fab	Antigen-binding fragment
FACS	Fluorescence-activated cell sorting
FOLH1	Folate hydrolase 1 (alternate for PSMA)
GPCR	G-protein coupled receptor
GM130	Golgi matrix protein 130
HBSS	Hank's balanced salt solution
HER2	Human epidermal growth factor receptor 2
HPEC	Human primary prostate epithelial cells
IGF1/2	Insulin-like growth factor 1/2
IGF1/2R	Insulin-like growth factor 1/2 receptor
IGFR-L1	Insulin-like growth factor receptor-like 1, also known as INCEPTOR
IgG	Immunoglobulin G
INCEPTOR	Insulin inhibitory receptor
Ins	Insulin
INSR	Insulin receptor (gene identifier)

IP	Immunoprecipitation
IR	Insulin receptor
IRS	Insulin receptor substrate
KIAA1324	alternate name for IGFR-L1
KLK3	Kallikrein 3 (alternate for PSA)
KO	Knockout
LAMP1	Lysosomal-associated membrane protein 1
M6PR	Mannose-6-phosphate receptor
MAPK	Mitogen-activated protein kinase
Mdm2	Mouse double minute 2 homolog
MOC	Mander's overlap coefficient
mTOR	Mammalian target of rapamycin
MVB	Multivesicular body
Nedd4	Neural-precursor expressed, developmentally down-regulated protein 4
NEPC	Neuroendocrine prostate cancer
PDGFR	Platelet-derived growth factor receptor
PI3K	Phosphoinositide 3-kinase
PIP3	Phosphatidylinositol-trisphosphate
PSA	Prostate-specific antigen
PSMA	Prostate-specific membrane antigen
PTEN	Phosphatase and tensin homologue
RFP	Red fluorescent protein
sgRNA	Single-guide RNA
Shc	Src-homology domain containing protein family
scFv	Single-chain variable fragment
TCGA	The cancer genome atlas
TGN	Trans-Golgi network
T2D	Type 2 diabetes mellitus
VEGFR	Vascular endothelial growth factor receptor
WT	Wildtype

II Summary

Diabetes mellitus is a widespread disease that causes severe complications and enormous costs to healthcare systems worldwide. The molecular basis of diabetes is defective insulin production and signalling. The aim of this thesis was to investigate the function of the novel receptor IGFR-L1 (IGF Receptor-Like 1), which negatively regulates insulin signalling in β -cells of the pancreas.

In the first part of this project, we describe that IGFR-L1 circulates between the cytoplasmic membrane, the endosomal-lysosomal system and the Golgi complex. For these analyses, we generated an IGFR-L1 fusion protein with the fluorescent protein Venus. We showed that internalisation of IGFR-L1-Venus occurred primarily via clathrin-mediated endocytosis. Further, IGFR-L1-Venus interacted with the insulin receptor and was transported via the same intracellular vesicles towards lysosomes or the Golgi compartment. In addition, we showed that loss of IGFR-L1 led to impaired endocytosis of insulin. We conclude that IGFR-L1 desensitises insulin and IGF1 (Insulin-like Growth Factor 1) signalling by modulating the intracellular trafficking of the insulin receptor and IGF1 receptor.

Furthermore, diabetes is a known risk factor for the development and progression of many cancer types, including prostate cancer. This is presumably due to growth-promoting effects of insulin and/or IGF1 signalling, as well as crosstalk with androgen signalling, which is the predominant driver of prostate cancer growth. In the second part of this project, we therefore aimed to investigate the potential function of IGFR-L1 in prostate cancer.

Analysis of publicly available data showed that IGFR-L1 expression is upregulated in prostate cancer compared to benign prostate tissue, and that it correlates with markers of disease progression. In our *in vitro* experiments, androgen depletion induced IGFR-L1 expression, but androgen receptor activation correlated with IGFR-L1 levels in single cells. This suggests that IGFR-L1 is involved in androgen signalling under androgen-deprived conditions. Further, IGFR-L1 overexpression promoted translocation of the IGF1 receptor to the plasma membrane and activated IGF1 signalling in prostate cancer cells. In a 3D cancer spheroid model, IGFR-L1 overexpression induced migration. We conclude that IGFR-L1 is involved in prostate cancer progression, likely by modulating IGF1 signalling.

In summary, IGFR-L1 is a potential target for diabetes and cancer treatment. We generated highly specific IGFR-L1 antibodies to possibly modulate insulin signalling in β -cells for diabetes therapy. Further, prostate cancer progression and metastasis could potentially be mitigated by blocking proliferative insulin / IGF1 pathways using IGFR-L1 antibodies.

1 Introduction

1.1 Mechanisms and Therapy of Diabetes

1.1.1 Pancreatic β -cells in Diabetes

Diabetes mellitus is a pandemic disease. In 2014, 422 million people worldwide suffered from diabetes, with steadily increasing incidence [1]. The mortality, due to diabetes-related high blood glucose, was 3.7 million in 2012. In Germany alone, around 7 million people are currently affected [2]. In type 1 diabetes mellitus, the insulin-producing pancreatic β -cells are lost due to autoimmune destruction [3]. The most common form, type 2 diabetes mellitus (T2D), is characterised by reduced sensitivity of the insulin receptor to insulin. The human pancreas consists of exocrine acinar cells, which produce digestive enzymes, and endocrine islets that contain four major hormone producing cell types: glucagon-secreting α -cells, insulin-secreting β -cells, somatostatin-releasing δ -cells and PP-cells (pancreatic polypeptide) [4].

In healthy individuals, the blood glucose levels are tightly regulated by insulin-mediated glucose uptake in peripheral tissues, i.e. skeletal muscle, adipose tissue and liver [5]. In T2D patients, it is anticipated that insulin resistance results in impaired glucose uptake in the peripheral tissues and increased insulin production in the pancreas. Thus, the circulating insulin levels are elevated in early disease stages. In later stages, chronic hyperglycemia leads to β -cell dysfunction and ultimately β -cell loss due to oxidative stress, cytotoxic intracellular calcium levels, endoplasmic reticulum stress and accumulation of lipids [6]. In addition to apoptosis, the reduction of functional β -cell mass in T2D is also due to loss of identity, i.e. β -cell dedifferentiation [7]. Eventually, continuous β -cell loss can lead to hypoinsulinemia, which not only leads to intensified hyperglycemia but also severe cardiovascular complications.

There are various approaches aiming to restore β -cell function. It has been shown that β -cell regeneration can occur after surgical or chemical injury [8]. Three distinct mechanisms are predominantly discussed in this context: replication of pre-existing β -cells, neogenesis from progenitor cells in the ductal epithelium, or transdifferentiation from exocrine or other

endocrine pancreatic cells, e.g. α -cells [4]. Among these, replication of β -cells is the prevailing mechanism of expansion after birth [9]. Although proliferation of β -cells is rare in adults, it has been reported in multiple studies [9-11]. It was shown that there are specific subsets within the heterogeneous β -cell population, that are not fully mature and capable of self-replication [12]. An ideal approach for regeneration of healthy β -cells would therefore be the controlled stimulation of endogenous proliferative pathways in β -cells, without risking the development of malignancies such as pancreatic cancer. Another strategy could be *in vitro* differentiation of pluripotent stem cells to mature β -cells for replacement therapy. However, the efficient differentiation of stem cells towards insulin-secreting cells has proven to be challenging [13, 14]. Interestingly, it was shown that insulin therapy, which is commonly prescribed to type 1 diabetics and to severely hyperglycemic type 2 diabetics, can stimulate β -cell redifferentiation, potentially due to reduced cellular stress [15]. Nonetheless, current treatments fail to stop disease progression, therefore we aim to improve diabetes therapy by β -cell regeneration.

1.1.2 The Insulin/IGF1 Signalling Pathway

To overcome insulin resistance, it is crucial to understand the downstream signalling pathways triggered by insulin (shown in Figure 1). The key players of the insulin/IGF signalling axis are insulin, the insulin-like growth factors IGF1 and IGF2, as well as their respective cell surface receptors [16]. Both the insulin receptor (IR) and the IGF1 receptor (IGF1R) belong to the family of receptor tyrosine kinases (RTKs), which also comprises the epidermal growth factor receptor (EGFR), platelet-derived growth factor receptor (PDGFR), vascular endothelial growth factor receptor (VEGFR), ephrin receptors, and many more. RTKs are composed of an extracellular domain (including, among others, the ligand-binding domain), a transmembrane domain and a cytoplasmic domain with tyrosine kinase activity [17]. The most well-studied function of the insulin signalling pathway is recruitment of the glucose transporter GLUT4 to the plasma membrane in adipose and muscle tissue, facilitating glucose uptake and storage.

Both the IR and IGF1R are composed of two α and two β subunits and they share similar sequences. There are, however, subtle differences, which determine preferential interaction

partners downstream of the receptors [18]. These differences explain the predominantly metabolic effect of IR in contrast to the mainly proliferative effect of IGF1R [19]. Ligand-binding induces autophosphorylation of IR and IGF1R and subsequent binding of adaptor proteins, specifically insulin receptor substrates (IRS) and src-homology domain containing proteins (Shc) [20]. These adaptor proteins then bind to the p85 subunit of the key regulator PI3K (phosphoinositide 3-kinase), thus facilitating the synthesis of PIP3 (phosphatidylinositol-trisphosphate) by PI3K. PIP3 recruits the serine/threonine kinase Akt to the cytoplasmic membrane. Akt can exert various cellular effects, e.g. inhibition of pro-apoptotic factors Bad and caspase 9 [21], stimulation of the proliferative factor mTOR (mammalian target of rapamycin) [22] or activation of the E3-ubiquitin ligase Mdm2 (mouse double minute 2 homolog) [23]. Mdm2 has diverse effects, such as degradation of the tumor suppressor p53. Moreover, Akt can induce AMPK (adenosine monophosphate-activated protein kinase), which regulates the cellular energy homeostasis. In addition to the PI3K/Akt pathway, IR and IGF1R can stimulate the MAPK cascade (mitogen-activated protein kinase), which induces expression of cell cycle genes, for instance via the transcription factor c-Fos [24].

In contrast to IR and IGF1R, the insulin-like growth factor 2 receptor (IGF2R), also known as cation-independent mannose-6-phosphate receptor (M6PR), does not activate signalling cascades. Rather, IGF2R scavenges for excess IGF2 at the plasma membrane and delivers enzymes from the Golgi network to the endosomal-lysosomal system [25]. Interestingly, it was shown that IGF2 is required for normal embryonic development of the pancreas, and defective IGF2 production leads to loss of β -cells [26]. The IGF2R contains 15 domains in the extracellular region with high sequence homology to the cation-dependent M6PR. IGF2 binds to domain 11, although domain 13 is required for high affinity binding. Domains 3, 5 and 9 bind M6P with varying affinities. In addition, the IGF2R can bind the protease plasminogen, associating to domain 1 [27].

There are two alternative splicing isoforms of Insulin Receptor (IR): the more common isoform IR-B is highly expressed in the liver, muscle and adipose tissue [28] and is mainly associated with metabolic signalling. The slightly shorter isoform IR-A is lacking the 12-amino acid long exon 11 of the entire 22 IR exons. Although IR-A is ubiquitously expressed, it is particularly important during embryonic development and in certain malignancies. IR-A displays a slightly higher affinity for insulin and significantly higher affinities for IGF1 and IGF2 [29]. Despite the

almost identical sequence of both receptors, there are differences in their downstream signalling pathways: it was demonstrated that in β -cells, IR-A activation triggers signalling via PI3K class I, while IR-B signalling recruits PI3K class II, leading to different transcriptional programs [30]. This has been attributed to varying plasma membrane localisations of both isoforms, thus facilitating the concentration of different adaptor proteins around the receptors [31].

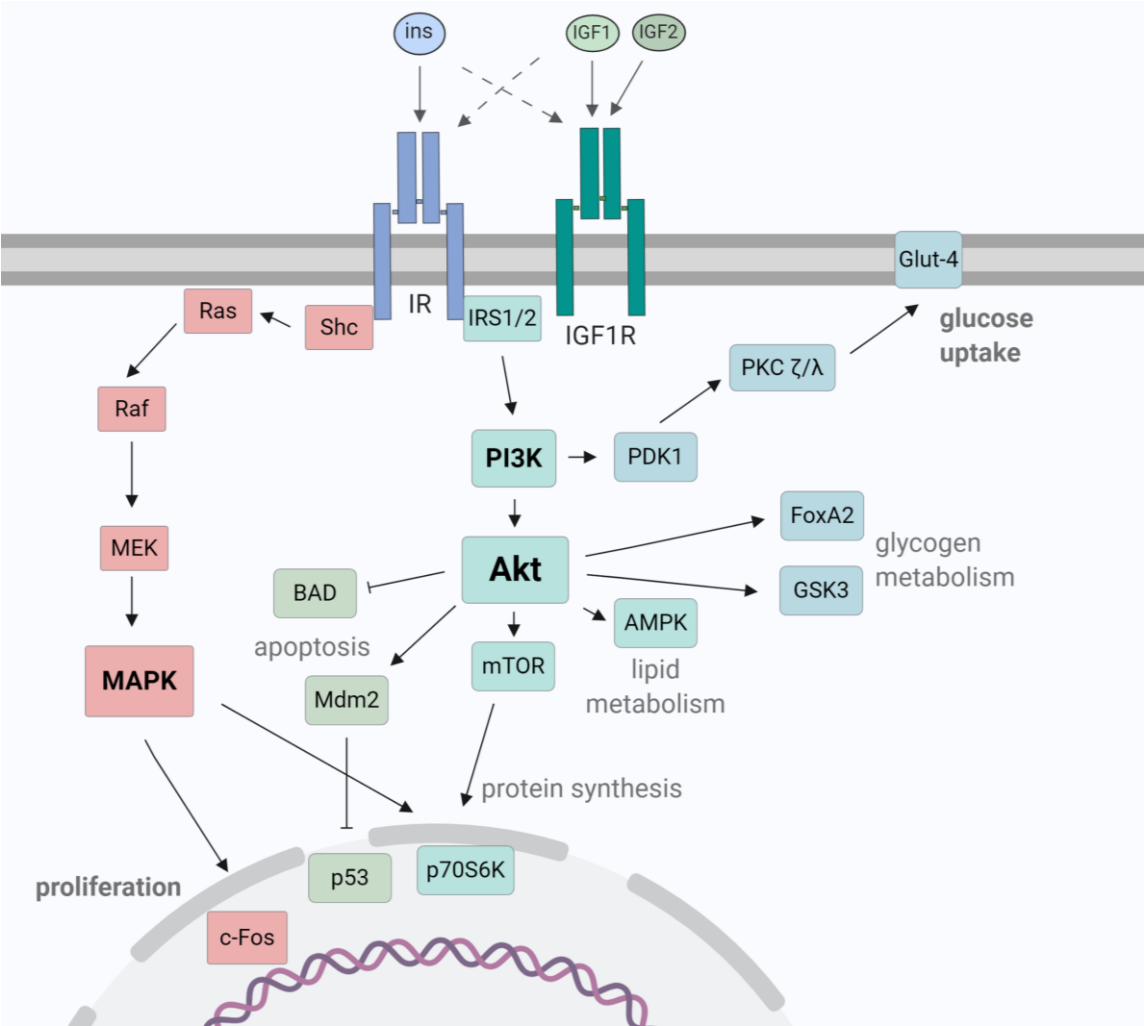


Figure 1: IR/IGF1R signalling via the MAPK and the PI3K/Akt pathway

Insulin receptor (IR) and Insulin-like growth factor 1 receptor (IGF1R) can trigger various cellular effects by signalling via the MAPK or the PI3K/Akt pathway. Figure was adapted from Belfiore et al. [29] and created with BioRender.com.

IR-A and IR-B, which are coexpressed in most tissues, are known to form heterodimers [29]. These heterodimers can be stimulated by insulin with an affinity similar to that of IR-A and IR-B homodimers, by IGF2 with an affinity similar to that of IR-A, and by IGF1 with lower affinity compared to both homodimers [32]. Similarly, hybrid receptors containing IR and IGF1R monomers have been observed. It was shown that these hybrid receptors are mainly stimulated by IGF1 binding [29].

In addition to the canonical pathways, it was recently suggested that there might be crosstalk between IR and IGF1R signalling and G-protein coupled receptors (GPCRs) [33]. Specifically, it was shown that β -arrestin, an important factor in GPCR signalling, might desensitise IGF1R signalling [34]. Furthermore, the IR has direct functions in gene regulation. For instance, it was recently shown that the IR is associated with RNA Polymerase II and that it can bind to gene promoters. Notably, a direct transcriptional upregulation of various insulin-related functions was observed upon IR binding to RNA Polymerase II [35]. Similarly, IGF1R was detected in the nucleus, suggesting a direct function in gene regulation [36].

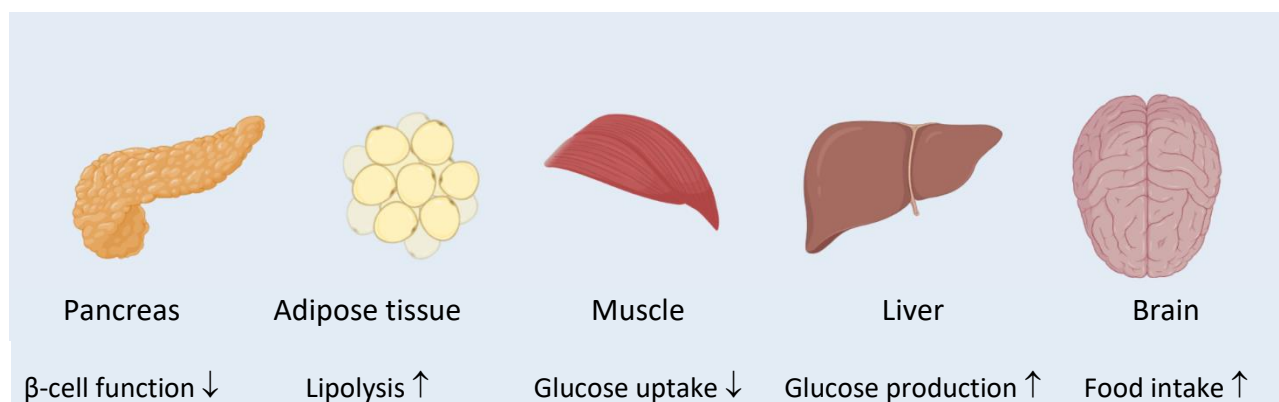


Figure 2: Effects of insulin resistance on important target organs

The predominant effects of insulin resistance are summarised by Kahn et al. [5]; organs were illustrated with BioRender.com.

The main target tissues for insulin action are adipose tissue and muscles (Figure 2). Additionally, high levels of the IR are expressed in the pancreas, liver, heart, lung, brain, spleen, placenta and kidney [37]. The effects of insulin on the brain are emerging as an important factor in normal organ function and in disease. In fact, it was described that the brain-specific insulin knockout mouse developed whole-body insulin resistance and obesity. Further, insulin administration has effects on cognitive function and eating behaviour [32]. As

the systemic functions of insulin are highly complex, targeting the insulin/IGF1 pathway can have potentially severe effects, which have to be thoroughly investigated.

1.1.3 Intracellular Trafficking of Receptor Tyrosine Kinases

Intracellular trafficking of receptors is a crucial factor in signalling regulation, as the rate of receptor endocytosis and recycling back to the cell surface determines the accessibility to ligands and interaction partners [38]. Numerous studies have shown that IR and IGF1R can be internalised via clathrin-mediated endocytosis [39] and via clathrin-independent pathways [40, 41] (Figure 3). Binding of clathrin to membrane-bound receptors is facilitated via adaptor proteins such as AP2. The μ 2 subunit of AP2 specifically recognises the sequence YXX Φ (X being any amino acid and Φ being a bulky hydrophobic amino acid) in cargo proteins. In addition, the AP2 subunit σ 2 recognises the dileucine motif ([DE]XXXL[LIM]). For clathrin-mediated endocytosis independent of AP2, clathrin-associated sorting proteins (CLASPS) function as adaptors [42]. It has been shown that some receptors are already pre-sorted at the cytoplasmic membrane, ensuring that they are not located in the same endosomes, although they use the same general endocytosis pathways [43].

Some proteins, such as IGF2R, have several motifs for different adaptor proteins (e.g. AP2, AP1), facilitating repeated cycling between different cellular compartments. Endocytosis of IGF2R is almost exclusively mediated via the YSKV motif binding to AP2. M6PRs (such as IGF2R) are recycled from early endosomes via AP1 and from late endosomes via Rab9. Generally, Rab proteins have important roles in receptor transport. Budding from the trans-Golgi network (TGN), where newly synthesized lysosomal enzymes are sorted, occurs via AP1 [25].

Clathrin-independent endocytosis can occur via actin rearrangements conferring macropinocytosis - although this mechanism has only been observed in cell types expressing very high levels of EGFR - or via caveolae [38]. Caveolae are flask-shaped membrane invaginations, which are structurally supported by three caveolin proteins. It is speculated that apart from endocytosis, caveolae can also function as scaffolds for signalling events. The most prominent function of caveolae is transcytosis, which enables rapid transport of ligands to neighbouring cells [44].

Caveolae are characterised by a high cholesterol concentration, similar to lipid rafts, which are dynamic microdomains in the plasma membrane where specific proteins are accumulated. It was shown that lipid rafts play an important role in pre-sorting receptors for various signalling pathways. For instance, insulin signalling in adipocytes relies on the localisation of signalling molecules to lipid rafts. Likewise, the subsequent translocation of GLUT4 to the plasma membrane is associated to lipid rafts [45].

After endocytosis, vesicles move towards the Golgi area along microtubules [38]. During the course of endosome maturation, the decreasing pH changes the interaction between sorting receptors such as the IGF2R and their cargo proteins [46]. In addition to acidification, this maturation is accompanied by a change in vesicle morphology towards multivesicular bodies (MVBs) (Figure 3). Proteases and other lysosomal enzymes are delivered to late endosomes from the TGN, resulting in further advancement to lysosomes. Proteins that are not sorted for recycling remain in lysosomes and are subsequently degraded. This process of sorting proteins for either recycling or degradation is dependent on the ubiquitination status of RTKs [47].

Most receptors are targeted for lysosomal degradation via lysine-63-linked polyubiquitination. This signal is recognised by the ESCRT machinery (endosomal sorting complexes required for transport) [48], which is composed of a variety of cytosolic proteins all containing ubiquitin-binding domains. Receptors that do not interact with the ESCRT complex are recycled to the plasma membrane. In addition to lysosomes, proteasomes play an important role in protein degradation. Proteins are marked for proteasomal degradation via differently linked ubiquitin chains, most importantly lysine-48-linked polyubiquitins [49]. In this context, the IR was shown to interact with the E3 ubiquitin ligases Nedd4 and MG53, while IGF1R binds to Mdm2, Nedd4 and c-Cbl [20].

The Nedd4 (neural-precursor expressed, developmentally down-regulated) family comprises nine structurally similar proteins, including Nedd4 and Nedd4-2, which have been implicated in the downregulation of growth factor receptors [50]. Importantly, ubiquitination by Nedd4 occurs at the TGN where correctly folded proteins are directed to the plasma membrane and misfolded proteins are ubiquitinated and sorted to the lysosome [51].

Transport of IGF2R back to the TGN occurs via different machineries, including the multiprotein complex retromer, as well as clathrin in association with AP1 and other adaptor proteins. The formation of vesicles containing retromer and the sorting mechanism of

retromer directing cargo towards the TGN is incompletely understood, but it seems to be distinct from the mechanism of clathrin-dependent vesicles. It has been proposed that early endosomes, late endosomes, lysosomes, MVBs and the TGN form an intricate tubular endosomal network where cargo proteins are constantly sorted and recycled via different sorting mechanisms, including clathrin and retromer [46].

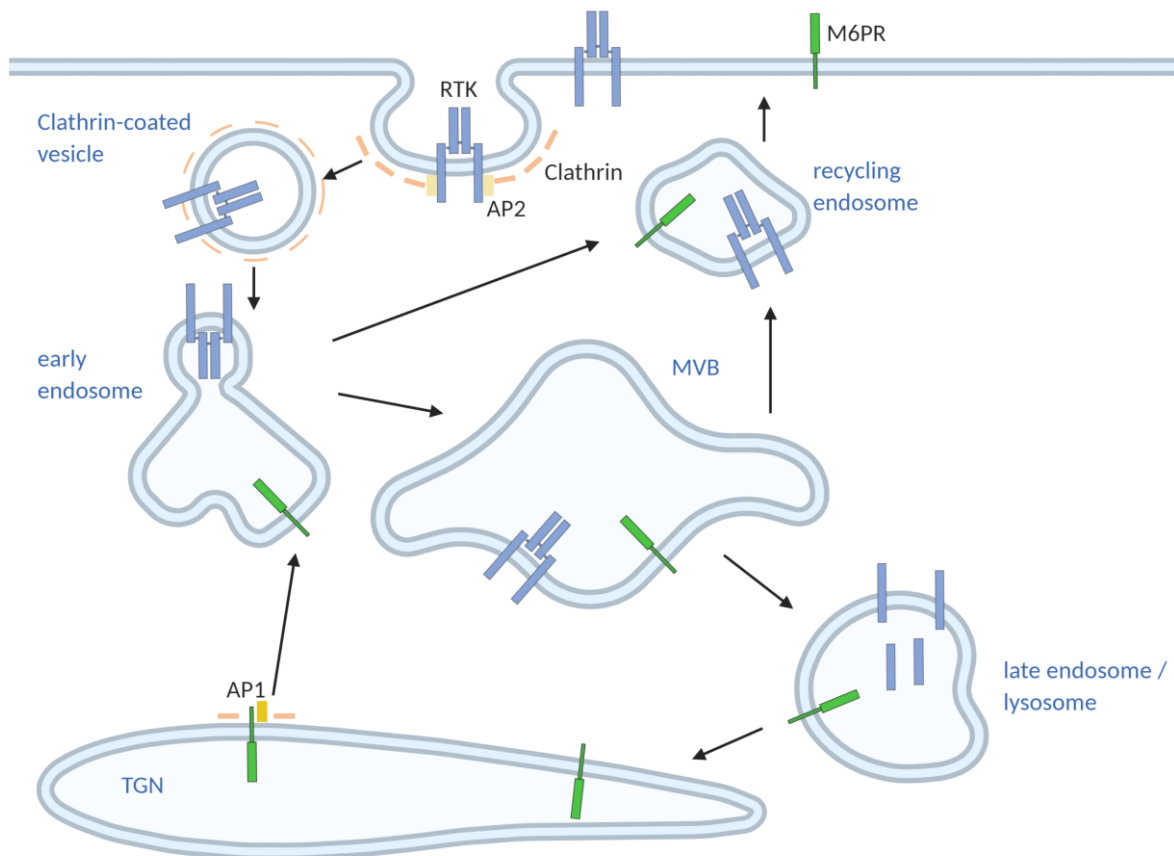


Figure 3: Intracellular trafficking in the endosomal/lysosomal system.

The trafficking of mannose-6-phosphate receptors (M6PR) was summarised by Ghosh et al. [25], while receptor tyrosine kinase (RTK) transport was illustrated by Goh et al. [38]. Figure was created with BioRender.com.

In cells expressing high levels of EGFR, a receptor recycling rate of up to 80% was observed. EGFR can either be recycled rapidly from early endosomes or slowly from the endocytic recycling compartment [52]. Endocytosis and recycling of RTKs, such as EGFR, is dependent on Rab proteins. Fast recycling from early endosomes is thought to be mediated by Rab4 and Rab35, whereas recycling from the endocytic recycling compartment to the cytoplasmic membrane relies on Rab11 [53]. However, this highly complex mechanism of endocytosis and

recycling requires a vast amount of regulatory proteins, such as other Rabs, polarity proteins and ADP-ribosylation factor (Arf) proteins.

In summary, RTKs undergo complex sorting mechanisms. Disturbances of these mechanisms can lead to severe signalling defects and trigger a variety of diseases, including diabetes. Thus, the modulation of IR endocytosis and/or recycling could be a promising approach towards re-establishing insulin signalling in diabetes.

1.1.4 Diabetes Treatment

To date, common therapies for T2D include lifestyle intervention, bariatric surgery and oral antidiabetics. Although lifestyle intervention relies on high intrinsic motivation of the patient, it was reported to significantly decrease the incidence of cardiovascular disease in T2D patients [54].

There are several classes of oral antidiabetics, including biguanides such as metformin, sulfonylureas, α - and β -glucosidase inhibitors and glitazones. Sulfonylureas act by increasing insulin availability. Mechanistically, glitazones are particularly interesting since they address the core issue of T2D, which is insulin resistance [55]. For this reason, they are often referred to as insulin sensitisers. They act as transactivators of the peroxisomal proliferator-activated receptor γ (PPAR γ), which is one of the key transcription factors involved in metabolic insulin signalling. Glitazones have been shown to decrease glucose levels, improve insulin sensitivity and reduce pathologically elevated glucose production in T2D patients [56].

The most commonly prescribed antidiabetic, metformin, is known to improve insulin sensitivity in liver, muscle and adipose tissue. This effect is likely attributed to several mechanisms, one of which is suppressing hepatic gluconeogenesis. Further, it has been shown that metformin is protective against cardiovascular disease and β -cell failure [57]. The positive cardiovascular effects of metformin are thought to be mediated by activation of AMPK and its downstream mediators, thus regulating the cellular energy metabolism. It was shown that insulin secretion in human β -cells is decreased after chronic culturing in high glucose concentrations. This effect can be prevented by treatment with metformin, likely by enhancing the cellular energy homeostasis [58]. In addition, metformin induces autophagy in

the mouse insulinoma cell line Min6 via AMPK signalling and protects Min6 cells against lipotoxicity [59]. Despite these positive effects, current oral antidiabetics merely treat diabetes in an acute manner, but do not cure the underlying disease; therefore, patients remain dependent on medication.

In more severe cases of T2D, many patients undergo bariatric surgery to restrict their caloric intake. Recent studies suggest that bariatric surgery yields better results in comparison to currently available oral antidiabetics [60]. T2D can be fully reversible when suitable measures such as strict lifestyle intervention and bariatric surgery are enforced [61]. However, as lifestyle intervention is a lengthy and challenging process, and bariatric surgery is highly invasive, the ideal diabetes treatment would be reversal of insulin resistance by oral medication.

1.1.5 Therapeutic Antibodies in Diabetes Therapy

A novel approach that is highly specific and therefore a safe treatment option for many diseases is the application of antibodies. In the context of T2D, not many therapeutic antibodies have been developed so far, yet there are several interesting concepts to explore. For instance, it was shown that antibodies against the fibroblast growth factor (FGF) receptor 1 can activate downstream signalling of the receptor, which leads to lipid oxidation and ketogenesis in the liver, as well as glucose uptake in the adipose tissue [62]. Another approach is targeting of the bone morphogenetic protein (BMP) 7 receptor. This factor is associated with repression of inflammation and stimulation of thermogenesis in adipose tissue, which could aid in balancing energy expenditure and blood glucose [63].

Recently, it was also shown that antibodies targeting Selenoprotein P could improve insulin secretion and glucose sensitivity in mouse models. Selenoprotein P, an extracellular metal binding protein, is produced mainly in the liver and has important functions in the cellular antioxidative system of target tissues, such as pancreas and skeletal muscle [64]. Similarly, treatment with an antibody against the adipokine aP2 improved glucose and insulin sensitivity in mice. The serum levels of this adipokine are significantly increased in obesity and metabolic diseases, as it is involved in regulating systemic metabolic adaptations [65].

Most promisingly, monoclonal antibodies against the serine protease PCSK9 (Proprotein convertase subtilisin/kexin 9) significantly lowered the cholesterol levels in multiple clinical trials without occurrence of adverse effects [66]. Given that many diabetics display hypercholesterolemia, supplementary treatment reducing cholesterol levels might be beneficial. However, there was no significant effect on the glucose metabolism of T2D patients [67]. In summary, there are various promising concepts, which could provide a basis for further development of therapeutic antibodies for diabetes treatment in the future.

1.1.6 Estrogen and Androgen Signalling in Diabetes

It is known that reproductive hormones are involved in regulation of the insulin signalling pathway, making these hormones of particular interest in diabetes research. During embryonic development, both estrogens and androgens are a key component of reproductive organ differentiation. In adults, estrogens mediate proliferation of female reproductive tissues, but they additionally have effects on skeletal homeostasis, lipid metabolism, electrolyte balance, skin physiology, the cardiovascular system and the central nervous system [68]. The main function of androgens is regulation of reproductive functions, such as spermatogenesis in males, but also ovarian function in females. While estrogens are primarily produced in ovaries and androgens in testes, both can be converted from steroid precursors in extragonadal tissues, specifically from dehydroepiandrosterone (DHEA) and dehydroepiandrosterone sulfate (Figure 4). In addition, circulating testosterone can be converted to 17 β -estradiol (E2) via aromatase [69]. Thus, the differential effects of estrogens and androgens on target tissues are difficult to determine.

Estrogen signalling is predominantly mediated by the estrogen receptors ER α and ER β , although there are additional receptors such as the estrogen-related receptor α (ERR α) and the membrane-bound G protein-coupled estrogen receptor 1 (GPER1) [68]. Androgen signalling occurs via the androgen receptor (AR). Due to their hydrophobic properties, estrogens and androgens can enter cells via free diffusion before binding to their receptors, which are cytosolic in the inactive state. Ligand-binding to steroid receptors causes a structural change, which allows the receptors to form dimers. The receptor-ligand dimers subsequently

translocate to the nucleus and function as transcription factors, in association with co-regulators [70]. The genomic sequences recognised by these receptors are referred to as estrogen response elements (ERE) or androgen response elements (ARE), respectively.

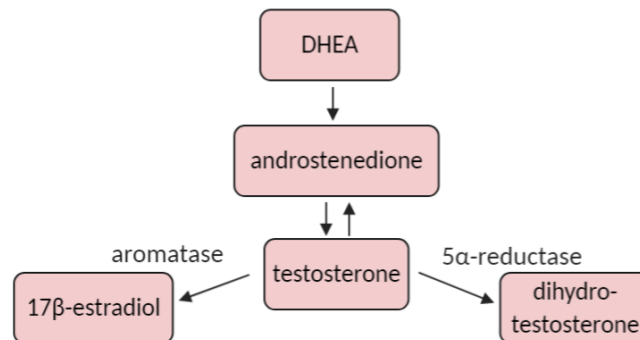


Figure 4: Conversion of steroids in extragonadal tissues

Circulating testosterone is converted to dihydrotestosterone or 17 β -estradiol in target tissues (illustration was adapted from Vrtacnik et al. [68] and created with BioRender.com).

It is known that the insulin/IGF1 pathway is heavily interlaced with estrogen and androgen signalling. Male T2D patients show lower testosterone levels, and testosterone replacement therapy is associated with a reduction in plasma glucose, indicating that the connection is bidirectional [71]. Aromatisation of testosterone to E2 plays an important role in this context. It has been shown that testosterone treatment reduces the body fat in males after androgen deprivation, while this effect is blocked by co-administration of aromatase inhibitors [72]. However, there is evidence that testosterone can also directly suppress white adipose tissue formation and promote muscle growth via AR signalling, possibly by induction of IGF1 expression [73].

In addition, androgens have a direct impact on β -cell function, as demonstrated by β -cell specific knockout of the AR in mice. The authors found a deregulation of a large number of genes involved in inflammation and cellular stress, as well as insulin secretion. This demonstrates that chronic androgen deficiency leads to β -cell failure [74]. In contrast, it is known that hyperandrogenism in women is associated with glucose intolerance and insulin resistance, although the mechanism is poorly understood [75].

Accordingly, various studies have demonstrated that estrogen treatment in diabetic women lowers blood glucose levels and improves insulin sensitivity [76]. Presumably, this is due to the physiologically active E2 protecting β -cells from oxidative stress and apoptosis. The stimulatory effect of E2 on insulin secretion has been extensively studied *in vitro* [76], and E2

has been shown to promote β -cell proliferation and regeneration *in vivo*, thus it could be an interesting treatment option for diabetes therapy [77]. However, due to the association of high estrogen levels with hormone-dependent cancers, estrogens are currently not approved for diabetes treatment. Therefore, approaches for targeted delivery of estrogen to the pancreas, e.g. via targeting of incretins, are being explored and have shown promising results in preclinical studies [78].

1.1.7 Link between Diabetes and Hormone-dependent Cancers

Hyperinsulinemia increases the risk for many cancer types [79]. Among males, prostate cancer is the third most frequent type of cancer [80]. However, despite the interlaced insulin and androgen signalling pathways, the prostate cancer risk is not increased in diabetes patients [81]. On the contrary, some studies reported a decreased risk [82]. One explanation could be the reduced testosterone levels in diabetics, specifically in patients with high BMI. However, the assumption that increased testosterone levels lead to higher prostate cancer risk remains controversial, as recent studies have reported that testosterone replacement therapy does not increase the prostate cancer prevalence [83]. Other possible mechanisms include certain gene variants that are present in diabetics, or the relative hypoinsulinemia in late stage type 2 and type 1 diabetes patients [82]. Nonetheless, evidence is accumulating that patients with diabetes are more frequently affected by metastatic prostate cancer and show higher mortality rates [84-86].

On the other hand, diabetes increases the risk for breast cancer [87]. Breast cancer is the second most common type of cancer in females [80]. Prostate cancer and breast cancer share remarkably similar growth mechanisms, as both rely on reproductive hormones, i.e. androgens, estrogens and progesterones [88].

By activating proliferation cascades, the insulin/IGF1 pathway is highly relevant in the intracellular signalling of cancer cells [89], including prostate cancer [90] and breast cancer [91]. Thus, it seems plausible that hyperinsulinemia is a driver for cancer progression. It has been speculated that neoplastic cells remain more insulin sensitive than liver, muscle or adipose tissue and can be growth-stimulated by elevated insulin levels [92]. It was shown *in*

vitro that high insulin concentrations increased the proliferation rate of prostate cancer cells [93]. Furthermore, diet-induced hyperinsulinemia in a murine *in vivo* xenograft model, accelerated prostate tumor growth [94].

Many studies have shown that individual variations in IGF1 levels have a large impact on cancer risk. Therefore, the development of IGF1R blocking antibodies seems like a promising approach for individual cancer therapy. However, treatment of cancer patients with these antibodies is associated with severe hyperglycemia and hyperinsulinemia. This is thought to be due to increased compensatory growth hormone secretion in the pituitary, leading to growth-hormone induced insulin resistance [92, 95].

Further, epidemiological studies have shown that low testosterone levels correlate to dyslipidemia, i.e. elevated cholesterol and triglyceride levels, and insulin resistance [96]. Androgen-deprivation therapy leads to hypogonadism, which seems to be a risk factor for metabolic syndrome [97]. Recent metabolomic studies have shown that androgen-deprivation therapy results in significant changes of metabolites associated with ketogenesis and fatty acid oxidation, and in higher glucose and insulin levels [98]. Thus, the connection between type 2 diabetes and prostate cancer appears to be bidirectional.

1.2 Proliferative Signalling in Prostate Cancer

1.2.1 Prostate Anatomy

The prostate is a secretory organ located beneath the bladder and shaped around the urethra. The function of the prostate is secretion of proteins, peptides and ions that form the basis of the seminal fluid. Embryonic development of the prostate starts in the 10th week of gestation from the urogenital sinus, which is derived from the endoderm. To initiate the budding of the prostate, AR activation in the surrounding mesenchymal tissue is required [99]. Histological classifications showed that it can be distinguished into three areas: the central, peripheral and transitional zone [100]. In contrast, the mouse prostate is composed of separate lobes with distinct morphology: the dorsal, ventral, lateral and anterior prostate. Nonetheless, the histology of mouse prostate epithelium is highly similar to human, thus the mouse is a valid model to study prostate histology [101]. The two dorsal prostate lobes are composed of small acini with columnar epithelium, while the acini of the ventral prostate are comparatively larger. The lateral prostate shows a flat epithelial layer. Distinctly, the anterior prostate is characterised by papillary structures. Based on histological comparisons and gene expression signatures [102], the dorsal prostate is analogous to the peripheral zone of the human prostate, while the anterior prostate is the counterpart to the human central zone. This is of interest as it is estimated that 70% of prostate cancers originate from the peripheral zone [103].

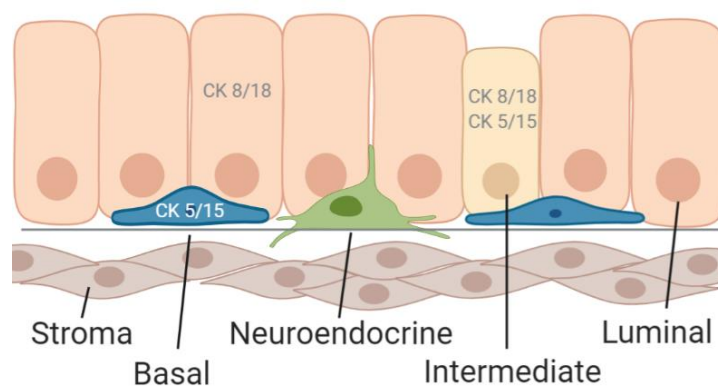


Figure 5: Structure of the prostate epithelium

Luminal cells are marked by cytokeratin (CK) 8 and 18 expression, basal cells characteristically express CK 5 and 15. Figure was adapted from Taylor et al. [104] and created with BioRender.com.

Growth of the prostate is very slow and directly depends on androgens for growth stimulation during development. In adults, the prostate is a growth-quiescent organ with low rates of both proliferation and apoptosis. In addition to androgens, estradiol has a role in prostate growth, via activation of ER β [105]. IGF1 has also been implicated in prostate growth. For instance, it was shown that the serine-protease prostate-specific antigen (PSA) can cleave insulin-like growth factor binding protein-3 (IGFBP-3), thereby increasing the local availability of IGF1 [106].

The prostate epithelium is comprised of four cell types (Figure 5): the secretory luminal cells; the basal cells, which are responsible for regeneration of luminal cells and for maintaining structural integrity of the epithelium [107]; the intermediate cells, which show histological characteristics of both luminal and basal cells; and finally, the rare neuroendocrine cells. By secreting peptide hormones, such as serotonin, calcitonin and somatostatin, neuroendocrine cells regulate the growth and differentiation of prostate epithelia [108]. Studying the function of normal prostate epithelium could provide insight into the mechanisms of carcinogenesis in the prostate.

1.2.2 Androgen Signalling in Prostate Cancer

Prostate growth and regeneration is regulated by androgens. The AR belongs to the group of steroid hormone receptors, along with estrogen receptors ER α and ER β , progesterone receptor, glucocorticoid receptor and mineralcorticoid receptor [70]. The most well-known ligand of the AR, testosterone, can be converted to 5 α -dihydrotestosterone (DHT) by 5 α -reductase, which is significantly more potent in binding to the cytosolic AR. The inactive form of AR is bound to chaperones, which are released upon binding of DHT, thus facilitating dimerisation of AR [109].

The dimerised AR is able to translocate to the nucleus and bind specific DNA sequences known as androgen response elements (AREs). AREs contain two hexamers with an inverted repeat in the second hexamer, separated by three arbitrary base pairs. The motif with the highest binding affinity was identified as AGAACAnnnTGTTCT (whereby n is any nucleotide), although it should be noted that many AREs show diverging base pairs in the palindromic consensus

sequence. It was shown that even half AREs, consisting of only one hexamer, can be bound by AR [110]. Binding of AR to AREs regulates transcription of target genes in the presence of coactivators or corepressors, including metabolic genes, specifically those required for aerobic glycolysis and anabolism [111]. In addition, there have been reports of membrane testosterone receptors, exerting rapid nongenomic actions such as secretion of PSA [112].

In some prostate cancer cells, specific AR splice variants, lacking the ligand binding domain, have been found. Although there are differences in the transcription of genes related to biosynthesis and metabolism compared to wildtype AR, the same set of cell cycle genes can be activated by the ligand-independent splice variant [113].

The AR contains three poly-glutamine repeats in the aminoterminal domain. In many proteins, including AR, mutations resulting in expansion of such poly-glutamine repeats can lead to significant structural changes. These proteins are associated with neurodegenerative diseases such as Huntington's disease and spinal bulbar muscular atrophy [114]. In summary, signalling via AR has differential effects that are not limited only to gonadal function.

1.2.3 Androgen-independent Prostate Cancer

The initial treatment for localised, non-metastatic prostate cancer is prostatectomy or radiotherapy (Figure 6). As prostate tumor growth depends on androgens, the preferred chemotherapeutical treatment is androgen deprivation, either via chemical castration or anti-androgens [115]. However, androgen deprivation therapy can eventually lead to androgen-independent tumors.

Several pathways are thought to be involved in the progression towards androgen-independent prostate cancer (AIPC) [116]. The androgen receptor (AR) can become hypersensitive to minimal androgen concentrations through various mutations. These tumors are usually the result of a selection process under low androgen conditions [117]. There are other mechanisms by which cells can increase AR sensitivity, e.g. increased stability or amplified levels of co-activators [118]. Another possibility is a local increase of androgens, specifically through an accelerated conversion rate of testosterone to the more potent

DHT [119]. In addition, the AR can become promiscuous through specific mutations, and bind to other steroid hormones or anti-androgens [120]. The most frequently occurring AR mutation is the T877A mutant, where threonine is replaced with alanine in the ligand binding domain. It was shown that this mutant is efficiently activated by progesterone and estradiol [121]. Interestingly, this mutant is often found in patients that were previously treated with the anti-androgen flutamide [120].

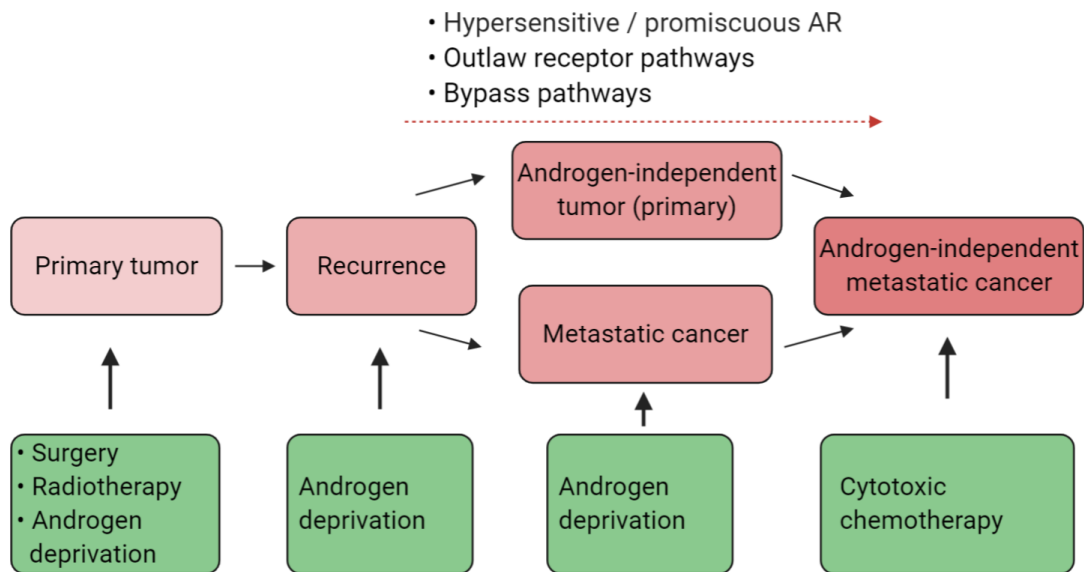


Figure 6: Therapeutical strategy in prostate cancer

After androgen deprivation, tumors often acquire alternative proliferative pathways. In late disease stages, cytotoxic chemotherapy is currently the only treatment option. The flowchart was adapted from Drake et al. [122] and created with BioRender.com.

Some tumors activate proliferation by switching to bypass pathways that utilise entirely different mechanisms, such as blocking apoptosis by upregulation of BCL2 (B-cell lymphoma protein 2) [123]. Finally, the AR can be cross-activated by other receptor pathways, creating a so-called ‘outlaw’ pathway (Figure 7). It has been demonstrated that AR can be efficiently activated by IGF1, EGF or KGF (keratinocyte growth factor) [124]. This is thought to occur through phosphorylation of Foxo1 via the PI3K/Akt pathway, leading Foxo1 to leave the nucleus and thus lose its ability to block AR [125]. Accordingly, immunohistochemical staining of human tissue samples showed IGF1R upregulation in prostate cancer after androgen-independent progression [126, 127]. Moreover, it has been described that HER2 (a member of the Human Epidermal growth factor Receptors) can mediate the expression of AR target genes in presence, but not in absence of AR [128]. It was suggested that this is due to increased Akt signalling, as Akt can phosphorylate AR and thereby facilitate AR dimerisation [129].

Strikingly, the well described tumor suppressor gene PTEN (phosphatase and tensin homologue) is mutated in a high percentage of prostate tumors. PTEN is a potent inhibitor of the PI3K/Akt pathway, thus this is another indication that the PI3K/Akt pathway has an important role in AR activation [130].

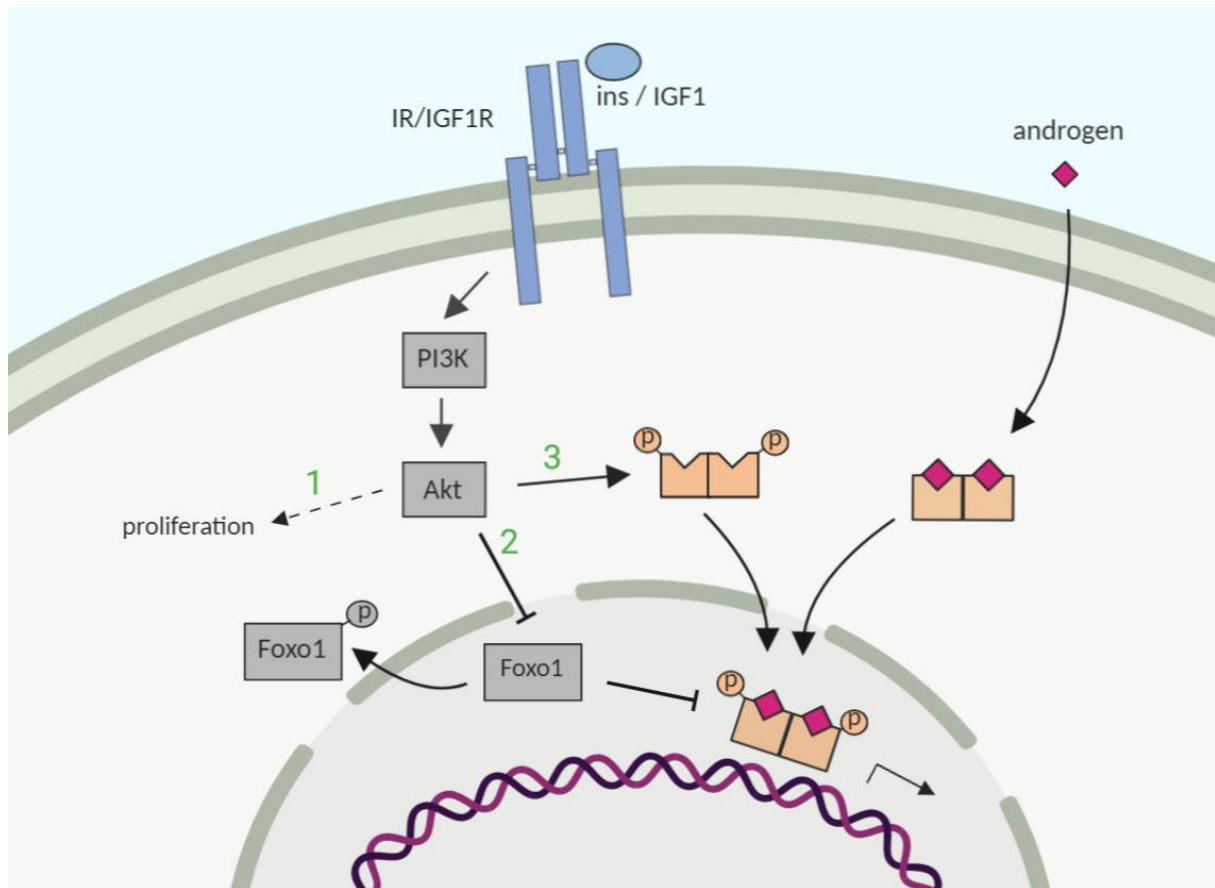


Figure 7: Mechanisms of insulin/IGF1 signalling in prostate cancer

1: IR and IGF1R activate proliferative pathways. 2: Akt phosphorylates Foxo1, which subsequently leaves the nucleus, thereby unblocking AR [125]. 3: Akt phosphorylates AR in absence of androgen, thus facilitating AR dimerisation and DNA binding [129]. Created with BioRender.com.

There is currently no efficacious treatment for AIPC. It was attempted to treat AIPC with enzalutamide (a second generation anti-androgen), however the response was modest [131]. Only slightly better results were achieved with a combination of the anti-androgen abiraterone acetate and the glucocorticoid prednisone [132]. Thus, the search for novel targets is ongoing.

1.2.4 Cell line Models of Prostate Cancer

The most widely used cell line model for androgen-dependent prostate cancer, LNCaP, was originally isolated in 1980 from a lymph node (LN) metastasis of prostate cancer (CaP) [133]. It was soon discovered that the cells retain their malignant phenotype and form tumors upon injection in mice, and that their proliferation can be modulated by different testosterone concentrations [134]. Co-inoculation of LNCaP cells and a bone stromal cell line into castrated male mice yielded the subline C4-2. LNCaP C4-2 cells had significantly reduced AR levels and could not be stimulated by varying testosterone concentrations, but retained their ability to form tumors [135]. Another widely used cell line, PC-3, was isolated from a bone metastasis of prostate adenocarcinoma in 1979. It was shown that PC-3 cells do not respond to testosterone and are therefore a useful model for AIPC [136]. Several years later, another cell line named MDA PCa 2b was established from an androgen-independent bone metastasis. In contrast to PC-3, this cell line showed androgen-stimulated expression of target genes [137].

1.2.5 Targeting Prostate Cancer via PI3K/Akt

The PI3K/Akt pathway is highly relevant in cancer metabolism and proliferation, specifically regarding the development of AIPC [138, 139]. Thus, the idea of blocking PI3K to decrease cancer growth and progression is intriguing. Indeed, PI3K inhibitors performed well in reducing prostate tumor growth in preclinical studies [140]. However, PI3K inhibitors have the negative effect of inducing severe hyperglycemia, likely by disrupting insulin signalling in peripheral organs [141, 142].

In addition, the efficacy of PI3K inhibitors often declines during the course of the treatment, presumably due to compensatory effects. It was demonstrated in xenograft models that insulin signalling can reactivate the loss of PI3K signalling achieved by PI3K inhibitors. The authors proposed that ketogenic diet could greatly improve the efficacy of PI3K inhibitors [143]. Accordingly, it was shown that insulin can induce mitogenic signalling exclusively via IR activation in prostate cancer cells. The authors concluded that IR activation can compensate for inhibition of other proliferative pathways [144].

It has also been suggested that inhibitors of mTOR, which is activated by Akt, should be co-administered to account for compensatory effects. Treatment with an mTOR inhibitor, along with an inhibitor of Akt or MAPK, showed consistent anti-tumoral activity *in vitro* and *in vivo*, while the efficacy of the mTOR inhibitor alone was ameliorated due to the feedback activation of MAPK signalling [145, 146].

Combination therapy with AR and PI3K inhibitors was effective against AIPC in an animal model, while single-agent treatment with an AR inhibitor or PI3K inhibitor activated compensatory growth pathways [147]. Interestingly, it was shown that AR signalling and activation is elevated in diabetic prostate cancer patients, suggesting that crosstalk between IR and AR signalling is highly relevant for cancer development and progression [148].

Clinical trials involving direct inhibition of IGF1R have shown promising results in AIPC [149]. Again, the efficacy of the treatment was significantly increased by co-treatment, in this case with the cytotoxic chemotherapeutic docetaxel. It was suggested that IGF1R inhibition sensitises prostate cancer cells to docetaxel [150]. Taken together, targeting insulin/IGF1 signalling might be beneficial in prostate cancer treatment.

1.2.6 Therapeutic Antibodies in Cancer

Monoclonal antibodies have been used with great success for the treatment of various cancer types. There are several mechanisms by which antibodies can induce tumor cell-specific apoptosis, either via immune modulation, activation of pro-apoptotic pathways or blocking of proliferative pathways, which are mainly mediated via RTKs [151]. Promising results have been achieved in breast cancer, particularly with anti-proliferative antibodies. The human epidermal growth factor receptor 2 (HER-2)-targeting antibody trastuzumab was shown to be effective and well-tolerated as a first-line treatment [152]. However, after a promising initial response, many tumors acquire resistance to trastuzumab. One of the contributors to trastuzumab resistance could be the insulin/IGF1 pathway. It has thus been suggested that trastuzumab should be used in combination with other therapeutics, e.g. IGF1R blocking antibodies [153]. In prostate cancer, phase II studies of the IGF1R inhibiting antibody

cixutumumab showed promising initial results [154]. However, a follow-up trial comparing cixutumumab to a VEGFR-targeting antibody showed limited efficacy of cixutumumab [155]. One of the most important factors in antibody design for cancer therapy is the *in vivo* specificity, as it determines the biodistribution, i.e. the ratio of antibody uptake in the tumor relative to healthy tissues. This specificity can be influenced by subtle changes in the physicochemical properties [156].

Other approaches aim for specific drug delivery to prostate cancer cells using conjugated antibodies. This can be done using either chemotherapeutics or radionuclides as conjugates. A well-studied target for this purpose is the prostate-specific membrane antigen (PSMA), as it is highly upregulated in prostate cancer [157]. For instance, a PSMA antibody conjugated to a microtubule-depolymerizing drug showed efficient tumor reduction in animal models with no apparent toxicity, while the administration of the drug alone showed only minor effects [158]. Although prostate cancer is radiation-sensitive, radiation is only feasible for localised tumors, as the toxicity to surrounding organs would be too high in metastatic prostate cancer. There are approaches to conjugate antibodies to radionuclides such as Lutetium-177 (^{177}Lu), which emits short-range β particles that will damage surrounding cells, as well as γ -radiation, facilitating computed tomography (CT) imaging at the same time. It was shown that a PSMA antibody conjugated to ^{177}Lu suppressed tumor growth in clinical trials and was well tolerated [159].

As EGFR is known to be involved in prostate cancer progression, it was proposed that the anti-EGFR antibody cetuximab, which is approved for therapy of colorectal cancer, might be beneficial in prostate cancer treatment. However, *in vitro* evaluations showed only a moderate response [160]. Although there are many promising alternatives in clinical trials, there is currently no approved antibody treatment for prostate cancer.

1.3 Identification of IGFR-L1

We have described a novel receptor, the IGF receptor-like 1 (IGFR-L1) (Figure 8). *In vivo* experiments showed that deletion of the *IGFR-L1* gene is fatal as knockout mice die within few hours after birth. Furthermore, the mice are characterised by hyperinsulinemia and hypoglycemia, suggesting that this novel receptor has a crucial function in glucose homeostasis. *In vitro* experiments in the mouse insulinoma cell line Min6 showed that deletion of the *Igfr-L1* gene increases the phosphorylation of key regulators in insulin/IGF1 signalling (IR, IGF1R and Akt). IGFR-L1 shows high sequence similarities to growth factor receptors such as IGF1R and EGFR within the cysteine-rich growth factor receptor domain. Further, the similarity between IGFR-L1 and IGF2R is very high within the M6PR domain (Figure 8).

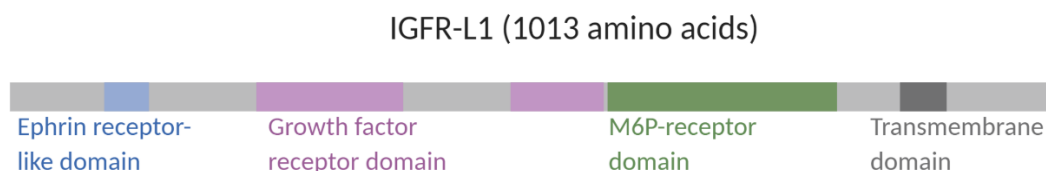


Figure 8: Domain structure of IGFR-L1

The protein sequence was analysed using the ENSEMBL database (transcript ID ENST00000369939.8 [161]). The recognised domains were extracted and annotated with BioRender.com.

Earlier studies have linked IGFR-L1 with various cancers. Initially, it was described as a biomarker in estrogen-dependent endometrial carcinoma and therefore termed estrogen-induced gene 121 (EIG121) [162]. It was subsequently shown that this gene, also known as KIAA1324, was associated with a good prognosis in gastric cancer and pancreatic neuroendocrine tumors [163, 164]. Contrarily, EIG121 was correlated to poor prognosis in ovarian cancer [165], and induced progression of endometrial cancer in an *in vitro* and *in vivo* model [166]. Based on its involvement in insulin signalling and its link to various cancers, we propose that IGFR-L1 could be a potential target molecule in diabetes or cancer therapy.

1.4 Scope of the Project

The first part of this project was the characterisation of IGFR-L1 in pancreatic β -cells. As we showed before that IGFR-L1 is related to insulin signalling, our aim was to investigate the molecular mechanisms underlying this interaction. As receptor trafficking is a crucial factor in signalling regulation, we aimed to analyse the intracellular trafficking behaviour of IGFR-L1 and find potential links to related receptors such as IR and IGF1R.

The second part focused on investigating the potential function of IGFR-L1 in benign prostate epithelium and prostate cancer cells. As discussed previously, hyperinsulinemia is a driver for prostate cancer progression. To develop novel treatment options for metastatic prostate cancer, it is therefore essential to understand the mechanisms of insulin/IGF1 signalling in cancer cells. Importantly, these findings can also be applied to other hormone-dependent cancers, such as breast cancer.

For these purposes, we established high affinity monoclonal antibodies, which are useful tools for various techniques in molecular biology. Eventually, these antibodies could be used to block receptor function and thereby alter insulin/IGF1 signalling. We propose that IGFR-L1 blocking antibodies present novel treatment options for diabetes or cancer. Alternatively, antibodies can be conjugated to small molecules for drug delivery.

2 Results

2.1 Establishment of IGFR-L1 antibodies

2.1.1 Antibody Screening

2.1.1.1 IGFR-L1 antibodies are functional in human cells

Antibodies against IGFR-L1 were generated using the hybridoma technique by R. Feederle (Monoclonal Antibody Core Facility, Helmholtz-Zentrum München) and Ü. Coskun (Paul-Langerhans Institute Dresden) (Figure 9). As an epitope, either the recombinant extracellular domain of IGFR-L1 or full-length IGFR-L1 embedded in an artificial plasma membrane (proteoliposomes) was used. Since the antibodies were raised against human IGFR-L1, the functionality was initially tested by immunocytochemistry, using the unpurified cell culture supernatant, on the human breast cancer cell line MCF7. As an internal positive control, the cells were co-stained with the previously established antibody 31A11 (mouse) or 16F6 (rat). Both 31A11 and 16F6 were raised against the recombinant cytoplasmic domain of IGFR-L1. Out of 37 newly generated antibodies, 24 showed a positive signal in immunocytochemistry of human cells (see Table 1 and Figure 10).

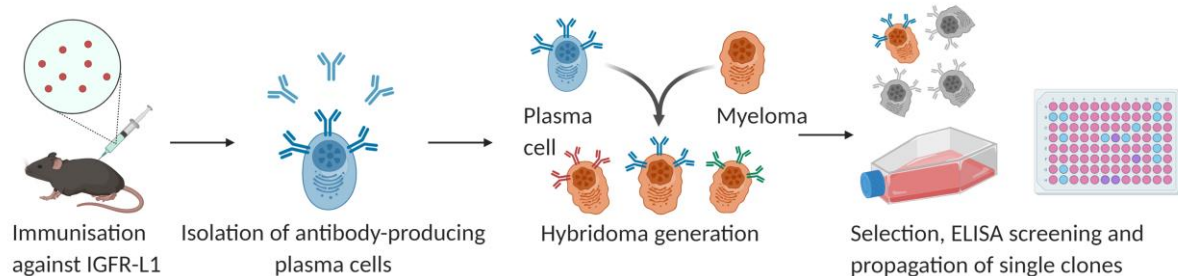


Figure 9: Antibody generation via the hybridoma technique

Mice were immunised against either the extracellular domain of recombinant IGFR-L1 or against IGFR-L1 embedded in proteoliposomes. The illustration was adapted from Hurrell et al. [167] and created with BioRender.com.

Table 1: Summarising list of all tested antibodies

Antibody	Subclass	Epitope	Signal human cells	Signal mouse cells	Unspecific signal KO cells	Dilution purified Ab
1C9	Rat IgG2c	Proteolip.	++	-	-	-
2A2	Rat IgG2c	Proteolip.	-			
2G6	Rat IgG2b	Rec.	++	+++	-	1:1000
5A2	Rat IgG2c	Proteolip.	-			
6B12	Rat IgG2c	Proteolip.	+	-	-	
6D12	Rat IgG2c	Rec.	++	-	-	1:5000
7C3	Rat IgG1	Proteolip.	+	+	-	
7E5	Rat IgG1	Proteolip.	++	-	-	1:1000
8A4	Rat IgG1	Proteolip.	+	+	+	
8B6	Rat IgG1	Proteolip.	-	-	-	
8D1	Rat IgG2a	Proteolip.	-			
8G5	Rat IgG2c	Proteolip.	-			
9F12	Rat IgG2a	Proteolip.	+++	-	-	
10B11	Rat IgG1	Rec.	+	-	-	1:100
10E5	Rat IgG1	Proteolip.	-			
11F4	Rat IgG1	Proteolip.	+++	++	-	1:100
12B4	Rat IgG1	Proteolip.	++	+	+	1:100
13E7	Rat IgG2a	Proteolip.	-			
14B2	Rat IgGa	Proteolip.	+	-	-	1:1000
16E10	Rat IgG2c	Proteolip.	-			
16H10	Rat IgG2a	Proteolip.	+++	+++	-	1:100
19A6	Rat IgG2b	Rec.	++	+++	-	1:1000
19F2	Rat IgG1	Proteolip.	-			
21E5	Rat IgG2a	Proteolip.	+	-	-	1:100
21G4	Rat IgG1	Proteolip.	-			
22G5	Rat IgG2a	Proteolip.	++	-	-	
24A12	Rat IgG2a	Proteolip.	+	-	-	
25D3	Mouse IgG2a	Proteolip.	+	-	-	
25E5	Mouse IgG2b	Proteolip.	-	-	-	
25E6	Mouse IgG2b	Proteolip.	-	-	-	
25F1	Mouse IgG2b	Proteolip.	+	-	-	
25F8	Mouse IgG3	Proteolip.	+	-	-	
25G6	Mouse IgG3	Proteolip.	+	-	-	
27B6	Mouse IgG2b	Proteolip.	-	-	-	
27D7	Mouse IgG3	Proteolip.	++	-	-	
30A7	Mouse IgG1	Proteolip.	++	+	-	
30G11	Mouse IgG3	Proteolip.	++	-	-	

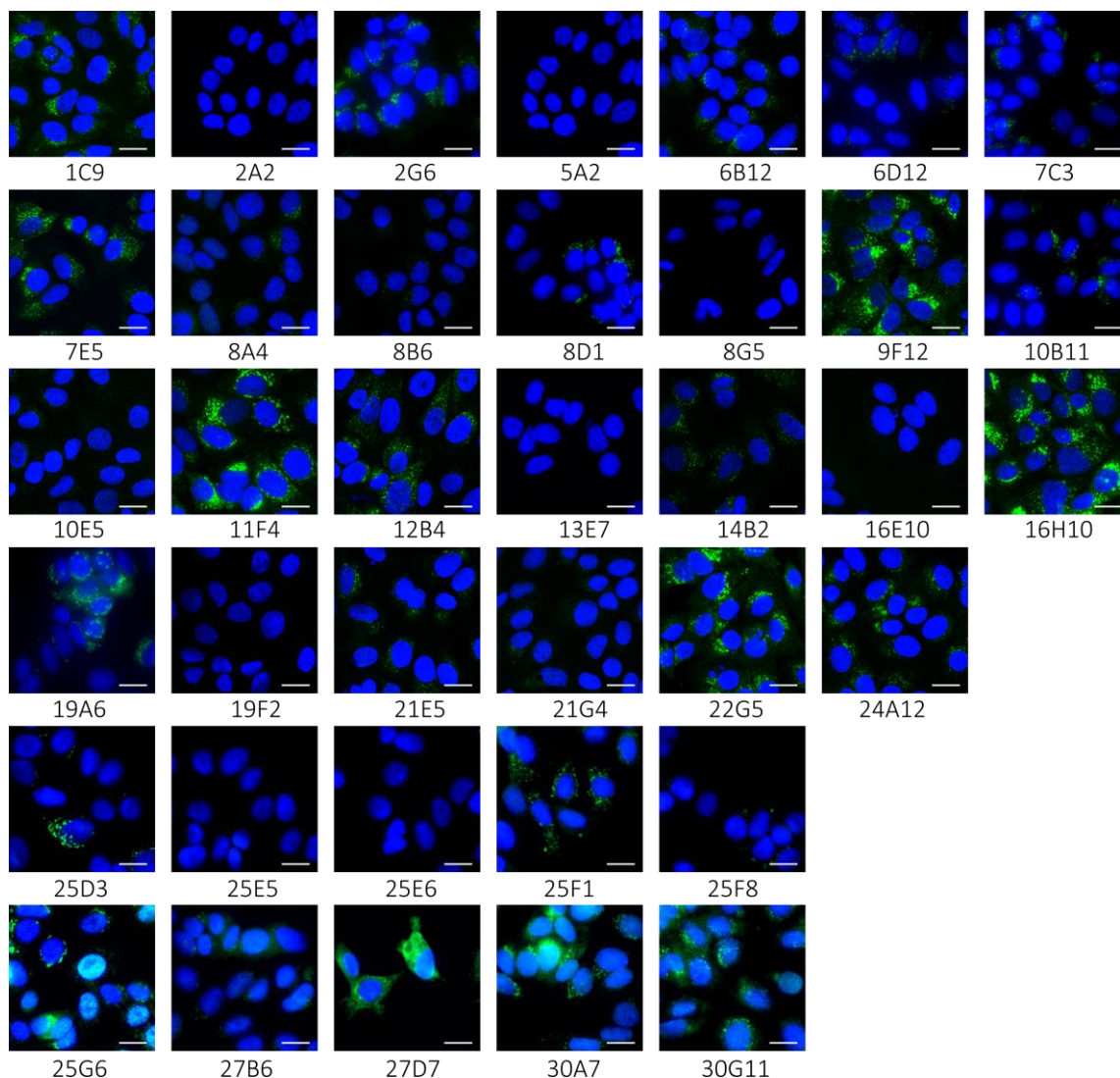


Figure 10: Screen of antibodies directed against IGFR-L1

All antibodies were initially tested via immunocytochemistry in the human cell line MCF7

(scale bar: 20 μm).

2.1.1.2 The subtype of mouse IGFR-L1 antibodies is confirmed

The subtypes of the IGFR-L1 antibodies generated in the mouse hybridoma cultures was not conclusively determined before. Thus, the subtypes were confirmed using a sandwich immunocytochemistry assay, where the fixed MCF7 cells were first incubated with the respective primary antibodies, followed by a rat anti-mouse IgG1 / IgG2a / IgG2b / IgG3 antibody, and finally with an AlexaFluor 647 tagged donkey anti-rat antibody. The anticipated

isotypes were correct for all antibodies except 30G11, where no signal was detected (Figure 11). Interestingly, the staining pattern of some mouse IgGs (25G6, 27D7 and 30A7) was slightly different compared to the staining pattern observed with most of the antibodies, indicating that there might be crossreactivity to other proteins (Figure 10 and Figure 11).

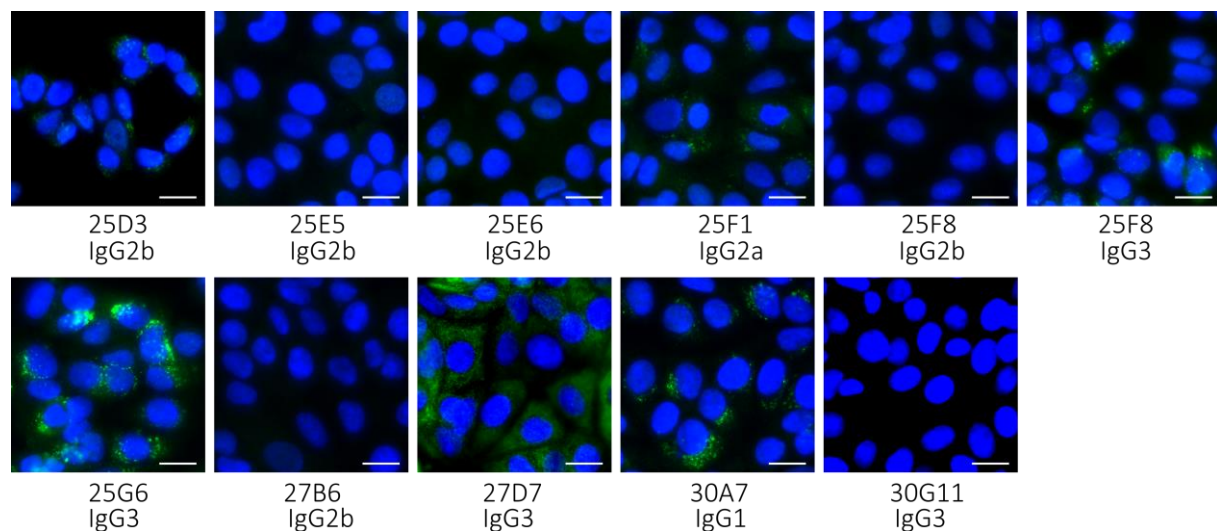


Figure 11: Determination of the active IgG subtype of mouse IGFR-L1 antibodies

The subtype of mouse antibodies was confirmed using subtype-specific antibodies (scale bar: 20 μ m).

2.1.1.3 Several IGFR-L1 antibodies are functional on mouse cells

The 24 functional antibodies were subsequently tested on the mouse insulinoma cell line Min6 to determine their reactivity for mouse Igfr-I1 (Figure 12). Only 8 antibodies showed a signal in Min6 cells, which means that 16 antibodies were specific for human IGFR-L1. The target specificity of the antibodies was determined using Igfr-I1 knockout (KO) Min6 cells. Two antibodies showed a weak unspecific signal in KO cells, indicating cross-reactivity to a different target. In summary, the clones 1C9, 6D12, 7E5, 9F12 and 22G5 showed a reliably strong cytoplasmic staining only in human cells, while 2G6, 11F4, 12B4, 16H10 and 19A6 displayed a strong signal in both human and mouse cells. These antibodies were selected as the best candidates for future experiments.

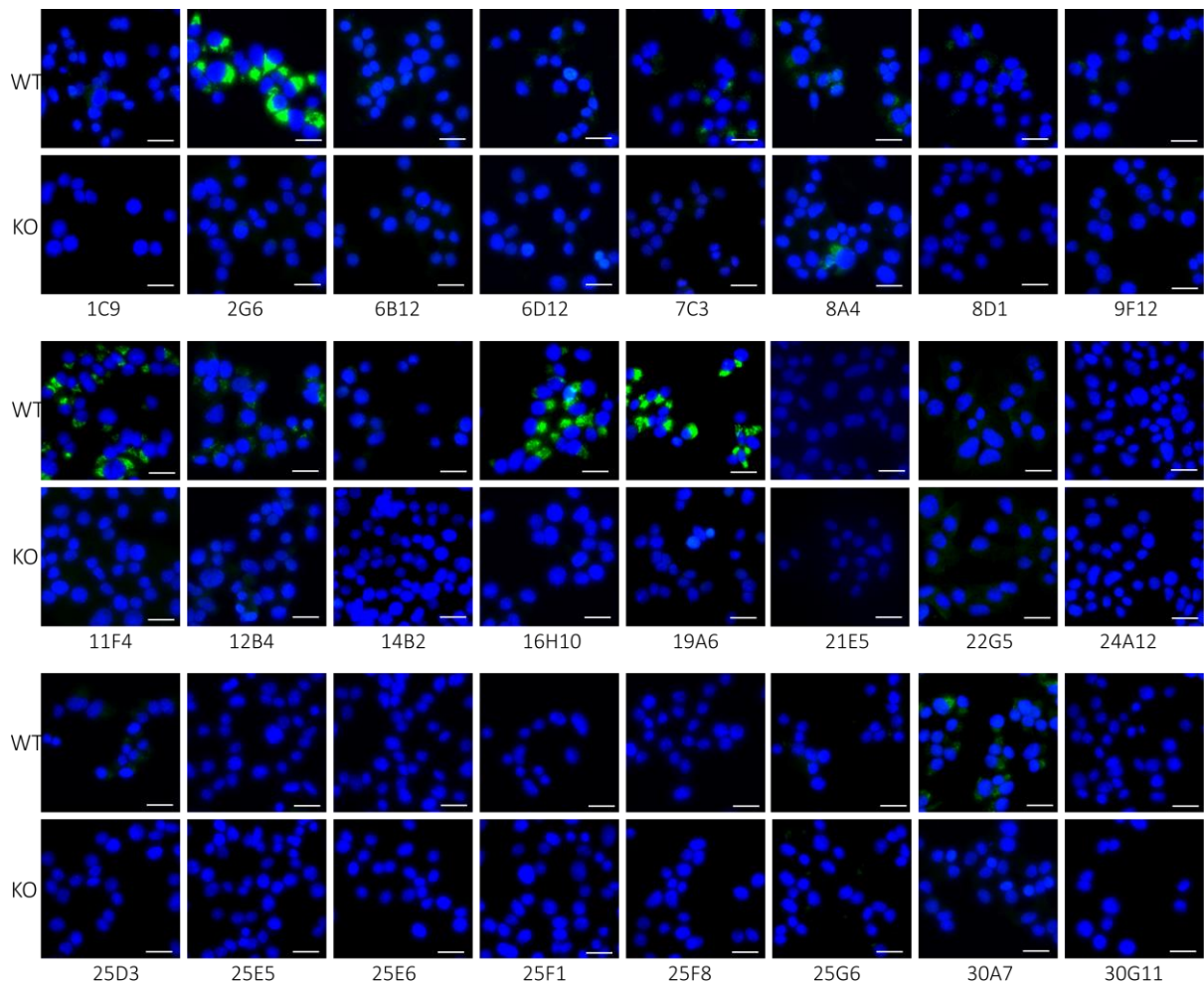


Figure 12: Specificity test of working antibodies in the mouse cell line Min6

The reactivity of IGFR-L1 antibodies against mouse Igfr-L1 was assessed via immunocytochemistry in Min6 cells (WT and Igfr-L1 KO; scale bar: 20 μ m).

2.1.1.4 Purified antibodies show high affinity in mouse and human cells

From the 24 functional hybridoma clones, only 12 were successfully stabilised (1C9, 2G6, 6B12, 6D12, 7E5, 10B11, 11F4, 12B4, 14B2, 16H10, 19A6 and 21E5). These clones were further cultured and their collected supernatant was column-purified by R. Feederle (Monoclonal Antibody Core Facility). To determine the optimal working concentration, the purified antibodies were tested on human and mouse cells in different dilutions (Figure 13 and Figure 14). Strikingly, antibody 1C9 was not reactive in the purified form. Further, 6D12 yielded

a strong specific signal in human cells, but no signal in mouse cells, as expected from previous experiments. The signal of 16H10 was comparatively weak, suggesting that the purification was less successful compared to other antibodies. In summary, based on their intense and reproducible staining signal in both mouse and human cell lines, antibodies 2G6 and 19A6 were selected as the most promising candidates for future experiments.

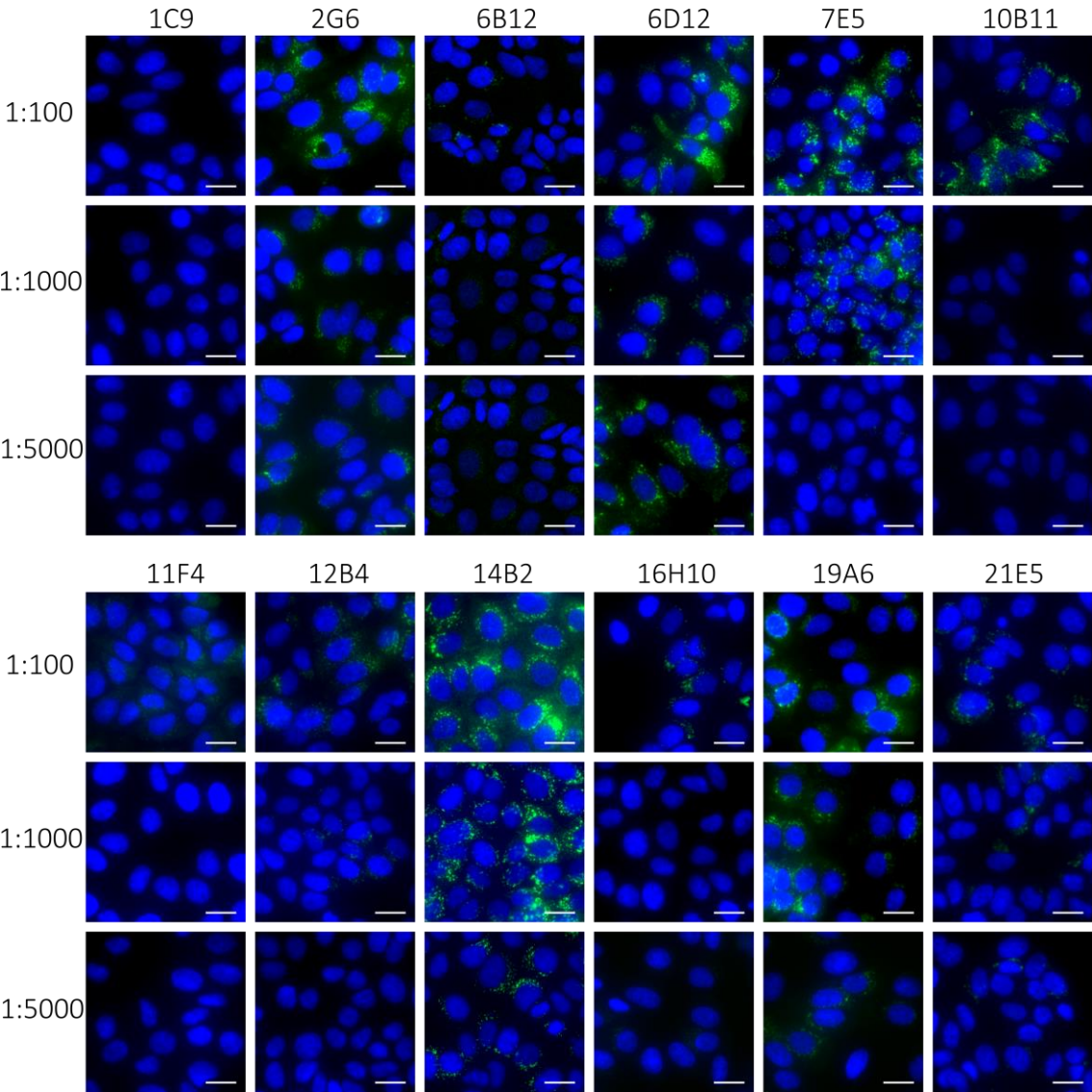


Figure 13: Concentration-dependent test of purified IGFR-L1 antibodies
The ideal dilution of purified antibodies was determined in the human cell line MCF7 (scale bar: 20 μ m).

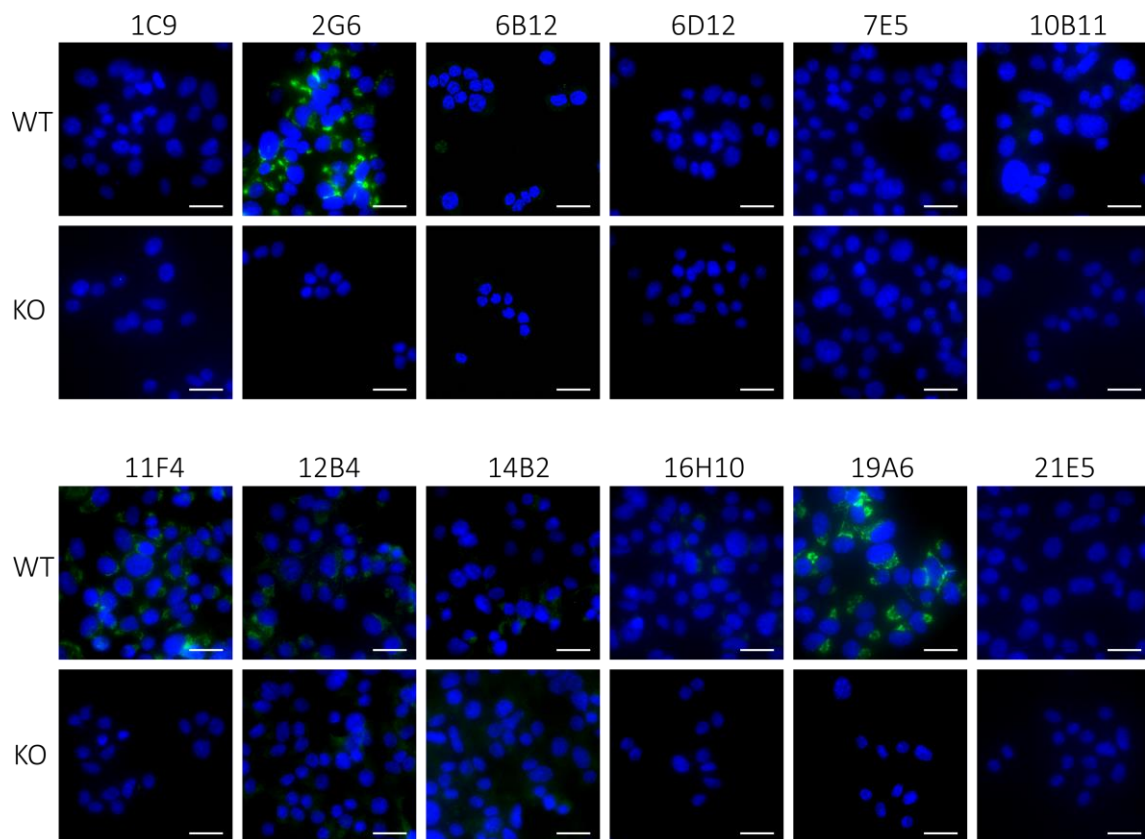


Figure 14: Test of purified IGFR-L1 antibodies in the mouse cell line Min6

The purified antibodies were validated in Min6 cells using a 1:1000 dilution (scale bar: 20 μ m).

2.1.1.5 Labelled antibodies are effective tools for live cell imaging

For use in live imaging and for potential *in vivo* experiments, the antibodies 6D12, 16H10 and 19A6 were labelled with Alexa Fluor 488, 555 and 647; 2G6 was labelled with Alexa Fluor 647. We tested the conjugated antibodies in MCF7 and Min6 cells by incubation with the antibodies in a 1:20 dilution at 37 °C for 1 hour (Figure 15). Interestingly, the AlexaFluor 488 and 647 labelled antibodies appeared to yield a stronger signal. In MCF7 cells, 2G6 was the strongest candidate, followed by 6D12 and 19A6. As 6D12 did not recognise mouse Igfr-L1 in earlier experiments, only the remaining three were tested in Min6, where 2G6 exhibited the strongest signal.

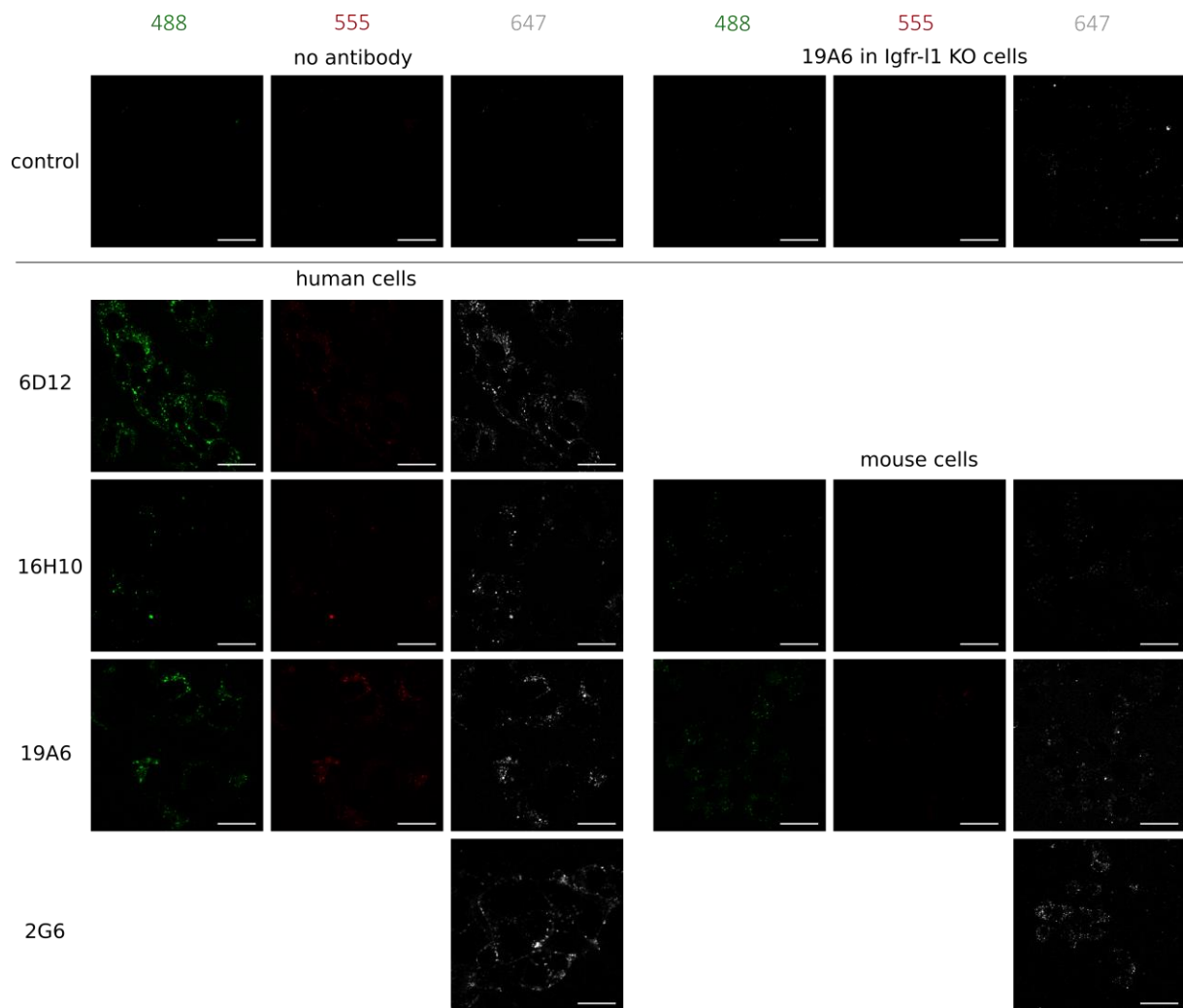


Figure 15: Test of labelled IGFR-L1 antibodies

Alexa Fluor 488, 555 or 647 labelled antibodies were tested in the human cell line MCF7 and in the mouse cell line Min6. The cells were incubated with the respective antibodies in a 1:20 dilution for 60 min at 37 °C and imaged in a live imaging chamber (scale bar: 20 µm).

2.1.2 Impact of IGFR-L1 Antibodies on Proliferation

Due to the domain structure of IGFR-L1 we hypothesised that it might have a role in insulin/IGF1 signalling. As both insulin and IGF1 can be potent growth factors, we analysed whether the proliferation rate of mouse insulinoma (Min6) cells are affected upon incubation with IGFR-L1 antibodies (Figure 16). Specifically, Min6 cells were incubated with the antibody 2G6 in different concentrations and proliferation was measured as EdU incorporation. Although there were slight variations in proliferation, these changes were not significant.

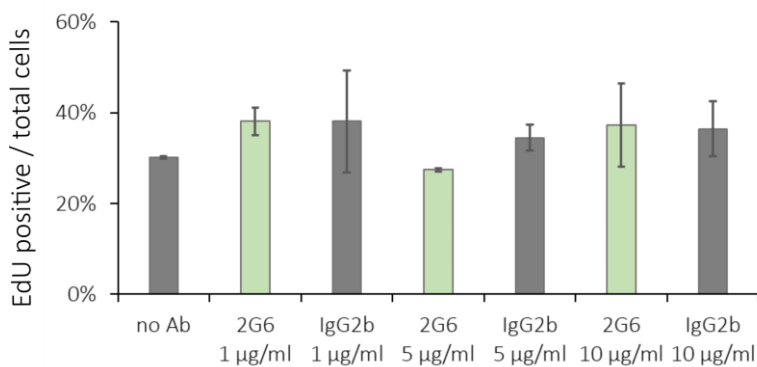


Figure 16: Proliferation assay in Min6 cells with IGFR-L1 Abs.

Min6 cells were incubated with the IGFR-L1 antibody 2G6 in different concentrations for 24 h, compared to the isotype (IgG2b) control antibody. EdU was added for 4 h, followed by EdU staining, imaging and automated counting (>300 cells/n in each condition, n=3).

In many cancer types, insulin/IGF1 signalling is important for growth and differentiation. Thus, we tested if IGFR-L1 antibodies can regulate the proliferation of the breast cancer cell line MCF7 (Figure 17). There was, however, no change in any of the tested conditions.

Next, we tested the effect of IGFR-L1 antibodies on the prostate cancer cell line LNCaP (Figure 18). However, we found that the proliferation of LNCaP cells is highly dependent on subtle changes in seeding density, and that they easily detach during washing steps. Thus, it was necessary to normalise the proliferation rate of each experiment on the respective control containing no antibody. Incubation with the antibody 19A6 led to a slight but insignificant increase in proliferation. Strikingly, incubation with 2G6 substantially decreased the

proliferation. This result suggests that IGFR-L1 antibodies might be able to reduce prostate cancer growth.

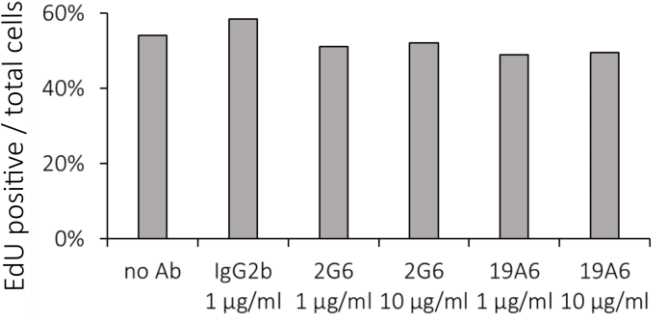


Figure 17: Proliferation assay in MCF7 cells with IGFR-L1 Abs.

MCF7 cells were incubated with the IGFR-L1 antibodies 2G6 or 19A6 for 24 h, compared to the isotype (IgG2b) control antibody. EdU was added for 4 h, followed by EdU staining, imaging and automated counting (n=1).

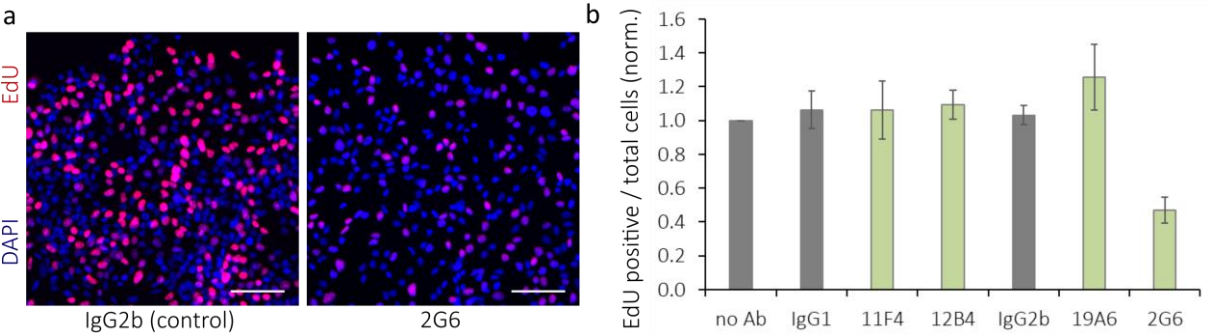


Figure 18: Proliferation assay in LNCaP cells with IGFR-L1 Abs.

LNCaP cells were incubated with the IGFR-L1 antibodies 11F4, 12B4, 19A6, 2G6 or their respective isotype controls at 10 µg/ml concentration for 24 h. EdU was added for 6 h. As an example, the EdU staining of 2G6-treated cells is shown (scale bar: 100 µm) (a). The EdU- and DAPI-positive cells were automatically counted and the ratio was normalised to the control without antibody (n=2, >300 cells/n per condition) (b).

2.2 Endocytosis and Intracellular Trafficking of IGFR-L1 in β -cells

2.2.1 Tool Generation

2.2.1.1 Interdomain-tagged IR fusion proteins are functional in Min6 cells

To observe the intracellular trafficking of the insulin receptor (IR) using time lapse imaging, we used expression constructs for IR-A and IR-B, which had a blue, green or red fluorescent protein (eBFP, eGFP or RFP) inserted between the transmembrane region and the ectodomain [40]. To test if these interdomain-tagged constructs are functional, Min6 cells were transfected with the constructs and imaged after 3 days. The eGFP- and RFP-tagged constructs were clearly visible (Figure 19a). In contrast, there was only autofluorescence observed in the cells transfected with eBFP-tagged constructs. The IR-A-RFP and IR-B-RFP constructs generated the strongest signal. The IR is expressed as a 210 kDa proreceptor, which is then cleaved into the α and β subunit in the endoplasmic reticulum [168]. To assess if these fusion proteins were correctly expressed and processed, Min6 cells transfected with IR-A-RFP or IR-B-RFP were lysed and analysed via Western blotting (Figure 19c). It was clearly visible that only a small fraction of RFP-tagged IR was processed compared to endogenous IR, as observed in the wild-type (WT) sample. This suggests that the processing and function of the interdomain-tagged IR fusion proteins might not be identical to endogenous IR. However, it was shown that the subcellular localisation of these IR fusion proteins mirrored endogenous IR [40], indicating that they are valid tools to study receptor trafficking.

2.2.1.2 IGFR-L1 is successfully fused to Venus

After successfully cloning the fluorescent protein Venus to the C-terminus of IGFR-L1 to generate a fusion construct (Figure 20a), Min6 cells were transiently transfected with this plasmid and imaged on a confocal microscope (Figure 20b). The transfected cells were subsequently stained with an IGFR-L1 antibody and a GFP antibody detecting the Venus tag (Figure 20c). As expected, some cells were only stained with the IGFR-L1 antibody; these were

presumably untransfected cells. Transfected cells were stained with both antibodies with almost complete overlap.

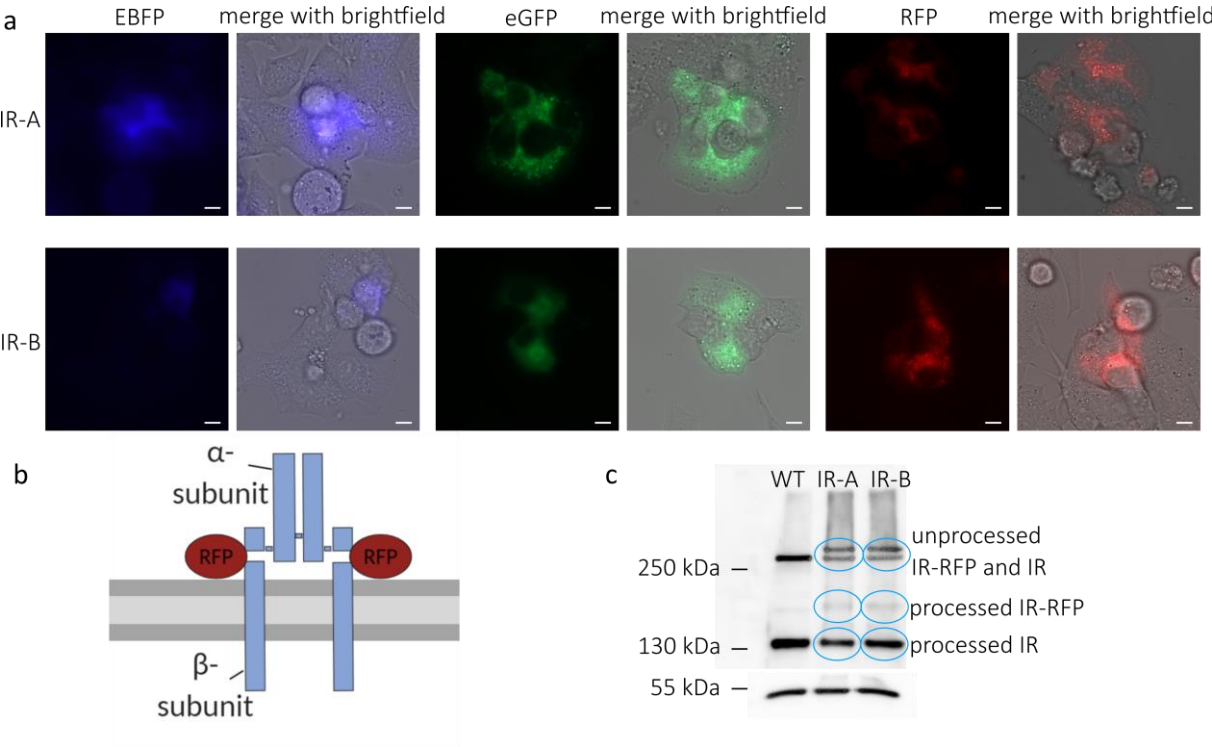


Figure 19: Validation of tagged IR constructs
 Min6 cells were transfected with the interdomain-tagged IR constructs and imaged after 3 days (scale bar: 20 μ m) (a). Schematic representation of the interdomain-tagged constructs, adapted from [40] (b). Western blot analysis of Min6 cells transfected with IR-A-RFP and IR-B-RFP shows processed and unprocessed IR (c).

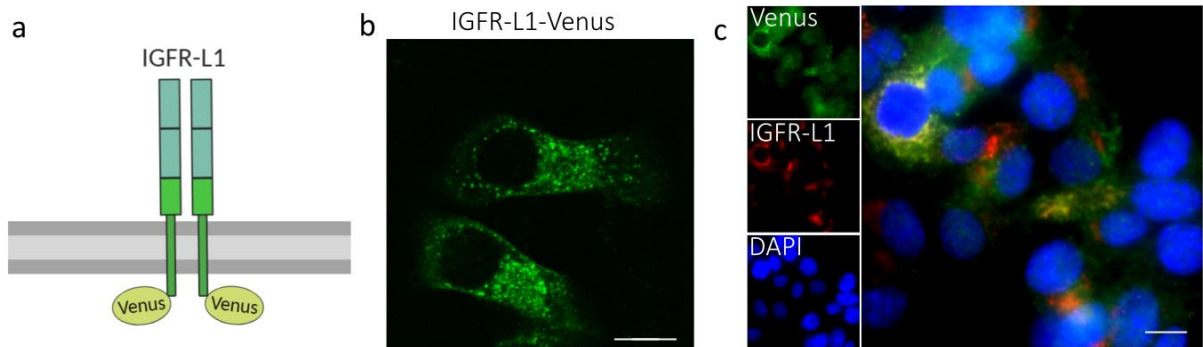


Figure 20: Initial validation of IGFR-L1-Venus
 Schematic representation of IGFR-L1-Venus (a). Min6 cells were transiently transfected with the expression plasmid pCAG-IGFR-L1-Venus and imaged directly on a confocal microscope after 2 days (b) or stained with an antibody against GFP (recognising Venus) and IGFR-L1 (scale bar: 10 μ m) (c).

2.2.1.3 IGFR-L1-Venus can be used for generation of a stable cell line

As the transfection efficiency in Min6 cells is generally low and experiments on transfected cells are therefore difficult, a stable cell line was generated by random integration of the plasmid pCAG-IGFR-L1-Venus. To this end, Min6 cells were transfected and subsequently selected with the antibiotic puromycin, as the plasmid contained a puromycin resistance gene expressed from the same promoter as IGFR-L1-Venus. Since not all resistant cells showed expression of the fusion construct, the resulting cell pool was sorted via FACS (Fluorescence-activated cell sorting), distinguishing cells with low, medium and high expression levels (Figure 21a). The difference between the three resulting cell lines was visualised via confocal microscopy (Figure 21b) and Western blot analysis (Figure 21c).

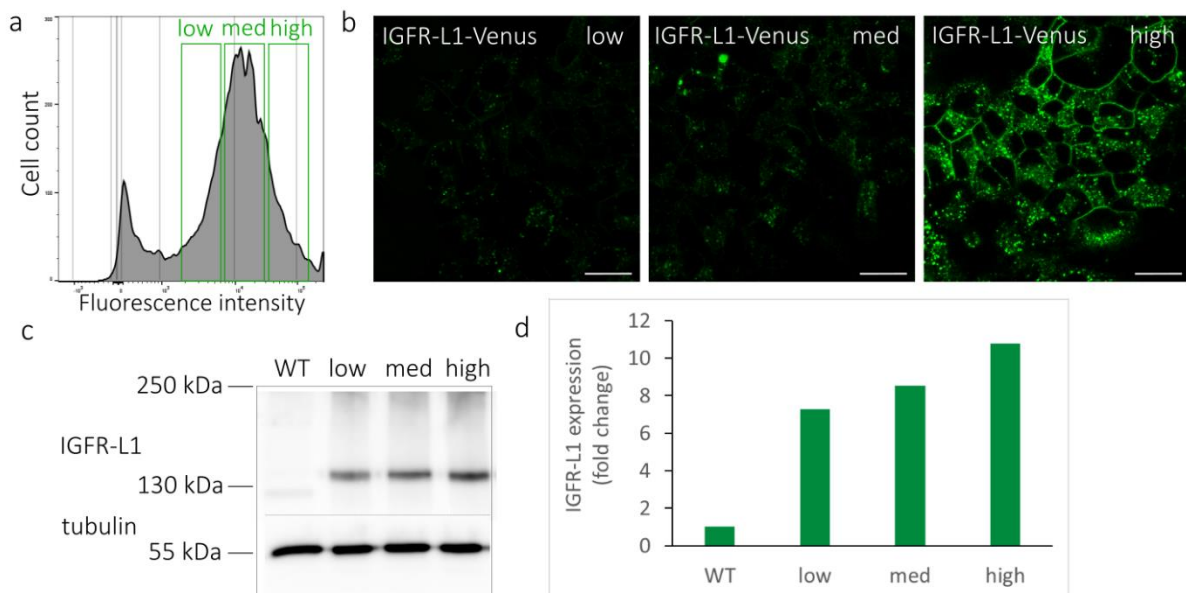


Figure 21: Generation of stable cell line Min6 IGFR-L1-Venus

After transfection of Min6 cells with IGFR-L1-Venus and selection with puromycin, the cells were sorted based on low, medium and high expression levels of IGFR-L1-Venus via FACS, the gates were set as indicated (a). For validation, the cells were subsequently imaged with constant settings (scale bar: 20 μ m) (b) and the IGFR-L1 levels were quantified via Western blot (c, d). The same procedure was performed in *Igfr-1* KO Min6 cells.

Importantly, the quantification of the Western blot bands (Figure 21d) showed that even in the cells with low IGFR-L1-Venus expression, the IGFR-L1-Venus levels were seven times higher than the endogenous IGFR-L1 levels in WT Min6. The localisation of IGFR-L1-Venus appeared to be different in cells with high expression levels, in particular the fluorescent signal

on the plasma membrane was more visible (Figure 21b). To minimise any adverse effects resulting from constant overexpression, the cells with low IGFR-L1-Venus levels were used for subsequent experiments, unless indicated otherwise.

2.2.2 Analysing the Trafficking Dynamics of IGFR-L1 in Live Cells

2.2.2.1 Subcellular localisation of IGFR-L1-Venus resembles IGFR-L1

The subcellular localisation of IGFR-L1 was previously analysed by Felizitas G.v. Hahn [169]. To confirm that IGFR-L1-Venus is a valid tool to analyse the trafficking behaviour of IGFR-L1, the stable cell line Min6 IGFR-L1-Venus was stained with the organelle markers EEA1 (early endosome antigen 1), Giantin, GM130 (Golgi matrix protein 130) and LAMP1 (lysosomal-associated membrane protein 1) antibodies. The Mander's Overlap Coefficient (MOC) and the Pearson's R value with IGFR-L1-Venus was calculated for each protein (Figure 22, Table 2). Similar to endogenous IGFR-L1 [170], IGFR-L1-Venus shows very high overlap with the medial-Golgi marker Giantin, the lysosome marker LAMP1 and the early endosome marker EEA1; followed by the cis-Golgi marker GM130 (Table 2). It should be noted that different LAMP1 antibodies were used for the analysis of IGFR-L1-Venus compared to endogenous IGFR-L1, thus these values were not comparable. Taken together, the localisation of IGFR-L1-Venus mirrors endogenous IGFR-L1.

Table 2: Colocalisation of endogenous IGFR-L1 or IGFR-L1-Venus with organelle markers

	Pearson's R value		MOC	
	IGFR-L1	IGFR-L1-Venus	IGFR-L1	IGFR-L1-Venus
EEA1	0.27	0.39	0.86	0.85
Giantin	0.79	0.76	0.95	0.91
GM130	0.71	0.67	0.78	0.80

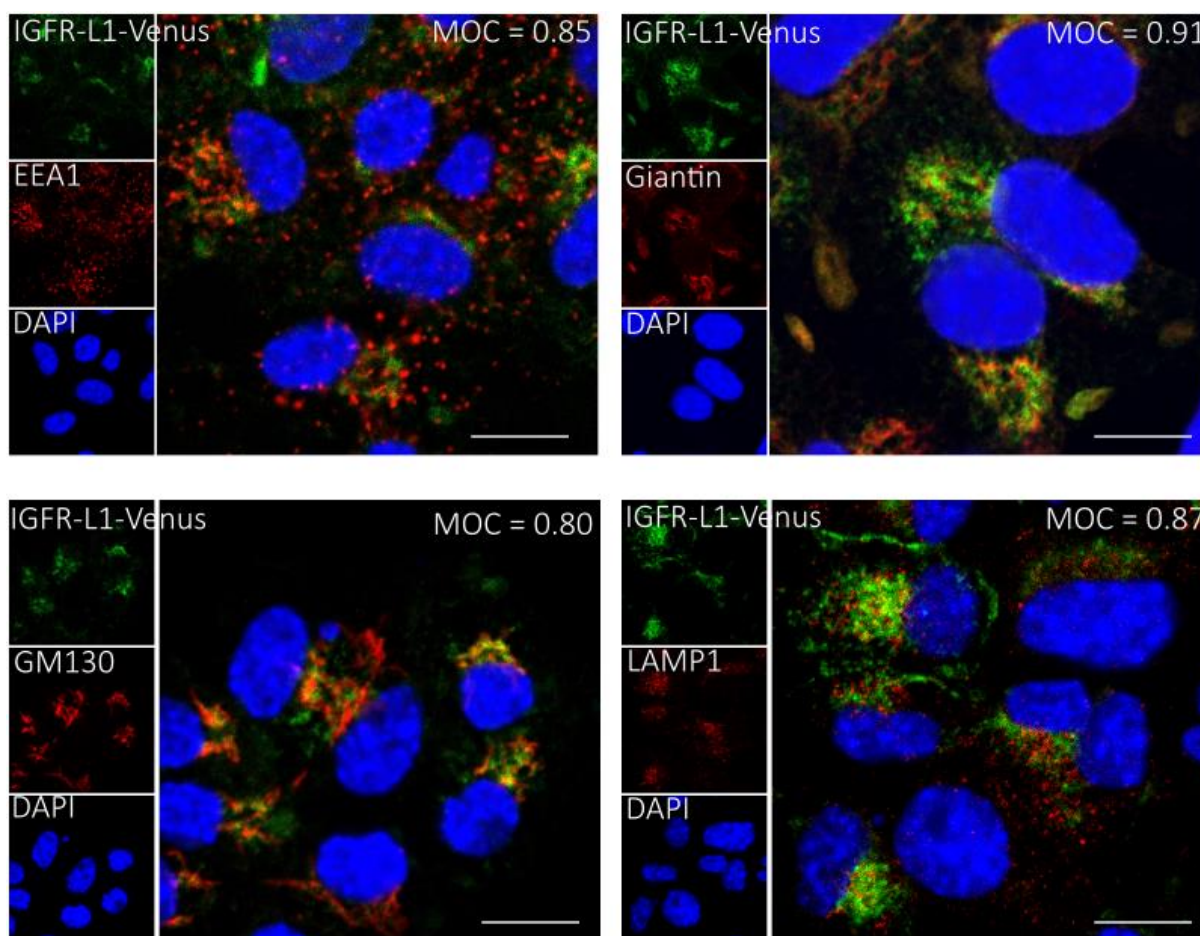


Figure 22: Staining of Min6 IGFR-L1-Venus with organelle markers

The stable cell line Min6 IGFR-L1-Venus was counterstained with EEA1, Giantin, GM130 and LAMP1 to analyse the subcellular localisation. As a measure for colocalisation, the MOC was calculated in >100 cells/n (n=3; scale bar: 10 μ m).

To analyse the trafficking of IGFR-L1-Venus in live cells, Min6 cells were co-transfected with IGFR-L1-Venus and a plasmid encoding a palmitoylation sequence, which specifically localised to the cytoplasmic membrane (Figure 23). Similarly, they were transfected with a marker plasmid for Golgi stacks or lysosomes (LAMP1). There was substantial overlap with all markers, indicating that IGFR-L1-Venus is cycling between the plasma membrane, the Golgi complex and the endosomal-lysosomal system. It should be noted that overexpression of two proteins can lead to artificial interaction; thus, the degree of colocalisation might be exaggerated. In addition, there was very high overlap between IGFR-L1 and Phogrin, which has an important role in insulin secretion. This suggests that IGFR-L1 might be involved in the secretory process.

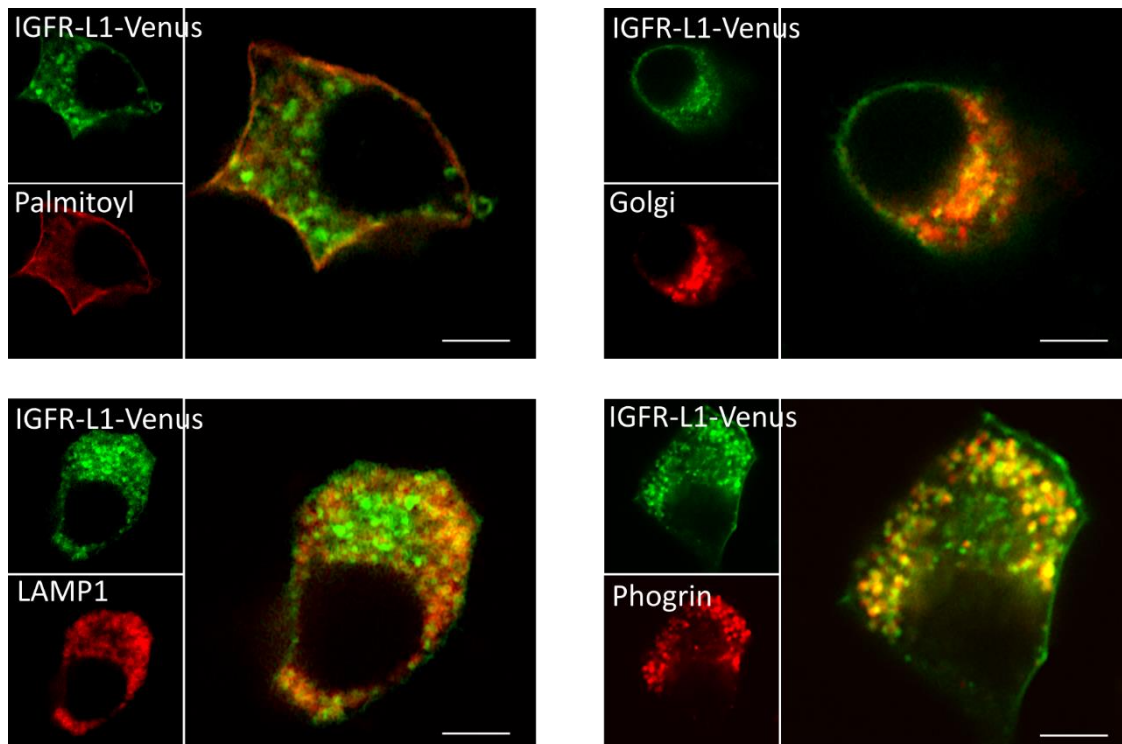


Figure 23: Transfection of Min6 cells with organelle marker plasmids

Min6 cells were co-transfected with pCAG-IGFR-L1-Venus and the plasmids pPalmitoyl-m-Turquoise2, pmTurquoise2-Golgi, pLAMP1-mCherry or Phogrin-mCherry. Images are representative for > 10 live cells/n (n=2; scale bar: 10 μ m).

2.2.2.2 IGFR-L1 antibodies are efficiently internalised

To study the cellular uptake and retention of IGFR-L1 antibodies and to observe IGFR-L1 endocytosis in a time-resolved manner, Min6 IGFR-L1-Venus cells were incubated with the fluorescently labelled antibody 19A6 (Figure 24). After 10 minutes, the antibody was clearly visible on the plasma membrane, while few intracellular dots were already observed, indicating that the antibody was at least partially internalised. After 60 minutes, most of the IGFR-L1-Venus containing vesicles were stained by the antibody, suggesting that the main pool of IGFR-L1-Venus had been saturated. The cells were imaged again after 1 day, showing most of the vesicles still positive for the antibody. After 3 days, some cells lacked any antibody signal, but presumably these were newly divided cells.

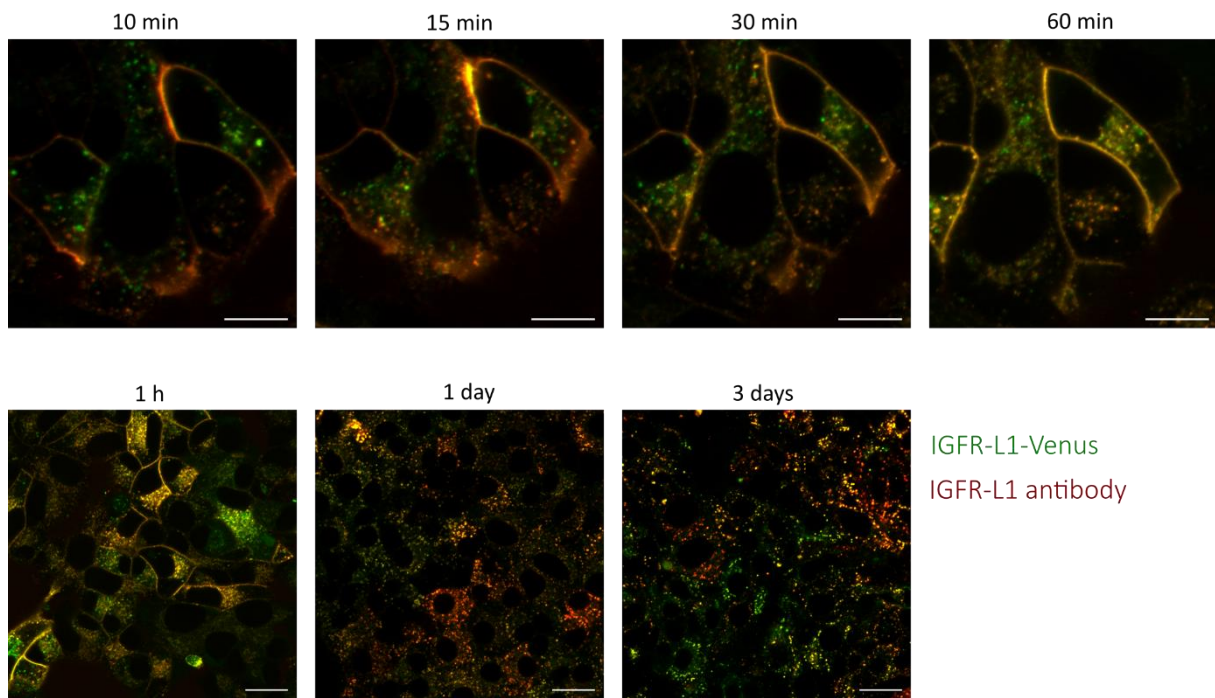


Figure 24: Internalisation time course of IGFR-L1 Ab

The Alexa Fluor 555 labelled antibody 19A6 was tested on Min6 IGFR-L1-Venus cells by incubation with 200 $\mu\text{g/ml}$ antibody in Min6 medium for 1 h. The cells were washed and subsequently cultured for 3 days. Images are representative of >20 cells per time point (scale bar: 10 μm).

The uptake dynamics of the IGFR-L1 antibody 2G6 were quantitatively assessed by incubating Min6 cells with the labelled antibody and measuring the fluorescence intensity after defined time points (Figure 25). The fluorescence intensity increased gradually during incubation with the Alexa Fluor 647-labelled antibody 2G6. Similar dynamics were observed for the antibody 19A6 (not shown), while the IgG2b isotype control showed no signal. Thus, the uptake of IGFR-L1 antibodies into Min6 cells was specific.

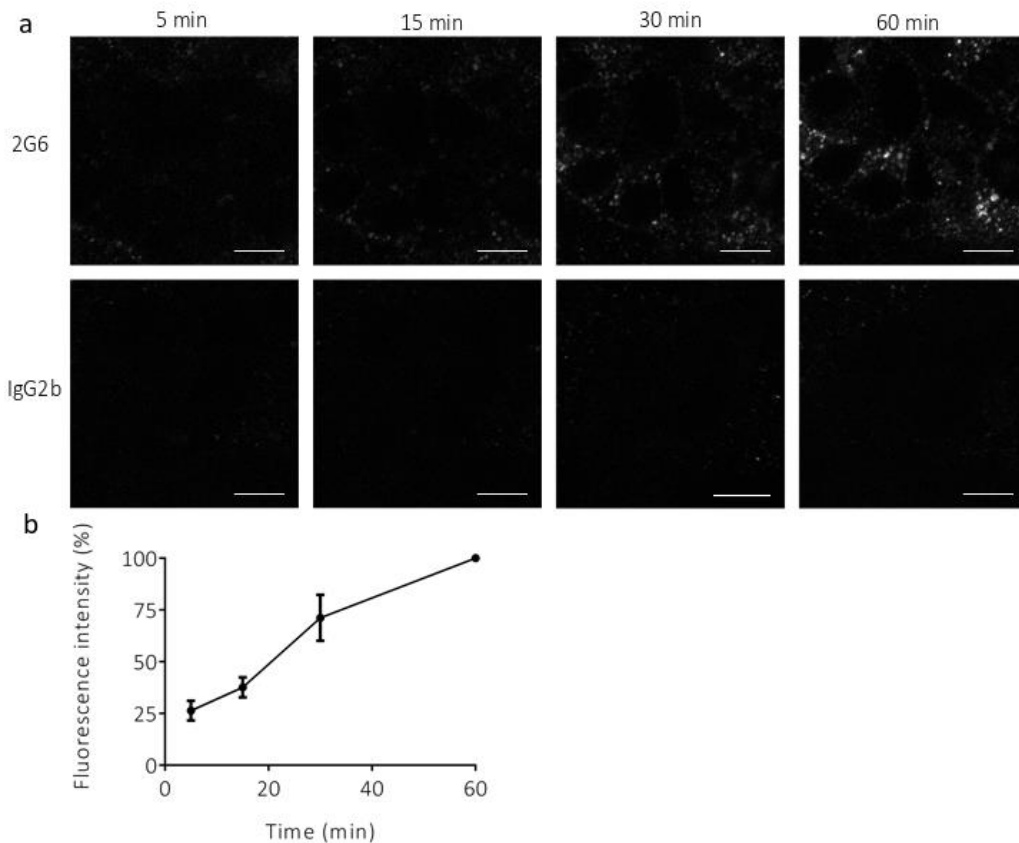


Figure 25: Quantification of IGFR-L1 Ab internalisation

Min6 IGFR-L1-Venus cells were incubated with 10 $\mu\text{g}/\text{ml}$ of the Alexa Fluor 647-labelled IGFR-L1 antibody 2G6, compared to the labelled IgG2b isotype control (a). The fluorescence intensity of 2G6 at each time point was quantified and normalised for each individual experiment (>25 cells/n per time point, n=3; scale bar: 10 μm) (b).

2.2.2.3 IGFR-L1-Venus is enriched in the Golgi complex under starvation

Insulin/IGF1 signalling is significantly affected by changes in environment, such as starvation. These changes can affect intracellular processes, such as recruitment of IR to the plasma membrane. To determine the behaviour of IGFR-L1 under starvation conditions, Min6 IGFR-L1-Venus cells were incubated for two hours with HBSS (Hank's balanced salt solution) and imaged at multiple timepoints (Figure 26a). During starvation, the signal increased in intracellular structures that resemble Golgi cisternae. In addition to static images, time-lapse movies with an interval of two seconds were taken to observe the trafficking dynamics. However, no significant changes in vesicle movement were visible after starvation (data not shown). To further investigate how the distribution of IGFR-L1 across the organelles was altered, the cells were counterstained with the Golgi marker giantin and the early endosome

marker EEA1 after defined time points. The overlap coefficient with IGFR-L1-Venus was calculated for both markers after different time points (Figure 26b,c).

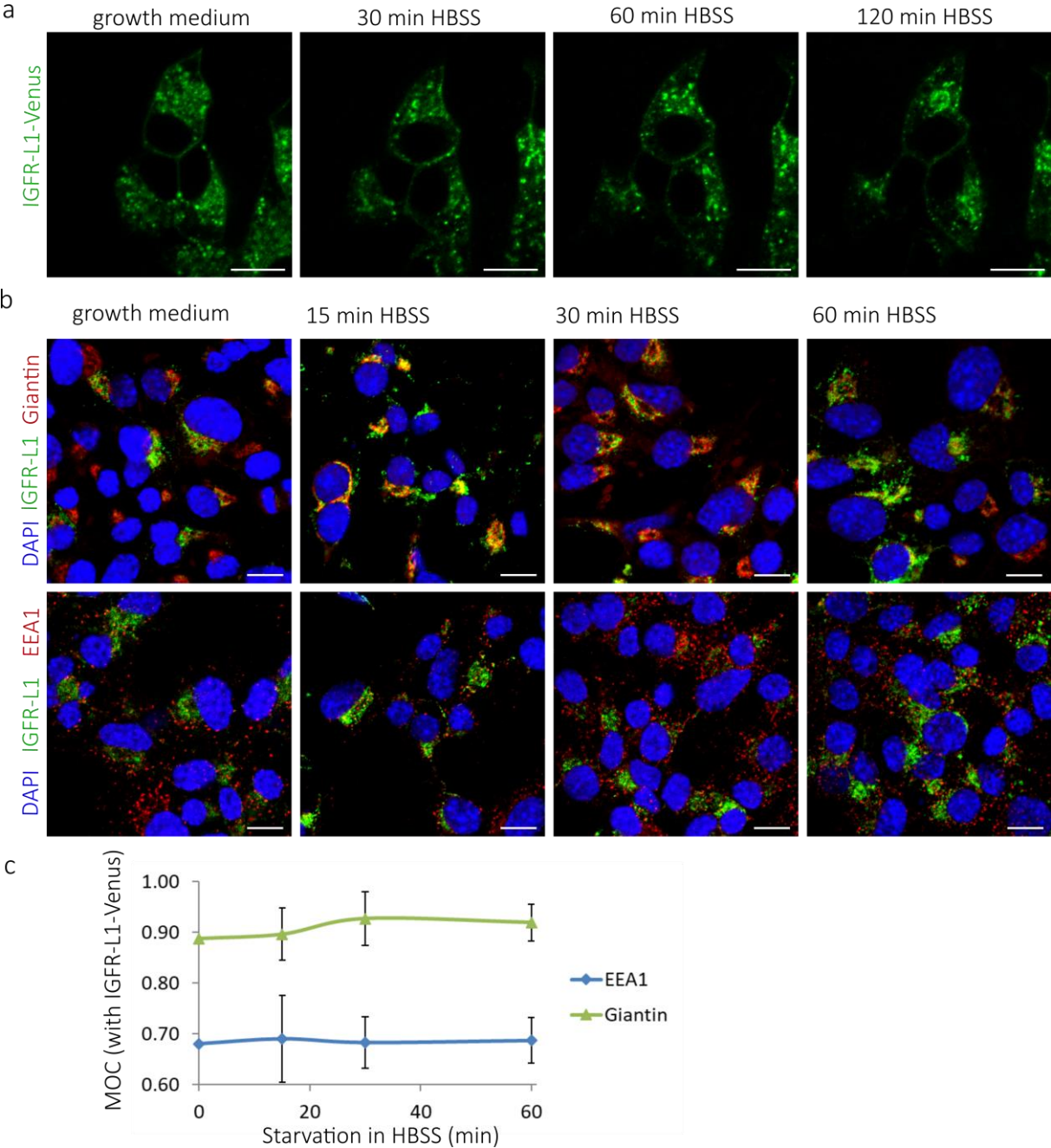


Figure 26: Starvation of Min6 IGFR-L1-Venus

Min6 IGFR-L1-Venus cells were starved in HBSS and observed live (>20 cells/n, n=6) (a), or fixated and counterstained with Giantin or EEA1 (scale bar: 10 μm) (b). As a measure for colocalisation, the MOC of IGFR-L1 and Giantin or EEA1 was calculated from >50 cells/n (n=2) (c).

Compared to normal Min6 growth medium, the overlap with giantin increased slightly in starvation conditions. This indicates that more IGFR-L1-Venus was localised in the Golgi stacks compared to normal growth conditions, although the effect was not significant. The overlap

of IGFR-L1-Venus with EEA1 did not change during the starvation. To confirm that the intracellular pool of IGFR-L1-Venus is moved towards the Golgi complex during starvation, pulse-chase experiments would be necessary in the future.

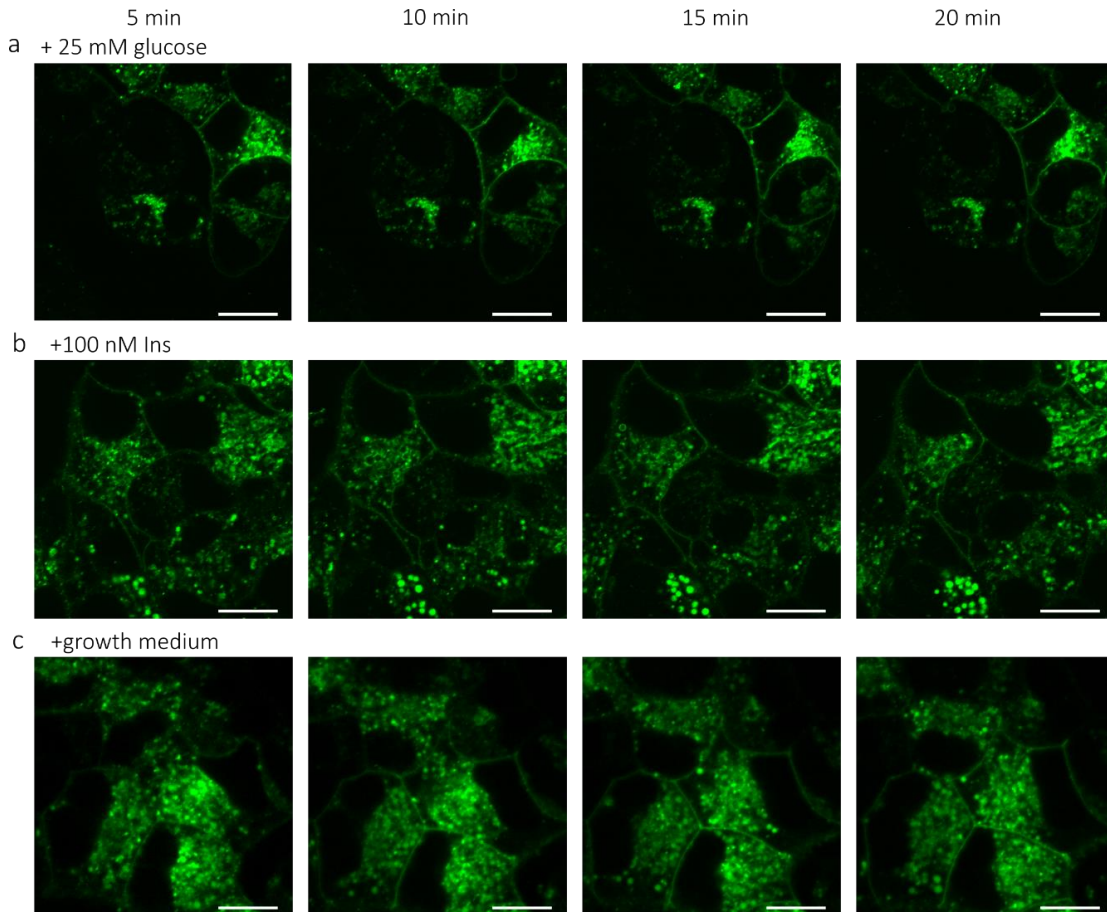


Figure 27: Stimulation of starved Min6 IGFR-L1-Venus

Min6 IGFR-L1-Venus were starved in HBSS for 2 hours and subsequently observed during treatment with 25 mM glucose in HBSS (a), 100 nM insulin in HBSS (b) or normal Min6 growth medium (c). The images are representative for >50 cells per condition (scale bar: 10 μ m).

As IGFR-L1 shares sequence similarities with IR, we hypothesised that IGFR-L1 might be involved in the intracellular trafficking of insulin and/or IR. If this is the case, the changes in IGFR-L1-Venus localisation observed during starvation might be due to decreased insulin or glucose concentration. Thus, Min6 IGFR-L1-Venus cells were starved for two hours in HBSS before being treated with glucose or insulin (Figure 27a,b). However, no significant changes were observed after the treatment. After addition of normal growth medium, the distribution of IGFR-L1-Venus was more vesicular again, closely resembling the original pattern

(Figure 27c). This observation shows that the changes introduced by starvation are reversible. It is possible that these changes were either introduced by the lack of a different factor other than glucose or insulin, or by several factors synergistically.

2.2.3 Influence of IGFR-L1 on IR Trafficking

2.2.3.1 IR-RFP shows the same localisation in Igfr-L1 knockout cells

As we speculated that IGFR-L1 might influence the trafficking of IR, we transfected WT and Igfr-L1 KO Min6 cells with the IR-A-RFP and IR-B-RFP constructs (Figure 28). The localisation pattern of IR-A-RFP and IR-B-RFP showed no differences between WT and KO. In addition to static images, time-lapse movies with an interval of 2 seconds were taken to monitor the trafficking dynamics, but again no difference was visible (data not shown).

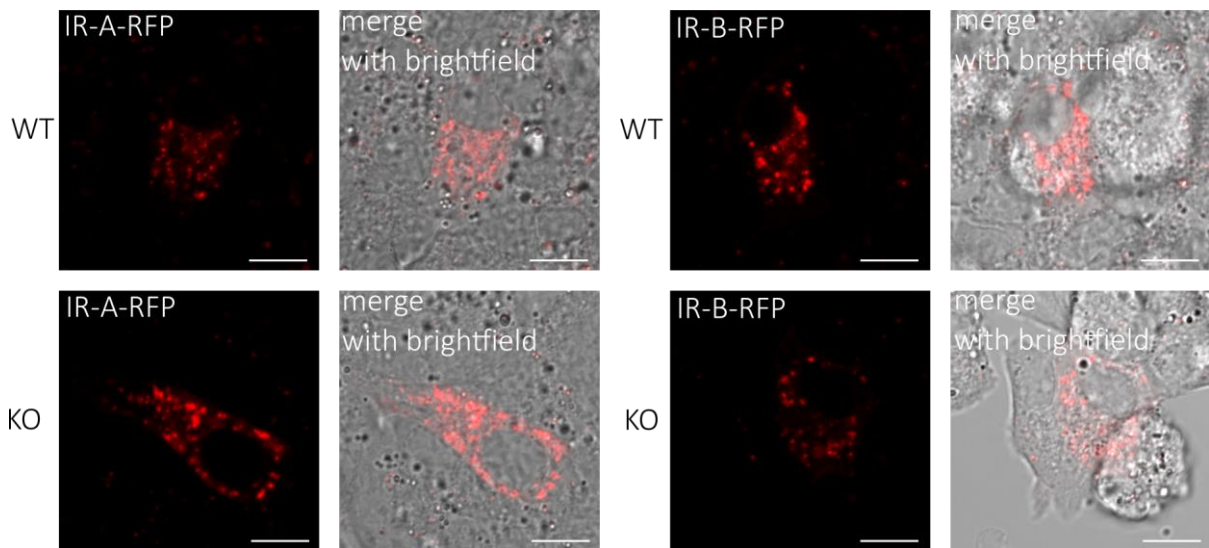


Figure 28: IR-RFP in Min6 WT vs. KO

WT and Igfr-L1 KO Min6 were transfected with the IR-A-RFP or IR-B-RFP constructs and imaged after 2 days. Images are representative for at least 12 cells per condition (scale bar: 10 μ m).

2.2.3.2 IGFR-L1-Venus and IR-RFP colocalise in vesicles and on the plasma membrane

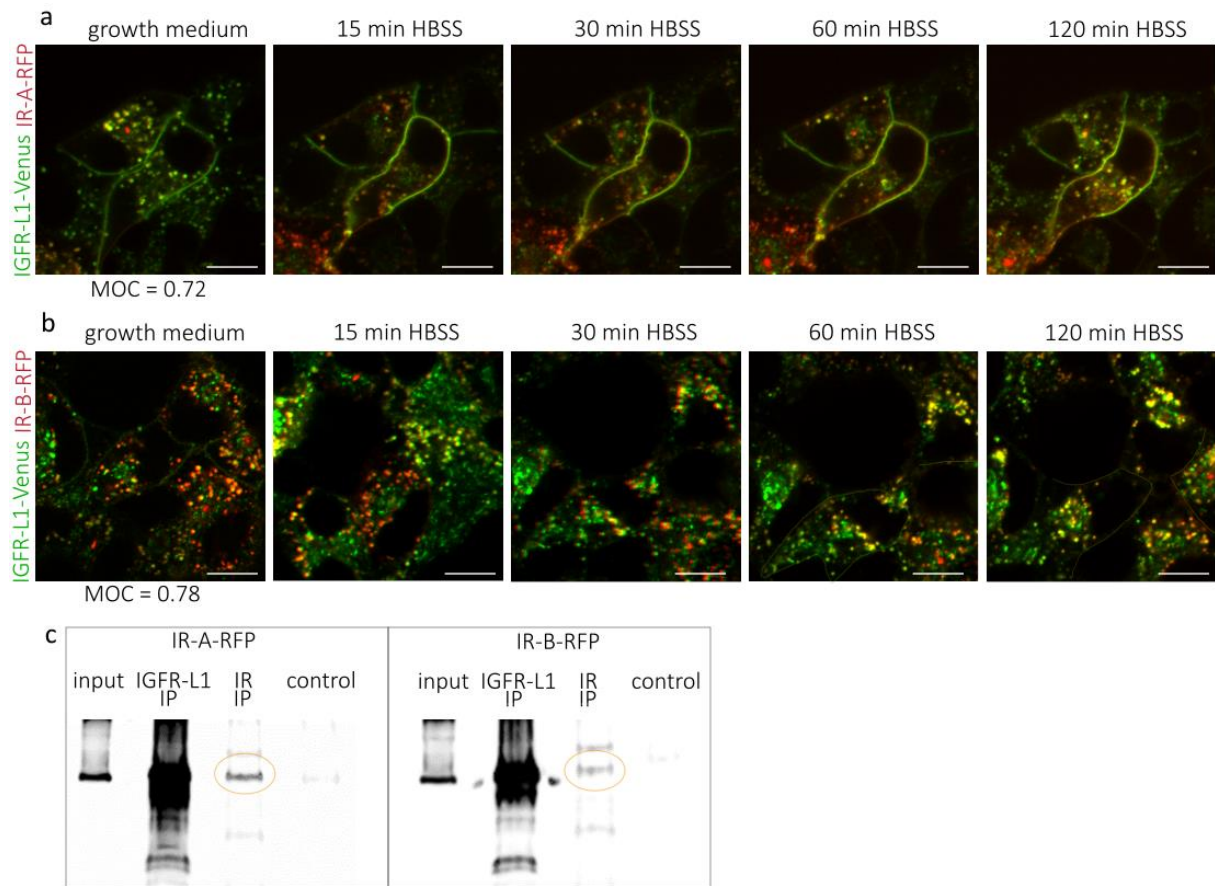


Figure 29: Potential interaction of IGFR-L1-Venus and IR-RFP

The stable cell lines Min6 IGFR-L1-Venus + IR-A-RFP (a) and IGFR-L1-Venus + IR-B-RFP (b) were imaged during starvation in HBSS (scale bar: 10 μ m). In Min6 growth medium, the MOC was calculated including >30 cells/n (n=2). For the Co-IP, both cell lines were lysed and the lysates were incubated with IGFR-L1 or IR-antibody conjugated magnetic beads (IGFR-L1 IP, IR IP) or beads only (control). The bands were detected with an IGFR-L1 antibody (n=3) (c).

As starvation in HBSS caused minor changes in the localisation of IGFR-L1-Venus (see 2.2.2.3 IGFR-L1-Venus is enriched in the Golgi complex under starvation), the procedure was repeated in stable Min6 cell lines simultaneously expressing IGFR-L1-Venus and IR-A-RFP or IR-B-RFP (Figure 29a,b). In normal growth conditions, it appeared there was more colocalisation between IGFR-L1-Venus and IR-B-RFP compared to IR-A-RFP. The overlap was therefore quantified by calculating the MOC; however, the difference was not significant.

To further analyse the interactions, co-immunoprecipitation (co-IP) was performed in both stable cell lines (Figure 29c). Although we successfully pulled down IGFR-L1 with an IR antibody

in both cell lines, the efficiencies varied between the individual experiments. Further, unspecific bands in the control samples were occasionally observed. Thus, a quantitative assessment of the pull-down efficiencies in each cell line was not possible. Nonetheless, this shows that IGFR-L1-Venus physically interacts with IR-RFP.

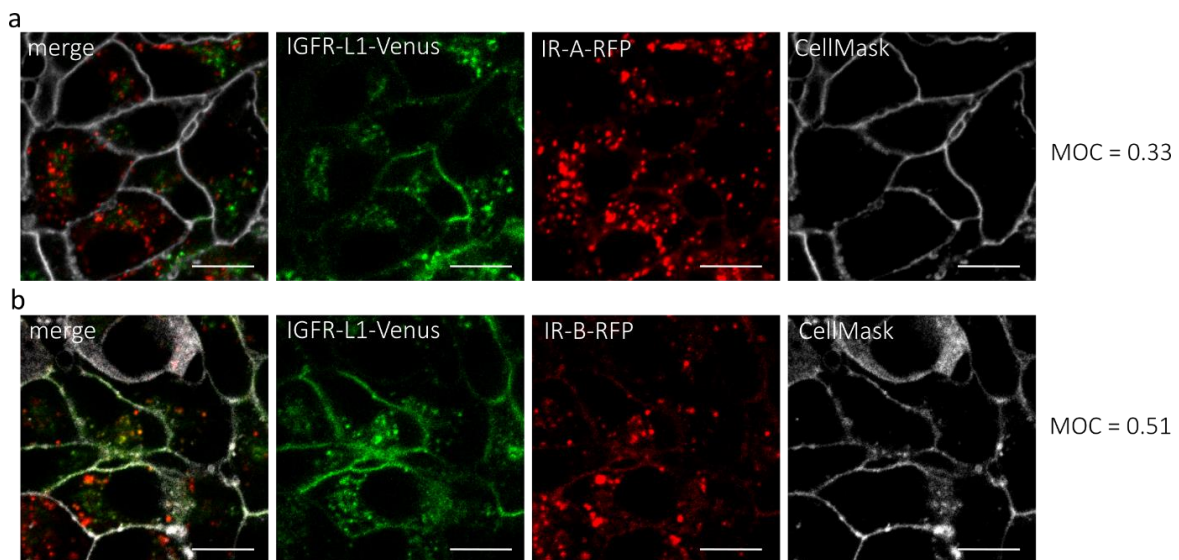


Figure 30: Colocalisation of IGFR-L1-Venus and IR-RFP on the plasma membrane

The stable cell lines IGFR-L1-Venus + IR-A-RFP (a) and IGFR-L1-Venus + IR-B-RFP (b) were starved for 1 hour in HBSS and counterstained with CellMask (scale bar: 10 μ m). The MOC in the membrane region was calculated by using CellMask to create a mask for colocalisation analysis of IGFR-L1-Venus vs. IR-RFP. >80 cells/n were quantified (n=3; p=0.011).

Interestingly, the constructs accumulated at the plasma membrane during the course of starvation and the overlap of IGFR-L1-Venus with both IR-A-RFP and IR-B-RFP increased during the starvation (Figure 29a,b). To visualise the increased overlap on the plasma membrane, the stable cell lines were starved in HBSS for 1 hour and counterstained with CellMask (Figure 30). To quantify the proximity between the receptors, the overlap between IGFR-L1-Venus and IR-A-RFP or IR-B-RFP was calculated specifically within the membrane region. The overlap between IGFR-L1-Venus and IR-B-RFP was significantly higher compared to IGFR-L1-Venus and IR-A-RFP. This finding suggests that IGFR-L1-Venus might have more interaction with IR-B-RFP at the plasma membrane. Remarkably, IR-A differs in only 12 amino acids from IR-B, but tends to activate proliferative rather than metabolic pathways [29]. If there is indeed more interaction of IGFR-L1-Venus with IR-B-RFP, this would be a hint towards a rather metabolic function of IGFR-L1. Thus, these interactions should be further investigated.

2.2.3.3 Insulin / IGF1 signalling is altered in Min6 IGFR-L1-Venus

As we had evidence that deletion of *Igfr-L1* in mice significantly increases insulin/IGF1 signalling [170], we wanted to investigate the influence of IGFR-L1 overexpression in Min6 cells. To this end, the protein levels of IR, IGF1R and pIR/pIGF1R (Figure 31) were analysed in Min6 cells with different IGFR-L1 expression levels (see also Figure 21). Strikingly, overexpression resulted in higher IGF1R levels, while IR levels were slightly lower. Stimulation with IGF1 increased the phosphorylated form pIR/pIGF1R accordingly. This shows that overexpression of IGFR-L1 modulates the IGF1R levels, although the experiment should be repeated in the same cell lines to obtain robust results.

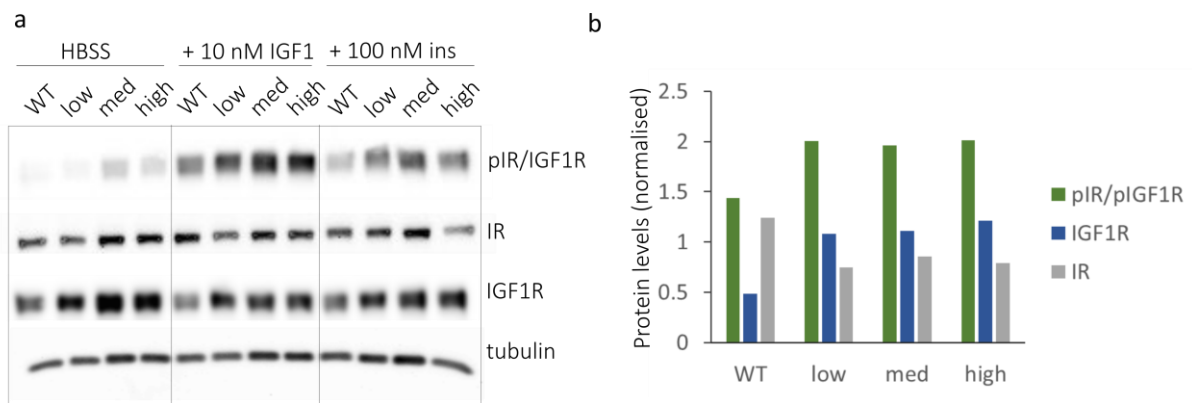


Figure 31: Insulin/IGF1 signalling in Min6 IGFR-L1-Venus

Western blot of proteins related to insulin/IGF1 signalling on Min6 IGFR-L1-Venus cells sorted according to expression levels in comparison to WT Min6 cells. The cells were starved in HBSS for 2 h and stimulated with 10 nM IGF1 or 100 nM insulin (a). The same procedure was applied for *Igfr-L1* KO Min6 cells with similar results (not shown). The protein levels in the samples stimulated with IGF1 were quantified and normalised on tubulin (b).

2.2.4 Clathrin-mediated Endocytosis of IGFR-L1

2.2.4.1 Mutant IGFR-L1-AP2*-Venus shows different localisation

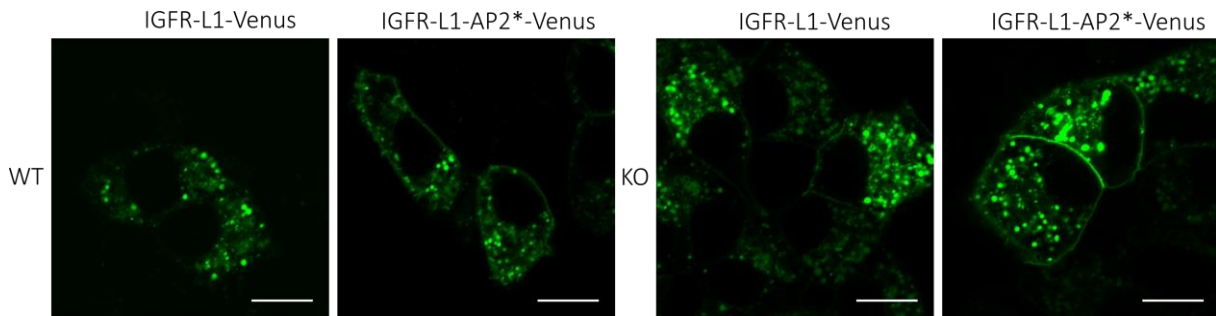


Figure 32: Initial test of Min6 IGFR-L1-AP2*-Venus

Min6 WT or Igfr-L1 KO cells were transfected with IGFR-L1-AP2*-Venus and imaged after 2 days (scale bar: 10 μ m).

The cytoplasmic tail of IGFR-L1 contains the AP2 binding motif YSKL, which strongly indicates internalisation by clathrin-mediated endocytosis. To confirm this hypothesis, we created the mutant construct pCAG-IGFR-L1-AP2*-Venus, where the amino acids tyrosine and leucine in the YSKL motif were replaced by alanine. To test this construct for functionality, WT and Igfr-L1 KO Min6 were transfected (Figure 32). In the WT cells, no significant difference was visible. This might be due to dimerisation of endogenous IGFR-L1 with IGFR-L1-AP2*-Venus. In the KO cells, the mutant construct appeared to be more localised at the plasma membrane.

2.2.4.2 The endocytosis of IGFR-L1-AP2*-Venus is disrupted

To confirm this observation, a stable cell line expressing IGFR-L1-AP2*-Venus was generated by transfecting the cell line Igfr-L1 KO Min6 with the construct pCAG-IGFR-L1-AP2*-Venus and selecting with puromycin, following the same procedure as for Min6 IGFR-L1-Venus (see Figure 21). The resulting cell line was counterstained with the membrane marker CellMask and the ratio of membrane-proximal signal to total signal was calculated (Figure 33a,b). We found that a higher fraction of IGFR-L1-AP2*-Venus resides on the plasma membrane

compared to IGFR-L1-Venus. This indicates that clathrin-mediated endocytosis of the mutant protein is impaired.

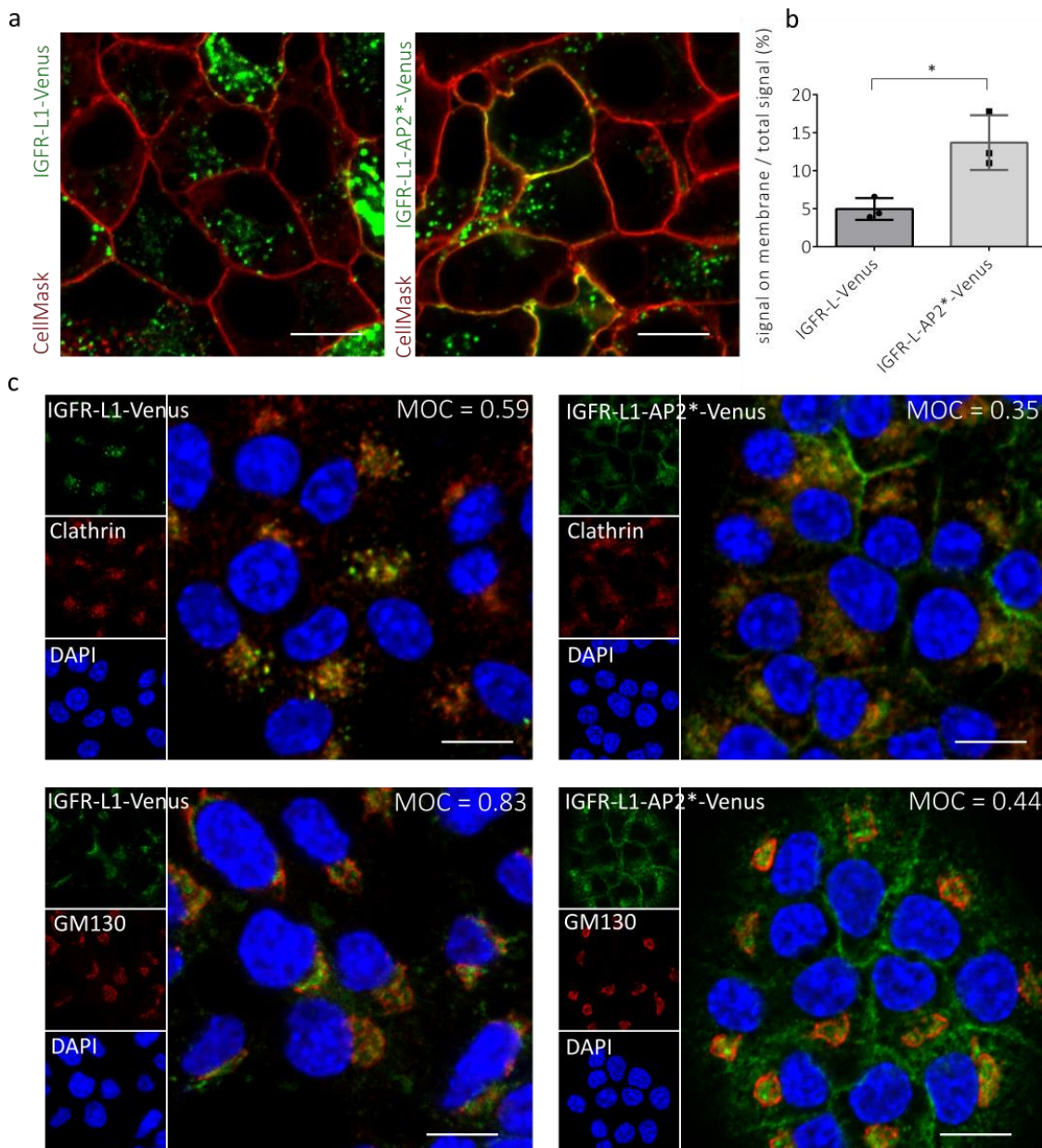


Figure 33: Subcellular localisation of IGFR-L1-AP2*-Venus

To analyse the ratio of normal or mutated IGFR-L1 on the cytoplasmic membrane, the stable cell lines Min6 IGFR-L1-Venus or Min6 IGFR-L1-AP2*-Venus were stained with CellMask, fixed and imaged immediately (a). For the quantification, >40 single cells/n were analysed using CellMask as a mask for colocalisation analysis and by drawing a ROI around the individual cell (n=3; p=0.018) (b). The fixed cell lines were counterstained with a Clathrin or GM130 antibody to show the colocalisation and quantified via the MOC (>80 cells/n, n=3; p=0.049 for clathrin and p=0.025 for GM130) (c). Scale bar: 10 μ m.

In addition, Min6 IGFR-L1-Venus and Min6 IGFR-L1-AP2*-Venus cells were stained with antibodies against clathrin or GM130 (Figure 33c). The colocalisation of clathrin with IGFR-L1-

Venus was high, but significantly lower with IGFR-L1-AP2*-Venus. This was expected, since AP2 binding is required for the uptake of target proteins into clathrin-coated vesicles. Likewise, the colocalisation of GM130 and IGFR-L1-AP2*-Venus was significantly lower compared to IGFR-L1-Venus. As clathrin is required for transport to and from the Golgi complex, this suggests that not only the endocytosis of IGFR-L1 is disrupted by the mutation, but also Golgi trafficking.

2.2.4.3 Endocytosis inhibitor dynasore blocks IGFR-L1 internalisation

To confirm that IGFR-L1 is internalised via clathrin-mediated endocytosis, Min6 IGFR-L1-Venus cells were incubated with the dynamin inhibitor dynasore, which blocks the formation of clathrin-coated vesicles. As expected, incubation with dynasore significantly increased the proportion of IGFR-L1-Venus on the plasma membrane (Figure 34).

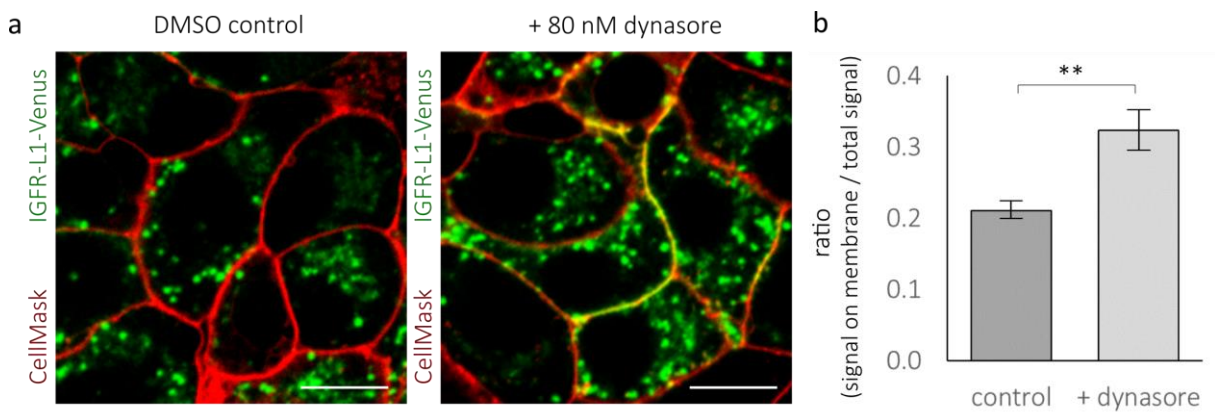


Figure 34: IGFR-L1 endocytosis inhibition

Min6 IGFR-L1-Venus cells were treated with 80 μ M dynasore in serum-free DMEM for 2 hours, compared to DMSO control (scale bar: 10 μ m) (a). The signal within the membrane region was quantified in >150 cells/n ($p=0.007$; $n=3$).

2.2.5 Insulin Uptake

2.2.5.1 Insulin uptake is delayed in Igfr-L1 KO cells

Due to the sequence similarities of IGFR-L1 with RTKs such as IR and EGFR, we speculated that IGFR-L1 might be involved in the uptake of insulin, either directly or indirectly via interaction with IR. To investigate this hypothesis, we incubated WT and Igfr-L1 KO Min6 with FITC-labelled insulin (Figure 35a). For reference, the cells were counterstained with CellMask. Initial observations suggested that in the KO Min6 cells more insulin remained in the membrane region after 15 minutes. To confirm this, the ratio of membrane-proximal signal to total signal was quantified (Figure 35b). Although there was slightly more signal in the membrane region of KO Min6, the variation was very high. Thus, the difference was not significant. Nonetheless, this suggests that insulin uptake might be delayed in KO Min6.

The endocytosis pathway of insulin in WT vs. KO cells was further investigated by incubation with labelled insulin for 15 minutes and subsequent co-staining with the early endosome marker EEA1 and the Golgi marker GM130 (Figure 35 c). In the KO cells, there was less overlap of insulin-FITC with both markers, which is consistent with reduced internalisation at early time points.

However, as there was no information available on the bioactivity of insulin-FITC, we tested the effect of incubation with insulin-FITC on Akt signalling (Figure 36). The pAkt signal appeared to increase slightly in immunostaining, although the background signal in the unstimulated condition was high, particularly in KO Min6. In Western blot, no significant increase in pAkt levels was observed after stimulation with insulin-FITC, while the induction using unlabelled insulin was as expected. Thus, the previous results should be confirmed using other reagents.

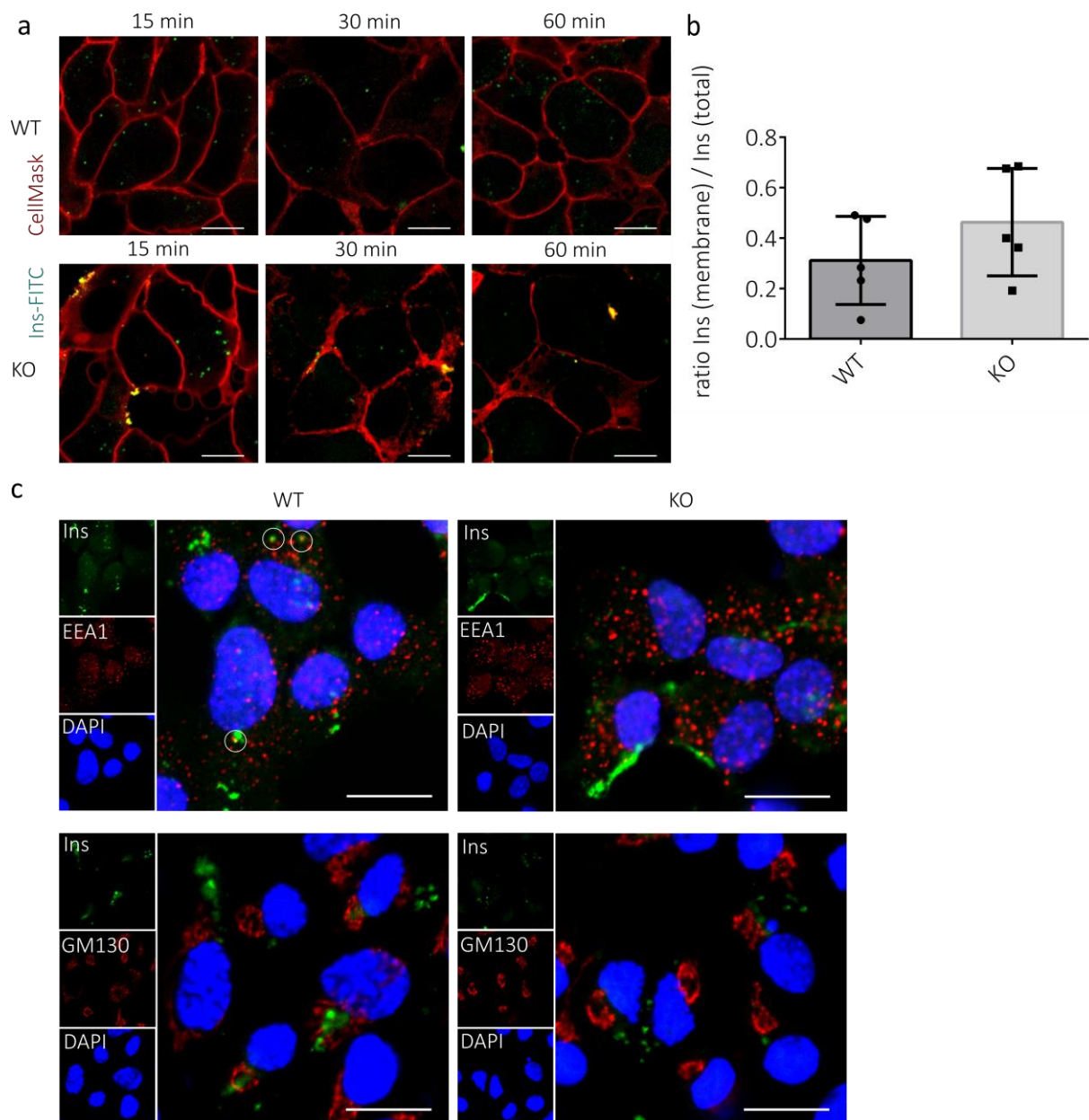


Figure 35: Internalisation of insulin-FITC in Min6

WT and Igfr-L1 KO Min6 were incubated with insulin-FITC for the indicated time points and counterstained with CellMask (a). The ratio of signal in the membrane region vs. total signal after 15 min was calculated (b) ($n=4$, >200 cells in total; $p=0.244$). The cells were incubated with FITC-insulin for 15 min and stained with EEA1 or GM130 antibodies (c) ($n=2$, >40 cells/ n ; scale bar: $20\ \mu\text{m}$).

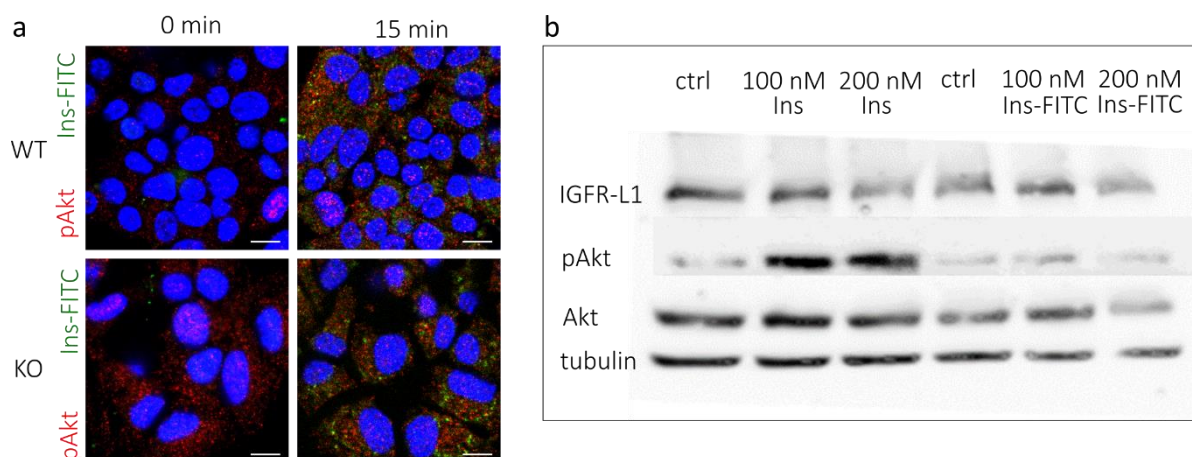


Figure 36: Biological activity of insulin-FITC

Insulin-FITC was tested for functionality by incubation of WT and IGFR-L1 KO Min6 with 100 nM insulin-FITC for 15 min after starvation in HBSS for 2 h, and subsequently stained for pAkt (40 cells/n, n=3; scale bar: 10 μ m) (a). WT Min6 cells were starved in HBSS for 2 h (ctrl) and incubated with insulin or insulin-FITC for Western blot analysis (b).

To overcome the constraints of reduced biological activity, we collaborated with O. Plettenburg (Institute of Medicinal Chemistry, Leibniz University Hannover) to instead design monovalently labelled insulin. The commercially available insulin-FITC is randomly labelled at multiple sites, which might be the reason for lacking insulin binding. As a label for monovalently conjugated insulin, we chose Alexa Fluor 546, due to the desirable quantum yield and fluorescence lifetime. After insulin-546 was validated by O. Plettenburg (data not shown), we performed a time-resolved insulin uptake assay (Figure 37a,b). To this end, we incubated WT and Igfr-L1 KO Min6 with insulin-546 for specified time points and counterstained with a silicon rhodamine (SiR)-labelled actin dye. There was significantly less insulin uptake in the KO cells after 15 and 30 minutes, thus confirming that the insulin uptake is delayed in Igfr-L1 KO cells. This suggests that IGFR-L1 has a role in insulin endocytosis.

As a control, the same experiment was performed with Alexa Fluor 647-labelled transferrin (Figure 37c). There was no difference in transferrin uptake in WT vs. Igfr-L1 KO Min6, which shows that the KO cells do not have a general endocytosis defect.

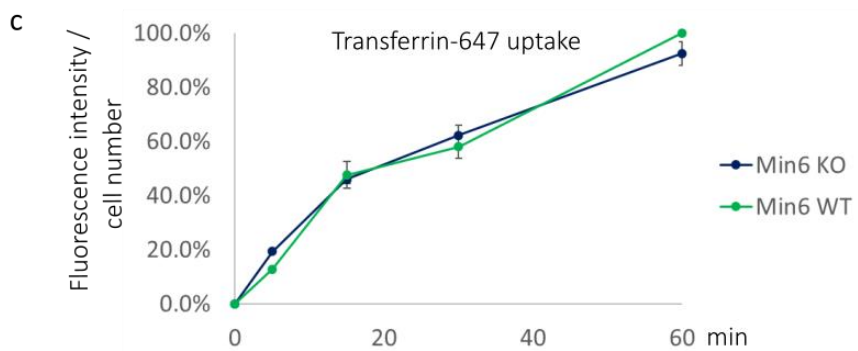
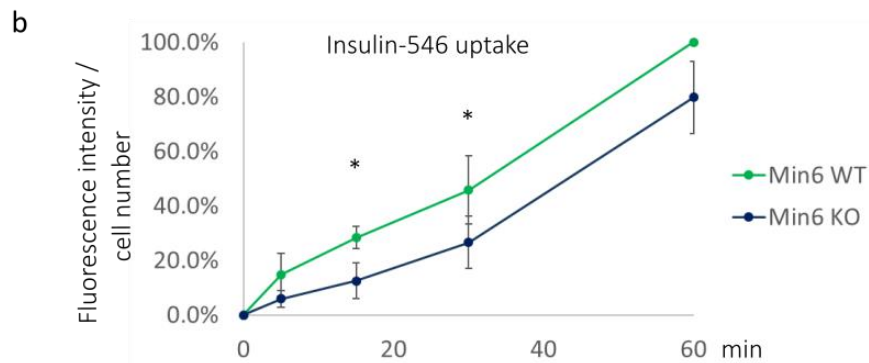
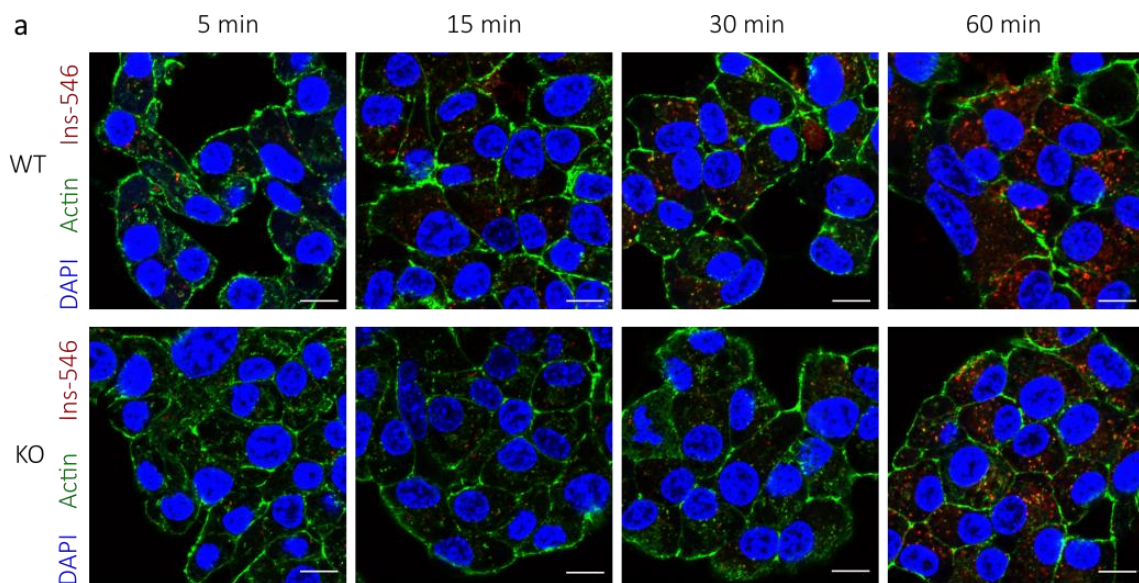


Figure 37: Internalisation of insulin-546

WT and IGFR-L1-KO Min6 were incubated with Alexa Fluor 546-labelled insulin for the indicated time points and counterstained with CellMask (scale bar: 10 μ m) (a). The fluorescence intensity was calculated and normalised on the cell number (>150 cells/n each time point, n=5; p=0.003 at 15 min and p=0.021 at 30 min). The uptake in WT Min6 at 60 min was defined as 100 % (b). The same experiment was performed with Alexa Fluor 647-labelled transferrin as a control (>150 cells/n each time point, n=3) (c).

2.2.5.2 Insulin and IGFR-L1 are simultaneously internalised

As mentioned previously, IGFR-L1 also shares sequence similarities with EGFR, in addition to IR. Therefore, we further investigated the potential role of IGFR-L1 in EGF uptake. To this end, the internalisation of insulin-FITC or Alexa Fluor 488-labelled EGF along with the IGFR-L1 antibody 19A6-555 was monitored (Figure 38). After 30 minutes, there was clearly visible overlap of insulin with the antibody, with most colocalising vesicles being plasma membrane-proximal. Contrarily, no overlap with EGF was observed, which suggests that EGF might be internalised in different vesicles than IGFR-L1, in contrast to insulin.

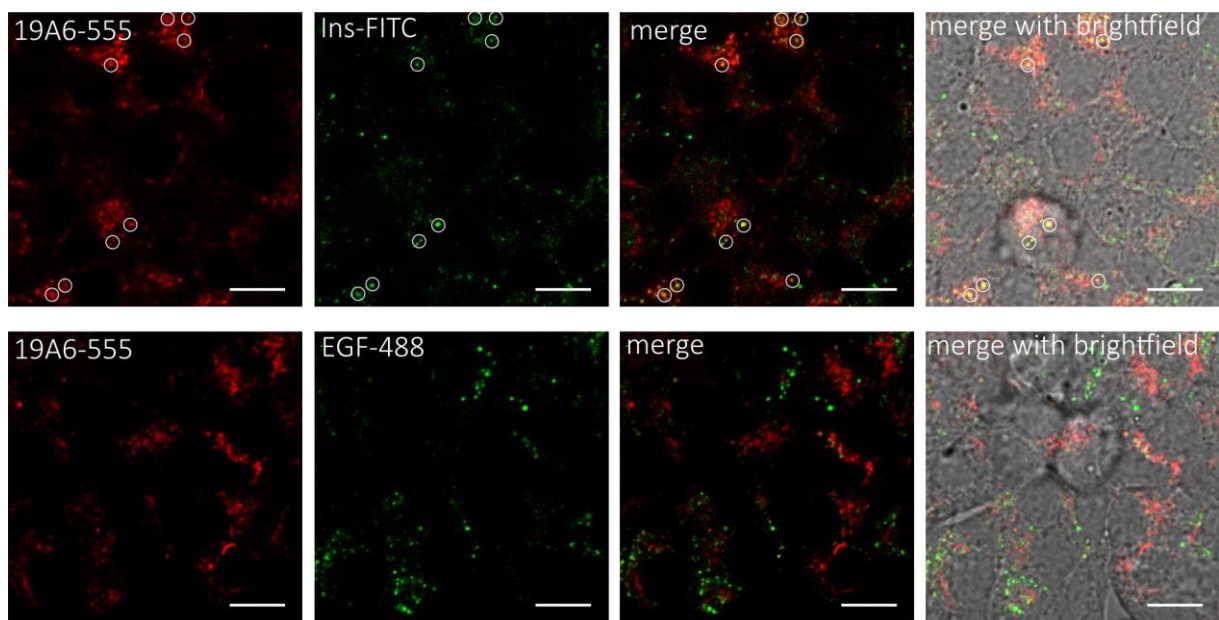


Figure 38: Live uptake of insulin-FITC and EGF-488 in Min6

Min6 cells were incubated with AlexaFluor555-labelled IGFR-L1 antibody 19A6 and insulin-FITC or AlexaFluor488-labelled EGF for 30 min. Images are representative for >50 cells (n=2), scale bar: 10 μ m.

To visualise insulin endocytosis in a time-resolved manner, the uptake dynamics were observed in 5-minute intervals (Figure 39). Vesicles showing overlapping signals for insulin-546 and the IGFR-L1 antibody 19A6-647 were already visible after 5 minutes, which shows that both are internalised simultaneously. After 15 minutes, there was a high degree of overlap between IGFR-L1-Venus, 19A6-647 and insulin-546. This observation shows that IGFR-L1 and insulin are internalised efficiently, and presumably in the same vesicles.

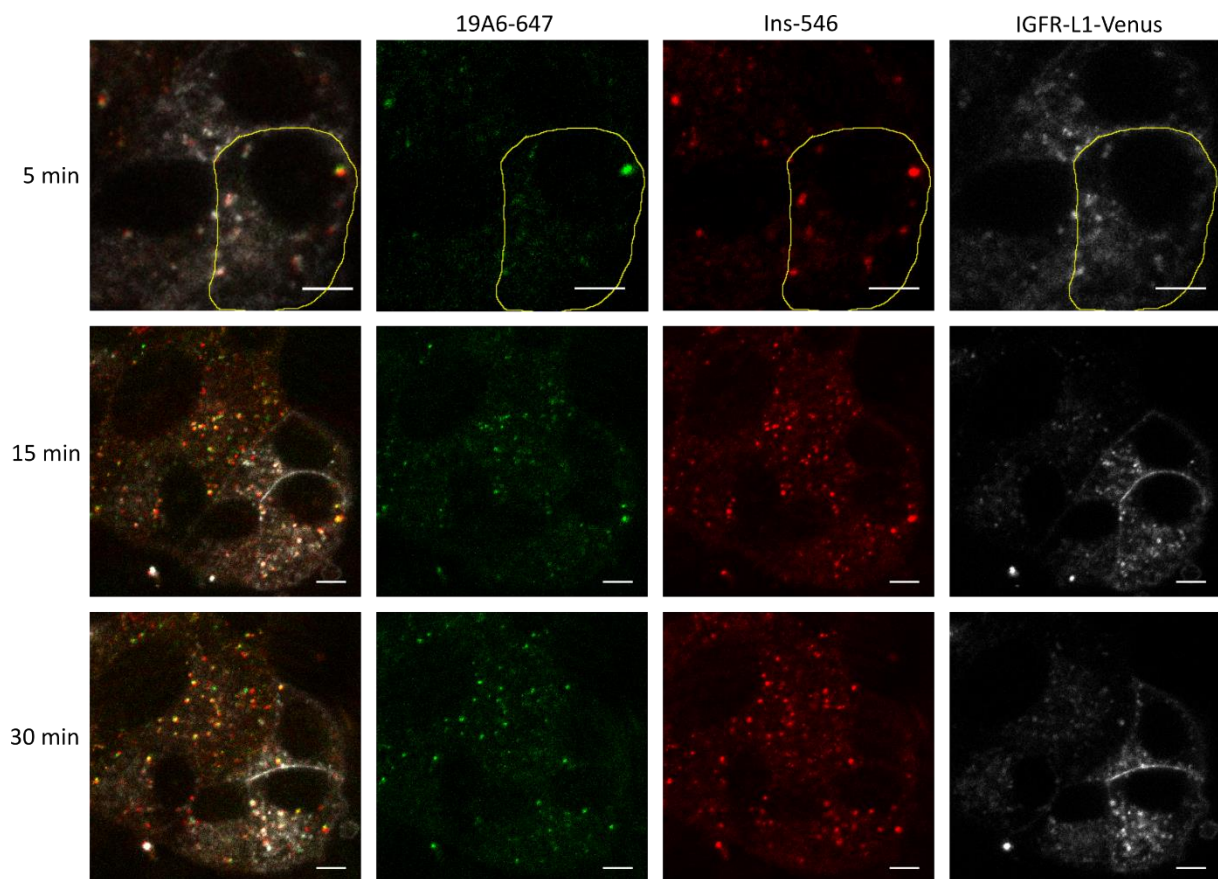


Figure 39: Live uptake of insulin-546 along with IGFR-L1 Ab

Min6 IGFR-L1-Venus cells were observed during incubation with 10 $\mu\text{g}/\text{ml}$ Alexa Fluor 647-labelled antibody 19A6 and 100 nM Alexa Fluor 546-labelled insulin. Images were taken after 5 minutes (zoomed in), 15 minutes and 30 minutes (scale bar: 5 μm). Images are representative for >50 cells/n each time point ($n=3$); similar results were obtained for the Alexa Fluor 647-labelled antibody 2G6 (not shown).

To analyse the impact of IGFR-L1 on the lysosomal transport of insulin, we incubated Min6 cells expressing IGFR-L1-Venus or IGFR-L1-AP2*-Venus with fluorescent labelled insulin, along with LysoTracker for lysosome staining (Figure 40). There was more overlap between insulin and LysoTracker in the cells expressing the unmutated IGFR-L1-Venus compared to the mutated protein. To quantify this effect, we calculated the MOC in both conditions. The overlap was indeed slightly lower in the IGFR-L1-AP2*-Venus expressing cells, where the endocytosis was impaired (see 2.2.4 Clathrin-mediated Endocytosis of IGFR-L1), although the difference was not significant. Nonetheless, this suggests that IGFR-L1 might be involved in the transport of insulin towards the lysosome. Further experiments are needed to verify this hypothesis.

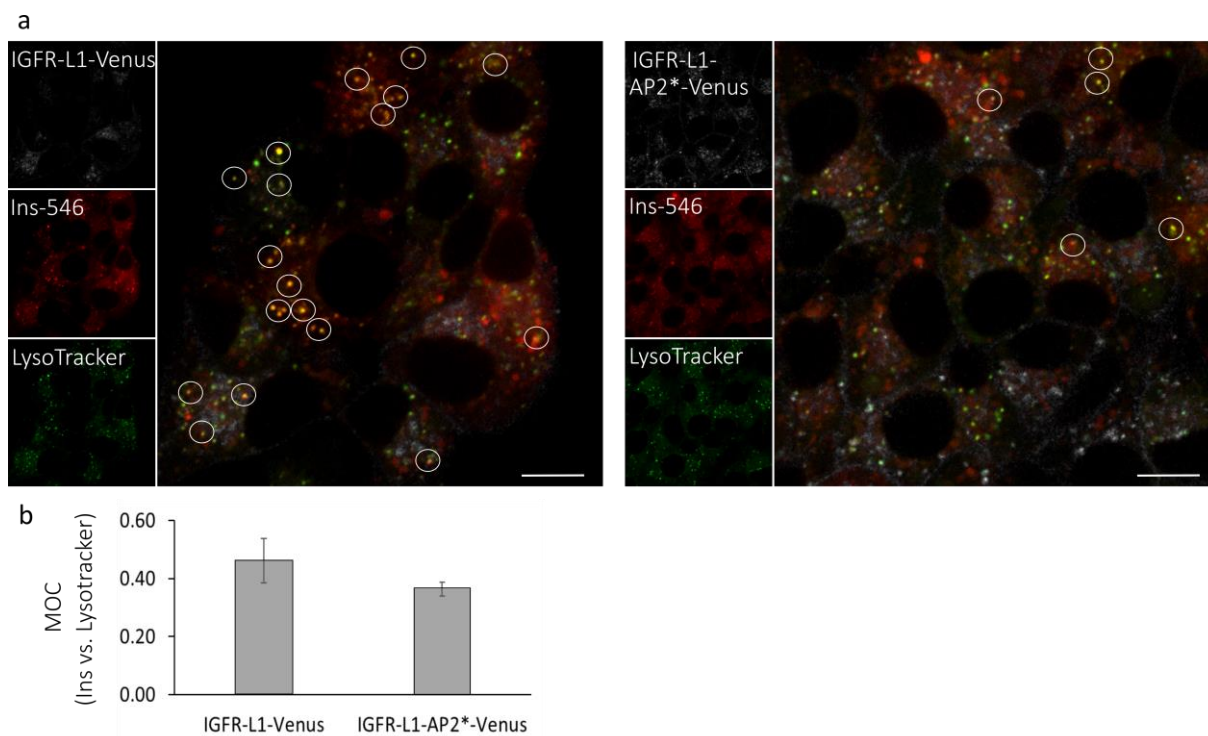


Figure 40: Lysosomal transport of insulin-546

Min6 IGFR-L1-Venus and Min6 IGFR-L1-AP2-Venus were incubated with 100 nM Alexa Fluor 546-labelled insulin, along with 100 nM LysoTracker Deep Red for 60 minutes (scale bar: 10 μ m). The clearly overlapping vesicles were circled. The MOC of Ins-546 vs. LysoTracker was calculated from >120 cells/n ($n=4$; $p=0.078$).*

2.3 The Role of IGFR-L1 in Cancer

2.3.1 IGFR-L1 expression in Benign Tissue

2.3.1.1 IGFR-L1 is expressed in secretory glands

Online databases such as the Human Protein Atlas are useful to get an overview of the expression of proteins in different tissues. Analysis of IGFR-L1 expression showed that *IGFR-L1* mRNA is not only expressed in the pancreas, but even higher in other gastrointestinal-associated tissues such as salivary glands, stomach and duodenum (Figure 41). In addition, *IGFR-L1* is expressed in gonadal tissues, i.e. cervix, uterus, breast, fallopian tube, endometrium, prostate and testis. Together with the initial discovery of IGFR-L1 as an estrogen-inducible gene [165], this indicates a potential involvement in sex hormone signalling. Importantly, the prostate is among the organs with highest *IGFR-L1* expression levels. The main function of all above-mentioned tissues is exocrine secretion, suggesting a potential role of IGFR-L1 in this process.

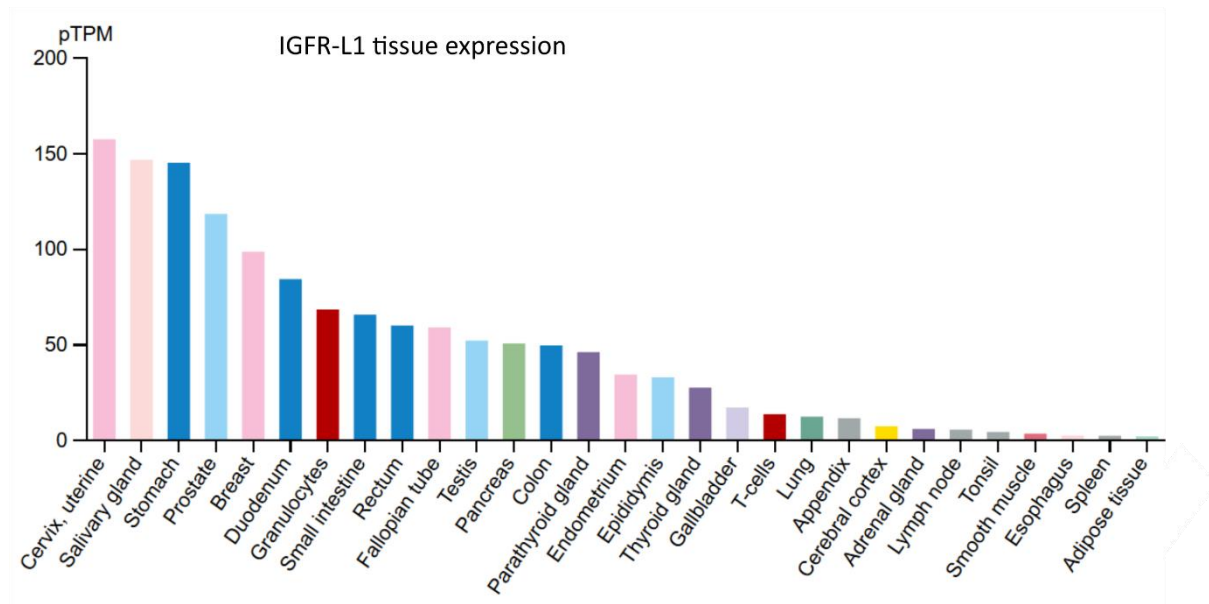


Figure 41: Expression of IGFR-L1 in normal human tissues

The mRNA expression data was retrieved via the Human Protein Atlas [171].

2.3.1.2 Igfr-L1 is expressed in secretory cells of the prostate epithelium

The mouse prostate is composed of four distinctive lobes: the dorsal, ventral, lateral and anterior lobe. To analyse the tissue distribution of Igfr-L1, we isolated prostates from WT mice and prepared cryosections. The sections were stained with actin and prostate-specific antigen (PSA) antibodies to visualise the prostate tissue (Figure 42). Igfr-L1 was expressed equally in all regions.

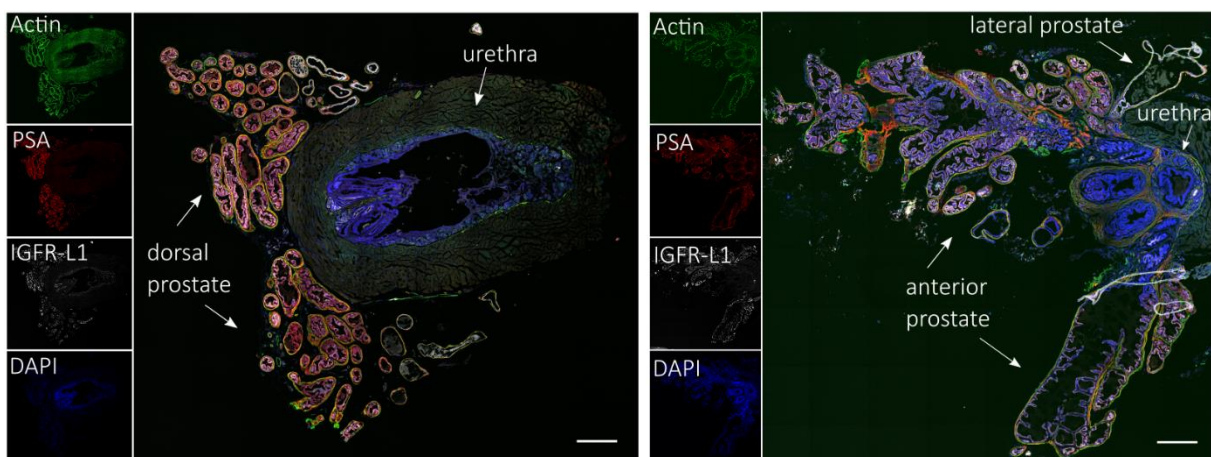


Figure 42: IGFR-L1 in different regions of the mouse prostate

Staining of Igfr-L1, PSA and smooth muscle actin in prostate sections of WT mice (images are representative of two mice). Scale bar: 500 μ m.

The prostate epithelium is composed of four main cell types: luminal (secretory) cells, basal cells, intermediate cells and neuroendocrine cells (see also Figure 5). The main cell types can be distinguished by co-staining with cytokeratin 5 (CK5) and cytokeratin 8/18 (CK8/18). Luminal cells express CK8 and 18, while basal cell express CK5 and 15. Intermediate cells display features of both cell types. Igfr-L1 was found in luminal and intermediate cells, but not in basal cells (Figure 43).

Neuroendocrine cells secrete peptides regulating growth and differentiation of prostate epithelial cells; among others, serotonin and somatostatin. In some neuroendocrine cells no Igfr-L1 expression was observed (Figure 44), whereas others displayed very weak expression. However, extensive analyses were not possible as these cells are very rare in the prostate epithelium. In addition to serotonin, we attempted staining neuroendocrine cells with

Chromogranin A; however, the tested antibodies were not functional on this tissue. Taken together, these results demonstrate that Igfr-L1 is expressed in secretory cells of the prostate epithelium.

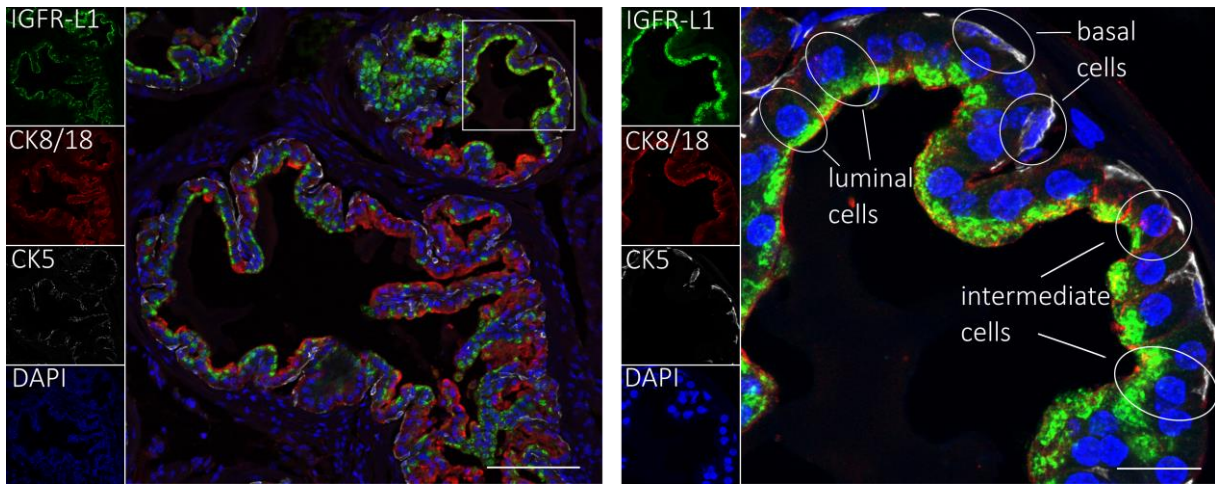


Figure 43: Cell type analysis of Igfr-L1 expression in WT mouse prostate section

Luminal cells are marked by CK8/18 expression, basal cells by CK5 expression, and intermediate cells express both CKs. Image is representative of 14 slices from dorsoventral and anterior prostate of 2 mice. Scale bar: 100 μ m (left) / 20 μ m (right, zoomed in).

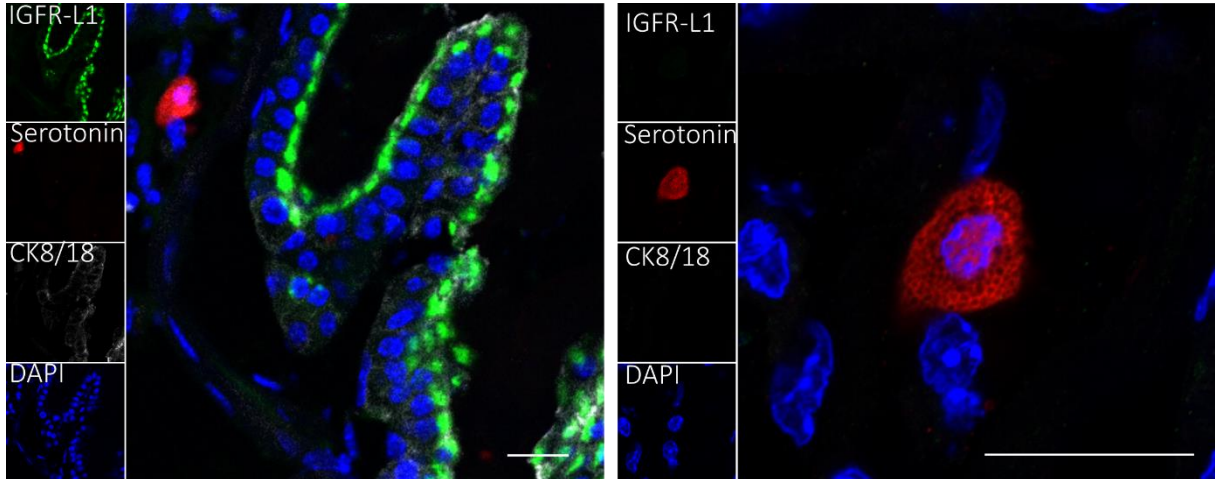


Figure 44: Analysis of Igfr-L1 expression in neuroendocrine cells

Neuroendocrine cells are characterised by serotonin and somatostatin expression. Images are representative of 8 slices from 2 WT mice, scale bar: 20 μ m (right side shows zoomed image).

2.3.1.3 Knockout of Igfr-L1 has no effect on AR signalling or polarity of the prostate

To investigate the *in vivo* function of Igfr-L1, generating a loss-of-function model is crucial. As Igfr-L1 KO mice die within hours after birth, we resorted to a ROSA26-CreERT2-inducible knockout model, where the Cre recombinase is induced by the estrogen receptor antagonist tamoxifen. In this model, the IGFR-L1 gene is flanked by loxP sites, which are recognised by the Cre recombinase, leading to excision of IGFR-L1. The Cre recombinase is fused to a modified estrogen receptor (ERT2), which is expressed under control of the ubiquitous ROSA26 locus. The fusion protein is activated by the estrogen receptor antagonist tamoxifen. It was previously shown that CreERT2 does not achieve complete deletion, but rather generates a genetic mosaic [172]. Therefore, the IGFR-L1 expressing and non-expressing cells can be directly compared within the same sample. The prostates of these mice were isolated 4 weeks after tamoxifen injection. The knockout efficiency was high, as approximately 90 % of the epithelial cells were negative for Igfr-L1 staining (Figure 45). To investigate any potential effects on androgen signalling, the slices were co-stained for AR; however, no significant difference in AR distribution or intracellular localisation was observed.

Based on the alignment of the stained nuclei, it appeared that the epithelium was less ordered in Igfr-L1 KO mice (+tamoxifen). Thus, we performed staining for the polarity markers laminin, ZO-1 and ezrin (Figure 46). The laminin-alpha1 subunit is clearly visible on the basal membrane of the epithelium, while ezrin is found at the apical membrane, as described in the literature [173]. ZO-1 is localised to tight junctions, thus the distribution of ZO-1 can further hint towards the degree of organisation in an epithelium. However, no significant changes were visible. As the morphology of the prostate epithelium varies greatly between the different lobes and even within the lobes, analyses of the epithelial organisation are particularly difficult in this tissue.

As a readout for downstream signalling, we attempted pAkt staining. However, there was no signal apart from unspecific background. Since it was shown that AR can be cross-activated by RTKs via Foxo1 [125], we attempted to assess the Foxo1 activation by comparing nuclear with cytoplasmic localisation. However, no Foxo1 signalling could be observed in luminal cells. Only the nuclear localisation in basal cells, where Igfr-L1 was not expressed, was visible (data not shown).

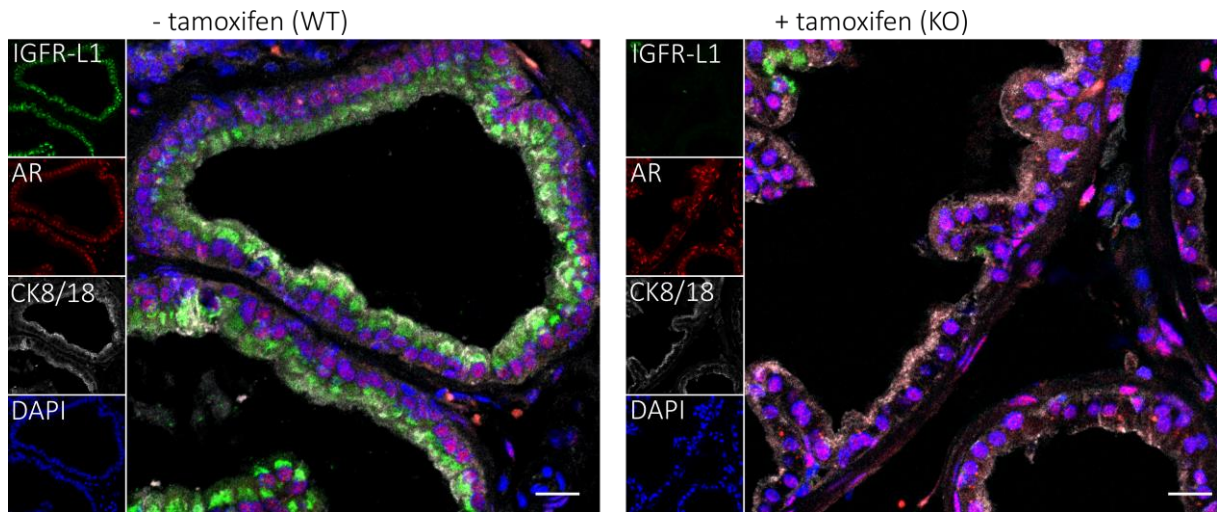


Figure 45: Localisation of AR in Igfr-L1 KO prostate

Prostate sections of Igfr-L1-flox mice induced with tamoxifen (right) and not induced (left) were stained for Igfr-L1, AR and CK8/18. Images are representative for 5 slices in different regions from each mouse (scale bar: 20 μ m).

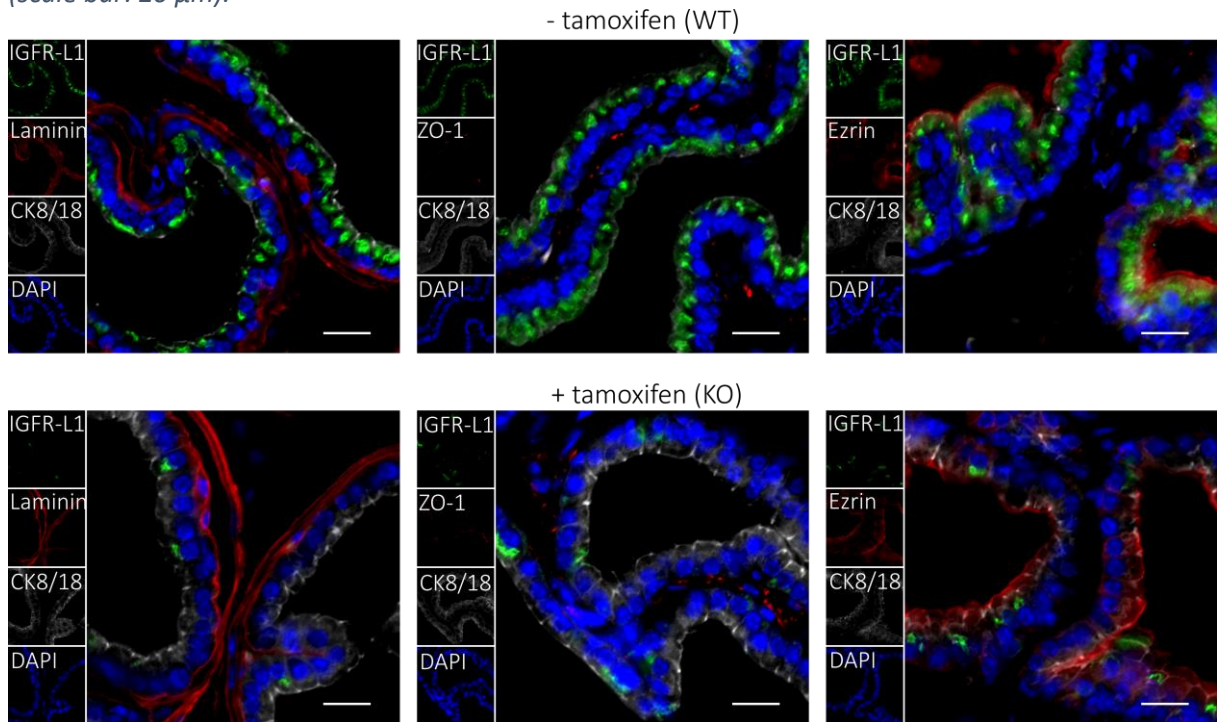


Figure 46: Polarity markers in Igfr-L1 KO prostate

Sections from Igfr-L1-flox mice (+/-tamoxifen) were stained for the polarity markers laminin, ZO-1 and ezrin. Images are representative for 2 slices in different regions from two mice (scale bar: 20 μ m).

2.3.1.4 Knockout of Igfr-L1 might increase proliferation of the prostate epithelium

It is known that IGF1 signalling is important for normal embryonic development of the prostate epithelium [174]. Thus, we speculated that Igfr-L1 might have an impact on proliferation in the adult prostate. To investigate this hypothesis, we stained prostate cancer sections with the proliferation marker Ki67 (Figure 47). While it seemed that there were more Ki67-positive cells in the Igfr-L1 KO prostates, the difference was not statistically significant. To complement this analysis, we attempted staining of the proliferating cell nuclear antigen (PCNA); however, none of the used antibodies worked on our tissue (data not shown). Thus, further experiments are needed to verify this result. For instance, mice could be injected with EdU before the sacrifice to facilitate EdU staining of tissue sections.

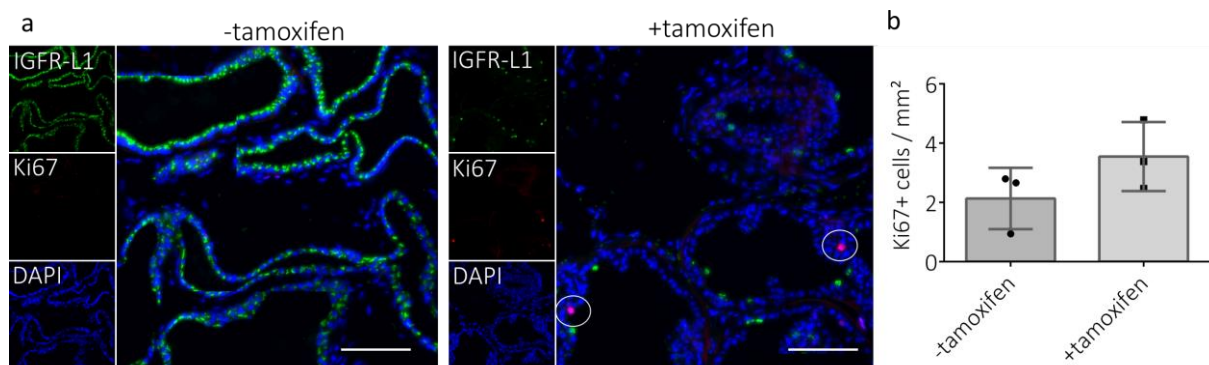


Figure 47: Proliferation of *Igfr-L1* KO prostate epithelium

Igfr-L1-flox mice (+/-tamoxifen) were stained for Ki67 (scale bar: 100 μ m) (a). To quantify proliferation, the Ki67+ cells in 14 sections from dorsolateral and from anterior prostate were counted for each animal (n=3) (b).

2.3.2 IGFR-L1 in Human Prostate Cancer

2.3.2.1 IGFR-L1 is differentially expressed in various cancers

The expression of *IGFR-L1* in benign and malignant tissues was studied using the publicly available dataset from The Cancer Genome Atlas (TCGA) (Figure 48). These data show that *IGFR-L1* is downregulated in pancreatic cancer, but upregulated in ovarian cancer, endometrial cancer, breast cancer and prostate cancer. This indicates that IGFR-L1 might have a role in hormone-dependent cancers.

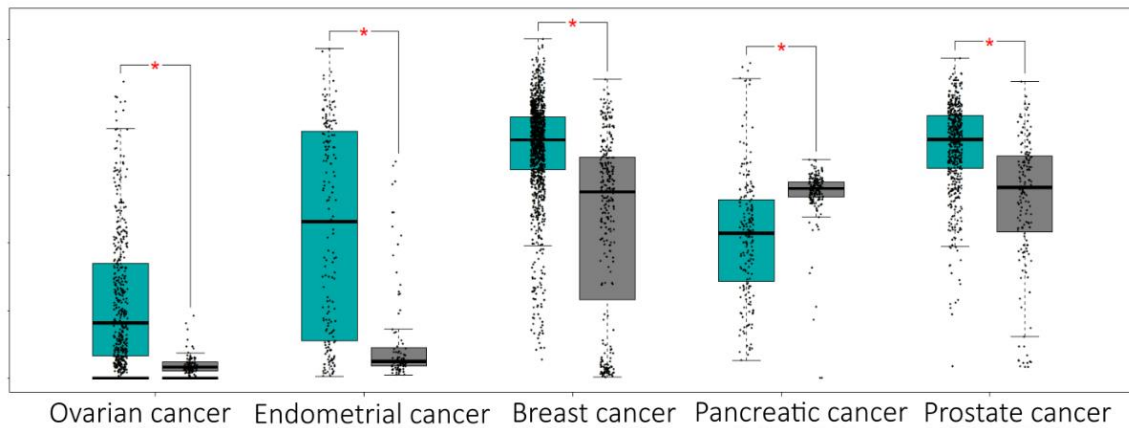


Figure 48: Expression of IGFR-L1 in various cancer types

Relative mRNA expression of IGFR-L1 in ovarian cancer, endometrial cancer, breast cancer, pancreatic cancer and prostate cancer (cyan), compared to benign tissue (grey). Data was collected by the TCGA project and retrieved via the GEPIA browser [175]).

2.3.2.2 IGFR-L1 is frequently mutated in later stages of prostate cancer

Mutations and amplifications of oncogenes often occur in malignancies. In prostate cancer, the most well-described mutation is gene amplification of *AR*, which occurs in around 20% of androgen-independent prostate cancer (AIPC) and 60% of neuroendocrine prostate carcinoma (NEPC) (Figure 49). Further, genes involved in RTK signalling are highly mutated, including *IGF1R*, *IR*, *EGFR*, and *PI3K*. Presumably, these genes are mutated since they provide a survival mechanism for cancer cells in androgen-deprived conditions. In comparison, mutations of *IGFR-L1* (6%) in AIPC are more frequent than of *IGF1R* (1%), and in a comparable range as *IR* (8%) and *EGFR* (9%) mutations. This suggests that IGFR-L1 is similarly important for prostate cancer progression as *IR* or *EGFR*.

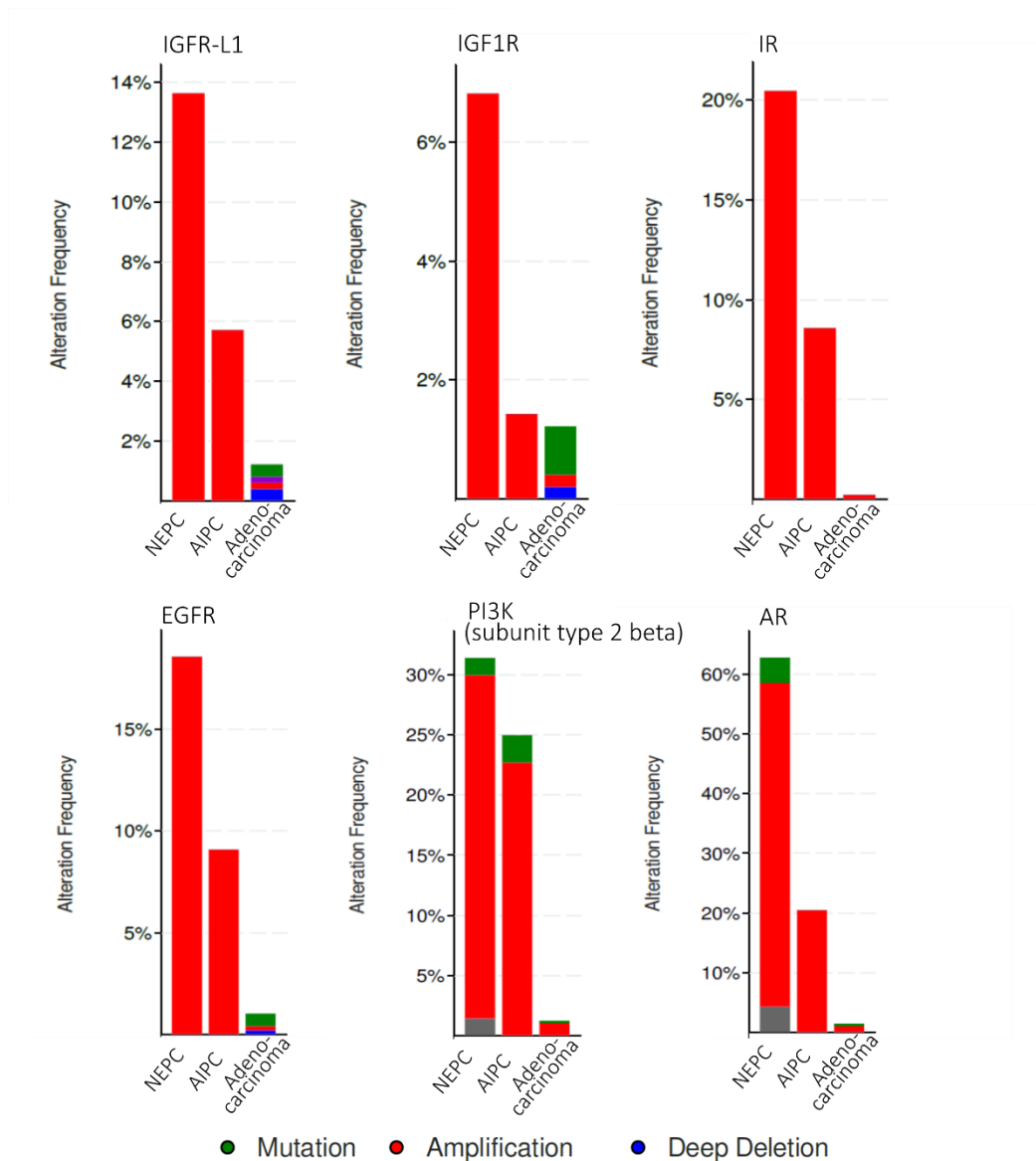


Figure 49: Mutation frequencies of genes potentially involved in prostate cancer

Data was collected by the TCGA project and extracted via CBioPortal [176], categorized by prostate adenocarcinoma, androgen-independent prostate cancer (AIPC) and neuroendocrine prostate carcinoma (NEPC).

In addition, we analysed the correlations of *IGFR-L1* mutations with mutations of factors involved in prostate cancer growth. Mutations of *IGFR-L1* frequently co-occur with mutations of *AR*, and the *AR*-regulated genes *PSA (KLK3)* and *PSMA (FOLH1)* (Table 3), which indicates a potential link to androgen signalling. Further, there was co-occurrence with *EGFR*, *IR*, *IGF2R*, *IGF1R* and *PI3K* (type 2 α and β). All these genes are involved in RTK signalling and thus in proliferative pathways that are alternative or complementary to androgen-dependent growth.

Table 3: Co-occurrence of mutations in the TCGA dataset and neuroendocrine prostate cancer dataset, retrieved via CBioPortal [176].

Mutation co-occurrence in prostate cancer								
A	B	Neither	A Not B	B Not A	Both	p-Value	q-Value	Tendency
IGFR-L1	AR	529	7	51	9	<0.001	<0.001	Co-occurrence
IGFR-L1	PSMA	565	10	15	6	<0.001	<0.001	Co-occurrence
IGFR-L1	PSA	558	9	22	7	<0.001	<0.001	Co-occurrence
IGFR-L1	EGFR	565	9	15	7	<0.001	<0.001	Co-occurrence
IGFR-L1	INSR	570	10	10	6	<0.001	<0.001	Co-occurrence
IGFR-L1	IGF2R	570	10	10	6	<0.001	<0.001	Co-occurrence
IGFR-L1	IGF1R	574	12	6	4	<0.001	<0.001	Co-occurrence
IGFR-L1	PIK3C2B	551	6	29	10	<0.001	<0.001	Co-occurrence
IGFR-L1	PIK3C2A	569	13	11	3	0.005	0.005	Co-occurrence

2.3.2.3 Expression of IGFR-L1 correlates with progression markers in prostate cancer

For expression analyses of prostate cancer samples, we correlated various genes of interest with *IGFR-L1*. The mRNA expression of *IGFR-L1* was positively correlated to expression of *AR* and the androgen-regulated genes *PSA* and *PSMA* (Figure 50a-c). Further, there was a striking positive correlation to *IGF1R*, *IR* and *EGFR* (Figure 50d-f). As these genes are amplified in late stages of prostate cancer, this indicates that *IGFR-L1* is upregulated during prostate cancer progression.

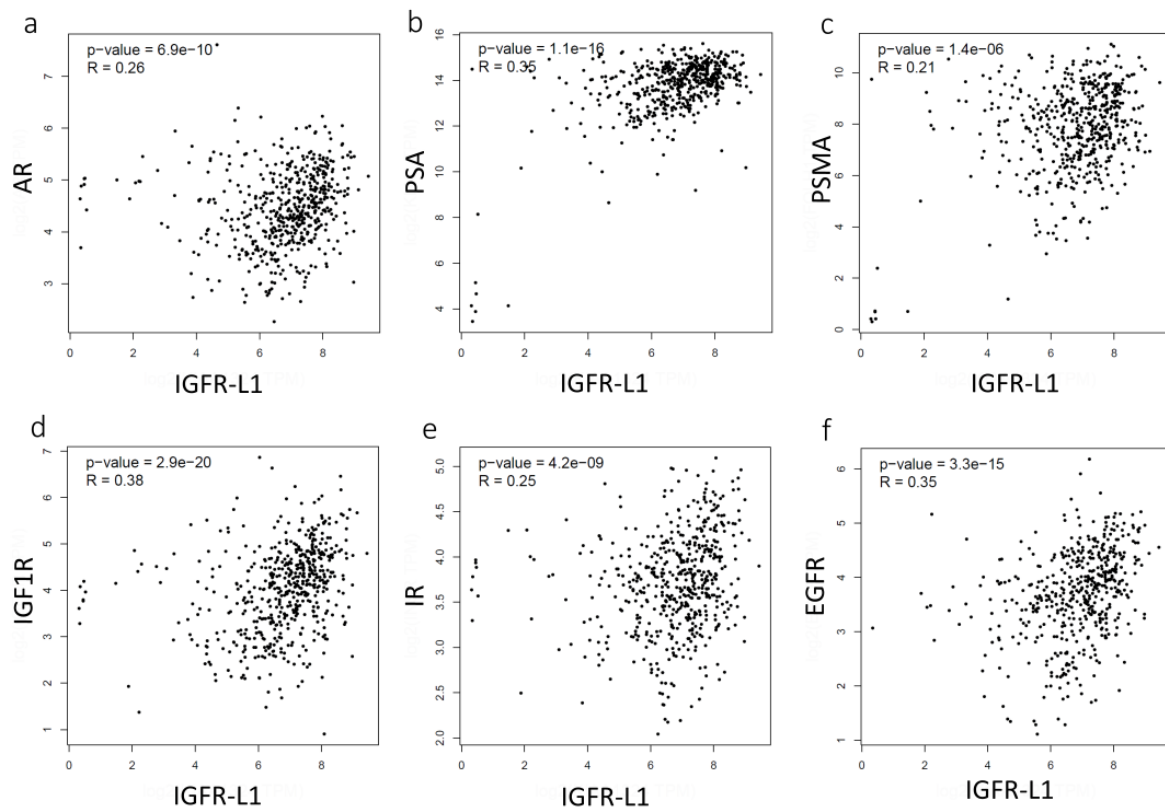


Figure 50: Correlation of IGFR-L1 and genes potentially involved in prostate cancer

The mRNA data was collected by the TCGA project and retrieved via the GEPIA browser [175].

2.3.3 Cell line Generation for Analysis of IGFR-L1 in Cancer

2.3.3.1 IGFR-L1 knockout in MCF7 and LNCaP cells via CRISPR/Cas9

To generate IGFR-L1 knockout cell lines, the CRISPR/Cas9 system was used. To this end, two sgRNAs (single guide RNAs) were designed to align to the region around the start codon of IGFR-L1 and were cloned into a pU6 plasmid containing an expression cassette for a fluorescent Cas9-Venus fusion recombinase. The breast cancer cell line MCF7 and the prostate cancer cell line LNCaP were transfected with the plasmid and sorted via FACS to enrich the successfully transfected cells (Figure 51), and single clones were isolated.

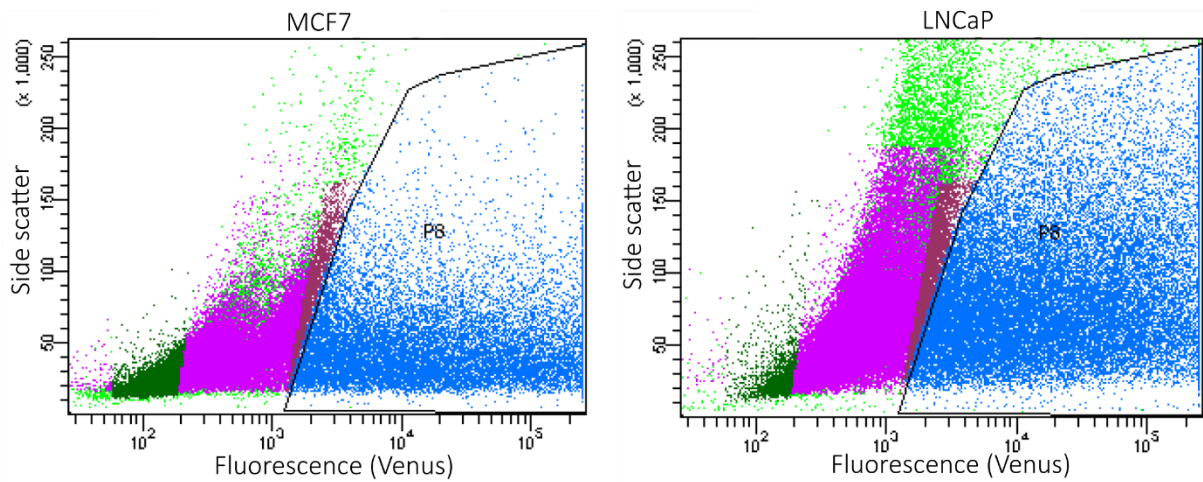


Figure 51: Sorting of cells transfected with sgRNA for CRISPR/Cas9 targeting

MCF7 and LNCaP cells were transfected with the vector pU6-sgRNA-CAG-Cas9-Venus and sorted via FACS after 2 days (the blue population was defined as Venus-positive).

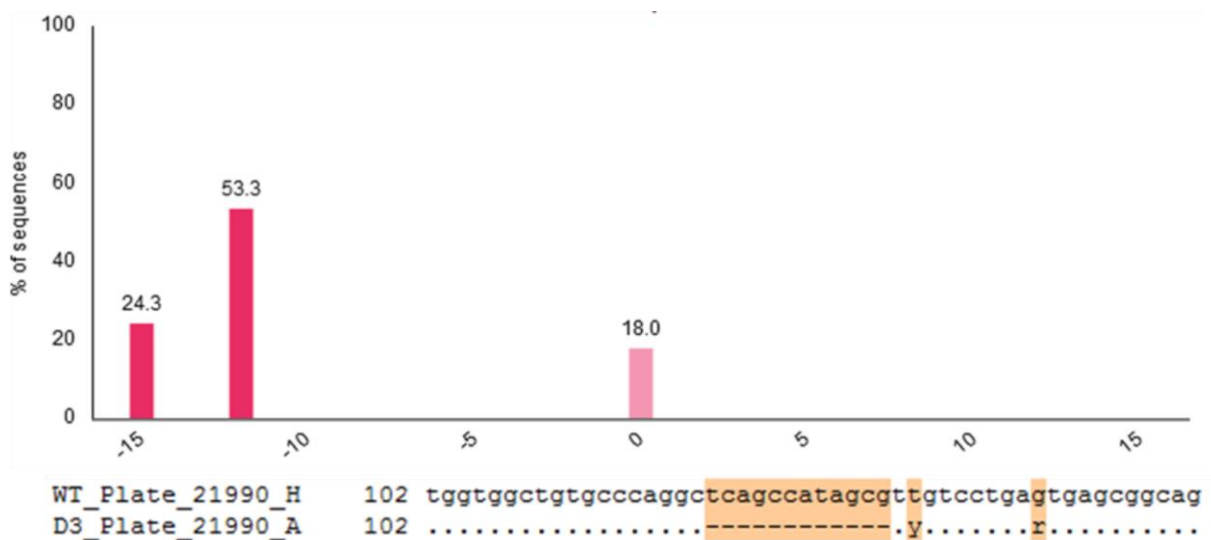


Figure 52: Sequencing of potential IGFR-L1 KO clones

For validation, the MCF7 clones were stained with IGFR-L1 antibodies (not shown) and sequenced. The above graph shows an example sequence (clone D3), analysed via the online tool TIDE (Tracking of Indels by Decomposition).

Despite multiple trials and variations in the culture conditions, LNCaP cells did not survive the procedure. The protocol was more suitable to MCF7 cells, as in the first try 96 MCF7 clones were successfully isolated and 31 clones survived over the following weeks. The mutation status of these clones was analysed by sequencing the *IGFR-L1* gene (Figure 52). However, only four of the clones had mutations on one allele, while the remaining 27 were WT. The graph indicates that 50 % of the analysed sequence shows a 12 base pair deletion and 25 % of

the sequence shows a 15 base pair deletion. This suggests that the clone D3 either has a gene duplication or consists of 2 clones, as 4 alleles are present. Immunohistochemical staining with two different IGFR-L1 antibodies directed against the cytoplasmic tail or against the ectodomain showed that all clones had normal IGFR-L1 expression. After two further tries there were 15 clones that appeared to be mixed clones and had a partial *IGFR-L1* deletion on at least one allele. However, after sub-cloning and expansion none of the clones had a full *IGFR-L1* deletion. Thus, different deletion strategies should be explored.

2.3.3.2 IGFR-L1-Venus overexpression in LNCaP cells

To induce overexpression of IGFR-L1, LNCaP cells were transfected with *IGFR-L1-Venus* (see 2.2.1.2 IGFR-L1 is successfully fused to Venus). To ensure that any observed effects are not an artefact of overexpression, a control cell line was generated by transfection with *Venus*, encoded on the same plasmid. Both cell lines were selected with puromycin and subsequently sorted via FACS to obtain a population of cells with similar expression levels (Figure 53).

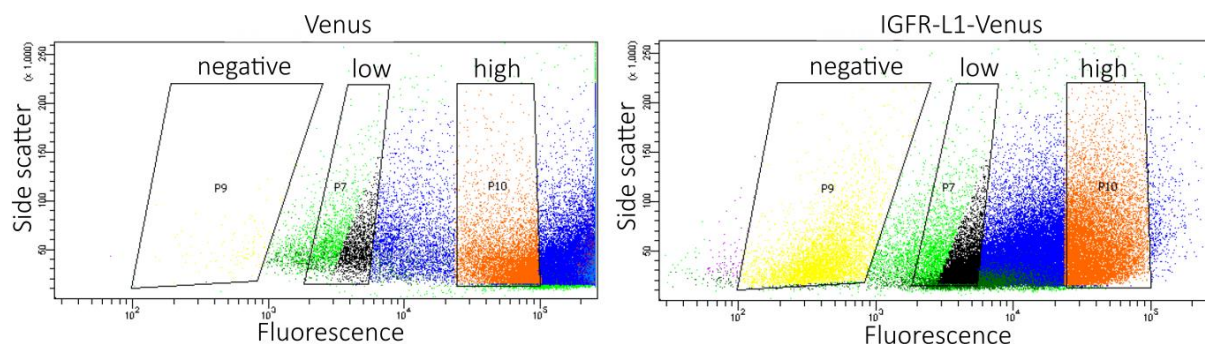


Figure 53: Generation of the stable cell lines LNCaP IGFR-L1-Venus / LNCaP Venus

LNCaP cells were transfected with the plasmid *pCAG-IGFR-L1-Venus* or *pCAG-Venus* as a control, selected with puromycin and sorted via FACS.

2.3.4 IGFR-L1 in Prostate Cancer Cells

2.3.4.1 IGFR-L1 is expressed in prostate cancer cells

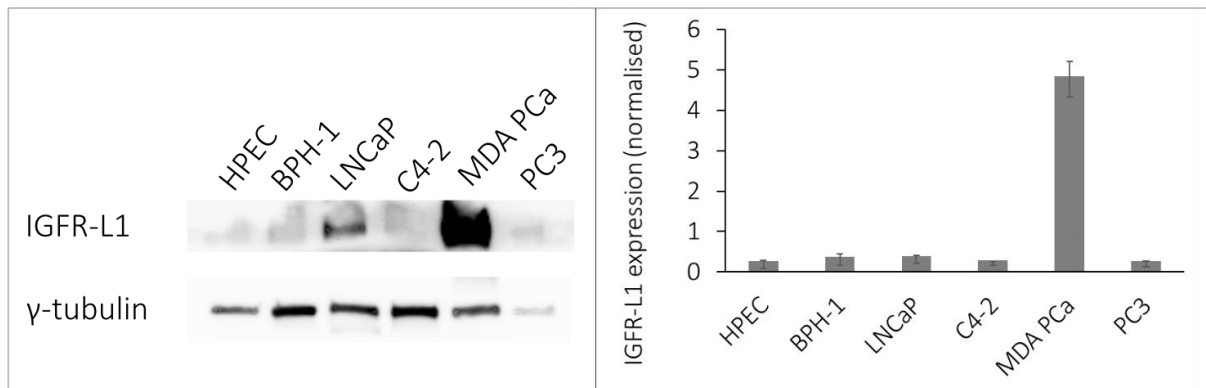


Figure 54: Expression of IGFR-L1 in prostate cancer cell lines

The expression levels of IGFR-L1 were analysed in various cell lines via Western blot and the band density was quantified ($n=3$).

The expression of IGFR-L1 was analysed in the androgen-dependent prostate cancer cell line LNCaP and the androgen-independent prostate cancer cell lines LNCaP C4-2, MDA PCa 2b and PC3. As a comparison, primary human prostate epithelial cells (HPEC) and the benign prostate hyperplasia cell line BPH-1 were included (Figure 54). All cell lines expressed IGFR-L1. Compared to the primary HPEC cells, the expression was slightly but insignificantly higher in BPH-1 and LNCaP. Interestingly, the expression in the androgen-independent cell lines LNCaP C4-2 and PC3 was slightly lower, while it was significantly higher in the cell line MDA PCa 2b, which was isolated from AIPC, but responds to androgen stimulation. This indicates that IGFR-L1 expression might vary in different prostate cancer subtypes. Since LNCaP is a widely used cell line in prostate cancer research and can be easily cultivated, LNCaP was chosen for further experiments.

The subcellular localisation of IGFR-L1 in LNCaP cells was assessed via co-staining with giantin, GM130 and LAMP1 (Figure 55). The distribution was similar compared to Min6 cells (see 2.2.2.1 Subcellular localisation of IGFR-L1-Venus resembles IGFR-L1). This shows that in prostate cancer cells IGFR-L1 is mainly localised to the endosomal-lysosomal system and the Golgi complex, similar to β -cells.

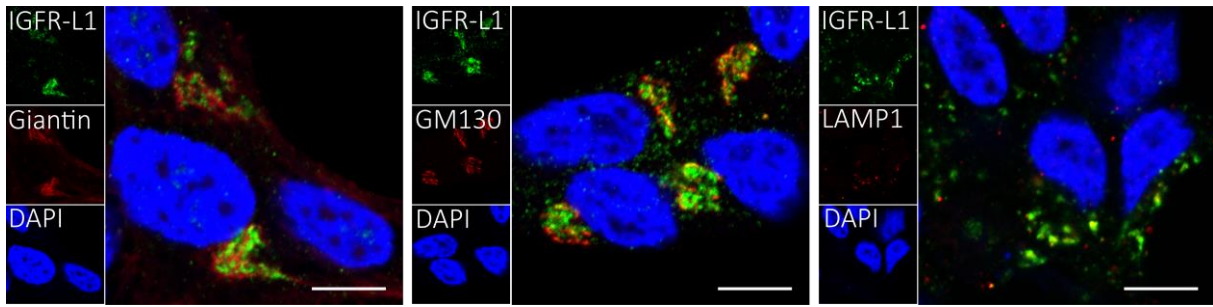


Figure 55: Subcellular localisation of IGFR-L1 in LNCaP cells

LNCaP cells were stained for IGFR-L1 along with Giantin, GM130 or LAMP1 to analyse the subcellular localisation.

2.3.4.2 IGFR-L1 overexpression does not influence proliferation in LNCaP cells

As insulin/IGF1 signalling promotes prostate cancer growth, we speculated that IGFR-L1 could influence the proliferation of prostate cancer cells. The proliferation of LNCaP cells overexpressing IGFR-L1-Venus was assessed by EdU staining, compared to LNCaP WT and LNCaP Venus cells (Figure 56). No significant difference could be observed between the cell lines. As this experiment was performed in normal growth medium containing androgens, it is possible that the effect was masked by active AR signalling.

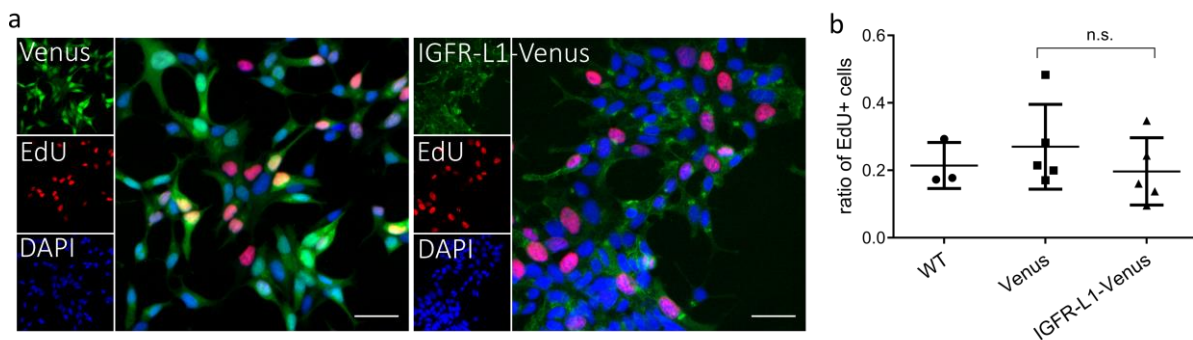


Figure 56: Proliferation of LNCaP IGFR-L1-Venus

The proliferation of LNCaP IGFR-L1-Venus cells was quantified via EdU staining (a) and automated cell counting (b), compared to LNCaP Venus and WT cells. For the quantification, >5000 cells/n were counted ($n=5$; $p=0.34$).

2.3.4.3 Migration of LNCaP cells is increased upon IGFR-L1 overexpression

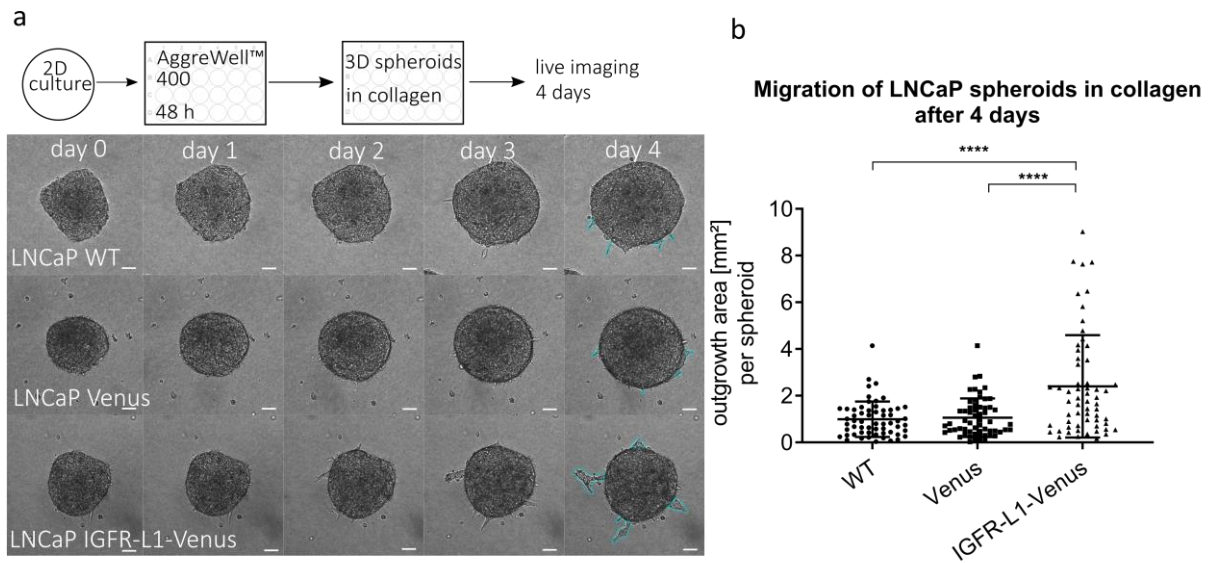


Figure 57: Migration of LNCaP IGFR-L1-Venus in a 3D assay

Migration of LNCaP spheroids in a collagen matrix (experimental scheme above) (scale bar: 50 μ m) (a). Quantification was done by measuring the outgrowth area of 60 spheroids for each cell line from 3 independent experiments, as shown in light blue colour ($p < 0.0001$; 2 outliers were removed using Grubb's outlier test) (b).

As an *in vitro* model for migration, LNCaP cells were aggregated to 3D cancer spheroids for 48 h, embedded in a collagen matrix and subsequently monitored for 4 days. The area of the migrating cells after 4 days was measured (Figure 57). The migration of IGFR-L1-Venus overexpressing spheroids was significantly higher compared to WT and control (Venus). This suggests that IGFR-L1 can promote migration in prostate cancer cells.

2.3.5 Potential Regulation of IGFR-L1 via Reproductive Hormone Signalling

2.3.5.1 IGFR-L1 seems to be estrogen-induced

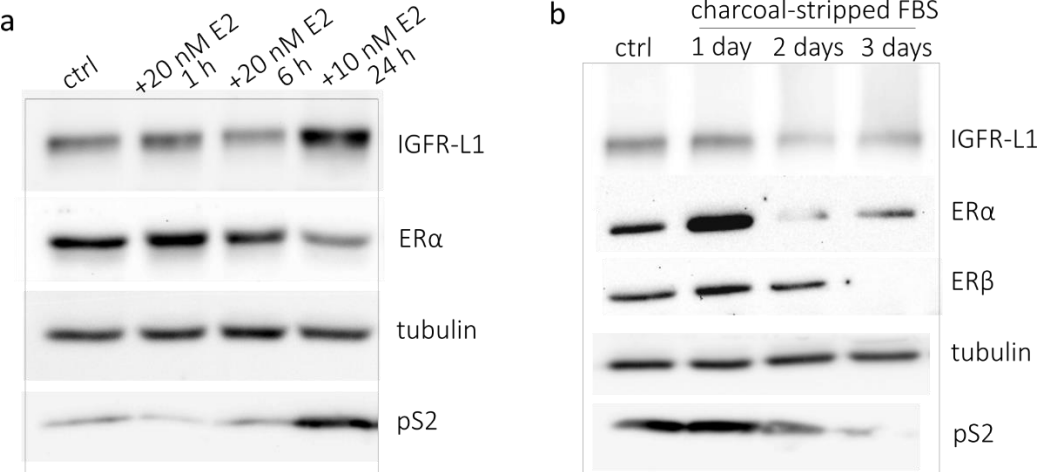


Figure 58: Estrogen induction or depletion of MCF7 cells

MCF7 cells were induced with 10 or 20 nM E2 for the indicated time points (a) or cultured in charcoal-stripped FBS without estrogen (b), and proteins relevant to estrogen signalling were detected via Western blot. Images are representative for 2 independent experiments.

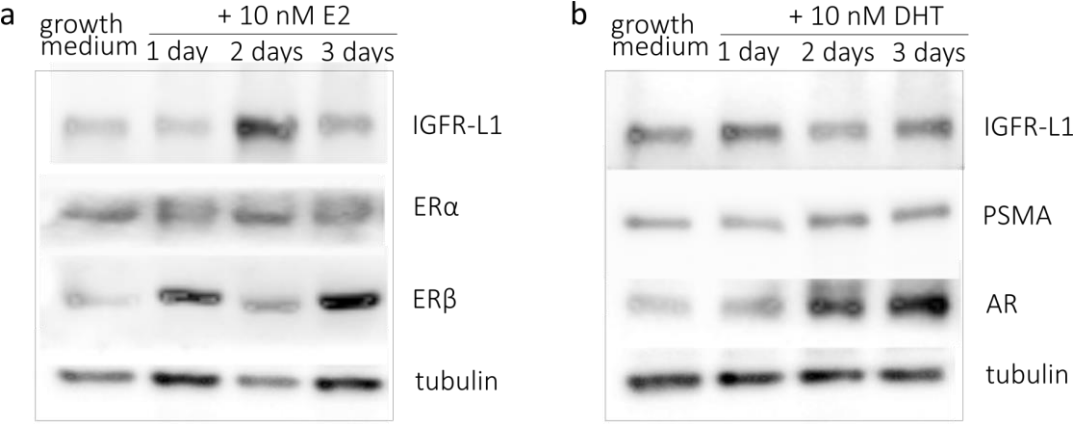


Figure 59: Estrogen or androgen induction of LNCaP cells

LNCaP cells were stimulated with 10 nM E2 (a) or dihydrotestosterone (DHT) (b) for up to 3 days. Images are representative for 2 independent experiments.

To assess whether IGFR-L1 is regulated by estrogens, the estrogen-dependent breast cancer cell line MCF7 was stimulated with E2 (Figure 58a). We found that IGFR-L1 was slightly increased after stimulation with 10 nM E2 for 24 hours. Accordingly, expression of the

estrogen-inducible protein pS2 was elevated, while the estrogen receptor α (ER α) was decreased, possibly due to negative feedback loops. Further, MCF7 cells were cultured in medium supplemented with charcoal-stripped FBS for up to 3 days (Figure 58b). Charcoal-stripped FBS contains only minimal amounts of steroid hormones. Thus, the estrogen signalling that is important for proliferation of MCF7 cells is diminished. IGFR-L1 expression was slightly decreased after 2 and 3 days. The estrogen receptors were markedly reduced, which indicates a transition to alternative proliferative pathways. Accordingly, pS2 expression was significantly reduced.

To confirm this effect in the prostate cancer cell line LNCaP, the cells were incubated with 10 nM E2 for up to 3 days (Figure 59a). IGFR-L1 expression was increased at 2 days, then declined to normal levels after 3 days. Expression of ER β was decreased at 2 days. As proliferation of LNCaP cells is androgen-dependent, LNCaP cells were further stimulated with DHT (Figure 59b). Induction with 10 nM DHT did not significantly change IGFR-L1 levels, while AR levels were increased. Taken together, these results suggest that IGFR-L1 is estrogen-inducible.

2.3.5.2 Androgen deprivation induces IGFR-L1 expression

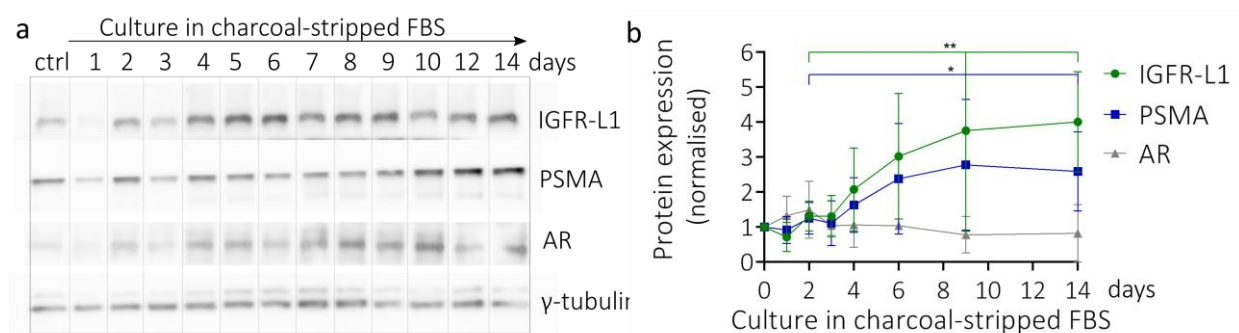


Figure 60: Androgen deprivation of LNCaP cells

WT LNCaP cells were cultured in RPMI1640 medium supplemented with charcoal-stripped FBS for 14 days. The control sample (ctrl) was cultured in RPMI1640 + charcoal-stripped FBS for 14 days, with the addition of 10 nM DHT (a). Band density was quantified, normalised on tubulin and normalised on the control for each experiment ($p=0.0049$ for IGFR-L1 and $p=0.0441$ for PSMA, $n=5$) (b).

As the growth of LNCaP cells is androgen-dependent, we investigated the effect of androgen deprivation on WT LNCaP cells (Figure 60). To this end, LNCaP cells were cultured in medium

supplemented with charcoal-stripped FBS and thereby depleted of steroid hormones for up to 14 days. During the observed time frame, AR expression slightly increased at first, but then dropped to levels below the control conditions. However, this effect was not significant. The expression of IGFR-L1 was significantly increased during androgen deprivation. Interestingly, the dynamics of PSMA upregulation were very similar to IGFR-L1. PSMA is negatively regulated by AR [177]; therefore, this suggests that IGFR-L1 is downregulated by AR signalling.

The increase of IGFR-L1 after androgen deprivation was also observed in immunocytochemistry (Figure 61a). The AR levels decreased overall; however, there were still individual cells with intense AR staining, specifically in the nucleus. As AR is translocated to the nucleus after activation, nuclear AR staining indicates active androgen signalling. Since the cells with strong AR staining also seemed to have high IGFR-L1 levels, we quantified the ratio of nuclear to total AR, depending on the IGFR-L1 fluorescence intensity, in single cells (Figure 61b). There was a significant positive correlation, which suggests that IGFR-L1 might be involved in maintaining AR signalling despite low androgen levels.

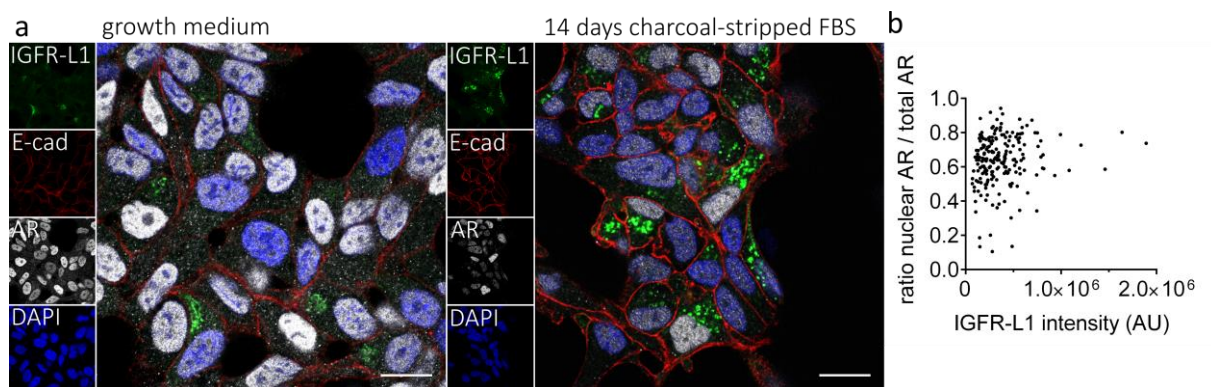


Figure 61: AR activation after androgen deprivation in LNCaP cells

LNCaP cells cultured in normal growth medium or in medium supplemented with charcoal-stripped FBS were stained for IGFR-L1, AR and E-cadherin (scale bar: 20 μ m) (a). The fluorescence intensity of IGFR-L1 and AR (nuclear/total) after 14 days of culture in charcoal-stripped FBS was quantified in >100 cells/n ($n=2$; $p=0.038$ in linear regression model) (b).

2.3.6 Insulin/IGF1 Signalling in Prostate Cancer Cells

2.3.6.1 IGFR-L1 physically interacts with IR and IGF1R

To investigate whether IGFR-L1 is involved in insulin/IGF1 signalling in prostate cancer cells, we analysed the physical interaction of IGFR-L1 with IGF1R and IR (Figure 62). This was done via co-IP in LNCaP cells. IGFR-L1 was successfully pulled down with an IGF1R and IR antibody, while there was no visible band in the control. Interestingly, the IGF1R levels in the input were comparatively low (barely visible next to the IGF1R- and IR-IP). This suggests that the pulldown was very efficient, and thus that a high fraction of IGF1R is bound by IGFR-L1.

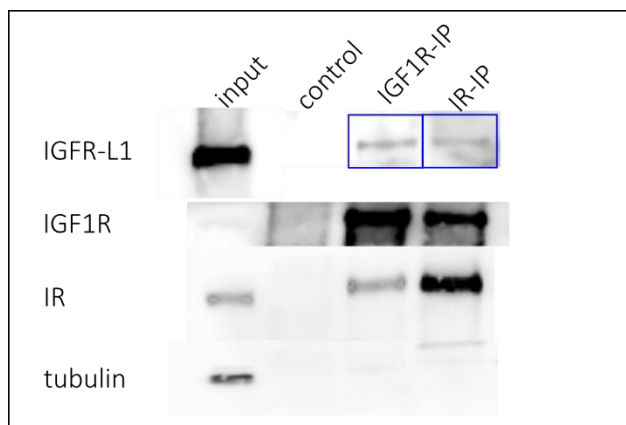


Figure 62: Co-IP of IGF1R/IR and IGFR-L1

The lysate of LNCaP IGFR-L1-Venus cells was incubated with an IGF1R (IGF1R-IP) or IR (IR-IP) antibody attached to magnetic beads, before eluting the beads and performing Western blot to detect IGFR-L1. The control sample contained magnetic beads only. To visualise the total protein levels, 20 µg of crude lysate were loaded (input).

2.3.6.2 Overexpression of IGFR-L1 induces IGF1R activation

Since IGFR-L1 expression in prostate cancer correlates with markers of disease progression (see 2.3.2.3), we analysed the insulin/IGF1 signalling in IGFR-L1-Venus overexpressing LNCaP cells. To this end, the cells were growth factor-depleted by culturing in serum-free medium, before they were stimulated with 10 nM IGF1, insulin or EGF (Figure 63). The levels of IGF1R

were increased in the overexpressing cells, both in serum-free medium and after induction with IGF1. Accordingly, the phosphorylation of IR/IGF1R was significantly increased after IGF1 stimulation. This could not be observed after stimulation with insulin, at a concentration where insulin almost exclusively activates IR [29]. The total levels of EGFR were slightly lower in IGFR-L1 overexpressing cells. The phosphorylation of EGFR was inconsistent. Taken together, these results indicate that IGFR-L1 promotes IGF1R activation, and possibly reduces EGFR levels.

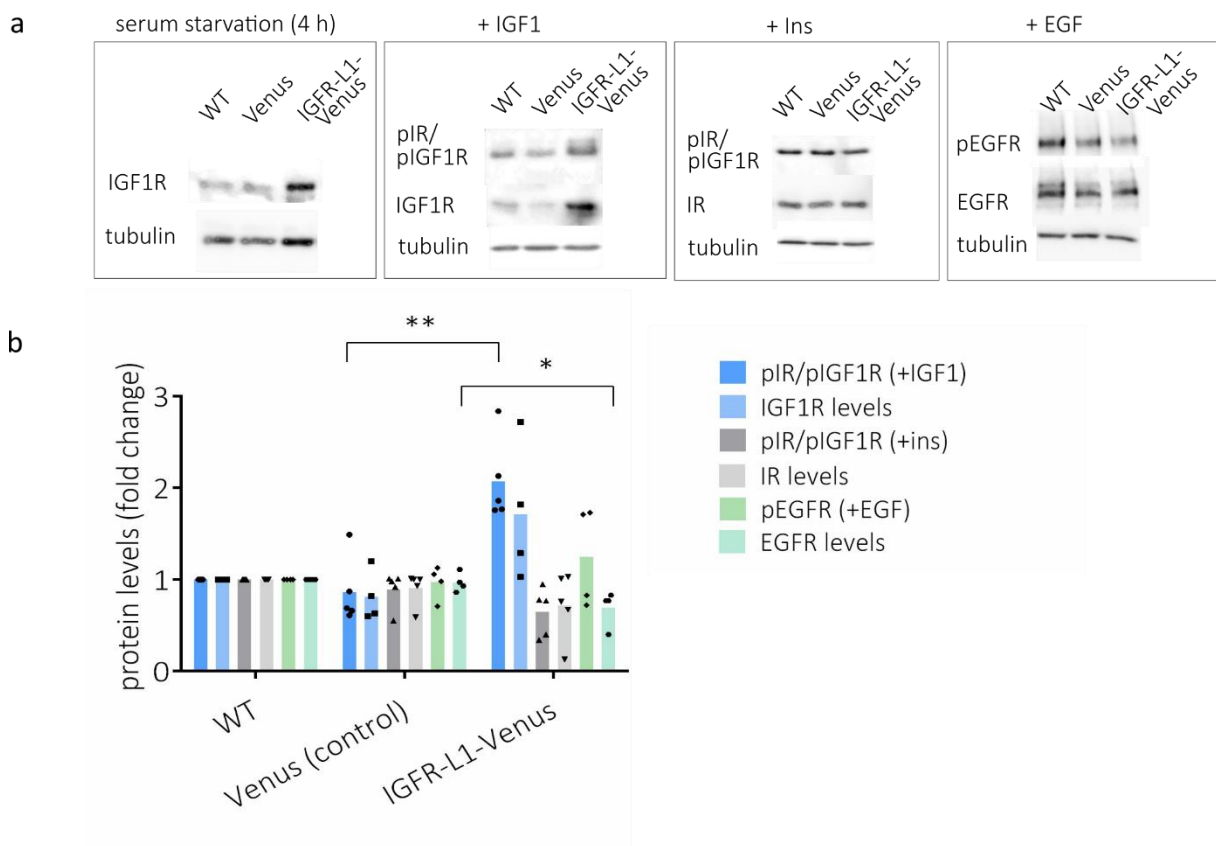


Figure 63: Insulin/IGF1 signalling in LNCaP IGFR-L1-Venus

LNCaP WT, LNCaP IGFR-L1-Venus or LNCaP Venus (control) were cultured in serum-free RPMI1640 for 4 hours and stimulated with 10 nM IGF1, 10 nM insulin or 10 nM EGF for 30 min (a). Band density was quantified and normalised on tubulin and loading control, then normalised on WT ($n=5$; $p=0.064$ for IGF1R, $p=0.001$ for pIR/pIGF1R and $p=0.049$ for EGFR) (b).

2.3.6.3 Insulin is co-internalised with IGFR-L1

To investigate whether IGFR-L1 is involved in the trafficking of RTKs in prostate cancer, we performed an endocytosis assay in LNCaP cells. To this end, the cells were incubated with

fluorescently labelled insulin or EGF, along with an IGFR-L1 antibody (Figure 64). Co-internalisation of the IGFR-L1 antibody was observed with insulin, while there was almost no overlap with EGF. This indicates that insulin is internalised in the same vesicles as IGFR-L1. It should be noted that at the used concentration of 100 nM insulin can bind to IGF1R or IR/IGF1R hybrids [29].

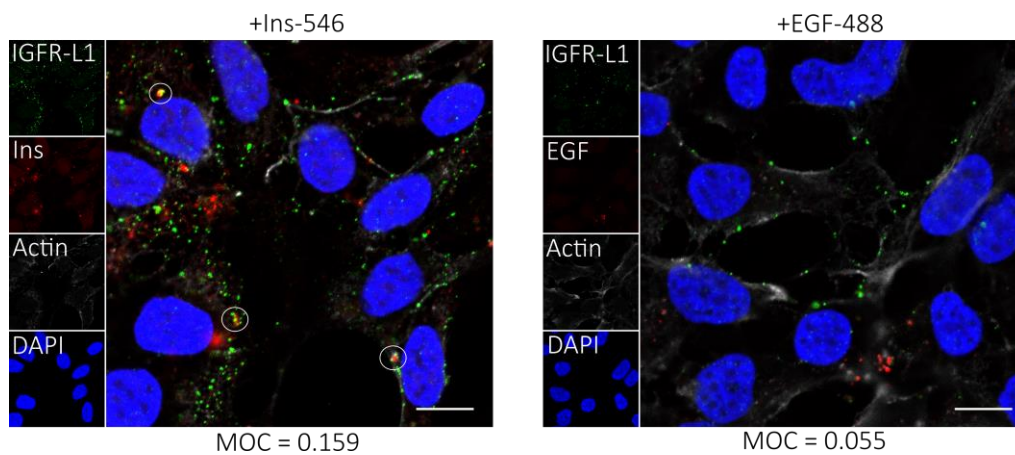


Figure 64: Endocytosis of insulin-546 or EGF-488 in LNCaP

WT LNCaP cells were incubated with 10 $\mu\text{g/ml}$ IGFR-L1 antibody 2G6 along with 100 nM insulin-546 or 1 $\mu\text{g/ml}$ EGF labelled with Alexa Fluor 488 for 60 min. The MOC was calculated from >50 cells/n ($n=3$; $p=0.005$; scale bar: 10 μm).

2.3.6.4 IGFR-L1 overexpression changes the localisation of IGF1R and EGFR

The potential involvement of IGFR-L1 in RTK trafficking was further investigated by co-staining of LNCaP cells with an E-cadherin antibody to mark the cell membrane and an IGF1R, EGFR or IR antibody (Figure 65). Strikingly, the membrane localisation of IGF1R was slightly but significantly increased in IGFR-L1-Venus overexpressing cells. Contrarily, there was slightly less EGFR on the membrane in overexpressing cells, although this effect was not significant. There was no change in IR localisation. This suggests that IGFR-L1 is involved in the trafficking of IGF1R and possibly EGFR.

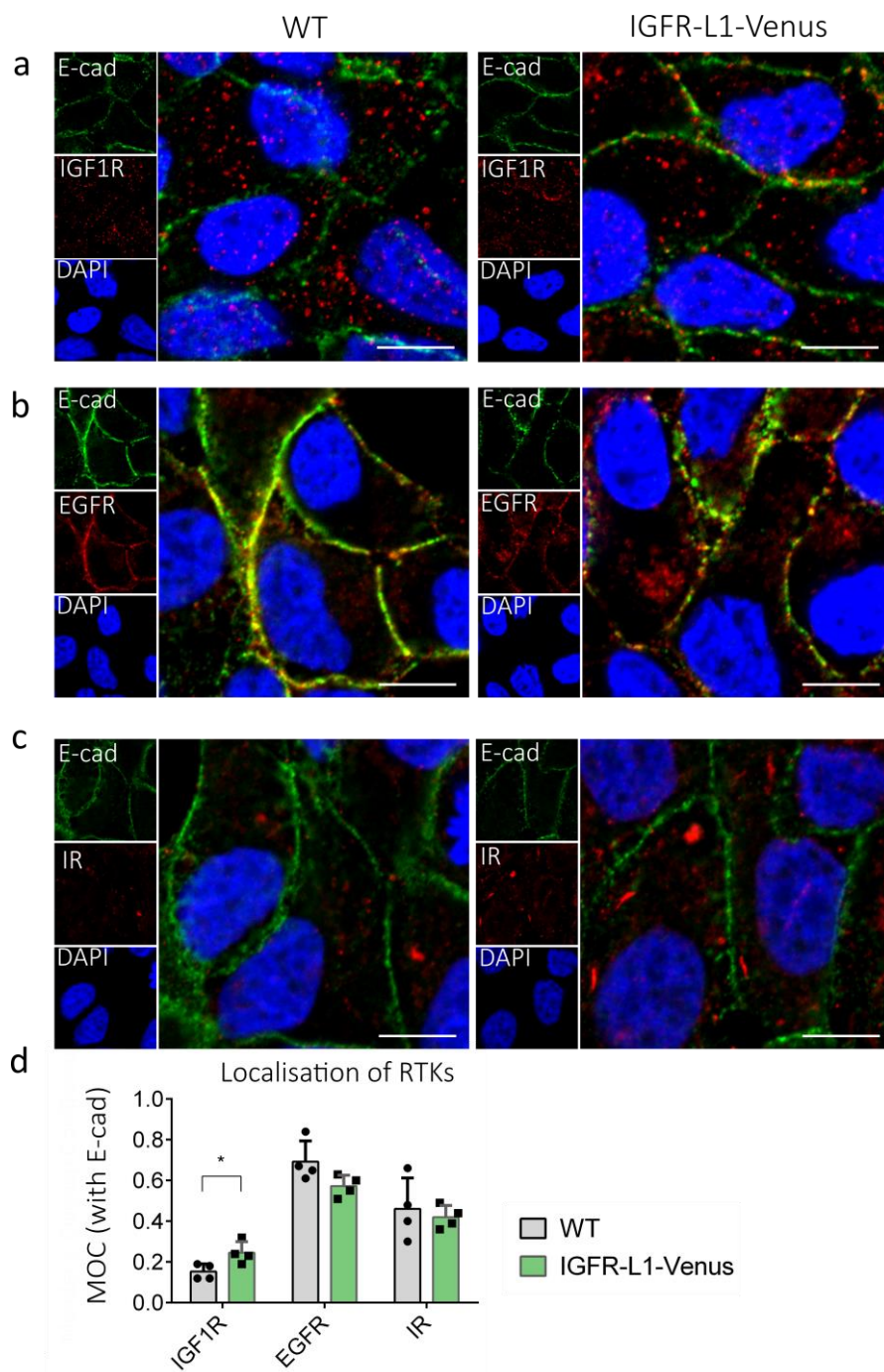


Figure 65: Localisation of RTKs in LNCaP IGFR-L1-Venus

LNCaP IGFR-L1-Venus cells were co-stained for E-cadherin and IGF1R (a) EGFR (b) or IR (c), compared to WT LNCaP cells (scale bar: 10 μ m). The MOC was calculated from >40 cells/n (n=4; p=0.040) (b).

2.3.7 Biodistribution of IGFR-L1 Antibody

2.3.7.1 Radioactive labelling of IGFR-L1 antibody does not diminish functionality

According to publicly available datasets, IGFR-L1 is upregulated in prostate cancer. Based on this, we speculated that IGFR-L1 antibodies might be a useful tool for cancer imaging or drug delivery. Thus, we conducted a proof-of-concept study injecting an IGFR-L1 antibody labelled with the radioactive nuclide ^{125}I into the tail vein of LNCaP xenograft mice. We first selected the most suitable antibody for this purpose by performing an uptake assay in LNCaP (Figure 66a). To this end, LNCaP cells were incubated with all purified IGFR-L1 antibodies and stained with a secondary antibody, to determine the intracellular fluorescence intensity reached by each antibody. The intensity was highest using the antibodies 2G6 or 7E5. As 2G6 was shown to be a very reliable tool in previous assays, we chose 2G6. Next, the uptake dynamics in LNCaP cells were visualised by incubating LNCaP IGFR-L1-Venus cells with fluorescently labelled 2G6 (Figure 66b).

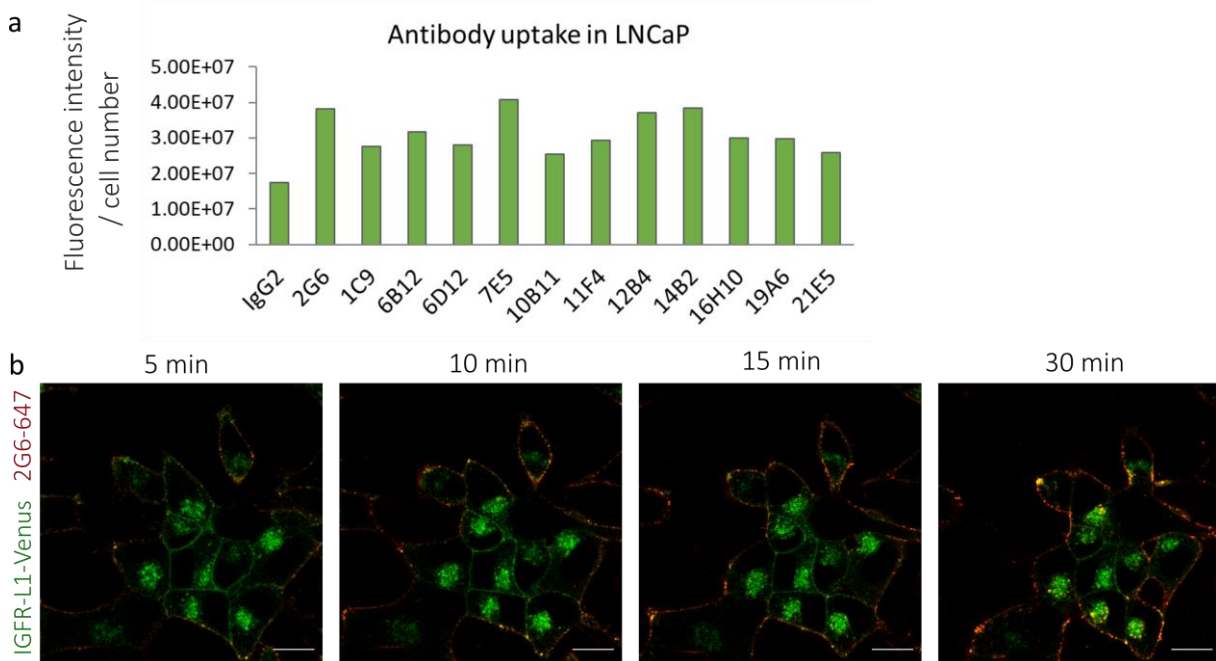


Figure 66: Internalisation assay using purified IGFR-L1 Abs in LNCaP cells

The cells were incubated for 60 min with $10\ \mu\text{g}/\text{ml}$ of the respective antibody, and then stained using an AlexaFluor488 anti rat antibody. The fluorescence intensity was measured and divided by cell number (>100 cells per condition) (a). LNCaP IGFR-L1-Venus cells were incubated with $10\ \mu\text{g}/\text{ml}$ AlexaFluor-647 conjugated antibody 2G6 and observed during progressing internalisation (scale bar: $20\ \mu\text{m}$) (b).

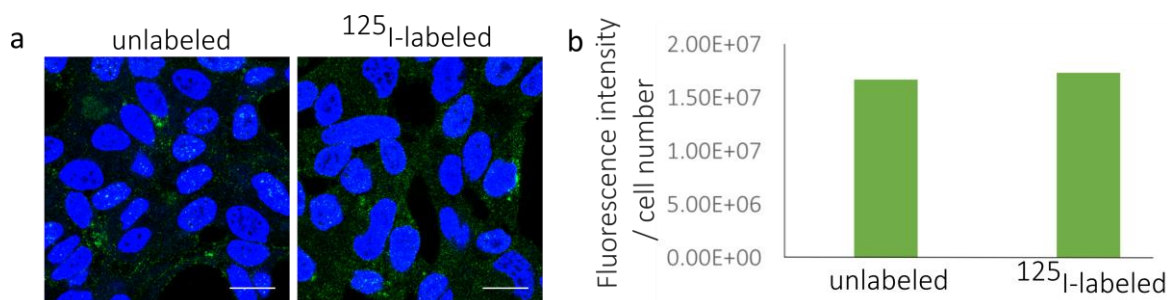


Figure 67: Validation of ¹²⁵I-labelled antibody

The IGFR-L1 antibody 2G6 was labelled with ¹²⁵I and both antibodies were tested on LNCaP cells in immunocytochemistry (scale bar: 20 μm) (a). The fluorescence intensity was measured and divided by cell number (>200 cells) (b).

The antibody was efficiently internalised and showed high colocalisation with IGFR-L1-Venus after 30 minutes. Compared to Min6 cells, the uptake in LNCaP cells seemed to be less, which could be due to generally reduced endocytosis activity.

The antibody was subsequently labelled with ¹²⁵I by M. Konrad from the group of H.J. Wester (Pharmaceutical radiochemistry, Technical University of Munich) according to previously published procedures [178]. The functionality of the labelled antibody was validated via immunocytochemistry (Figure 67). Although the overall intensity was low due to insufficient cell permeabilization prior to staining, there was no difference between the ¹²⁵I-labelled and the unlabelled antibody. This suggests that the ¹²⁵I-labelled antibody is still capable of binding IGFR-L1. However, as the staining intensity was very low, this should be investigated more thoroughly, for instance via binding assays.

2.3.7.2 IGFR-L1 antibody is not specifically accumulated in xenograft tumor

The tail vein injection of ¹²⁵I-labelled 2G6 or the ¹²⁵I-labelled IgG2b isotype control antibody into LNCaP xenograft mice was performed by M. Konrad. After 24 h the mice were sacrificed and all organs of interest were harvested and measured on a gamma counter (Figure 68). Interestingly, there was higher uptake of 2G6 compared to the isotype control in the salivary glands (submandibular and parotid gland) and the stomach, suggesting that the uptake was specific. This is plausible, since the highest expression of IGFR-L1 was found in uterus, stomach

and salivary glands (see 2.3.1.1 IGFR-L1 is expressed in secretory glands). In the tumor, however, the uptake of the isotype control was higher than the 2G6 uptake, showing that the uptake was clearly not specific. It should be noted that a high amount of radioactivity was still in the blood, which suggests that the chosen time point was too short to achieve clearance of the antibody.

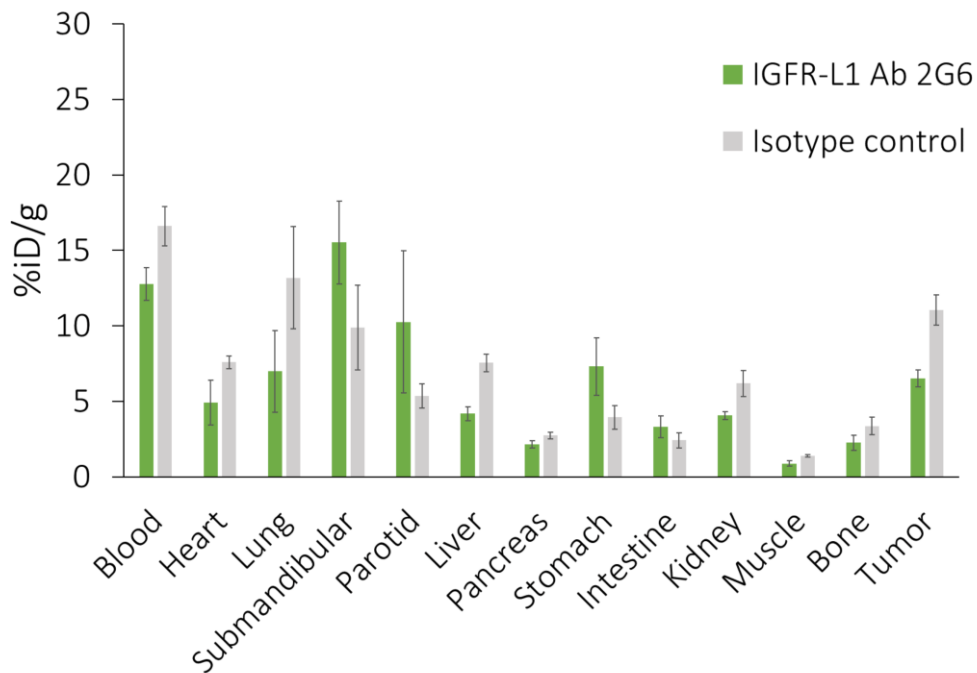


Figure 68: Biodistribution of the ^{125}I -labelled antibody 2G6

Distribution of labelled 2G6 compared to labelled IgG2b isotype control in LNCaP xenograft mice (n=4). Male CB-17 SCID mice were subcutaneously injected with WT LNCaP cells for tumorigenesis, and after 5 weeks the ^{125}I -labelled antibodies were injected into the tail-vein. The mice were sacrificed after 24 h and the organs were measured on a gamma counter. Accumulation of the antibody is shown in % of the injected dose (decay-corrected) per gram of organ weight.

3 Discussion

3.1 Endocytosis and Intracellular Trafficking of IGFR-L1

3.1.1 Endocytosis Pathways of IGFR-L1

The aim of this thesis was to elucidate the function of IGFR-L1 in insulin signalling of pancreatic β -cells and cancer cells. To resolve the mechanism of IGFR-L1 in insulin/IGF1 signalling, a clear understanding of the involved endocytosis pathways is crucial. The cytoplasmic tail of IGFR-L1 contains a recognition sequence for the adaptor protein AP2, which facilitates clathrin-mediated endocytosis by binding to cargo proteins and clathrin, thereby assembling to a scaffold for endocytic vesicles [42]. The mutant construct IGFR-L1-AP2*-Venus was unable to bind AP2 and thus accumulated on the cytoplasmic membrane. Further, the mutant construct showed less localisation to the Golgi region, which demonstrates that along with endocytosis, transport to the Golgi complex is also disrupted. Budding of clathrin-coated vesicles from the trans-Golgi is mainly mediated by AP1 binding [25], which is assumed not to be affected by the mutation. Thus, it is conceivable that the balance between transport to and from the trans-Golgi is skewed, resulting in less accumulation of IGFR-L1-AP2*-Venus in the Golgi complex.

Similar results were obtained by incubating Min6 cells expressing IGFR-L1-Venus with the dynamin inhibitor dynasore. Dynamin is an important factor in clathrin-mediated endocytosis. It was shown that dynamin is necessary for the release of fully formed clathrin-coated pits. Dynasore blocks the enzymatic activity of dynamin, and thereby interferes with the pinching of clathrin-coated pits [179]. Thus, these results confirm that IGFR-L1 is internalised via clathrin-mediated endocytosis. Since endocytosis was not completely blocked in both experiments, it is likely that IGFR-L1 can additionally be internalised via clathrin-independent mechanisms.

Although clathrin-mediated endocytosis is the classical pathway for IR internalisation, there is evidence that clathrin-independent internalisation has an important role. It was revealed that IR-A is internalised through clathrin-dependent and independent pathways, although only clathrin-mediated endocytosis directs IR-A towards lysosomal degradation [180]. In adipocytes, it was demonstrated that IR is rapidly internalised in caveolae and that insulin internalisation cannot be blocked by inhibitors of clathrin-mediated endocytosis. This suggests

that caveolin-dependent endocytosis is the preferred pathway of IR internalisation in this cell type, particularly in early phases of insulin signalling [181]. In endothelial cells, it was shown that insulin is transcytosed in caveolae to facilitate insulin signalling in interstitial muscle fibers [182]. So far, a potential involvement of IGFR-L1 in transcytosis remains to be investigated.

Endocytosis is a crucial mechanism for signalling depletion. One method of endocytic signal depletion is dissociation of IR and IGF1R from their ligands and transport to the lysosome for degradation. Another route, specific to IGF2, is the scavenging of excess IGF2 from the plasma membrane by IGF2R. However, internalisation of RTKs does not inevitably lead to signalling attenuation, as ligand-receptor complexes can be sustained in signalling endosomes [183]. It was suggested that prolonged association of IR and IGF1R with their ligands favours mitogenic signalling over metabolic signalling, since slow-dissociating insulin analogues led to stimulation of mitogenic pathways [184, 185]. Furthermore, the endocytosis dynamics of IR can be ligand-dependent. Specifically, it was shown that binding of IGF2 to IR-A decelerates internalisation and thus sustains the downstream stimulus, compared to insulin binding to IR-A [180]. In the case of IGF1R and EGFR, it is known that a large fraction of active receptors is retained in early endosomes [186]. In contrast, endosomal signalling seems to have a less important role in insulin signalling, as it was demonstrated that insulin-IR-complexes dissociate rapidly, mainly in early endosomes [168]. The IR system even contains a specific mechanism to decrease endosomal signalling, in the form of a pH-sensitive insulinase [187].

Whether receptors are sorted towards the lysosome or towards recycling endosomes after endocytosis is determined by their ubiquitination status and thus by the presence of ubiquitin ligases [188]. Receptors that are lysine-63-polyubiquitinated bind to ESCRT for lysosomal transport. There are different potential mechanisms by which ESCRT regulates intracellular signalling: by rapid sequestering of receptors into MVBs or by retaining receptors in endosomes for a prolonged period, thereby sustaining signalling. It has been suggested that the preferred mechanism could be cell-type dependent [189]. Thus, it is plausible that the expression levels of IGFR-L1 could be one of the factors determining the fate of receptors sorted by ESCRT. This could explain the seemingly contradictory effects of IGFR-L1 knockout and overexpression. To investigate the potential involvement of IGFR-L1 in receptor sorting,

the lysosomal transport of RTKs should be tracked in pulse-chase experiments, and the influence of IGFR-L1 knockout or overexpression on lysosomal trafficking should be analysed.

3.1.2 Regulation of Insulin/IGF1 signalling

Due to the domain structure of IGFR-L1 and the hyperinsulinemic and hypoglycemic phenotype of *Igfr-L1* KO mice, we hypothesised that IGFR-L1 desensitises insulin signalling in β -cells [170]. We provided evidence that IGFR-L1 is in close proximity to IR. For instance, IGFR-L1-Venus showed a high degree of colocalisation with IR-A-RFP and IR-B-RFP, although the overlap with IR-B-RFP was slightly higher compared to IR-A-RFP on the cytoplasmic membrane. To determine if IGFR-L1 preferentially interacts with IR-B, more extensive research is required. To begin with, the co-immunoprecipitation of IGFR-L1-Venus with IR-A-RFP or IR-B-RFP needs further optimisation, to make it suitable for quantitative analysis. However, results obtained in cell lines overexpressing both proteins simultaneously should be handled with caution, as the high intracellular concentration of both proteins can lead to artificial binding. In addition, we have shown in live cell imaging that insulin was internalised via the same vesicles as IGFR-L1, which is another indication that IGFR-L1 is in close proximity to IR.

Accordingly, the uptake kinetics of insulin were delayed in *Igfr-L1* knockout cells, suggesting a direct involvement of IGFR-L1 in insulin endocytosis. The fluorescently labelled insulin-546 used in these experiments was conjugated via azide-alkyne click chemistry, where insulin was chemically modified at a single residue. Similar labelling strategies were applied to other proteins, which did not lose their biological activity or change their 3D structure after the labelling procedure [190, 191]. Therefore, we assume that the fluorescent label does not change the endocytic behaviour of insulin.

Further, we have shown that overexpression of IGFR-L1 in Min6 cells increased IGF1R levels, and consistently increased the phosphorylation of IR/IGF1R. This indicates that, in addition to regulating IR trafficking, IGFR-L1 is also involved in IGF1R trafficking. One explanation for the observed increase of IGF1R in IGFR-L1 overexpressing cells is that high levels of IGFR-L1 might lead to enhanced recycling of IGF1R. It has to be taken into account that, in many experiments,

insulin and IGF1 signalling cannot be accurately separated for several reasons. First, insulin can function as a ligand for IGF1R at higher concentrations [29]. Second, the antibody used to detect the active phosphorylated receptors in this study recognises both the tyrosine phosphorylation site 1135/1136 of IGF1R and the tyrosine 1150/1151 phosphorylation of IR. None of the currently available commercial antibodies were able to distinguish between both receptors. Third, it is possible that during the co-immunoprecipitation, IR/IGF1R hybrids are pulled down. Due to the complex interactions of IR and IGF1R, we anticipate that IGFR-L1 is involved in the regulation of both insulin and IGF1 signalling.

There is evidence that IR is less abundant on the cytoplasmic membrane in diabetes patients. On this basis, it has been proposed that the rate of IR endocytosis, which is determined by various IR binding proteins, is an essential factor in the development of insulin resistance [192]. This is also reflected in mutated IR, which is occasionally found in patients with severe hyperinsulinemia. Some of these mutants have been observed in either increased or reduced levels at the plasma membrane, suggesting impaired endocytosis. Other mutants remain in the ER/Golgi after synthesis, indicating a defect in maturation or subsequent transport towards the plasma membrane [193]. Taken together, this shows that trafficking of IR is crucial to maintain normal insulin signalling.

It is known that feedback mechanisms are crucial for the regulation of insulin signalling. For instance, it was shown that activated mTOR changes the phosphorylation pattern of IRS proteins and thereby reduces insulin signalling in adipocytes [194, 195]. We propose that IGFR-L1 regulates insulin signalling in β -cells as an additional feedback mechanism, to prevent autocrine stimulation by newly released insulin. Attenuation of insulin signalling in β -cells is highly relevant, as it was shown that β -cell-specific insulin resistance can contribute to T2D [196, 197].

3.1.3 Model of IGFR-L1 Trafficking

In this study, we demonstrate that IGFR-L1 is localised at the plasma membrane, in the endosomal-lysosomal system and in Golgi cisternae. Live cell imaging showed that IGFR-L1 antibodies are rapidly internalised from the cytoplasmic membrane and transported to intracellular structures, such as Golgi/ER, where the antibodies were partially retained for several days. The labelled antibodies colocalised with the fusion protein IGFR-L1-Venus in live cell imaging. Thus, we conclude that IGFR-L1 circulates between these compartments and is involved in the sorting of signalling receptors.

Starvation of Min6 cells affected the trafficking of IGFR-L1-Venus, resulting in higher accumulation in the Golgi complex. This could be a consequence of decreased growth factor signalling, leading to less IGFR-L1 needed at the plasma membrane and in endosomes. The Golgi complex, in this context, could serve as a reservoir. It was shown that the trans-Golgi contains a storage pool of IGF2R [198], thus it seems plausible that IGFR-L1 shows similar behaviour. In addition, IGFR-L1 could play a role in protein sorting from the trans-Golgi network, where misfolded proteins are directed towards endosomes for subsequent lysosomal degradation.

Taken together, the close proximity of IGFR-L1 to IR and the modulation of insulin/IGF1 signalling in IGFR-L1 knockout and overexpressing cells indicate that IGFR-L1 regulates the endocytosis of IR and/or IGF1R. IGFR-L1 is predestined for lysosomal transport, since it contains a M6PR domain. Further, we observed overlap between insulin, IGFR-L1-Venus and a lysosomal marker, and we showed that the overlap was less in IGFR-L1-AP2*-Venus expressing cells. Thus, we hypothesise that IGFR-L1 is involved in the sorting of IR/IGF1R towards the lysosome.

In secretory cells, intraluminal vesicles within MVBs can be secreted as exosomes, after fusion of the MVB with the plasma membrane [199]. Interestingly, it was shown that many proteins secreted by the prostate epithelium are packaged into exosomes, which can regulate various sperm cell functions. In addition, it was proposed that they have immune-modulatory effects and promote prostate cancer survival [200]. Taken together with the expression of IGFR-L1 in secretory cells, such as β -cells and luminal prostate cells, it seems likely that IGFR-L1 has an

additional role in secretion, possibly via exosomes. Further experiments are necessary to investigate this hypothesis.

In addition, it is likely that a fraction of IGFR-L1, along with IR and IGF1R as its cargo, is recycled back to the plasma membrane. As the fate of RTKs after endocytosis is mainly dependent on ubiquitination, and thus interaction with ubiquitin ligases, it is possible that the preferred pathway is cell-type dependent.

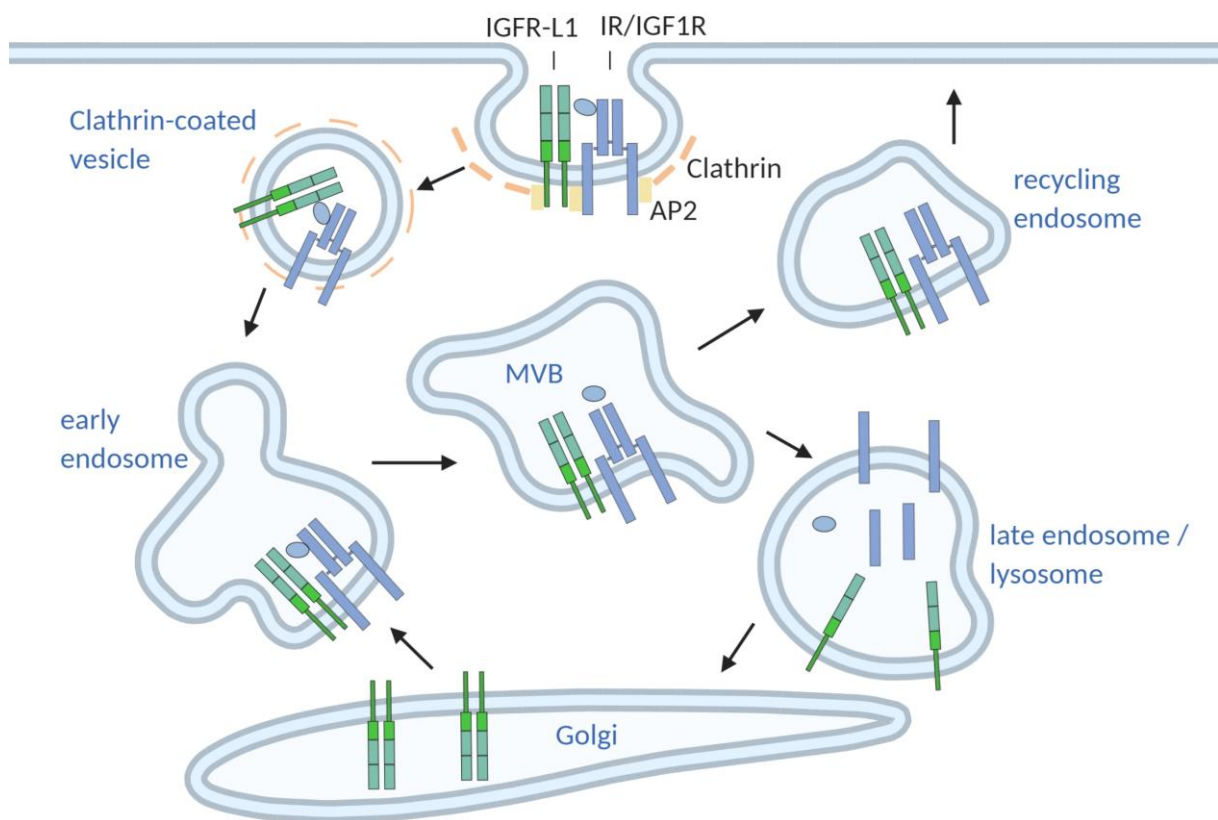


Figure 69: Current model of the mechanistic function of IGFR-L1

We hypothesise that IGFR-L1 modulates the clathrin-mediated endocytosis of IR/IGF1R via direct or indirect interaction. The receptors are then transported towards the endosomal/lysosomal system. It is possible that IGFR-L1 additionally has a function in recycling of IR/IGF1R. The main pool of IGFR-L1 is located in the Golgi complex, which likely serves as a reservoir. Created with BioRender.com.

3.2 The Role of IGFR-L1 in Cancer

3.2.1 IGFR-L1 in Benign Tissues

In addition to the pancreas, IGFR-L1 is highly expressed in female reproductive organs (uterus, breast tissue and fallopian tube), male tissues (prostate and testis) and the gastrointestinal tract. As all these organs are exocrine glands, it is possible that IGFR-L1 has a role in secretion. In addition, IGFR-L1 is expressed in the pituitary gland. Taken together with the high levels in female and male tissues, this points to a potential involvement of IGFR-L1 in the hypothalamus-pituitary-gonadal axis. The hypothalamus produces gonadotropin-releasing hormone (GnRH), which induces the release of luteinizing hormone and follicle stimulating hormone from the pituitary gland. These factors subsequently regulate the production of estradiol in the ovaries and the production of testosterone in the testes. Regulation of the hypothalamus-pituitary-gonadal axis relies heavily on feedback mechanisms that are mainly mediated by kisspeptin, but also other hormones such as leptin and adiponectin [201].

We have shown that in the murine prostate epithelium, IGFR-L1 is expressed in luminal cells and intermediate cells, both of which have secretory functions. Furthermore, there was no expression in basal cells. Although it is commonly anticipated that basal cells are responsible for regeneration of the prostate epithelium, there is evidence that luminal cells can differentiate into a fully functional epithelium *in vitro* [202]. In this context, it should be noted that luminal cells are the main cells of origin for prostate cancer development [203].

The function of neuroendocrine cells in the prostate epithelium is not fully understood. It was shown that there are specific subtypes of neuroendocrine cells expressing different neurosecretory peptides, including chromogranin A and B, serotonin, calcitonin peptides and somatostatin. Similar to neuroendocrine cells in other tissues, it is anticipated that prostate neuroendocrine cells regulate secretion, differentiation and proliferation of the epithelium [204]. Our research showed that only few neuroendocrine cells displayed weak IGFR-L1 expression, while others were conclusively negative for IGFR-L1. Thus, it is conceivable that only specific neuroendocrine subtypes express IGFR-L1. Due to the importance of secretory cells in both the pancreas and the prostate, the potential role of IGFR-L1 should be

further investigated by assessing the activity of secretory pathways in IGFR-L1 knockout or overexpressing cells.

In our inducible Igfr-L1 KO model, there was no apparent difference in AR expression or localisation between IGFR-L1 WT and KO cells in the prostate epithelium. Moreover, analysis of polarity markers did not show any differences in epithelial organisation. Interestingly, the proliferation of the prostate epithelium seemed to be higher in Igfr-L1 KO mice, although further experiments are needed to confirm this result. Nonetheless, it would be compatible with the results obtained in pancreata of E16.5 embryonic mice, where we showed that endocrine cell proliferation is markedly increased in the Igfr-L1 KO mice [170]. We assume that increased proliferation in Igfr-L1 KO cells occurs due to enhanced insulin/IGF1 signalling.

3.2.2 Expression of IGFR-L1 in Cancer

According to publicly available datasets, IGFR-L1 is downregulated in pancreatic cancer. This is consistent with a report showing that pancreatic neuroendocrine tumors with favourable prognosis express higher IGFR-L1 levels, compared to more advanced tumors [164].

Conversely, overall IGFR-L1 expression is upregulated in ovarian cancer, endometrial cancer and breast cancer. Interestingly, IGFR-L1 expression seems to differ among the subtypes of female cancers. Initially, it was found that IGFR-L1 was induced by estrogen replacement therapy in endometrial carcinoma and that IGFR-L1 expression declined with increasing tumor grade. However, the expression was still higher in grade 3 endometrial carcinoma compared to benign tissue [162]. *In vitro*, it was shown that IGFR-L1 promoted endometrial tumor growth and was associated with autophagy [205].

In ovarian cancer subtypes, IGFR-L1 was higher in endometrioid ovarian carcinoma compared to high-grade serous ovarian carcinoma and clear cell carcinoma [206, 207]. However, it was demonstrated that high IGFR-L1 levels in high-grade serous ovarian carcinoma predicted shorter survival [165]. In breast cancer, it was found that hormone-receptor positive tumors showed higher IGFR-L1 overexpression [208]. Based on these results, it was suggested that IGFR-L1 could be used as a prognostic marker to identify tumors with active hormone signalling and thus to select personalised treatment options [209].

Mutation and amplification of oncogenes, as well as deletion of tumor suppressor genes, is a common mechanism of cancer development and progression. The most prominent oncogene in prostate cancer is AR. Gene duplications and mutations towards hypersensitive AR variants facilitate tumor growth, particularly in androgen-deficient conditions [117]. Further, PI3K is frequently mutated in many cancer types, including prostate cancer, as it is a master regulator of metabolic and proliferative pathways. Specifically in androgen-independent tumors, the PI3K pathway is crucial for cancer survival. In addition to the proliferative function of PI3K/Akt signalling, it was shown that Akt can cross-activate AR [125]. Since PI3K/Akt signalling is activated by RTKs, the high amplification rates of IR, IGF1R and EGFR are consistent with this rationale. The alteration frequency of IGFR-L1 is in a similar range, indicating that it might be equally important for tumor growth. Consistently, *IGFR-L1* mutations co-occur with mutations of *AR* and with mutations of RTK signalling components. This suggests that dedifferentiated tumors, which have high mutation rates of various oncogenes, gain an additional selective advantage through mutation of IGFR-L1.

The expression level of *IGFR-L1* correlates with the expression of *AR* according to publicly available data. Further, it is positively correlated to the AR-regulated genes *PSA* and *PSMA*, which are known hallmarks of disease progression [210, 211]. This suggests that IGFR-L1 expression is linked to the androgen status of the tumor. In addition, *IGFR-L1* is correlated to *IR*, *IGF1R* and *EGFR*, which again points to an upregulation of IGFR-L1 in tumors that switched to alternative proliferative pathways rather than canonical AR signalling. In summary, IGFR-L1 is differentially expressed in various cancers, and correlates with tumor progression in prostate cancer.

3.2.3 Cell line Development for Cancer Research

For functional analysis of IGFR-L1 in cancer cells, we attempted CRISPR/Cas9-mediated deletion in LNCaP and MCF7 cells. The CRISPR/Cas9 technique is a powerful tool for genome editing. Naturally occurring CRISPR systems are immune mechanisms used by bacteria as a response to foreign DNA. Thereby the foreign DNA is cleaved by the Cas9 nuclease, after

hybridisation with the transactivating CRISPR RNA (tracrRNA). In mammalian cells, the Cas9 nuclease can be introduced by exogenous expression, along with single guide RNAs (sgRNA), which hybridise with the gene of interest and direct the nuclease to a specific cleavage site [212].

To date, there are only two publications on successful CRISPR/Cas9 knockout in LNCaP cells. In the first one, a similar approach as in this work was used to delete FOXA1 [213]. However, the authors do not show complete knockout, but only a downregulation of FOXA1 in several clones, without providing a mechanistic explanation. The second one aimed at targeted deletion of AR in LNCaP cells [214]. To this end, they delivered Cas9 and three different sgRNAs using lentiviruses and performed experiments two days after transduction on the resulting mixed clones. As a result of differential transduction efficiencies, they observed partial knockout. While they detected effects on cell proliferation, they conceded that the transduction itself might influence the proliferation and thus the method has limitations.

Generally, it seems that researchers working with cancer cell lines preferentially use knock-down strategies via RNA interference. One reason for this is undoubtedly the fact that cancer cells show a very high degree of genetic abnormalities such as chromosomal rearrangements, polyploidy, gene fusions or gene duplications [215]. It was shown that LNCaP cells are already tetraploid at early passages, and that they acquire additional structural rearrangements during prolonged culture [216]. It is conceivable that IGFR-L1 might be among the genes that are amplified in LNCaP, which complicates CRISPR/Cas9-targeting approaches. Therefore, alternative strategies, such as RNA interference, should be explored.

3.2.4 Regulation of IGFR-L1

As previously mentioned, IGFR-L1 is most highly expressed in female and male tissues, which indicates a potential association to reproductive hormone signalling. We showed that IGFR-L1 is likely induced by β -estradiol, as already implicated when it was first discovered in endometrial carcinoma and termed estrogen-inducible gene (EIG121) [162].

IGFR-L1 was more highly expressed in the androgen-dependent cell lines LNCaP and MDA Pca 2b compared to the androgen-independent cell lines LNCaP C4-2 and PC3, which

suggests that IGFR-L1 is linked to the androgen status of cancer cells. Stimulation of LNCaP cells with DHT did not show an effect on IGFR-L1 expression. However, the experimental conditions could be further optimised. For instance, IGF1 as an additive might modify the effect of DHT on IGFR-L1, as it was previously shown that IGF1 amplifies AR activation by DHT [125].

Androgen-deprivation of LNCaP cells by culture with charcoal-stripped FBS leads to upregulation of IGFR-L1. The levels of the androgen-regulated protein PSMA increase during a similar time frame. PSMA is an enzyme with hydrolase and peptidase function, which likely has metabolic benefits for the cancer cell. It is known that PSMA is significantly overexpressed in prostate cancer and increases with cancer progression [217]. PSMA is negatively regulated by AR, presumably due to downregulation of the PSMA enhancer PSME through activated AR [177]. In addition, studies have shown that PSMA is increased after androgen-deprivation of prostate cancer patients [218, 219]. Based on the similar change in expression after androgen-deprivation in LNCaP cells, we hypothesise that IGFR-L1, like PSMA, is androgen-regulated. Due to the highly connected estrogen and androgen signalling pathways, it is conceivable that this regulation is indirect and mediated via estrogen.

After culture of LNCaP cells in charcoal-stripped FBS for 14 days, the ratio of nuclear AR to total AR correlated with IGFR-L1 expression levels. It is known that androgen deprivation induces differentiation of LNCaP towards a more aggressive neuroendocrine cancer-like cell type [220]. Thus, this indicates that IGFR-L1 could be involved in maintaining cell growth in androgen-deficient conditions. There are contradictory reports on AR expression after culture in charcoal-stripped FBS. While the first report attempting androgen deprivation of LNCaP cells demonstrated AR downregulation [220], others have shown AR upregulation [221, 222]. In this study, AR levels seemed to slightly increase at first, then decline to slightly lower levels compared to growth conditions. It is conceivable that AR expression changes during the transition from androgen-dependent to androgen-independent growth. In summary, we showed that IGFR-L1 expression relies on reproductive hormone signalling in cancer cells.

3.2.5 Function of IGFR-L1 in Prostate Cancer

To elucidate the function of IGFR-L1 in prostate cancer cells, we analysed the implications of IGFR-L1 in RTK signalling. We previously established that in β -cells IGFR-L1 is involved in the intracellular trafficking of IR and IGF1R. In prostate cancer cells overexpressing IGFR-L1, we showed that IGF1R levels, along with IGF1R activation, are markedly increased. In contrast, the expression levels of EGFR are slightly but significantly decreased. It is therefore possible that IGFR-L1 is additionally involved in the trafficking of EGFR.

The localisation of IGF1R and EGFR was altered in IGFR-L1 overexpressing cells, compared to WT LNCaP cells. IGF1R was more localised to the membrane in IGFR-L1 overexpressing cells, which might go along with decreased lysosomal degradation of IGF1R and/or increased recycling to the plasma membrane. This rationale is consistent with the observed increased IGF1R levels. Vice versa, less EGFR was localised to the membrane in IGFR-L1 overexpressing cells. Together with decreased EGFR levels, this suggests higher rates of lysosomal degradation.

In addition, we demonstrated that insulin is internalised in IGFR-L1-containing vesicles. Notably, insulin can bind to IGF1R with a half maximal binding value of 30 nM [29], which means that at the concentration used in our endocytosis assay (100 nM), it activates IGF1R in addition to IR. Further, insulin potently binds IR/IGF1R hybrid receptors with a similar affinity as IR-A or IR-B homodimers (around 1 nM half maximal binding) [29]. LNCaP cells express similar levels of IR and IGF1R in normal growth conditions, according to publicly available RNA data [223]. It is therefore likely that a large fraction of IR and IGF1R are present as hybrid receptors. The anticipated co-internalisation of IGFR-L1 and IGF1R in prostate cancer cells strengthens the hypothesis of IGFR-L1-dependent sorting of IGF1R.

Conversely, we did not observe overlap of IGFR-L1 and EGF in our endocytosis assay. Since EGF is bound exclusively by EGFR [224], it is possible that uptake of EGF is a rare event in LNCaP cells under growth conditions, and thus no overlap could be observed. Another possibility could be that interaction of IGFR-L1 and EGFR occurs only in the non-ligand-bound state. Further studies are needed to verify if IGFR-L1 interacts with EGFR. This would be a prerequisite for determining whether IGFR-L1 is involved in EGFR trafficking. It was speculated

before that IGFR-L1 might regulate the degradation of EGFR in breast cancer [208], although a mechanistic explanation was not provided. As we showed that EGFR is downregulated, but IGF1R is upregulated in IGFR-L1 overexpressing cells, it is possible that EGFR is downregulated upon increased IGF1R activation, via negative feedback loops.

The proliferation of LNCaP cells was not affected by overexpression of IGFR-L1. When considering the results obtained from Igfr-L1 KO mouse prostate epithelium and embryonic mouse pancreata [170], it would rather be expected that IGFR-L1 overexpression decreases proliferation. However, this is not consistent with the upregulation of IGFR-L1 in human prostate cancer. Moreover, IGFR-L1 overexpression increased IGF1 signalling in prostate cancer cells, and it is known that insulin/IGF1 signalling can propagate mitogenic effects [79]. We propose that IGFR-L1 has differential effects depending on the cellular context, which would explain the upregulation in some cancer types versus downregulation in others. For instance, it is possible that the observed decrease of EGFR in IGFR-L1 overexpressing LNCaP cells balances the increase of IGF1R levels.

Moreover, IGFR-L1 overexpression significantly increased the migration of LNCaP cells. This was assessed in a 3D spheroid invasion assay, as it is the closest approximation to *in vivo* tumor dissemination. Multicellular spheroids closely mimic solid tumors, while embedding in a collagen matrix is a surrogate for the ECM invaded by cancer cells *in vivo* [225]. It is known that migration of cancer cells can be induced via IGF1 [90, 226, 227]. Thus, it is conceivable that IGFR-L1 acts via IGF1R to preferentially activate migration rather than proliferation.

The IGF2R, which is structurally related to IGFR-L1, has a dual function in carcinogenesis. On the one hand, it is responsible for the degradation of IGF2, thus preventing IGF2 from activating IGF1R or IR-A. On the other hand, IGF2R has other ligands that might have differential effects. These include retinoic acid and multiple M6P-conjugated ligands, including leukaemia inhibitory factor (a regulator of cell differentiation) and cathepsin D (a lysosomal enzyme associated with cancer cell proliferation) [228]. Generally, IGF2R is considered a tumor suppressor, as studies have reported loss of heterozygosity in various cancers, including breast cancer, ovarian cancer and lung cancer [228]. In cervical cancer, however, IGF2R was upregulated and led to reduced apoptosis, likely due to its role in lysosomal degradation of misfolded proteins [229]. In prostate cancer, IGF2R was lost in 40 % of the analysed patients [230]. It was demonstrated that PC3 cells overexpressing IGF2R proliferate less, which

is consistent with lower IGF2 signalling via IGF1R. However, PC3 cells expressing a mutant IGF2R unable to bind IGF2 showed higher proliferation, as did LNCaP cells expressing either mutant or WT IGF2R. The authors speculated that the M6P binding function of IGF2R has a proliferative effect, opposing the antiproliferative effect of IGF2 binding, which is more pronounced in PC3 compared to LNCaP cells [231]. This is an interesting concept that might similarly apply to IGFR-L1, as we observed seemingly contradictory roles of IGFR-L1 depending on the cellular context. Further research is required to investigate this possibility.

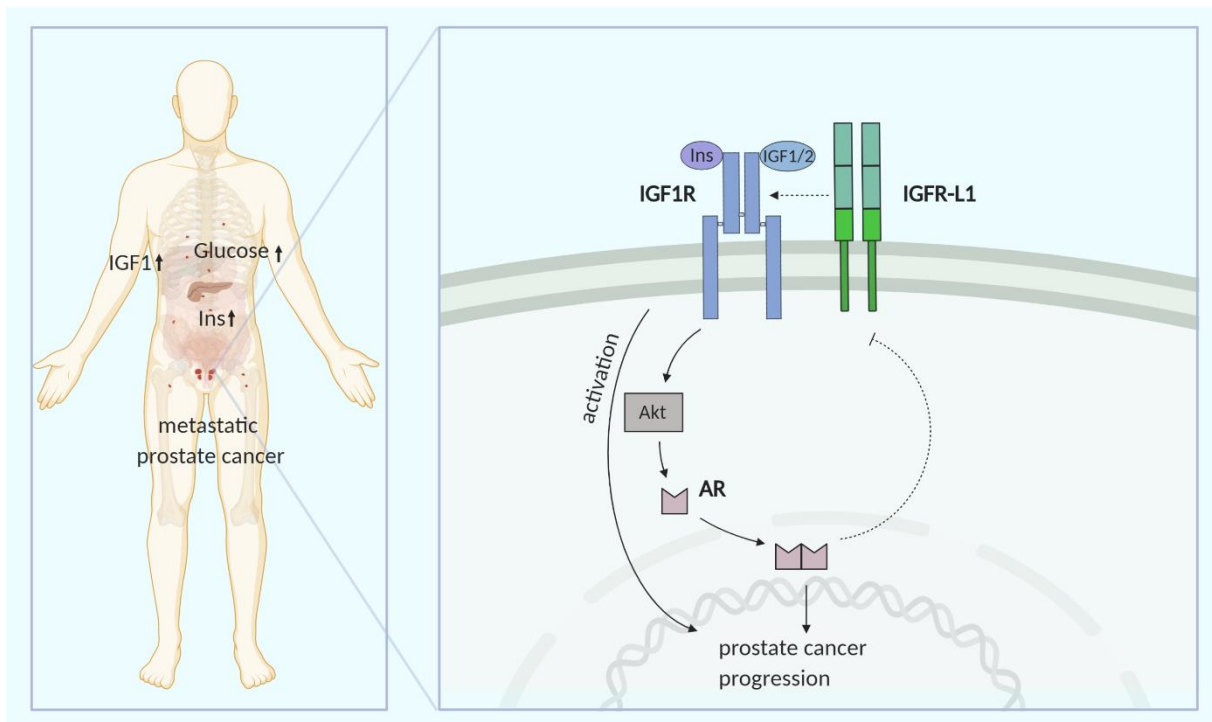


Figure 70: Hypothetical model of IGFR-L1 function in prostate cancer

Diabetics have an increased risk for metastatic prostate cancer, presumably due to elevated serum insulin and IGF1 levels. It is known that IGF1R can cross-activate AR, even in absence of androgens. We hypothesise that IGFR-L1 enhances IGF1R activation, and thereby promotes prostate cancer progression. Our results suggest that IGFR-L1 is negatively regulated by AR via negative feedback regulation. Created with BioRender.com.

3.2.6 Biodistribution

We propose that IGFR-L1 is upregulated during the course of prostate cancer progression. Thus, we investigated the potential use of IGFR-L1 as a diagnostic marker. We showed that IGFR-L1 antibodies are internalised into prostate cancer cells and they can be labelled with ^{125}I without loss of function. Due to its long half life, ^{125}I is well suited for proof-of-concept studies. In addition, the straightforward labelling of proteins is an advantage over other radionuclides, as all aromatic amino acids unspecifically react with iodine. However, ^{125}I is not commonly used for imaging, as it does not emit positrons and therefore is not detectable via positron emission tomography (PET). It can be detected via single photon emission computed tomography (SPECT); however, this technique provides low spatial resolution. Suitable radionuclides for PET imaging include ^{18}F , ^{11}C or ^{68}Ga [232]. Thus, for a potential clinical use of radioactive labelled IGFR-L1 antibodies, alternative conjugation strategies should be explored.

Our biodistribution experiment showed no specific uptake of the IGFR-L1 antibody in the tumor; remarkably, the uptake of the isotype control antibody was higher. It is possible that slightly higher amounts of the isotype control were injected, since tail vein injection is technically challenging. Interestingly, there was very high uptake of the IGFR-L1 antibody in the submandibular and parotid salivary gland, as well as in the stomach. Given that IGFR-L1 is highly expressed in stomach and salivary glands, it seems plausible that this was specific uptake. A high fraction of both the IGFR-L1 and the isotype antibody was in the blood, which indicates insufficient clearance. This was expected, since it was shown that the blood clearance half life of IgGs can be up to 5 days in mice [233]. For instance, PSMA is widely used as a target for prostate cancer imaging and drug delivery, due to its high expression in prostate cancer, particularly in advanced stages [157]. Biodistribution studies using an ^{125}I -labelled antibody directed against PSMA revealed that even 3 days after injection a high fraction of the antibody was in the circulating blood, and only marginally higher amounts specifically accumulated in the tumor [234]. It is therefore possible that the time frame of 24 h was too short to observe specific uptake in the tumor.

The slow blood clearance is one of the reasons that intact antibodies are rarely used for cancer diagnosis or treatment. In addition, the use of mouse or rat antibodies could lead to immune response in patients [233]. Thus, multiple strategies of engineering small antibody fragments

have been described. For instance, the Fab (antigen-binding) fragment of antibodies is sufficient to induce biological responses and is therefore used in the formulation of several therapeutics [235]. These fragments can be made even smaller by only using the single-chain variable fragment (scFv). The smallest antibody fragments are derived from the variable domain of a camelid antibody, and are frequently termed nanobodies. Moreover, small antibody fragments can be conjugated to nanoparticles, which can, for instance, function as specific drug carriers [236]. Therefore, to achieve a good biodistribution of an IGFR-L1 antibody, it should eventually be reduced to a recombinant antibody fragment.

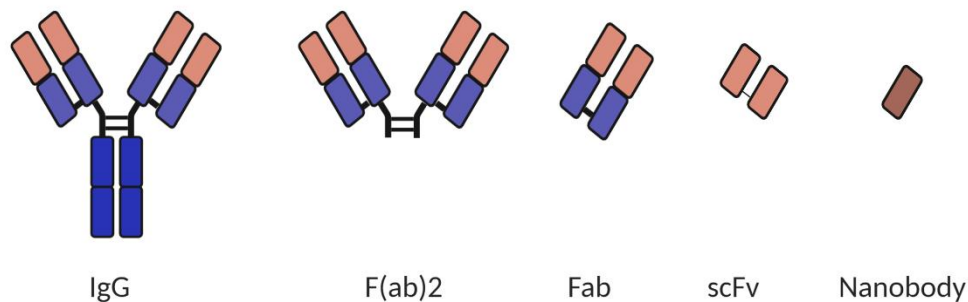


Figure 71: Structure of a full-length IgG and commonly used antibody fragments

To achieve a more desirable biodistribution, antibody fragments are used, such as Fab (antigen-binding fragment), scFv (single-chain variable fragment) or nanobodies, which are derived from structurally different camelid antibodies. The illustration was adapted from Alibakshi et al. [236] and created with BioRender.com.

3.3 Targeting IGFR-L1 using Antibodies

For *in vitro* and *in vivo* targeting of IGFR-L1, we generated highly specific antibodies. Out of 37 tested IGFR-L1 antibodies, 24 worked in immunocytochemistry of human cells. This provides a good basis to screen for functionally active antibodies. The two antibody clones 2G6 and 19A6, which were generated against the recombinant extracellular domain of IGFR-L1, showed very reliable and intense signals in both human and mouse cells. Thus, these antibodies would be the best candidates for future *in vivo* experiments. Since other antibodies

were equally well internalised into LNCaP cells as 2G6, those antibodies should be additionally considered for potential human translation.

Our proliferation assay on the human prostate cancer cell line LNCaP showed that the antibody clone 2G6 decreased proliferation. However, the results obtained from this assay were variable, thus it should be further optimised. For instance, FACS analysis after EdU pulse could be an alternative to immunocytochemistry. After optimisation, all purified antibodies should be tested in different concentrations to achieve more robust results.

Most of the antibodies were generated against IGFR-L1 embedded in proteoliposomes, since these structures provide a near-physiological environment. Proteoliposomes are bilayer spheres of a defined mixture of phospholipids and cholesterol, filled with an aqueous buffer [237]. Further, it is difficult to reconstitute the structure of transmembrane proteins in solution. If single domains are used, they often have slightly different conformations than in the native protein. For generation of IGFR-L1 proteoliposomes, the full-length receptor was embedded into the artificial bilayer, similarly to previous approaches [238, 239]. Liposome assembly can be further improved using nanoparticles designed to facilitate the correct implementation of membrane proteins into liposomes [239]. It is possible that additional optimisations of the proteoliposome formation could enhance the affinity and specificity of IGFR-L1 antibodies.

There have been many approaches to enhance the process of antibody development, for instance via phage display techniques. The basis of these concepts is fusion of the antigen to a bacteriophage surface protein to allow for recombinant antibody selection and amplification in bacterial cells. Using this artificial approach, antibody sequences can be specifically tailored to achieve the desired properties [240]. In summary, there are multiple possibilities to improve the affinity, stability and biodistribution of IGFR-L1 antibodies in the future.

3.4 Conclusion

Taken together, our results showed that IGFR-L1 desensitises insulin and IGF1 signalling in pancreatic β -cells, by facilitating clathrin-mediated endocytosis of IR and IGF1R. As IR and IGF1R dissociate from their ligands after endocytosis and are routed towards the lysosome for degradation, their downstream signalling is attenuated. In prostate cancer cells, IGFR-L1 enhances IGF1R activation, presumably by regulating receptor recycling, leading to the hypothesis that the exact mechanism of IGFR-L1 varies in different cell types. We showed that IGFR-L1 is estrogen-inducible and correlates to the androgen status of prostate cancer cells. Thus, it is possible that the function of IGFR-L1 depends on the activation of steroid hormone signalling, determining preferential proliferative and metabolic pathways. IGFR-L1 is a promising new target for the modulation of insulin/IGF1 signalling in the treatment of diabetes or hormone-dependent cancers. Further research is necessary to validate the potential of IGFR-L1 antibodies as drug candidates.

4 Materials and Methods

4.1 Methods

4.1 Animal Breeding

Breeding of WT mice was performed by S. Schirge and L. Appel (Institute of Diabetes and Regeneration Research, Helmholtz-Zentrum München). The German Animal Protection Act and the approved guidelines of the Society of Laboratory Animals (GV-SOLAS) and the Federation of Laboratory Animal Science Associations (FELASA) were applied. The mice with the genotype CD1xC57BL were 4 months old. IGFR-L1-flox/Rosa-CreERT2 mice were bred by G. Collden (Institute of Diabetes and Obesity, Helmholtz-Zentrum München). To achieve conditional knockout of IGFR-L1, the 5 months old mice were injected with 100 mg/kg body weight and sacrificed 4 weeks post administration.

4.2 Cell Culture

Min6 M9, K8 and K20 cells were maintained in DMEM with 4.5 g/l glucose and L-glutamine supplemented with 10 % FBS and 70 μ M 2-Mercaptoethanol. The subcultivation ratio was 1:4 to 1:6 every 5-7 days, with medium change every 2-3 days. For passaging, the cells were rinsed with DPBS and incubated with 0.05 % Trypsin until they started detaching (2-5 min). The suspension was subsequently centrifuged and resuspended in fresh medium. LNCaP and LNCaP C4-2 cells were cultured in RPMI 1640 with L-Glutamine with 10 % FBS. To model androgen deprivation, the cells were cultured in RPMI 1640 without phenol red, supplemented with 10 % charcoal-stripped FBS. In the control sample, 10 nM Dihydrotestosterone were added to the charcoal-stripped medium. During the time course, the medium was changed every 2 days. HPEC, BPH-1, PC3 and MDA PCa 2b cells were cultivated in the respective medium recommended by the vendor.

4.3 Molecular Cloning

Ligation was performed using T4 DNA ligase (1:20 dilution) over night at 16 °C with a backbone to insert ratio of 1 : 3 to 1 : 10. The ligation products were transformed into E.coli DH5 α

ultracompetent cells by 42 °C heat shock for 45 seconds, followed by cultivation in LB medium at 37 °C for 1 hour and streaking on LB Agar plates with ampicillin. Plasmids from the picked colonies were isolated using the Qiagen Plasmid Mini Kit and sequenced using the BigDye Terminator v3.1 Kit. Readout was done by the Core Facility Next Generation Sequencing at Helmholtz-Zentrum München. Plasmid amplification was performed using the Qiagen Plasmid PLUS Midi Kit or Plasmid Maxi Kit.

4.4 IGFR-L1-Venus and IGFR-L1-AP2*-Venus Cloning strategy

The IGFR-L1 sequence was PCR-amplified from pCMV-KIAA1324-WT [163] using forward and reverse primers KIAA_NotI_Fw and KIAA_NotI_Rev. The PCR product, as well as the vector pKS-Venus, were digested with the restriction enzyme NotI, purified using the Qiagen Gel Extraction Kit and ligated. Subsequently, the resulting plasmid pKS-IGFR-L1-Venus was digested with NotI and SpeI, while the desired backbone pCAG-H2B was digested with NotI and NheI. Both products were gel-purified and ligated as described before, generating pCAG-IGFR-L1-Venus. The success of the reaction was confirmed by diagnostic digest with AhdI and EcoRI, and plasmids from the positive colonies were isolated and sequenced using the primers Seq_KIAA_3HA_F3-F8, EP-038, EP-184 and KIAA-AFT.Beg-R.

For IGFR-L1-AP2*-Venus, pCAG-IGFR-L1-Venus was digested with AscI and BglII and gel-purified. The product was ligated with the oligonucleotide encoding IGFR-L1-ASKA where the AP2 binding motif YSKL was changed to ASKA (ordered from Thermo Fisher), thereby generating pCAG-IGFR-L1-AP2*-Venus. The cloning of IGFR-L1-Venus and IGFR-L1-AP2*-Venus was performed jointly with A. Morshedi (Institute of Diabetes and Regeneration Research).

4.5 Transfection

Min6, LNCaP and PC3 cells were transfected using Lipofectamine 2000 according to the manufacturer protocol, 24 h after seeding in a 6 cm cell culture dish. Stable cell lines overexpressing the fluorescent fusion protein IGFR-L1-Venus, IGFR-L1-AP2*-Venus or Venus only were generated by transfection and subsequent selection with 1 µg/ml puromycin for

approx. 4 weeks. The cells were then sorted according to expression levels via FACS to ensure that clones with similar expression levels were analysed. Similarly, stable cell lines coexpressing IGFR-L1-Venus and IR-A-RFP or IR-B-RFP were generated by co-transfection and selection with 1 µg/ml puromycin and 500 µg/ml geneticin.

4.6 Fluorescence-Activated Cell Sorting (FACS)

To prepare the transfected cells for sorting, they were detached using trypsin, centrifuged and resuspended in growth medium (1 ml medium for 2-3 million cells). The cell suspension was filtered into 5 ml round bottom tubes with cell strainer cap and stored on ice. The FACS Aria was set up and calibrated using Accudrop Beads according to manufacturer instructions. Untransfected cells were sorted to adjust the forward/side scatter and to control for autofluorescence. The gates were set to the desired fluorescence intensity to sort transfected cells with different expression levels. After sorting, the cell suspension was centrifuged and plated in 10 cm dishes for further culturing.

4.7 Live Imaging

The fluorescent constructs were visualised with a Zeiss LSM 880 confocal microscope. To this end, cells were seeded in µ-slide 8 well chambers 2-3 days before analysis and mounted on a 37 °C heated imaging chamber with 5 % CO₂ supply. For live imaging, Immersol 518F for 37 °C was used on a 63 x objective. The detector settings were either kept at standard settings, or changed to the AiryScan detector (Beam Splitter 488/561, R-S-mode) for fast imaging.

4.8 CRISPR/Cas9 Knockout

For targeting via CRISPR/Cas9, 4 single guide RNAs (sgRNAs) were cloned simultaneously into the vector E298 using gibbon assembly. The vector contains the Cas9 endonuclease to facilitate genetic modification and the fluorescent protein Venus for cell sorting. The cloning was performed jointly with J. Siehler (Institute of Diabetes and Regeneration Research). Sequencing and amplification of the plasmid was done as described (see 4.3 Molecular

Cloning). Subsequently, MCF-7 and LNCaP cells were transfected with the E298 vector using Lipofectamine and sorted via FACS after 24 h to separate the successfully transfected cells. These cells were then either seeded in 10 cm dishes at a very low density for colony picking, or in 96 well plates, with 1 cell per well. These clones were expanded into two 96 well plates, one of which was grown to full confluency for DNA isolation. To this end, the wells were washed with PBS and incubated with 50 μ l DNA Lysis Buffer at 60 °C over night in a humid atmosphere. The DNA was precipitated using 100 μ l cold NaCl/ethanol (75 mM Na Cl in 100 % ethanol) for 30 min at room temperature. The plate was carefully inverted and the wells were washed with 150 μ l 70 % ethanol three times and DNA was dissolved in 25 μ l TE buffer. DNA was sequenced using the BigDye Terminator v3.1 Kit and the readout was done by the Core Facility Next Generation Sequencing at Helmholtz-Zentrum München.

4.9 Antibody Generation

Monoclonal antibodies against the cytoplasmic tail or ectodomain of IGFR-L1 were generated by R. Feederle (MAB, HMGU München) and Ü. Coskun. (PLI, Dresden). Purification and fluorescent labelling was performed by R. Feederle. Antibodies were tested for functionality using immunocytochemistry in human MCF7 cells and mouse Min6 cells. The specificity of the antibodies was determined using Igfr-L1 KO Min6 cells. The isotype of rat antibodies was determined by R. Feederle. Isotype-specific antibodies for the isotype test of mouse antibodies were provided by R. Feederle.

4.10 Immunohistochemistry

Cells were seeded in μ -slide 8 well chambers (ibidi) at a density of 25000 - 50000 cells per well and were fixed after 3 days in 4% PFA for 10 min at RT and permeabilized for 15 min at RT.

Isolated mouse prostates were fixed overnight in 4 % PFA at 4 °C, dehydrated in a sucrose gradient ranging from 7.5 to 30% sucrose (in PBS) and embedded in tissue freezing medium before cutting 10 μ m sections and transferring to a microscope slide. The frozen sections were rehydrated in PBS for 5 x 5 min and permeabilized in 0.5% Triton-X100 for 20 min at RT.

The cells or sections were incubated with blocking solution for 1 h at RT and subsequently incubated with the respective primary antibodies overnight at 4 °C. After washing with PBS-T, the secondary antibodies were added in 1:800 dilution for 2 h at RT. For subsequent nuclear counterstaining, DAPI (1:500 dilution) was used. Samples were stored in Elvanol and imaged on a Zeiss LSM 880 AiryScan.

For signal amplification of pAkt staining, the Tyramide SuperBoost Kit (Life Technologies) was used according to the manufacturer's protocol. To achieve membrane staining, live cells were incubated with CellMask™ Deep Red plasma membrane stain (1:2000, 5 min), fixed in 4% PFA and imaged immediately.

4.11 Western Blot

Cells were lysed in RIPA buffer supplemented with protease inhibitor cocktail, as well as phosphatase inhibitor cocktail 2 and 3 (1:100 dilution). Lysates were centrifuged in a tabletop centrifuge at 14000 rpm for 4 °C. Protein concentrations were determined using the BCA protein assay kit (Thermo Fisher). SDS-PAGE in 7.5 % acrylamide gels and immunoblot on PVDF membrane were carried out in a BioRad electrophoresis chamber and transfer system. The membranes were blocked in 5% milk powder in TBS-T for 1h at RT and incubated with the respective primary antibodies overnight at 4 °C.

The membranes were washed in TBS-T for 3 x 10 min, and incubated for 2h at room temperature with the secondary antibodies conjugated to horseradish peroxidase (1: 10 000 dilution), before again being washed with TBS-T. The bands were detected using the Clarity Western ECL Substrate kit and imaged in a ChemStudio2A (Analytik Jena). Quantification was performed via densitometric analysis in ImageJ.

4.12 Co-immunoprecipitation

Min6 cells stably expressing IGFR-L1-Venus and IR-A-RFP or IR-B-RFP or LNCaP cells expressing IGFR-L1-Venus were seeded 2-3 days before. They were lysed in Co-IP lysis buffer and centrifuged at 14000 rpm, 4 °C for 10 min. The protein concentration of the lysate was determined via the BCA protein assay kit. Around 400 µl lysate (at a concentration of 1 µg/µL)

was incubated with the indicated antibody for 2 h at 4 °C under rotation. Sure Beads Protein G magnetic beads were blocked in 5 % BSA in PBS for 1 h at 4 °C and were then added to the sample during overnight incubation at 4 °C (10 µl beads / 100 µg protein). Beads were washed 3x with 100 µl lysis buffer and eluted with pre-made Laemmli-buffer with DTT for 5 min at 96 °C for subsequent Western Blot analysis. The Co-IP in LNCaP cells was performed by S. Bilekova (Institute of Diabetes and Regeneration Research).

4.13 Proliferation Assay

To assess the proliferation of MCF7 or Min6 cells, they were seeded in in µ-slide 8 well chambers. LNCaP cells were seeded in 384-well clear bottom plates previously coated with Poly-L-Lysine (1:100 dilution in PBS) for 2 h to enhance attachment. After 2 days the cells were incubated with 10 µM 5-ethynyl-2'-deoxyuridine (EdU) for 8 h, fixed with 4 % PFA and stored in PBS at 4 °C. EdU was labelled with the Click-iT EdU Cell Proliferation Kit (Invitrogen,). Images were taken on a Zeiss Axio Observer Z1.

4.14 Endocytosis Assay in LNCaP

The endocytosis of insulin and EGF in LNCaP cells was analysed as previously described, in cooperation with M. Katsburg (Institute of Diabetes and Regeneration Research) [241]. Briefly, the cells were incubated with 10 µg/ml rat anti-IGFR-L1 antibody (#2G6, purified), along with 100 nM AlexaFluor546-labelled insulin (kindly provided by Oliver Plettenburg, Institute for Medicinal Chemistry, Helmholtz-Zentrum München) or 100 nM AlexaFluor488-labelled EGF. The assay was performed in normal LNCaP medium for 60 min at 37 °C. The cells were then fixated with 4 % PFA for 10 min and permeabilized for 15 min at RT. To visualise the IGFR-L1 antibody, secondary anti-rat IgG Alexa Fluor® 488 or anti-rat IgG Cy3 was added for 2 h at RT. The cells were counterstained with SiR-Actin (1:1000 dilution) and DAPI. The colocalisation of the IGFR-L1 antibody with labelled insulin / EGF was calculated using the ImageJ Plugin JaCoP with manual thresholding.

4.15 Insulin Uptake Assay in Min6

Min6 WT and Igfr-I1 KO cells in μ -slide 8 well chambers were starved for 1h in HBSS and stimulated with 100 nM insulin-546 for different time points until fixation in 4% PFA. The cytoskeleton was visualised using SiR-actin and nuclei with DAPI. Confocal images were taken with a Zeiss LSM 880 microscope and quantified with ImageJ as fluorescent intensity of insulin-546 divided by the cell number.

4.16 Migration Assay

The migration of LNCaP was performed in a 3D spheroid assay, as previously described [241]. To form LNCaP spheroids, the AggreWell 400 24 well plates were used. The wells were rinsed using AggreWell Rinsing Solution, centrifuged at 1300 rcf for 5 min and washed with RPMI 1640. Each well was filled with 1 ml prewarmed LNCaP medium before adding the cell suspension (1.2 million cells in 1 ml), which is the adequate cell density to form spheroids containing approx. 1000 cells. The plate was centrifuged at 100 rcf for 3 min and incubated for 48 h. The spheroids were carefully collected in a 37 μ m reversible cell strainer, sedimented for a few minutes and resuspended in 1.2 ml of a prepared 10 μ M collagen solution buffered with 10 mM HEPES and approx. 15 mM NaOH, which was used for titrating the solution to a neutral pH. The cell suspension was equally distributed between 4 wells of a 24 well plate and incubated for 4 hours at 37 °C. After the collagen had solidified, 1 ml of LNCaP medium and 200 μ l of mineral oil, which prevents evaporation, were added to each well and the plate was mounted on a Zeiss Axio Observer Z1 using incubation at 37 °C and 5 % CO₂ supply for live cell imaging. The area of the cells leaving the spheroid was measured by hand-drawing ROIs in ImageJ.

4.17 Image Processing in ImageJ

The fluorescence intensity of a specific channel was measured automatically using a self-written IJ1 Macro code. In parallel, the cell number in each image was counted (based on DAPI).

```

fileExtension = ".czi";
run("Bio-Formats Macro Extensions");
dir=getDirectory("Choose a Directory");
cziFileList = getFileList(dir);

for (file=0; file<cziFileList.length; file++) {
    if (endsWith(cziFileList[file], fileExtension)) {
        Ext.setd(dir + cziFileList[file]);
        Ext.getSeriesCount(seriesCount);
        for (series=1; series<=seriesCount; series++) {
            //open and define image
            run("Bio-Formats Importer", "open=[" + dir + cziFileList[file] + "] autoscale color_mode=Colorized rois_import=[ROI manager] view=Hyperstack
            stack_order=XYZT series_" + series);
            imageName = getTitle();
            run("Split Channels");
            redCh = "C2-" + imageName;
            DAPI = "C3-" + imageName;

            //count cells
            selectWindow(DAPI);
            setAutoThreshold("Default dark");
            run("Threshold...");
            setThreshold(5900, 65535);
            setOption("BlackBackground", true);
            run("Convert to Mask", "method=Default background=Dark calculate black");
            run("Fill Holes", "slice");
            run("Watershed", "slice");
            run("Analyse Particles...", "size=500-Infinity pixel show=Outlines display summarize slice");
            selectWindow("Results");
            saveAs("Results", dir + imageName + "_Count" + ".csv");
            run("Clear Results");

            //measure intensity
            selectWindow(redCh);
            run("Set Measurements...", "area mean modal min integrated median redirect=None decimal=1");
            run("Measure");
            selectWindow("Results");
            saveAs("Results", dir + imageName + "_Intensity" + ".csv");
            run("Close All");
        }
    }
}

```

Unless specified otherwise, the Mander's Overlap Coefficient was calculated using the ImageJ plugin Coloc2, which was run automatically by the following code:

```

dir = getDirectory("Choose a Directory");
processFiles(dir);
//define function to extract MOC and PCC values from log
function extractValueFromLog(logString, indicator) {
    extractedValue = "NaN";
    indexOfIndicator = indexOf(logString, indicator);
    if (indexOfIndicator < 0) {
        print("Log does not contain \" + indicator + "\"!");
    }
    else {
        stringFollowingIndicator = substring(logString, indexOfIndicator + lengthOf(indicator));
        indexOffFollowingLineBreak = indexOf(stringFollowingIndicator, "\n");
        extractedValue = substring(stringFollowingIndicator, 0, indexOffFollowingLineBreak);
    }
    return extractedValue;
}
function processFiles(currentDir) {
    fileList = getFileList(currentDir);
    for(i=0; i<fileList.length; i++) {
        csvFileContent = "image name;PCC;PCCabovethreshold;M1;tM1;M2;tM2;\n";
        if(endsWith(fileList[i], ".tif")) {
            //open and define image
            open(currentDir+fileList[i]);
            imageName = getTitle();
            print("Analyzing image " + imageName);
            run("Split Channels");
            redCh = imageName + " (red)";
            greenCh = imageName + " (green)";
            selectWindow(greenCh);
            run("Duplicate...", "title=[copy_" + greenCh + "]");
            copyOfGreenCh = getTitle();

            //set threshold to define a mask for measurement
            selectWindow(copyOfGreenCh);
            run("Options...", "iterations=1 count=1 black");
            setOption("BlackBackground", true);
            run("Convert to Mask", "method=Mean background=Dark calculate black");
            run("Fill Holes", "stack");
        }
    }
}

```

```

//run Coloc2
run("Coloc 2", "channel_1=[\" + greenCh + \"] channel_2=[\" + redCh + \"] roi_or_mask=[\" + copyOfGreenCh + \"] threshold_regression=Costes
display_images_in_result li_histogram_channel_1 li_histogram_channel_2 li_icq spearmans_rank_correlation manders_correlation
kendalls_tau_rank_correlation 2d_intensity_histogram costes_significance_test psf=3 costes_randomisations=100");

//extract MOC and PCC values from log
logString = getInfo("Log");
PCCIndicator = "Pearson's R value \\\(no threshold\\), ";
PCC = extractValueFromLog(logString, PCCIndicator);
PCCthresholdIndicator = "Pearson's R value \\\(above threshold\\), ";
PCCthreshold = extractValueFromLog(logString, PCCthresholdIndicator);
M1valueIndicator = "Manders' M1 (Above zero intensity of Ch2), ";
M1value = extractValueFromLog(logString, M1valueIndicator);
tmValue1Indicator = "Manders' tM1 (Above autothreshold of Ch2), ";
tmValue1 = extractValueFromLog(logString, tmValue1Indicator);
M2valueIndicator = "Manders' M2 (Above zero intensity of Ch1), ";
M2value = extractValueFromLog(logString, M2valueIndicator);
tmValue2Indicator = "Manders' tM2 (Above autothreshold of Ch1), ";
tmValue2 = extractValueFromLog(logString, tmValue2Indicator);
if (endsWith(dir, "\\\")) {
    dir = dir + "\\\";
}

csvFileContent += "\\n\" + imageName + \";\" + PCC + \";\" + PCCthreshold + \";\" + M1value + \";\" + tmValue1 + \";\" + M2value + \";\" + tmValue2;
selectWindow("Log");
saveAs("Text", dir + "/" + imageName);
print("\\Clear");
run("Close All");
csvFile = File.open(dir + "values_" + imageName + ".csv");
print(csvFile, csvFileContent);
File.close(csvFile);

} else if (endsWith(fileList[i], ".tif")) {
    processFiles(currentDir + fileList[i]);
} else {
    print(dir + fileList[i]);
}
}
return csvFileContent;
}

```

To assess the proliferation of various cell lines, EdU positive and DAPI positive cells were counted (in previously separated images) using the following code:

```

dir = getDirectory("Choose a Directory ");
processFiles(dir);
function processFiles(currentDir) {
    fileList = getFileList(currentDir);
    for(i=0; i<fileList.length; i++) {
        if(endsWith(fileList[i], ".tif")) {
            open(currentDir+fileList[i]);
            imageName = getTitle();
            run("16-bit");
            run("Auto Threshold", "method=Default white");
            run("Watershed");
            run("Analyse Particles...", "size=500-10000 pixel show=Outlines display summarize slice");
            selectWindow("Drawing of " + imageName);
            saveAs("PNG", dir + imageName + "count");
            run("Close All");
        }
    }
    selectWindow("Results");
    saveAs("Results", dir + imageName + "_Count" + ".csv");
}

```

4.18 Statistics

Statistical analysis was performed using GraphPad Prism 8 (GraphPad Software, Inc.). The Shapiro-Wilk test was applied to test the data set for normality. In case of normal distribution

or in case of small sample sets, the statistical significance was determined via two-tailed, unpaired student's t test. If required, outliers were identified by Grubb's outlier test.

4.19 Bioinformatic Analyses

To analyse the tissue distribution of IGFR-L1, mRNA expression data was extracted from the Human Protein Atlas (<https://www.proteinatlas.org/ENSG00000116299-KIAA1324/tissue>). These data were collected by Illumina RNA-sequencing of specimen from the Uppsala Biobank. The domain structure of IGFR-L1 was analysed using the Ensembl database [161], aligned with the IGFR-L1 sequence via SnapGene Viewer (Insightful Science; available at snapgene.com) and illustrated with BioRender.com. The gene expression data of IGFR-L1 in prostate cancer was extracted from the TCGA dataset using the GEPIA web server [175] and mutation data in the TCGA and Neuroendocrine Prostate Cancer [242] datasets was searched in CBioPortal [176]. All databases were reviewed for potential changes on the 18.09.2020.

4.2 Materials

4.2.1 General Lab ware

4.2.1.1 Machines

Agarose Gel Chamber	Midi 450 (Neolab)
Balance	Scout Pro (Ohaus)
Cell counter	Countess II Automated Cell Counter (Thermo Fisher) / TC20 Automated cell counter (BioRad)
Cell culture centrifuge	Universal 320 R (Hettich)
Cell culture hood	HeraSafe KS 12 (ThermoScientific)
Cell culture incubator	BBD 6220 (ThermoScientific)
Centrifuge	5430 R (Eppendorf)
Confocal microscope	LSM 880 AiryScan (Zeiss)
Cryostat	CM1860 (Leica)
Epifluorescence microscope	Axio Observer Z1 (Zeiss)
FACS	BD FACS Aria III (BD)
Gel chamber	Mini Trans-Blot Cell (BioRad)
Live imaging chamber	Heating insert P2000 / Incubator XL (Pecon)
Magnetic Stirrer	RH basic 2 (IKA)
PCR machines	Personal Thermocycler (Biometra) / PXE0.2 Thermo Cycler (Thermo Fisher)
pH meter	Mettler Toledo (Hanna Instruments)
Pipette controller	Accu-jet pro pipette controller (BrandTech)
Pipettes	1000 µl / 200 µl / 10 µl Eppendorf Pipettes (Eppendorf)
Plate reader	Varioskan LUX (Thermo Fisher)
Water purification system	Millipore Q-POD, 0.22 µl filter (Merck)
Western blot developer	ChemStudio 2A (Analytik Jena)
Western blot transfer	Trans-Blot Turbo Blotting System (BioRad)

4.2.1.2 Consumables

Blotting paper	Whatman / GE Healthcare
Cell scraper 25 cm	Sarstedt
Countess Cell Counting Slides	Invitrogen
Cryotubes 1.8 ml	Nunc
Eppendorf tubes 1.5 ml / 2.0 ml	Eppendorf
Falcon tubes 15 ml / 50 ml	Falcon / Corning
Freezing Containers	Nalgene / Thermo Fisher
Immuno-Blot PVDF Membrane	BioRad
Micro tubes 0.5 ml / 2.0 ml	Sarstedt
Pasteur pipettes	Fisher Scientific

PCR tubes	Kisker Biotech
Pipette 2 ml / 5 ml / 10 ml / 25 ml / 50 ml	Greiner
Pipette tips 10 µl / 20 µl / 200 µl / 1000 µl	Sarstedt

4.2.1.3 Kits

Alexa Fluor™ 555 Tyramide SuperBoost™ Kit, goat anti-rabbit IgG-150 slides	LIFE Technologies (Invitrogen)	B40923
BigDye® Terminator v3.1 Cycle Sequencing Kit	Thermo Fisher	4337458
Click-iT™ EdU Cell Proliferation Kit for Imaging with Alexa Fluor™ 647	Invitrogen	C10340
Gel Extraction Kit	Qiagen	28704
Nano-Glo Luciferase Assay	Promega	N1110
PCR Purification Kit	Qiagen	28104
Pierce BCA Protein Assay Kit	Thermo Fisher	23225
Plasmid Maxi Kit	Qiagen	12162
Plasmid Mini Kit	Qiagen	12125
Plasmid PLUS Midi Kit	Qiagen	12943

4.2.2 Cell Culture

4.2.2.1 Cell lines

BPH-1	DSMZ	ACC 143
HEK293LTV	Cell Biolabs	LTV-100
Human Prostate Epithelial cells	Merck Millipore	SCCE019
LNCaP	ATCC	CRL-1740
LNCaP C4-2	ATCC	CRL-3314
MCF7	ATCC	HTB-22
Min6 Igfr-I1 KO (clone E10)	Amir Morshedi	Ansarullah et al. [170]
Min6 M9/K8/K20	Susumu Seimo	Minami et al. [243], [244]
PC3	CLS	300312

4.2.2.2 Cell culture media formulations

Min6 Medium	DMEM high glucose 10 % FBS 70 µM 2-mercaptoethanol 1 % P/S
Min6 Medium for live imaging	DMEM no phenol red 10 % FBS 70 µM 2-mercaptoethanol

MCF7 Medium	1 % P/S DMEM high glucose 10 % FBS
LNCaP Medium	10 nM beta-estradiol RPMI 1640 10 % FBS
LNCaP Medium for live imaging	RPMI no phenol red 10 % FBS
HEK293LTV Medium	DMEM high glucose 10 % FBS
PC3 Medium	DMEM high glucose 10 % FBS
BPH-1 Medium	RPMI 1640 20 % FBS 20 ng/ml testosterone 5 µg/ml transferrin 5 ng/ml sodium selenite 5 µg/ml insulin
MDA PCa 2b Medium	Ham's F12K 20 % FBS 10 ng/ml EGF 0.005 mM phosphoethanolamine 45 nM sodium selenite 0.005 mg/ml insulin
Hank's Balanced Salt Solution (HBSS)	114 mM NaCl 47 mM KCl 1.2 mM KH ₂ PO ₄ 1.16 mM MgSO ₄ 2.5 mM CaCl ₂ 25.5 mM NaHCO ₃ , pH 7.2 20 mM HEPES (added fresh)

4.2.2.3 Cell culture media and additives

2-Mercaptoethanol	Life Technologies	31350-010
5alpha-dihydrotestosterone (DHT)	Sigma-Aldrich	D-073-1ML
AggreWell Rinsing Solution	STEMCELL	7010
Apo Transferin Human	Sigma Aldrich	T4382-100MG
B-estradiol bioreagent	Sigma-Aldrich	E2758-1G
Collagen solution from bovine skin	Sigma-Aldrich	C4243
DMEM 5X, with 4.5 g/l D(+)-Glucose (High Glucose), w/o L-Glutamine, w/o NaHCO ₃	Neolab	010554B
DMEM, high glucose, L-Glut, Phenol Red,		
Sodium Pyruvate	Gibco	41966-052
DPBS	Gibco	14190-169

Dulbecco's Modified Eagle's Media 2X, With 4.5 mg/L Glucose and L-Glutamine	Merck Millipore	SLM-202-B
EGF / Epidermal Growth Factor Protein (recombinant human)	Biomol	PKSH031641.500
EpiGRO Human Prostate Complete Media	Merck Millipore	SCMP001
FBS good	Pan	P40-37500
FBS, Charcoal stripped	Sigma-Aldrich	F6765
Geneticin 50mg/ml	Gibco	10131019
Ham's F-12K (Kaighn's) Medium-500 mL	Life Technologies	21127022
IGF-I Rec. human (receptor grade), GroPep	ibt Eagle Biosciences	CU100
Insulin solution human	Sigma-Aldrich	I9278
Lipofectamine® 2000 Transfection Reagent	Life Technologies	11668030
Lipofectamine® 3000 Transfection Reagent	Life Technologies	L3000015
O-phosphorylethanolamine	Sigma-Aldrich	P0503-1G
Opti-MEM I Reduced Serum Medium	LIFE Technologies	31985062
Pen/Strep	Gibco	15140-122
Polybrene Transfection Reagent	Sigma-Aldrich	TR-1003
Poly-L-lysine	VWR	L7240
Puromycin	Thermo Fisher	A1113803
RPMI 1640 Medium, no phenol red	Life Technologies Gibco	11835030
RPMI 1640 with L-Glutamine, Phenol Red	Gibco	21875-034
RPMI 1640, no phenol red	Gibco	11835030
Sodium selenite	Sigma-Aldrich	9133
Testosterone	component of EpiGRO kit	SCMP001
Tet-system approved FBS	Clontech / Takara	631106
Trypsin, 0,05%	Invitrogen	253000-054
VEGF-A	Bio-Rad	PBP027

4.2.2.4 General cell culture materials

μ-slide 8 well	ibidi	80826
12-well plates	Falcon	353043
24-well plates	Falcon	353047
37 μm reversible strainer	STEMCELL	27250
384-well clear bottom plates	Corning	3770
48-well plates	Falcon	353078
5ml polystyrene round bottom with cell strainer	VWR/ Omnilab	FALC352235
6-well plates	Falcon	353046
96-well multiwell plate, flat bottom	Nunc	167008
Cell culture dish 10 cm	Nunc	150350
Cell culture dish 6 cm	Nunc	150288
FACS Accudrop Beads	BD	345249
FACS Flow Sheath Fluid	BD	342003

4.2.3 Molecular Cloning

4.2.3.1 Plasmids

pCAG-H2B	Ingo Burtscher	
pCAG-Kozak-Venus	Ingo Burtscher	
pKS-Venus	Ingo Burtscher	
pCMV-KIAA-HA	Seong-Jin Kim	Kang et al. [163]
pU6-sgRNA-CAG-Cas9-Venus	Ralf Kühn	Yumlu et al. [245]
InsRA-TagRFP	James D. Johnson	Boothe et al. [40]
InsRB-TagRFP	James D. Johnson	Boothe et al. [40]
Phogrin-mCherry	Joachim Goedhart	
pLAMP1-mCherry	Joachim Goedhart	
pmTurquoise2-Golgi	Joachim Goedhart	Addgene plasmid # 36205
pPalmitoyl-mTurquoise2	Joachim Goedhart	Addgene plasmid # 36209

4.2.3.2 Primers

KIAA_NotI_Fw	AGTCGGTAGCGGCCGCATGGCTGAGCCTGGGCACAG	Eurofins
KIAA_NotI_Rev	CTGGACACGCGGCCGCACAGGTCCATGTCTAGGCCTCCT	Eurofins
KIAA_MluI_Fw_A	AAAACGCGTCCACCATGGCTGAGCCTGGGC	Eurofins
Venus_SpeI_Re_A	AAAGCTAGCCTTGTACAGCTCGTCCATGCC	Eurofins
KIAA_HA_MluI_Fw	AAAACGCGTATGGCTGAGCCTGGGCACA	Eurofins
KIAA_HA_NheI_Re	AAAGCTAGCGCTTACCCTGCGTAATCTGGAAC	Eurofins

4.2.3.3 Sequencing primers

SEQ-KIAA-3HA-F3	CTGCTGAGTCCACCGGGAAC	Eurofins
SEQ-KIAA-3HA-F4	CCCAGCTTGCACAGACAAAGATTATT	Eurofins
SEQ-KIAA-3HA-F5	CGGTGATGGCAGACACAGAG	Eurofins
SEQ-KIAA-3HA-F6	GATTCAGGAACCTGCCACTCCT	Eurofins
SEQ-KIAA-3HA-F7	CCAATGATGTGACCCAGTCCTG	Eurofins
SEQ-KIAA-3HA-F8	ATCTTTACCAGCAAGAAGTCACTCTTTG	Eurofins
EP-038	CAAGATCCGCCACAACATCG	Eurofins
EP-184	ATGTTGTGGCGGATCTTG	Eurofins
KIAA-AFT.BEG-R	CAGTACCTCTTTGCAGGCATGAAGC	Eurofins

4.2.3.4 sgRNAs

Beg2-Fw	CACCGGG GACAACGCTATGGCTGAGCC	Eurofins
Beg2-Rev	AAACGGCTCAGCCATAGCGTTGTCCCC	Eurofins
g3-Fw	CACCGGGGAACTGAGAGGCGCATACCC	Eurofins
g3-Rev	AAACGGGTATGCGCCTCTCAGTTCCCC	Eurofins
g4-Fw	CACCGGGAAGCTCCGGTCCCCTTCCCT	Eurofins
g4-Rev	AAACAGGGAACGGGACCGGAGCTTCCC	Eurofins
g5-Fw	CACCGGGGGCGCATACCCCGGCTGTGG	Eurofins
g5-Rev	AAACCACAGCCGGGGTATGCGCCCC	Eurofins

4.2.3.5 IGFR-L1-ASKA oligonucleotide

TTGCCAAGATCTACTCCATCAATGTCACCAATGTTATGAATGGTGTGGCCTCCTACTGCCGTCCCTGT
GCCCTAGAAGCCTCTGATGTGGGCTCCTCCTGCACCTTTGTCTGCTGGTTACTATATTGACCGAGA
TTCAGGAACCTGCCACTCCTGCCCCACTAACACAATTCTGAAAGCCCACCAGCCTTATGGTGTCCAGG
CCTGTGTGCCCTGTGGTCCAGGGACCAAGAACAACAAGATCCACTCTCTGTGCTACAACGATTGCAC
CTTCTCACGCAACACTCCGACCAGGACTTTCAACTACAACCTTCTCCGCTTTGGCAAACACTGTCACCT
TGCTGGAGGGCCAAGCTTCACTTCAAAGGGCTGAAATACTTCCATCACTTTACCCTCAGTCTCTGTG
GAAACCAGGGTAGGAAAATGTCTGTGTGCACCGACAATGTCACTGACCTCCGGATTCCCTGAGGGTG
AGTCAGGGTTCTCAAATCTATCACAGCCTACGTCTGCCAGGCAGTCATCATCCCCCAGAGGTGACA
GGCTACAAGGCCGGGTTTCTCACAGCCTGTGACCTTGCTGATCGACTTATTGGGGTGACAACAG
ATATGACTCTGGATGGAATCACCTCCCCAGCTGAACTTTTCCACCTGGAGTCCTTGGGAATACCGGAC
GTGATCTTCTTTTATAGGTCCAATGATGTGACCCAGTCTGACAGTTCTGGGAGATCAACCACCATCCG
CGTCAGGTGCAGTCCACAGAAAAGTGTCCCTGGAAGTTTGTGCTGCCAGGAACGTGCTCGGATGG
GACCTGTGATGGCTGCAACTTCACTTCTGTGGGAGAGCGCGGCTGCTTGCCCGCTCTGCTCAGTG
GCTGACTACCATGCTATCGTCAGCAGCTGTGTGGCTGGGATCCAGAAGACTACTTACGTGTGGCGAG
AACCCAAGCTATGCTCTGGTGGCATTCTCTGCCTGAGCAGAGAGTCACCATCTGCAAACCATAGAT
TTCTGGCTGAAAGTGGGCATCTCTGCAGGCACCTGTAAGTCCATCCTGCTCACCGTCTTGACCTGCTA
CTTTTGGAAAAGAATCAAAAAGTACAGTACAAGGCCTCCAAGGCGGTGATGAATGCTACTCTCAAG
GACTGTGACCTGCCAGCAGCTGACAGCTGCGCCATCATGGAAGGCGAGGATGTAGAGGACGACCTC
ATCTTTACCAGCAAGAAGTCACTCTTTGGGAAGATCAAATCATTTACCTCCAAGAGGACTCCTGATGG
ATTTGACTCAGTGCCGCTGAAGACATCCTCAGGAGGCCTAGACATGGACCTGTGCGGCCGCGCCACC
ATGTCTAGAATGGTGTGAGCAAGGGCGAGGAGCTGTTACCGGGGTGGTGCCCATCCTGGTGTGAGCTG
GACGGCGACGTAAACGGCCACAAGTTCAGCGTGTCCGGCGAGGGCGAGGGCGATGCCACCTACGG
CAAGCTGACCCTGAAGCTGATCTGCACCACCGGCAAGCTGCCCGTGCCCTGGCCCACCTCGTGACC
ACCCTGGGCTACGGCCTGCAGTGCTTCGCCCCTACCCCGACCACATGAAGCAGCACGACTTCTTCA
AGTCCGCCATGCCCGAAGGCTACGTCCAGGAGCGCACCATCTTCTTCAAGGACGACGGCAACTACAA
GACCCGCGCCGAGGTGAAGTTCGAGGGCGACACCCTGGTGAACCGCATCGAGCTGAAGGGCATCG
ACTTCAAGGAGGACGGCAACATCCTGGGGCACAAGCTGGAGTACAACACTACAACAGCCACAACGTCT
ATATCACCGCCGACAAGCAGAAGAACGGCATCAAGGCCAAGTCAAGATCCGCCACAACATCGAGG
ACGGCGGCGTGCAGCTCGCCGACCACTACCAGCAGAACACCCCATCGGCCGACGGCCCCGTGCTGC
TGCCCGACAACCACTACCTGAGCTACCAGTCCGCCCTGAGCAAAGACCCCAACGAGAAGCGCGATCA
CATGGTCTGCTGGAGTTCGTGACCGCCGCGGGATCACTCTCGGCATGGACGAGCTGTACAAGGG
CGCGCCATAAAT

4.2.3.6 PCR cycle

Forward primer	1 μ l
Reverse primer	1 μ l
Template	50 - 100 ng
5 x Phusion buffer	5 μ l
dNTPs (10 mM)	0.25 μ l
DMSO	0.75 μ l
Phusion polymerase	0.25 μ l
Nuclease-free water	filled up to 25 μ l

98 °C	30 s	} 36 x
98 °C	10 s	
69 °C	30 s	
72 °C	90 s	
72 °C	5 min	
16 °C	storage	

4.2.3.7 Buffers and solutions

LB Medium	1 % Tryptone 1 % Yeast 0.5 % NaCl
Ampicillin	Ampicilin 10 mg/ml ddH2O
E.coli DH5 α competent cells	E.coli DH5 α LB medium TFB I / TFB II buffer
DNA Lysis Buffer	10 mM Tris (pH7.5) 10mM EDTA 10mM NaCl 0,5% (w/v) Sarcosyl Proteinase K (1mg/ml) Ethanol (96%, 70%), -20°C 5M NaCl
TE Buffer	10 mM Tris pH 7.6 1 mM EDTA
TFB I Buffer (pH 5.8)	15 % Glycerol 100 mM RbCl ₂ 50 mM MnCl ₂ 10 nM CaCl ₂ 30 mM potassium acetate
TFB II Buffer (pH 7.0)	15 % Glycerol 10 mM MOPS

75 mM CaCl₂
10 mM RbCl₂

4.2.3.8 Enzymes and other reagents

Ascl	NEB	R0558L
BglII	NEB	R0144S
Big Dye	LIFE Technologies	4337449
MluI	NEB	R0198S
NheI-HF	NEB	R3131S
NotI-HF	NEB	R3189L
Phusion high Fidelity DNA Polymerase	NEB	M0530 S
SpeI-HF	NEB	R3133S
T4 DNA Ligase	NEB	M0202S
1 kb DNA Ladder	NEB	N3232S
100 bp DNA Ladder	NEB	N3231S

4.2.4 Immunohistochemistry and Imaging

4.2.4.1 Reagents for imaging

Alexa Fluor® 488 EGF complex	Life technology	E13345
CellMask Deep Red	Thermo Fisher	C10046
Insulin-AlexaFluor546	Oliver Plettenburg	Ansarullah et al. [170]
Insulin FITC-labelled	Sigma-Aldrich	I3661
LysoTracker Deep Red	Thermo Fisher	L12492
SiR-Actin Kit	Cytoskeleton	CY-SC001

4.2.4.2 Materials for Immunohistochemistry

Jung Tissue Freezing Medium	Leica	(14)020108926
Microscope Slides	Thermo Scientific	J1800AMNZ
Cover slips, 24 x 50 mm # 1.5	Menzel-Gläser / VWR	MENZBB024050SC13
Mouse on Mouse (M.O.M.) Blocking Reagent	Biozol	MKB-2213-1
Donkey serum	Merck / Millipore	S30-100ml
Immersion Oil 518F	Carl Zeiss Microscopy	7510347
Immersion oil 518 F for 37°C	Carl Zeiss Microscopy	7646030

4.2.4.3 Buffers

PFA	4 % PFA in PBS, heated to 60 °C
PBS 10 x	1.37 M NaCl 26.8 mM KCl 0.1 M Na ₂ HPO ₄ 13.8 mM KH ₂ PO ₄
PBS-T	PBS pH 7.4 0.1 % Tween-20
Permeabilization solution	0.25 % Triton-X100 100 mM Glycine in PBS
Blocking Solution	0,1 % Tween 10% FBS 0,1% BSA 3% donkey serum
DAPI	200 µg/ml DAPI in PBS
Elvanol	25 % Glycerol , , 100 mM Tris 10 % Mowiol (Polyvinyl alcohol) 100 mM Tris pH 8.0 (dissolved over night in water bath) 2 % 1,4-Diazabicyclo[2.2.2]octan (DABCO)

4.2.5 Western Blot

4.2.5.1 Western blot reagents

Protease inhibitor cocktail	Sigma-Aldrich	P8340
Phosphatase inhibitor cocktail 2	Sigma-Aldrich	P5726
Phosphatase inhibitor cocktail 3	Sigma-Aldrich	P0044
Clarity Western ECL Substrate	BioRad	1705061
SuperSignal West Femto Maximum Sensitivity	Life Technologies	34095
Sure Beads Protein G magnetic beads	BioRad	161-4023
QuickStart Bovine Serum Albumin Standard	BioRad	500-0207

4.2.5.2 Ingredients for 2 Western blot gels (7.5 %)

Separating gel			Stacking gel		
Acrylamide	5.6	ml	Acrylamide	1.0	ml
Separating gel buffer	5.6	ml	Stacking gel buffer	1.9	ml
H ₂ O	11.3	ml	H ₂ O	4.7	ml
Temed	30	μl	Temed	15	μl
APS 10%	225	μl	APS 10%	75	μl

4.2.5.3 Western blot buffers

Co-IP lysis buffer	20 mM Tris/HCl pH 7.4 150 mM NaCl 1 mM EDTA 1 % Triton X-100
RIPA buffer	25 mM Tris pH 8 150 mM NaCl 1 % NP-40 0.5 % Deoxycholate 0.1 % SDS
5x Laemmli Buffer	50 % Glycerol 10 % SDS 0.05 % Bromophenol blue 0.3 M Tris pH 6.8 50 mM EDTA
TBS 10 x	1.5 M NaCl 100 mM Tris/HCl pH 7.4
TBS-T	TBS 10 x, ddH ₂ O 0.2 % Tween-20
Running buffer 10 x	0.25 M Tris 1.92 M Glycine 1 % SDS
Separating gel buffer 4 x	1.5 M Tris pH 8.8 0.4 % SDS
Stacking gel buffer 4 x	0.5 M Tris pH 6.8 0.4 % SDS
Anode buffer I	300 mM Tris pH 10.4 10 % Methanol
Anode buffer II	25 mM Tris pH 10.4 10 % Methanol
Cathode buffer	25 mM Tris pH 9.4 40 mM Glycine 10 % Methanol

4.2.6 Antibodies

4.2.6.1 Primary Antibodies

Akt, Pan- (C67E7)	Cell signalling	4691
Akt, Phospho- (Ser473) (D9E)	Cell signalling	4060
Androgen Receptor	Santa Cruz	sc-7305
Androgen Receptor	Abcam	ab133273
Cadherin - E (24E10)	Cell Signalling	3195
Cadherin - E (DECMA-1)	E. Kremmer	
Chromogranin A (Chr-A)	Abcam	ab15160
Chromogranin A (Chr-A)	Aviva Systems Biology	OASA09165
Chromogranin A (Chr-A) (C-20)	Santa Cruz	sc-1488
Chromogranin A (Chr-A) (Bovine), SP-1	Immunostar	20085
Chromogranin A (Chr-A) (C-12)	Santa Cruz	sc-393941
Chromogranin A (Chr-A) (Porcine), SP-1	Immunostar	20086
Clathrin Heavy Chain	Cell signalling	2410
Clathrin Heavy Chain	Cell signalling	4796
Cytokeratin 5	Abcam	ab53121
Cytokeratin 8 (TROMA-I)	DSHB	TROMA-I
Cytokeratin 8 + 18	OriGene	BP5007
EEA1	Life technologies	PA517228
EGF Receptor (D38B1)	Cell Signalling	4267S
EGF Receptor, Phospho-(Tyr1068) (D7A5)	Cell Signalling	3777T
ERGIC53	Santa Cruz	sc-66880
ER α (Estrogen receptor alpha) (H226)	Santa Cruz	sc-53493
Estrogen Inducible Protein pS2	abcam	ab92377
Estrogen receptor beta	DSHB	CWK-F12
Ezrin	Merck Millipore	07-130
FoxO1 (C29H4)	Cell Signalling	2880
GAPDH	Merck Biosciences	CB1001
Giantin	BioLegend	924302
GM130	BD	610822
IGF1 Receptor β , Phospho- (Tyr1135/1136) -Insulin Receptor β , Phospho- (Tyr1150/1151)	Cell signalling	3024
IGF1R beta (D23H3)	Cell signalling	9750
IGFR-L1	R. Feederle / Ü. Coskun	16F6 (rat), 2G6 (rat) or 31A11 (mouse)
Insulin (C27C9)	Cell signalling	3014
Insulin Receptor (IR) beta (C-19)	Santa Cruz	sc-711
Insulin, (Pro-) C-peptide	DSHB Hybridoma	GN-ID4-c
Ki67	abcam	ab15580
Ki67	Abcam	ab16667
Ki67 (D2H10)	Cell Signalling	9027S

Ki67 (SolA15), eBioscience™	LIFE Technologies	14-5698-82
Ki67, conjugated with DyLight650	LSBio	LS-C181326-100
Laminin beta 1 [LT3]	Abcam	ab44941
LAMP1 (CD107a)	BD	553792
PCNA	Abcam	ab29
PCNA (PC10)	Cell signalling	2586S
PCNA (PC10)	Santa Cruz Biotech.	sc-56
PSA (Prostate Specific Antigen)	Abcam	ab53774
PSMA (FOLH1)	Abcam	ab19071
Serotonin (5-HT)	Neuromics	RA20080
Smooth muscle actin, alpha-	Abcam	ab21027
Somatostatin	R&D Systems	MAB2358
TGN46	Abcam	ab16059
Tubulin-gamma	Sigma	T5326
VEGF Receptor 2	Cell Signalling	2479
ZO-1	DSHB	R26.4C-c

4.2.6.2 Secondary Antibodies

donkey anti rabbit IgG 647	Invitrogen	A31573
donkey anti-goat IgG 488	Invitrogen	A11055
donkey anti-guinea pig Alexa 488	Dianova	706-545-148
donkey anti-mouse IgG 488	Invitrogen	A21202
donkey anti-mouse IgG 555	Invitrogen	A31570
donkey anti-rabbit IgG 488	Invitrogen	A21206
donkey anti-rabbit IgG 555	Invitrogen	A31572
donkey anti-rat Alexa 488	Life Technologies	A-21208
donkey anti-rat IgG 647	Dianova	712-605-150
donkey anti-rat IgG 647	Dianova	712-605-150
goat anti-guinea pig IgG 633	Invitrogen	A21105
goat anti-Mouse IgG (H+L), HRP	Dianova/Jackson	DAB-087641
goat anti-mouse IgG 633	Invitrogen	A21052
goat anti-Rabbit IgG (H+L), HRP	Dianova/Jackson	DAB-087729
goat Anti-Rat IgG, Light Chain specific, HRP	Dianova/Jackson	112-035-175
rabbit anti-rat IgG, HRP	abcam	ab6734

5 References

1. WHO, *Global report on diabetes*. 2016: WHO Library Cataloguing-in-Publication Data.
2. Deutsche Diabetes Gesellschaft (DDG), D.D.-H., *Deutscher Gesundheitsbericht Diabetes 2020 - Die Bestandsaufnahme*. Diabetes-Journal, 2019.
3. Atkinson, M.A., G.S. Eisenbarth, and A.W. Michels, *Type 1 diabetes*. The Lancet, 2014. **383**(9911): p. 69-82.
4. Pan, F.C. and C. Wright, *Pancreas organogenesis: From bud to plexus to gland*. Developmental Dynamics, 2011. **240**(3): p. 530-565.
5. Kahn, S.E., R.L. Hull, and K.M. Utzschneider, *Mechanisms linking obesity to insulin resistance and type 2 diabetes*. Nature, 2006. **444**(7121): p. 840-846.
6. Rhodes, C.J., *Type 2 Diabetes-a Matter of β -Cell Life and Death?* Science, 2005. **307**(5708): p. 380-384.
7. Salinno, C., et al., *β -Cell Maturation and Identity in Health and Disease*. International journal of molecular sciences, 2019. **20**(21): p. 5417.
8. Xu, X., et al., *β Cells Can Be Generated from Endogenous Progenitors in Injured Adult Mouse Pancreas*. Cell, 2008. **132**(2): p. 197-207.
9. Butler, P.C., et al., *The replication of β cells in normal physiology, in disease and for therapy*. Nature Clinical Practice Endocrinology & Metabolism, 2007. **3**(11): p. 758-768.
10. Teta, M., et al., *Growth and Regeneration of Adult β Cells Does Not Involve Specialized Progenitors*. Developmental Cell, 2007. **12**(5): p. 817-826.
11. Rosado-Olivieri, E.A., et al., *Identification of a LIF-Responsive, Replication-Competent Subpopulation of Human β Cells*. Cell Metabolism, 2020. **31**(2): p. 327-338.e6.
12. Bader, E., et al., *Identification of proliferative and mature β -cells in the islets of Langerhans*. Nature, 2016. **535**(7612): p. 430-434.
13. Reznia, A., et al., *Reversal of diabetes with insulin-producing cells derived in vitro from human pluripotent stem cells*. Nature Biotechnology, 2014. **32**(11): p. 1121-1133.
14. Jennings, R.E., et al., *Human pancreas development*. Development, 2015. **142**(18): p. 3126-3137.
15. Wang, Z., et al., *Pancreatic β Cell Dedifferentiation in Diabetes and Redifferentiation following Insulin Therapy*. Cell Metabolism, 2014. **19**(5): p. 872-882.
16. Clayton, P.E., et al., *Growth hormone, the insulin-like growth factor axis, insulin and cancer risk*. Nature Reviews Endocrinology, 2011. **7**(1): p. 11-24.
17. Gutmann, T., et al., *Cryo-EM structure of the complete and ligand-saturated insulin receptor ectodomain*. Journal of Cell Biology, 2019. **219**(1).
18. Cai, W., et al., *Domain-dependent effects of insulin and IGF-1 receptors on signalling and gene expression*. Nature communications, 2017. **8**(1): p. 1-14.
19. Pandini, G., et al., *Insulin/insulin-like growth factor I hybrid receptors have different biological characteristics depending on the insulin receptor isoform involved*. J Biol Chem, 2002. **277**(42): p. 39684-95.
20. Girnita, L., et al., *Something old, something new and something borrowed: emerging paradigm of insulin-like growth factor type 1 receptor (IGF-1R) signaling regulation*. Cellular and Molecular Life Sciences, 2014. **71**(13): p. 2403-2427.
21. Cardone, M.H., et al., *Regulation of Cell Death Protease Caspase-9 by Phosphorylation*. Science, 1998. **282**(5392): p. 1318.
22. Dupont, J., et al., *The Insulin-like Growth Factor Axis in Cell Cycle Progression*. Horm Metab Res, 2003. **35**(11/12): p. 740-750.

23. Mayo, L.D. and D.B. Donner, *A phosphatidylinositol 3-kinase/Akt pathway promotes translocation of Mdm2 from the cytoplasm to the nucleus*. Proceedings of the National Academy of Sciences, 2001. **98**(20): p. 11598.
24. Yamaguchi, Y., et al., *Ligand-binding properties of the two isoforms of the human insulin receptor*. Endocrinology, 1993. **132**(3): p. 1132-1138.
25. Ghosh, P., N.M. Dahms, and S. Kornfeld, *Mannose 6-phosphate receptors: new twists in the tale*. Nature Reviews Molecular Cell Biology, 2003. **4**(3): p. 202-213.
26. Calderari, S., et al., *Defective IGF2 and IGF1R protein production in embryonic pancreas precedes beta cell mass anomaly in the Goto-Kakizaki rat model of type 2 diabetes*. Diabetologia, 2007. **50**(7): p. 1463-1471.
27. Brown, J., E.Y. Jones, and B.E. Forbes, *Keeping IGF-II under control: Lessons from the IGF-II-IGF2R crystal structure*. Trends in Biochemical Sciences, 2009. **34**(12): p. 612-619.
28. Benecke, H., J.S. Flier, and D.E. Moller, *Alternatively spliced variants of the insulin receptor protein. Expression in normal and diabetic human tissues*. The Journal of Clinical Investigation, 1992. **89**(6): p. 2066-2070.
29. Belfiore, A., et al., *Insulin receptor isoforms and insulin receptor/insulin-like growth factor receptor hybrids in physiology and disease*. Endocrine reviews, 2009. **30**(6): p. 586-623.
30. Leibiger, B., et al., *Selective Insulin Signaling through A and B Insulin Receptors Regulates Transcription of Insulin and Glucokinase Genes in Pancreatic β Cells*. Molecular Cell, 2001. **7**(3): p. 559-570.
31. Uhles, S., et al., *Isoform-specific insulin receptor signaling involves different plasma membrane domains*. Journal of Cell Biology, 2003. **163**(6): p. 1327-1337.
32. Issad, T., C. Blanquart, and C. Gonzalez-Yanes, *The use of bioluminescence resonance energy transfer for the study of therapeutic targets: application to tyrosine kinase receptors*. Expert Opinion on Therapeutic Targets, 2007. **11**(4): p. 541-556.
33. Janssen, J.A., *New Insights from IGF-IR Stimulating Activity Analyses: Pathological Considerations*. Cells, 2020. **9**(4): p. 862.
34. Zheng, H., et al., *Selective recruitment of G protein-coupled receptor kinases (GRKs) controls signaling of the insulin-like growth factor 1 receptor*. Proceedings of the National Academy of Sciences, 2012. **109**(18): p. 7055-7060.
35. Hancock, M.L., et al., *Insulin receptor associates with promoters genome-wide and regulates gene expression*. Cell, 2019. **177**(3): p. 722-736. e22.
36. Aleksic, T., et al., *Type 1 Insulin-like Growth Factor Receptor Translocates to the Nucleus of Human Tumor Cells*. Cancer Research, 2010. **70**(16): p. 6412-6419.
37. Kaplan, S.A., *The insulin receptor*. J Pediatr, 1984. **104**(3): p. 327-36.
38. Goh, L.K. and A. Sorokin, *Endocytosis of receptor tyrosine kinases*. Cold Spring Harbor perspectives in biology, 2013. **5**(5): p. a017459.
39. Ceresa, B.P., et al., *Inhibition of clathrin-mediated endocytosis selectively attenuates specific insulin receptor signal transduction pathways*. Mol Cell Biol, 1998. **18**(7): p. 3862-70.
40. Boothe, T., et al., *Inter-domain tagging implicates caveolin-1 in insulin receptor trafficking and Erk signaling bias in pancreatic beta-cells*. Molecular Metabolism, 2016. **5**(5): p. 366-378.
41. McClain, D.A. and J.M. Olefsky, *Evidence for Two Independent Pathways of Insulin-Receptor Internalization in Hepatocytes and Hepatoma Cells*. Diabetes, 1988. **37**(6): p. 806.
42. Traub, L.M., *Tickets to ride: selecting cargo for clathrin-regulated internalization*. Nature Reviews Molecular Cell Biology, 2009. **10**(9): p. 583-596.
43. Leonard, D., et al., *Sorting of EGF and transferrin at the plasma membrane and by cargo-specific signaling to EEA1-enriched endosomes*. Journal of Cell Science, 2008. **121**(20): p. 3445.
44. Hansen, C.G. and B.J. Nichols, *Exploring the caves: cavins, caveolins and caveolae*. Trends in Cell Biology, 2010. **20**(4): p. 177-186.
45. Bickel, P.E., *Lipid rafts and insulin signaling*. American Journal of Physiology-Endocrinology And Metabolism, 2002. **282**(1): p. E1-E10.

46. Bonifacino, J.S. and R. Rojas, *Retrograde transport from endosomes to the trans-Golgi network*. Nature reviews Molecular cell biology, 2006. **7**(8): p. 568-579.
47. Wong, E.S.M., et al., *Sprouty2 attenuates epidermal growth factor receptor ubiquitylation and endocytosis, and consequently enhances Ras/ERK signalling*. The EMBO Journal, 2002. **21**(18): p. 4796-4808.
48. Ren, X. and J.H. Hurley, *VHS domains of ESCRT-0 cooperate in high-avidity binding to polyubiquitinated cargo*. The EMBO Journal, 2010. **29**(6): p. 1045-1054.
49. Grice, G.L. and J.A. Nathan, *The recognition of ubiquitinated proteins by the proteasome*. Cellular and Molecular Life Sciences, 2016. **73**(18): p. 3497-3506.
50. Yang, B. and S. Kumar, *Nedd4 and Nedd4-2: closely related ubiquitin-protein ligases with distinct physiological functions*. Cell Death & Differentiation, 2010. **17**(1): p. 68-77.
51. Ingham, R.J., G. Gish, and T. Pawson, *The Nedd4 family of E3 ubiquitin ligases: functional diversity within a common modular architecture*. Oncogene, 2004. **23**(11): p. 1972-1984.
52. Sorkin, A., et al., *Recycling of epidermal growth factor-receptor complexes in A431 cells: identification of dual pathways*. Journal of Cell Biology, 1991. **112**(1): p. 55-63.
53. Grant, B.D. and J.G. Donaldson, *Pathways and mechanisms of endocytic recycling*. Nature Reviews Molecular Cell Biology, 2009. **10**(9): p. 597-608.
54. Chen, L., et al., *Effect of lifestyle intervention in patients with type 2 diabetes: A meta-analysis*. Metabolism, 2015. **64**(2): p. 338-347.
55. Mudaliar, S. and R.R. Henry, *New oral therapies for type 2 diabetes mellitus: the glitazones or insulin sensitizers*. Annual review of medicine, 2001. **52**(1): p. 239-257.
56. Stumvoll, M. and H.-U. Häring, *Glitazones: clinical effects and molecular mechanisms*. Annals of Medicine, 2002. **34**(3): p. 217-224.
57. Yang, X., et al., *Metformin, beyond an insulin sensitizer, targeting heart and pancreatic β cells*. Biochimica et Biophysica Acta (BBA) - Molecular Basis of Disease, 2017. **1863**(8): p. 1984-1990.
58. Masini, M., et al., *Prevention by metformin of alterations induced by chronic exposure to high glucose in human islet beta cells is associated with preserved ATP/ADP ratio*. Diabetes Research and Clinical Practice, 2014. **104**(1): p. 163-170.
59. Jiang, Y., et al., *Metformin plays a dual role in MIN6 pancreatic β cell function through AMPK-dependent autophagy*. International journal of biological sciences, 2014. **10**(3): p. 268.
60. Mingrone, G., et al., *Bariatric Surgery versus Conventional Medical Therapy for Type 2 Diabetes*. New England Journal of Medicine, 2012. **366**(17): p. 1577-1585.
61. Taylor, R., *Type 2 Diabetes*. Diabetes care, 2013. **36**(4): p. 1047-1055.
62. Wu, A.-L., et al., *Amelioration of Type 2 Diabetes by Antibody-Mediated Activation of Fibroblast Growth Factor Receptor 1*. Science Translational Medicine, 2011. **3**(113): p. 113ra126-113ra126.
63. Ussar, S., S.G. Vienberg, and C.R. Kahn, *Receptor Antibodies as Novel Therapeutics for Diabetes*. Science Translational Medicine, 2011. **3**(113): p. 113ps47-113ps47.
64. Mita, Y., et al., *Selenoprotein P-neutralizing antibodies improve insulin secretion and glucose sensitivity in type 2 diabetes mouse models*. Nature Communications, 2017. **8**(1): p. 1658.
65. Burak, M.F., et al., *Development of a therapeutic monoclonal antibody that targets secreted fatty acid-binding protein aP2 to treat type 2 diabetes*. Science translational medicine, 2015. **7**(319): p. 319ra205-319ra205.
66. Stein, E.A., et al., *Effect of a monoclonal antibody to PCSK9 on LDL cholesterol*. New England Journal of Medicine, 2012. **366**(12): p. 1108-1118.
67. Cao, Y.X., et al., *Effect of proprotein convertase subtilisin/kexin type 9 (PCSK9) monoclonal antibodies on new-onset diabetes mellitus and glucose metabolism: a systematic review and meta-analysis*. Diabetes, Obesity and Metabolism, 2018. **20**(6): p. 1391-1398.
68. Vrtačnik, P., et al., *The many faces of estrogen signaling*. Biochimica medica: Biochimica medica, 2014. **24**(3): p. 329-342.
69. Matsumoto, T., et al., *The androgen receptor in health and disease*. Annual review of physiology, 2013. **75**: p. 201-224.

70. Tan, M.H.E., et al., *Androgen receptor: structure, role in prostate cancer and drug discovery*. *Acta Pharmacologica Sinica*, 2015. **36**(1): p. 3-23.
71. Corona, G., et al., *Type 2 diabetes mellitus and testosterone: a meta-analysis study*. *International Journal of Andrology*, 2011. **34**(6pt1): p. 528-540.
72. Finkelstein, J.S., et al., *Gonadal Steroids and Body Composition, Strength, and Sexual Function in Men*. *New England Journal of Medicine*, 2013. **369**(11): p. 1011-1022.
73. Gentile, M.A., et al., *Androgen-mediated improvement of body composition and muscle function involves a novel early transcriptional program including IGF1, mechano growth factor, and induction of β -catenin*. *Journal of molecular endocrinology*, 2010. **44**(1): p. 55.
74. Xu, W., et al., *Androgen receptor-deficient islet β -cells exhibit alteration in genetic markers of insulin secretion and inflammation. A transcriptome analysis in the male mouse*. *Journal of Diabetes and its Complications*, 2017. **31**(5): p. 787-795.
75. Navarro, G., et al., *The role of androgens in metabolism, obesity, and diabetes in males and females*. *Obesity*, 2015. **23**(4): p. 713-719.
76. Tiano, J.P. and F. Mauvais-Jarvis, *Importance of oestrogen receptors to preserve functional β -cell mass in diabetes*. *Nature Reviews Endocrinology*, 2012. **8**(6): p. 342.
77. Ren, Z., et al., *Oestrogen regulates proliferation and differentiation of human islet-derived precursor cells through oestrogen receptor alpha*. *Cell Biology International*, 2010. **34**(5): p. 523-530.
78. Sachs, S., et al., *Targeted pharmacological therapy restores β -cell function for diabetes remission*. *Nature Metabolism*, 2020. **2**(2): p. 192-209.
79. Belfiore, A. and R. Malaguarnera, *Insulin receptor and cancer*. *Endocrine-related cancer*, 2011. **18**(4): p. R125-R147.
80. Bray, F., et al., *Global cancer statistics 2018: GLOBOCAN estimates of incidence and mortality worldwide for 36 cancers in 185 countries*. *CA: A Cancer Journal for Clinicians*, 2018. **68**(6): p. 394-424.
81. Crawley, D., et al., *A systematic review of the literature exploring the interplay between prostate cancer and type two diabetes mellitus*. *Ecancermedicalsecience*, 2018. **12**: p. 802-802.
82. Kasper, J.S., Y. Liu, and E. Giovannucci, *Diabetes mellitus and risk of prostate cancer in the health professionals follow-up study*. *International Journal of Cancer*, 2009. **124**(6): p. 1398-1403.
83. Klap, J., M. Schmid, and K.R. Loughlin, *The Relationship between Total Testosterone Levels and Prostate Cancer: A Review of the Continuing Controversy*. *The Journal of Urology*, 2015. **193**(2): p. 403-414.
84. Bensimon, L., et al., *Type 2 diabetes and the risk of mortality among patients with prostate cancer*. *Cancer Causes & Control*, 2014. **25**(3): p. 329-338.
85. Cai, H., et al., *Diabetes mellitus is associated with elevated risk of mortality amongst patients with prostate cancer: a meta-analysis of 11 cohort studies*. *Diabetes/Metabolism Research and Reviews*, 2015. **31**(4): p. 336-343.
86. Currie, C.J., et al., *Mortality after incident cancer in people with and without type 2 diabetes: impact of metformin on survival*. *Diabetes care*, 2012. **35**(2): p. 299-304.
87. Larsson, S.C., C.S. Mantzoros, and A. Wolk, *Diabetes mellitus and risk of breast cancer: A meta-analysis*. *International Journal of Cancer*, 2007. **121**(4): p. 856-862.
88. Risbridger, G.P., et al., *Breast and prostate cancer: more similar than different*. *Nature Reviews Cancer*, 2010. **10**(3): p. 205-212.
89. Gallagher, E.J. and D. LeRoith, *Diabetes, cancer, and metformin: connections of metabolism and cell proliferation*. *Annals of the New York Academy of Sciences*, 2011. **1243**(1): p. 54-68.
90. Hellawell, G.O., et al., *Expression of the Type 1 Insulin-like Growth Factor Receptor Is Up-Regulated in Primary Prostate Cancer and Commonly Persists in Metastatic Disease*. *Cancer Research*, 2002. **62**(10): p. 2942-2950.
91. Yang, Y. and D. Yee, *Targeting insulin and insulin-like growth factor signaling in breast cancer*. *Journal of mammary gland biology and neoplasia*, 2012. **17**(3-4): p. 251-261.

92. Pollak, M., *The insulin and insulin-like growth factor receptor family in neoplasia: an update.* Nature Reviews Cancer, 2012. **12**(3): p. 159-169.
93. Vikram, A. and G. Jena, *Diet-Induced Hyperinsulinemia Accelerates Growth of Androgen-Independent PC-3 Cells In Vitro.* Nutrition and Cancer, 2012. **64**(1): p. 121-127.
94. Venkateswaran, V., et al., *Association of Diet-Induced Hyperinsulinemia With Accelerated Growth of Prostate Cancer (LNCaP) Xenografts.* JNCI: Journal of the National Cancer Institute, 2007. **99**(23): p. 1793-1800.
95. Gualberto, A. and M. Pollak, *Emerging role of insulin-like growth factor receptor inhibitors in oncology: early clinical trial results and future directions.* Oncogene, 2009. **28**(34): p. 3009-3021.
96. Laaksonen, D.E., et al., *Testosterone and sex hormone-binding globulin predict the metabolic syndrome and diabetes in middle-aged men.* Diabetes care, 2004. **27**(5): p. 1036-1041.
97. Braga-Basaria, M., et al., *Metabolic Syndrome in Men With Prostate Cancer Undergoing Long-Term Androgen-Deprivation Therapy.* Journal of Clinical Oncology, 2006. **24**(24): p. 3979-3983.
98. Chi, J.T., et al., *Metabolomic effects of androgen deprivation therapy treatment for prostate cancer.* Cancer Medicine, 2020.
99. Takeda, H. and C. Chang, *Immunohistochemical and in-situ hybridization analysis of androgen receptor expression during the development of the mouse prostate gland.* Journal of Endocrinology, 1991. **129**(1): p. 83-NP.
100. Timms, B.G., *Prostate development: a historical perspective.* Differentiation, 2008. **76**(6): p. 565-577.
101. Oliveira, D.S.M., et al., *The mouse prostate: a basic anatomical and histological guideline.* Bosnian journal of basic medical sciences, 2016. **16**(1): p. 8-13.
102. Berquin, I.M., et al., *Expression Signature of the Mouse Prostate.* Journal of Biological Chemistry, 2005. **280**(43): p. 36442-36451.
103. McNeal, J.E., et al., *Zonal distribution of prostatic adenocarcinoma. Correlation with histologic pattern and direction of spread.* The American journal of surgical pathology, 1988. **12**(12): p. 897-906.
104. Renea, A.T., T. Roxanne, and P.R. Gail, *Stem cells in prostate cancer: treating the root of the problem.* Endocrine-Related Cancer, 2010. **17**(4): p. R273-R285.
105. Hayward, S.W. and G.R. Cunha, *THE PROSTATE: DEVELOPMENT AND PHYSIOLOGY.* Radiologic Clinics of North America, 2000. **38**(1): p. 1-14.
106. Thomas, L.N., et al., *Insulin-like growth factor binding protein 5 is associated with involution of the ventral prostate in castrated and finasteride-treated rats.* The Prostate, 1998. **35**(4): p. 273-278.
107. Kurita, T., et al., *Role of p63 and basal cells in the prostate.* Development, 2004. **131**(20): p. 4955.
108. Anthony Di Sant'Agnese, P., *Neuroendocrine differentiation in human prostatic carcinoma.* Human Pathology, 1992. **23**(3): p. 287-296.
109. Srinivas-Shankar, U. and F.C.W. Wu, *Drug Insight: testosterone preparations.* Nature Clinical Practice Urology, 2006. **3**(12): p. 653-665.
110. Wilson, S., J. Qi, and F.V. Filipp, *Refinement of the androgen response element based on ChIP-Seq in androgen-insensitive and androgen-responsive prostate cancer cell lines.* Scientific reports, 2016. **6**: p. 32611.
111. Massie, C.E., et al., *The androgen receptor fuels prostate cancer by regulating central metabolism and biosynthesis.* The EMBO Journal, 2011. **30**(13): p. 2719-2733.
112. Papakonstanti, E.A., et al., *A Rapid, Nongenomic, Signaling Pathway Regulates the Actin Reorganization Induced by Activation of Membrane Testosterone Receptors.* Molecular Endocrinology, 2003. **17**(5): p. 870-881.
113. Hu, R., et al., *Distinct Transcriptional Programs Mediated by the Ligand-Dependent Full-Length Androgen Receptor and Its Splice Variants in Castration-Resistant Prostate Cancer.* Cancer Research, 2012. **72**(14): p. 3457.

114. Davies, P., et al., *Consequences of poly-glutamine repeat length for the conformation and folding of the androgen receptor amino-terminal domain*. J. Mol. Endocrinol, 2008. **41**(5): p. 301-314.
115. Sharifi, N., J.L. Gulley, and W.L. Dahut, *Androgen Deprivation Therapy for Prostate Cancer*. JAMA, 2005. **294**(2): p. 238-244.
116. Feldman, B.J. and D. Feldman, *The development of androgen-independent prostate cancer*. Nature Reviews Cancer, 2001. **1**(1): p. 34-45.
117. Visakorpi, T., et al., *In vivo amplification of the androgen receptor gene and progression of human prostate cancer*. Nature Genetics, 1995. **9**(4): p. 401-406.
118. Gregory, C.W., et al., *A Mechanism for Androgen Receptor-mediated Prostate Cancer Recurrence after Androgen Deprivation Therapy*. Cancer Research, 2001. **61**(11): p. 4315.
119. Makridakis, N., et al., *A Prevalent Missense Substitution That Modulates Activity of Prostatic Steroid 5 α -Reductase*. Cancer Research, 1997. **57**(6): p. 1020.
120. Taplin, M.-E., et al., *Selection for Androgen Receptor Mutations in Prostate Cancers Treated with Androgen Antagonist*. Cancer Research, 1999. **59**(11): p. 2511-2515.
121. Veldscholte, J., et al., *A mutation in the ligand binding domain of the androgen receptor of human LNCaP cells affects steroid binding characteristics and response to anti-androgens*. Biochemical and biophysical research communications, 1990. **173**(2): p. 534-540.
122. Drake, C.G., *Prostate cancer as a model for tumour immunotherapy*. Nature Reviews Immunology, 2010. **10**(8): p. 580-593.
123. Colombel, M., et al., *Detection of the apoptosis-suppressing oncoprotein bc1-2 in hormone-refractory human prostate cancers*. The American journal of pathology, 1993. **143**(2): p. 390-400.
124. Culig, Z., et al., *Androgen Receptor Activation in Prostatic Tumor Cell Lines by Insulin-like Growth Factor-I, Keratinocyte Growth Factor, and Epidermal Growth Factor*. Cancer Research, 1994. **54**(20): p. 5474-5478.
125. Fan, W., et al., *Insulin-like growth factor 1/insulin signaling activates androgen signaling through direct interactions of Foxo1 with androgen receptor*. J Biol Chem, 2007. **282**(10): p. 7329-38.
126. Krueckl, S.L., et al., *Increased Insulin-Like Growth Factor I Receptor Expression and Signaling Are Components of Androgen-Independent Progression in a Lineage-Derived Prostate Cancer Progression Model*. Cancer Research, 2004. **64**(23): p. 8620-8629.
127. Nickerson, T., et al., *In Vivo Progression of LAPC-9 and LNCaP Prostate Cancer Models to Androgen Independence Is Associated with Increased Expression of Insulin-like Growth Factor I (IGF-I) and IGF-I Receptor (IGF-IR)*. Cancer Research, 2001. **61**(16): p. 6276-6280.
128. Craft, N., et al., *A mechanism for hormone-independent prostate cancer through modulation of androgen receptor signaling by the HER-2/neu tyrosine kinase*. Nature Medicine, 1999. **5**(3): p. 280-285.
129. Wen, Y., et al., *HER-2/neu promotes androgen-independent survival and growth of prostate cancer cells through the Akt pathway*. Cancer research, 2000. **60**(24): p. 6841-6845.
130. Phin, S., M. Moore, and P. Cotter, *Genomic Rearrangements of PTEN in Prostate Cancer*. Frontiers in Oncology, 2013. **3**(240).
131. Schrader, A.J., et al., *Enzalutamide in Castration-resistant Prostate Cancer Patients Progressing After Docetaxel and Abiraterone*. European Urology, 2014. **65**(1): p. 30-36.
132. Ryan, C.J., et al., *Abiraterone acetate plus prednisone versus placebo plus prednisone in chemotherapy-naïve men with metastatic castration-resistant prostate cancer (COU-AA-302): final overall survival analysis of a randomised, double-blind, placebo-controlled phase 3 study*. The Lancet Oncology, 2015. **16**(2): p. 152-160.
133. Horoszewicz, J., et al., *The LNCaP cell line—a new model for studies on human prostatic carcinoma*. Progress in clinical and biological research, 1980. **37**: p. 115-132.

134. Horoszewicz, J.S., et al., *LNCaP model of human prostatic carcinoma*. *Cancer research*, 1983. **43**(4): p. 1809-1818.
135. Wu, H.C., et al., *Derivation of androgen-independent human LNCaP prostatic cancer cell sublines: role of bone stromal cells*. *International journal of cancer*, 1994. **57**(3): p. 406-412.
136. Kaighn, M., et al., *Establishment and characterization of a human prostatic carcinoma cell line (PC-3)*. *Investigative urology*, 1979. **17**(1): p. 16-23.
137. Navone, N.M., et al., *Establishment of two human prostate cancer cell lines derived from a single bone metastasis*. *Clinical Cancer Research*, 1997. **3**(12): p. 2493-2500.
138. Hopkins, B.D., M.D. Goncalves, and L.C. Cantley, *Insulin-PI3K signalling: an evolutionarily insulated metabolic driver of cancer*. *Nature Reviews Endocrinology*, 2020.
139. Zhao, L. and P.K. Vogt, *Class I PI3K in oncogenic cellular transformation*. *Oncogene*, 2008. **27**(41): p. 5486-5496.
140. Raynaud, F.I., et al., *Biological properties of potent inhibitors of class I phosphatidylinositide 3-kinases: from PI-103 through PI-540, PI-620 to the oral agent GDC-0941*. *Molecular Cancer Therapeutics*, 2009. **8**(7): p. 1725-1738.
141. Juric, D., et al., *Phase I Dose-Escalation Study of Taselisib, an Oral PI3K Inhibitor, in Patients with Advanced Solid Tumors*. *Cancer Discovery*, 2017. **7**(7): p. 704-715.
142. Bendell, J.C., et al., *Phase I, dose-escalation study of BKM120, an oral pan-Class I PI3K inhibitor, in patients with advanced solid tumors*. *J Clin Oncol*, 2012. **30**(3): p. 282-290.
143. Hopkins, B.D., et al., *Suppression of insulin feedback enhances the efficacy of PI3K inhibitors*. *Nature*, 2018. **560**(7719): p. 499-503.
144. Weinstein, D., et al., *Insulin receptor compensates for IGF1R inhibition and directly induces mitogenic activity in prostate cancer cells*. 2014. **3**(1): p. 24.
145. Carracedo, A., et al., *Inhibition of mTORC1 leads to MAPK pathway activation through a PI3K-dependent feedback loop in human cancer*. *The Journal of Clinical Investigation*, 2008. **118**(9): p. 3065-3074.
146. O'Reilly, K.E., et al., *mTOR Inhibition Induces Upstream Receptor Tyrosine Kinase Signaling and Activates Akt*. *Cancer Research*, 2006. **66**(3): p. 1500-1508.
147. Carver, Brett S., et al., *Reciprocal Feedback Regulation of PI3K and Androgen Receptor Signaling in PTEN-Deficient Prostate Cancer*. *Cancer Cell*, 2011. **19**(5): p. 575-586.
148. Lutz, S.Z., et al., *Androgen receptor overexpression in prostate cancer in type 2 diabetes*. *Mol Metab*, 2018. **8**: p. 158-166.
149. Chen, H.X. and E. Sharon, *IGF-1R as an anti-cancer target--trials and tribulations*. *Chinese journal of cancer*, 2013. **32**(5): p. 242-252.
150. Niu, X.-B., et al., *Insulin-like growth factor-I induces chemoresistance to docetaxel by inhibiting miR-143 in human prostate cancer*. *Oncotarget*, 2017. **8**(63): p. 107157-107166.
151. Ludwig, D.L., et al., *Monoclonal antibody therapeutics and apoptosis*. *Oncogene*, 2003. **22**(56): p. 9097-9106.
152. Vogel, C.L., et al., *Efficacy and Safety of Trastuzumab as a Single Agent in First-Line Treatment of HER2-Overexpressing Metastatic Breast Cancer*. *Journal of Clinical Oncology*, 2002. **20**(3): p. 719-726.
153. Nahta, R., et al., *Insulin-like Growth Factor-I Receptor/Human Epidermal Growth Factor Receptor 2 Heterodimerization Contributes to Trastuzumab Resistance of Breast Cancer Cells*. *Cancer Research*, 2005. **65**(23): p. 11118-11128.
154. Hussain, M., et al., *A phase II randomized study of cixutumumab (IMC-A12: CIX) or ramucirumab (IMC-1121B: RAM) plus mitoxantrone (M) and prednisone (P) in patients (pts) with metastatic castrate-resistant prostate cancer (mCRPC) following disease progression (PD) on docetaxel (DCT) therapy*. *Journal of Clinical Oncology*, 2012. **30**(5_suppl): p. 97-97.
155. Hussain, M., et al., *A randomised non-comparative phase II trial of cixutumumab (IMC-A12) or ramucirumab (IMC-1121B) plus mitoxantrone and prednisone in men with metastatic docetaxel-pretreated castration-resistant prostate cancer*. *European journal of cancer (Oxford, England : 1990)*, 2015. **51**(13): p. 1714-1724.

156. Scott, A.M., J.P. Allison, and J.D. Wolchok, *Monoclonal antibodies in cancer therapy*. Cancer Immunity Archive, 2012. **12**(1): p. 14.
157. Wester, H.-J. and M. Schottelius, *PSMA-Targeted Radiopharmaceuticals for Imaging and Therapy*. Seminars in Nuclear Medicine, 2019. **49**(4): p. 302-312.
158. Henry, M.D., et al., *A Prostate-Specific Membrane Antigen-Targeted Monoclonal Antibody–Chemotherapeutic Conjugate Designed for the Treatment of Prostate Cancer*. Cancer Research, 2004. **64**(21): p. 7995-8001.
159. Tagawa, S.T., et al., *Phase II Study of Lutetium-177–Labeled Anti-Prostate-Specific Membrane Antigen Monoclonal Antibody J591 for Metastatic Castration-Resistant Prostate Cancer*. Clinical Cancer Research, 2013. **19**(18): p. 5182-5191.
160. Dhupkar, P., et al., *Effects of anti-EGFR antibody cetuximab on androgen-independent prostate cancer cells*. Anticancer research, 2010. **30**(6): p. 1905-1910.
161. Cunningham, F., et al., *Ensembl 2019*. Nucleic Acids Research, 2018. **47**(D1): p. D745-D751. https://www.ensembl.org/Homo_sapiens/Transcript/Exons?db=core;g=ENSG00000116299;r=1:109114115-109206781;t=ENST00000369939 - last accessed on 18.09.2020
162. Deng, L., et al., *Identification of a novel estrogen-regulated gene, EIG121, induced by hormone replacement therapy and differentially expressed in type I and type II endometrial cancer*. Clin Cancer Res, 2005. **11**(23): p. 8258-64.
163. Kang, J.M., et al., *KIAA1324 Suppresses Gastric Cancer Progression by Inhibiting the Oncoprotein GRP78*. Cancer Res, 2015. **75**(15): p. 3087-97.
164. Estrella, J.S., et al., *Expression of estrogen-induced genes and estrogen receptor beta in pancreatic neuroendocrine tumors: implications for targeted therapy*. Pancreas, 2014. **43**(7): p. 996-1002.
165. Schlumbrecht, M.P., et al., *Molecular clustering based on ER α and EIG121 predicts survival in high-grade serous carcinoma of the ovary/peritoneum*. Modern Pathology, 2011. **24**(3): p. 453-462.
166. Xiaomin Ran, P.Z., Keqiang Zhang, *Autophagy plays an important role in stemness mediation and the novel dual function of EIG121 in both autophagy and stemness regulation of endometrial carcinoma JEC cells*. International Journal of Oncology, 2017. **51**: p. 644-656.
167. Hurrell, J.G., *Monoclonal hybridoma antibodies: techniques and applications*. 2018: CRC press.
168. Knutson, V.P., *Cellular trafficking and processing of the insulin receptor1*. The FASEB Journal, 1991. **5**(8): p. 2130-2138.
169. Hahn, F.G.v., *Hedgehog and insulin signalling in beta-cell biology and glucose metabolism*. PhD Thesis, 2018.
170. Ansarullah, et al., *Inceptor counteracts insulin signalling in β -cells to control glycaemia*. Nature, 590, pages 326–331 (2021)
171. Uhlen, M., et al., *A pathology atlas of the human cancer transcriptome*. Science, 2017. **357**(6352): p. eaa2507. <https://www.proteinatlas.org/ENSG00000116299-KIAA1324/tissue> - last accessed on 18.09.2020
172. Hameyer, D., et al., *Toxicity of ligand-dependent Cre recombinases and generation of a conditional Cre deleter mouse allowing mosaic recombination in peripheral tissues*. Physiological Genomics, 2007. **31**(1): p. 32-41.
173. Aumailley, M., *The laminin family*. Cell Adhesion & Migration, 2013. **7**(1): p. 48-55.
174. Ruan, W., et al., *Evidence that insulin-like growth factor I and growth hormone are required for prostate gland development*. Endocrinology, 1999. **140**(5): p. 1984-1989.
175. Tang, Z., et al., *GEPIA: a web server for cancer and normal gene expression profiling and interactive analyses*. Nucleic Acids Research, 2017. **45**(W1): p. W98-W102. <http://gepia.cancer-pku.cn/detail.php?gene=KIAA1324> - last accessed on 18.09.2020
176. Cerami, E., et al., *The cBio cancer genomics portal: an open platform for exploring multidimensional cancer genomics data*. Cancer Discov, 2012. **2**(5): p. 401-4.

https://www.cbioportal.org/results/cancerTypesSummary?case_set_id=all&gene_list=ELAPO R1&cancer_study_list=prostate_dkfz_2018%2Cprad_msk_2019%2Cprad_mich%2Cprad_su2c_2019%2Cprad_su2c_2015%2Cprad_mcspc_mskcc_2020%2Cnepc_wcm_2016%2Cprad_broad_2013%2Cprad_broad%2Cprad_cpcg_2017%2Cprad_fhrc%2Cprad_cdk12_mskcc_2020%2Cprad_mskcc%2Cprad_mskcc_2014%2Cprad_p1000%2Cprad_eururo_2017%2Cprad_mskcc_cheny1_organoids_2014%2Cprad_mskcc_2017%2Cprad_mpcproject_2018&Z_SCORE_THRESHOLD=2.0&RPPA_SCORE_THRESHOLD=2.0&profileFilter=mutations%2Cfusion%2Ccna%2Cgistic&geneset_list=%20&tab_index=tab_visualize&Action=Submit
- last accessed on 18.09.2020

177. Ghosh, A. and W.D.W. Heston, *Tumor target prostate specific membrane antigen (PSMA) and its regulation in prostate cancer*. Journal of Cellular Biochemistry, 2004. **91**(3): p. 528-539.
178. Gupta, S., S. Batra, and M. Jain, *Antibody labeling with radioiodine and radiometals*, in *Drug Delivery System*. 2014, Springer. p. 147-157.
179. Macia, E., et al., *Dynasore, a Cell-Permeable Inhibitor of Dynamin*. Developmental Cell, 2006. **10**(6): p. 839-850.
180. Morcavallo, A., et al., *Insulin and insulin-like growth factor II differentially regulate endocytic sorting and stability of insulin receptor isoform A*. Journal of Biological Chemistry, 2012. **287**(14): p. 11422-11436.
181. Fagerholm, S., et al., *Rapid Insulin-Dependent Endocytosis of the Insulin Receptor by Caveolae in Primary Adipocytes*. PLOS ONE, 2009. **4**(6): p. e5985.
182. Wang, H., et al., *The vascular endothelial cell mediates insulin transport into skeletal muscle*. American Journal of Physiology-Endocrinology and Metabolism, 2006. **291**(2): p. E323-E332.
183. Balbis, A., et al., *Compartmentalization of signaling-competent epidermal growth factor receptors in endosomes*. Endocrinology, 2007. **148**(6): p. 2944-2954.
184. Bevan, A.P., et al., *The role of insulin dissociation from its endosomal receptor in insulin degradation*. Molecular and Cellular Endocrinology, 2000. **164**(1-2): p. 145-157.
185. Falck Hansen, B., et al., *Sustained signalling from the insulin receptor after stimulation with insulin analogues exhibiting increased mitogenic potency*. Biochemical Journal, 1996. **315**(1): p. 271-279.
186. Wiley, H.S. and P.M. Burke, *Regulation of receptor tyrosine kinase signaling by endocytic trafficking*. Traffic, 2001. **2**(1): p. 12-18.
187. Authier, F., et al., *Endosomal proteolysis of insulin by an acidic thiol metalloprotease unrelated to insulin degrading enzyme*. Journal of biological chemistry, 1994. **269**(4): p. 3010-3016.
188. Woodman, P., *ESCRT proteins, endosome organization and mitogenic receptor down-regulation*. Biochemical Society Transactions, 2009. **37**(1): p. 146-150.
189. Wegner, C.S., L.M.W. Rodahl, and H. Stenmark, *ESCRT Proteins and Cell Signalling*. Traffic, 2011. **12**(10): p. 1291-1297.
190. van Dongen, S.F.M., et al., *Single-Step Azide Introduction in Proteins via an Aqueous Diazo Transfer*. Bioconjugate Chemistry, 2009. **20**(1): p. 20-23.
191. Lohse, J., et al., *Targeted Diazotransfer Reagents Enable Selective Modification of Proteins with Azides*. Bioconjugate Chemistry, 2017. **28**(4): p. 913-917.
192. Choi, E., et al., *Mitotic regulators and the SHP2-MAPK pathway promote IR endocytosis and feedback regulation of insulin signaling*. Nature Communications, 2019. **10**(1): p. 1473.
193. Hall, C., H. Yu, and E. Choi, *Insulin receptor endocytosis in the pathophysiology of insulin resistance*. Experimental & Molecular Medicine, 2020: p. 1-10.
194. Copps, K. and M. White, *Regulation of insulin sensitivity by serine/threonine phosphorylation of insulin receptor substrate proteins IRS1 and IRS2*. Diabetologia, 2012. **55**(10): p. 2565-2582.
195. Haruta, T., et al., *A Rapamycin-Sensitive Pathway Down-Regulates Insulin Signaling via Phosphorylation and Proteasomal Degradation of Insulin Receptor Substrate-1*. Molecular Endocrinology, 2000. **14**(6): p. 783-794.
196. Goldfine, A.B. and R.N. Kulkarni, *Modulation of β -cell function: a translational journey from the bench to the bedside*. Diabetes, Obesity and Metabolism, 2012. **14**(s3): p. 152-160.

197. Ueki, K., et al., *Total insulin and IGF-I resistance in pancreatic β cells causes overt diabetes*. Nature genetics, 2006. **38**(5): p. 583-588.
198. Brown, W., *Cation-independent mannose 6-phosphate receptors are concentrated in trans Golgi elements in normal human and I-cell disease fibroblasts*. European journal of cell biology, 1990. **51**(2): p. 201-210.
199. Février, B. and G. Raposo, *Exosomes: endosomal-derived vesicles shipping extracellular messages*. Current opinion in cell biology, 2004. **16**(4): p. 415-421.
200. Aalberts, M., T.A. Stout, and W. Stoorvogel, *Prostasomes: extracellular vesicles from the prostate*. Reproduction, 2014. **147**(1): p. R1-R14.
201. Tsatsanis, C., et al., *The impact of adipose tissue-derived factors on the hypothalamic-pituitary-gonadal (HPG) axis*. Hormones, 2015. **14**(4): p. 549-562.
202. Chua, C.W., et al., *Single luminal epithelial progenitors can generate prostate organoids in culture*. Nature cell biology, 2014. **16**(10): p. 951-961.
203. Wang, Z.A., et al., *Luminal cells are favored as the cell of origin for prostate cancer*. Cell reports, 2014. **8**(5): p. 1339-1346.
204. Szczyrba, J., et al., *Neuroendocrine cells of the prostate derive from the neural crest*. Journal of Biological Chemistry, 2017. **292**(5): p. 2021-2031.
205. Ran, X., P. Zhou, and K. Zhang, *Autophagy plays an important role in stemness mediation and the novel dual function of EIG121 in both autophagy and stemness regulation of endometrial carcinoma JEC cells*. International Journal of Oncology, 2017. **51**(2): p. 644-656.
206. Fridley, B.L., et al., *Transcriptomic Characterization of Endometrioid, Clear Cell, and High-Grade Serous Epithelial Ovarian Carcinoma*. Cancer Epidemiology and Prevention Biomarkers, 2018. **27**(9): p. 1101-1109.
207. Dieters-Castator, D.Z., et al., *Proteomics-derived biomarker panel improves diagnostic precision to classify endometrioid and high-grade serous ovarian carcinoma*. Clinical Cancer Research, 2019. **25**(14): p. 4309-4319.
208. Meseure, D., et al., *Altered Expression of Three EGFR Posttranslational Regulators MDGI, MIG6, and EIG121 in Invasive Breast Carcinomas*. Analytical Cellular Pathology, 2020. **2020**: p. 9268236.
209. Zhong, Q., et al., *Integrative analysis of genomic and epigenetic regulation of endometrial cancer*. Aging (Albany NY), 2020. **12**(10): p. 9260.
210. Edwards, J., et al., *Androgen receptor gene amplification and protein expression in hormone refractory prostate cancer*. British Journal of Cancer, 2003. **89**(3): p. 552-556.
211. Perner, S., et al., *Prostate-specific membrane antigen expression as a predictor of prostate cancer progression*. Human Pathology, 2007. **38**(5): p. 696-701.
212. Sander, J.D. and J.K. Joung, *CRISPR-Cas systems for editing, regulating and targeting genomes*. Nature biotechnology, 2014. **32**(4): p. 347-355.
213. Albayrak, G., et al., *FOXA1 knock-out via CRISPR/Cas9 altered Casp-9, Bax, CCND1, CDK4, and fibronectin expressions in LNCaP cells*. Experimental Biology and Medicine, 2018. **243**(12): p. 990-994.
214. Wei, C., et al., *CRISPR/Cas9 targeting of the androgen receptor suppresses the growth of LNCaP human prostate cancer cells*. Molecular medicine reports, 2018. **17**(2): p. 2901-2906.
215. Mitelman, F., B. Johansson, and F. Mertens, *The impact of translocations and gene fusions on cancer causation*. Nature Reviews Cancer, 2007. **7**(4): p. 233-245.
216. König, J., et al., *Cytogenetic characterization of several androgen responsive and unresponsive sublines of the human prostatic carcinoma cell line LNCaP*. Urological Research, 1989. **17**(2): p. 79-86.
217. Eder, M., et al., *PSMA as a target for radiolabelled small molecules*. European Journal of Nuclear Medicine and Molecular Imaging, 2013. **40**(6): p. 819-823.
218. Meller, B., et al., *Alterations in androgen deprivation enhanced prostate-specific membrane antigen (PSMA) expression in prostate cancer cells as a target for diagnostics and therapy*. EJNMMI Research, 2015. **5**(1): p. 66.

219. Murga, J.D., et al., *Synergistic co-targeting of prostate-specific membrane antigen and androgen receptor in prostate cancer*. *The Prostate*, 2015. **75**(3): p. 242-254.
220. Ta-Chun, Y., et al., *Androgen deprivation induces human prostate epithelial neuroendocrine differentiation of androgen-sensitive LNCaP cells*. *Endocrine-Related Cancer Endocr Relat Cancer*, 2006. **13**(1): p. 151-167.
221. Fraser, J.A., et al., *hASH1 nuclear localization persists in neuroendocrine transdifferentiated prostate cancer cells, even upon reintroduction of androgen*. *Scientific reports*, 2019. **9**(1): p. 1-15.
222. Sha, J., et al., *Upregulated KDM4B promotes prostate cancer cell proliferation by activating autophagy*. *Journal of Cellular Physiology*, 2020. **235**(3): p. 2129-2138.
223. Edgar, R., M. Domrachev, and A.E. Lash, *Gene Expression Omnibus: NCBI gene expression and hybridization array data repository*. *Nucleic Acid Research*, 2002. **1**: p. 207-10.
[https://www.ncbi.nlm.nih.gov/geo/profiles?term=\(\(IR\)%20OR%20IGF1R\)%20AND%20LNCaP](https://www.ncbi.nlm.nih.gov/geo/profiles?term=((IR)%20OR%20IGF1R)%20AND%20LNCaP) - last accessed on 18.09.2020
224. Roskoski, R., *The ErbB/HER family of protein-tyrosine kinases and cancer*. *Pharmacological Research*, 2014. **79**: p. 34-74.
225. Kramer, N., et al., *In vitro cell migration and invasion assays*. *Mutation Research/Reviews in Mutation Research*, 2013. **752**(1): p. 10-24.
226. Pandini, G., et al., *Androgens Up-regulate the Insulin-like Growth Factor-I Receptor in Prostate Cancer Cells*. *Cancer Research*, 2005. **65**(5): p. 1849-1857.
227. Burfeind, P., et al., *Antisense RNA to the type I insulin-like growth factor receptor suppresses tumor growth and prevents invasion by rat prostate cancer cells in vivo*. *Proceedings of the National Academy of Sciences*, 1996. **93**(14): p. 7263-7268.
228. Martin-Kleiner, I. and K.G. Troselj, *Mannose-6-phosphate/insulin-like growth factor 2 receptor (M6P/IGF2R) in carcinogenesis*. *Cancer letters*, 2010. **289**(1): p. 11-22.
229. Takeda, T., et al., *Upregulation of IGF2R evades lysosomal dysfunction-induced apoptosis of cervical cancer cells via transport of cathepsins*. *Cell Death & Disease*, 2019. **10**(12): p. 876.
230. Hu, C.K., et al., *Loss of heterozygosity of M6P/IGF2R gene is an early event in the development of prostate cancer*. *Prostate Cancer and Prostatic Diseases*, 2006. **9**(1): p. 62-67.
231. Schaffer, B.S., et al., *Opposing roles for the insulin-like growth factor (IGF)-II and mannose 6-phosphate (Man-6-P) binding activities of the IGF-II/Man-6-P receptor in the growth of prostate cancer cells*. *Endocrinology*, 2003. **144**(3): p. 955-966.
232. Kraeber-Bodéré, F., et al., *Tumor immunotargeting using innovative radionuclides*. *International journal of molecular sciences*, 2015. **16**(2): p. 3932-3954.
233. Batra, S.K., et al., *Pharmacokinetics and biodistribution of genetically engineered antibodies*. *Current Opinion in Biotechnology*, 2002. **13**(6): p. 603-608.
234. Tolmachev, V., et al., *Development of a 124I-labeled version of the anti-PSMA monoclonal antibody capromab for immunoPET staging of prostate cancer: Aspects of labeling chemistry and biodistribution*. *International journal of oncology*, 2014. **44**(6): p. 1998-2008.
235. Elvin, J.G., R.G. Couston, and C.F. van der Walle, *Therapeutic antibodies: Market considerations, disease targets and bioprocessing*. *International Journal of Pharmaceutics*, 2013. **440**(1): p. 83-98.
236. Alibakhshi, A., et al., *Targeted cancer therapy through antibody fragments-decorated nanomedicines*. *Journal of Controlled Release*, 2017. **268**: p. 323-334.
237. Czogalla, A., et al., *Validity and applicability of membrane model systems for studying interactions of peripheral membrane proteins with lipids*. *Biochimica et Biophysica Acta (BBA) - Molecular and Cell Biology of Lipids*, 2014. **1841**(8): p. 1049-1059.
238. Jespersen, L.K., et al., *Use of proteoliposomes to generate phage antibodies against native AMPA receptor*. *European Journal of Biochemistry*, 2000. **267**(5): p. 1382-1389.
239. Chen, W., et al., *Unidirectional Presentation of Membrane Proteins in Nanoparticle-Supported Liposomes*. *Angewandte Chemie International Edition*, 2019. **58**(29): p. 9866-9870.

240. Miersch, S. and S. Sidhu, *Synthetic antibodies: concepts, potential and practical considerations*. *Methods*, 2012. **57**(4): p. 486-498.
241. Katharina Wißmiller, A.F., Stefan Z. Lutz, Sara Bilekova, Miriam Katsburg, Arnulf Stenzl, Martin Heni, Lucia Berti, Hans-Ulrich Häring and Heiko Lickert, *Inceptor correlates with markers of prostate cancer progression and modulates insulin/IGF1 signaling and cancer cell migration*. in revision.
242. Beltran, H., et al., *Divergent clonal evolution of castration-resistant neuroendocrine prostate cancer*. *Nature Medicine*, 2016. **22**(3): p. 298-305.
243. Iwasaki, M., et al., *Establishment of new clonal pancreatic β -cell lines (MIN6-K) useful for study of incretin/cyclic adenosine monophosphate signaling*. *Journal of Diabetes Investigation*, 2010. **1**(4): p. 137-142.
244. Minami, K., et al., *Insulin secretion and differential gene expression in glucose-responsive and -unresponsive MIN6 sublines*. *American Journal of Physiology-Endocrinology and Metabolism*, 2000. **279**(4): p. E773-E781.
245. Yumlu, S., et al., *Efficient gene editing of human induced pluripotent stem cells using CRISPR/Cas9*, in *CRISPR Gene Editing*. 2019, Springer. p. 137-151.

III List of Figures

Figure 1: IR/IGF1R signalling via the MAPK and the PI3K/Akt pathway.....	7
Figure 2: Effects of insulin resistance on important target organs.....	8
Figure 3: Intracellular trafficking in the endosomal/lysosomal system.....	11
Figure 4: Conversion of steroids in extragonadal tissues	15
Figure 5: Structure of the prostate epithelium	18
Figure 6: Therapeutical strategy in prostate cancer	21
Figure 7: Mechanisms of insulin/IGF1 signalling in prostate cancer	22
Figure 8: Domain structure of IGFR-L1.....	26
Figure 9: Antibody generation via the hybridoma technique.....	28
Figure 10: Screen of antibodies directed against IGFR-L1	30
Figure 11: Determination of the active IgG subtype of mouse IGFR-L1 antibodies	31
Figure 12: Specificity test of working antibodies in the mouse cell line Min6	32
Figure 13: Concentration-dependent test of purified IGFR-L1 antibodies	33
Figure 14: Test of purified IGFR-L1 antibodies in the mouse cell line Min6	34
Figure 15: Test of labelled IGFR-L1 antibodies.....	35
Figure 16: Proliferation assay in Min6 cells with IGFR-L1 Abs.	36
Figure 17: Proliferation assay in MCF7 cells with IGFR-L1 Abs.	37
Figure 18: Proliferation assay in LNCaP cells with IGFR-L1 Abs.	37
Figure 19: Validation of tagged IR constructs	39
Figure 20: Initial validation of IGFR-L1-Venus.....	39
Figure 21: Generation of stable cell line Min6 IGFR-L1-Venus	40
Figure 22: Staining of Min6 IGFR-L1-Venus with organelle markers	42
Figure 23: Transfection of Min6 cells with organelle marker plasmids.....	43
Figure 24: Internalisation time course of IGFR-L1 Ab	44
Figure 25: Quantification of IGFR-L1 Ab internalisation	45
Figure 26: Starvation of Min6 IGFR-L1-Venus.....	46
Figure 27: Stimulation of starved Min6 IGFR-L1-Venus.....	47
Figure 28: IR-RFP in Min6 WT vs. KO.....	48
Figure 29: Potential interaction of IGFR-L1-Venus and IR-RFP	49
Figure 30: Colocalisation of IGFR-L1-Venus and IR-RFP on the plasma membrane	50
Figure 31: Insulin/IGF1 signalling in Min6 IGFR-L1-Venus	51
Figure 32: Initial test of Min6 IGFR-L1-AP2*-Venus.....	52
Figure 33: Subcellular localisation of IGFR-L1-AP2*-Venus	53
Figure 34: IGFR-L1 endocytosis inhibition.....	54
Figure 35: Internalisation of insulin-FITC in Min6	56
Figure 36: Biological activity of insulin-FITC.....	57
Figure 37: Internalisation of insulin-546	58
Figure 38: Live uptake of insulin-FITC and EGF-488 in Min6.....	59
Figure 39: Live uptake of insulin-546 along with IGFR-L1 Ab.....	60
Figure 40: Lysosomal transport of insulin-546.....	61
Figure 41: Expression of IGFR-L1 in normal human tissues	62
Figure 42: IGFR-L1 in different regions of the mouse prostate	63

Figure 43: Cell type analysis of Igfr-L1 expression in WT mouse prostate section.....	64
Figure 44: Analysis of Igfr-L1 expression in neuroendocrine cells.....	64
Figure 45: Localisation of AR in Igfr-L1 KO prostate	66
Figure 46: Polarity markers in Igfr-L1 KO prostate.....	66
Figure 47: Proliferation of Igfr-L1 KO prostate epithelium	67
Figure 48: Expression of IGFR-L1 in various cancer types.....	68
Figure 49: Mutation frequencies of genes potentially involved in prostate cancer.....	69
Figure 50: Correlation of IGFR-L1 and genes potentially involved in prostate cancer	71
Figure 51: Sorting of cells transfected with sgRNA for CRISPR/Cas9 targeting	72
Figure 52: Sequencing of potential IGFR-L1 KO clones	72
Figure 53: Generation of the stable cell lines LNCaP IGFR-L1-Venus / LNCaP Venus.....	73
Figure 54: Expression of IGFR-L1 in prostate cancer cell lines.....	74
Figure 55: Subcellular localisation of IGFR-L1 in LNCaP cells.....	75
Figure 56: Proliferation of LNCaP IGFR-L1-Venus	75
Figure 57: Migration of LNCaP IGFR-L1-Venus in a 3D assay	76
Figure 58: Estrogen induction or depletion of MCF7 cells.....	77
Figure 59: Estrogen or androgen induction of LNCaP cells.....	77
Figure 60: Androgen deprivation of LNCaP cells.....	78
Figure 61: AR activation after androgen deprivation in LNCaP cells	79
Figure 62: Co-IP of IGF1R/IR and IGFR-L1	80
Figure 63: Insulin/IGF1 signalling in LNCaP IGFR-L1-Venus	81
Figure 64: Endocytosis of insulin-546 or EGF-488 in LNCaP	82
Figure 65: Localisation of RTKs in LNCaP IGFR-L1-Venus.....	83
Figure 66: Internalisation assay using purified IGFR-L1 Abs in LNCaP cells.....	84
Figure 67: Validation of ¹²⁵ I-labelled antibody	85
Figure 68: Biodistribution of the ¹²⁵ I-labelled antibody 2G6	86
Figure 69: Current model of the mechanistic function of IGFR-L1	92
Figure 70: Hypothetical model of IGFR-L1 function in prostate cancer.....	100
Figure 71: Structure of a full-length IgG and commonly used antibody fragments	102

IV List of Tables

Table 1: Summarising list of all tested antibodies	29
Table 2: Colocalisation of endogenous IGFR-L1 or IGFR-L1-Venus with organelle markers ...	41
Table 3: Co-occurrence of mutations in the TCGA dataset and neuroendocrine prostate cancer dataset, retrieved via CBioPortal.	70

V Acknowledgements

I am very grateful to **Prof. Dr. Heiko Lickert** for giving me the opportunity to conduct research in his lab, to use state-of-the-art equipment and to thrive in an excellent environment. His guidance and inspiration were highly appreciated.

Likewise, I am thankful to **Dr. Anja Zeigerer** and **Prof. Dr. Hans-Jürgen Wester** for their co-supervision and many helpful suggestions to improve my research project.

My gratefulness extends to **Prof. Dr. Martin Heni**, **PD Dr. Stefan Z. Lutz** and **Dr. Lucia Berti** (Institute of Diabetes and Metabolic Disease, HMGU, Tübingen) for a great collaboration, and especially to **PD Dr. Andras Franko**, who has been very helpful in terms of improving data analysis and writing strategies of our publication. Further, I want to thank **Dr. Gustav Colldén** (Institute of Diabetes and Obesity, HMGU, Munich) for cooperation on *in vivo* experiments.

Many of my experiments would not have been possible without **Dr. Regina Feederle** and **Andrew Flatley** (Monoclonal Antibody Core Facility, HMGU, Munich), as well as **Dr. Ünal Coskun** and **Dr. Michal Grzybek** (Paul Langerhans institute, HMGU, Dresden), who were responsible for the design, manufacturing and quality control of monoclonal antibodies. Likewise, I want to thank **Prof. Dr. Oliver Plettenburg** and **Christin Ahlbrecht** (Institute of Medicinal Chemistry, HMGU, Hannover) for the design and synthesis of fluorescently labelled insulin. In addition, I am thankful to **Matthias Konrad** and **Prof. Dr. Hans-Jürgen Wester** (Chair of Pharmaceutical Radiochemistry, TUM) for their help with biodistribution experiments.

My sincere gratitude belongs to **Dr. Felizitas Gräfin von Hahn** and **Dr. Amir Morshedi** for welcoming me to the group, teaching me new methods and advising me in all work-related issues. Many thanks also to the rest of the receptor team, including **Miriam Katsburg**, **Sára Bileková**, **Johanna Siehler**, **Fataneh Fathi-Far**, **Sarah Homberg**, **Dr. Chirag Jain** and **Dr. Ansarullah**. Further, I am grateful to **Dr. Silvia Schirge**, **Dr. Ingo Burtscher** and **Dr. Mostafa Bakhti** for advice on new experiments and lab techniques. Moreover, I want to thank **Dr. Joanne van Vuuren**, **Dr. Mostafa Bakhti** and **Prof. Dr. Heiko Lickert** for highly useful suggestions on my thesis. Of course, all my colleagues at the Institute of Diabetes and Regeneration Research greatly contributed to my motivation.

In particular, I am delighted to have made such great friends as **Anna Blöchinger**, **Sára Bileková**, **Johanna Siehler** and **Lena Oppenländer**, who have not only helped me in the lab on various occasions, but also made every lunch break and many evenings worthwhile.

Last but not least I want to thank my friends from school and from university, including but not limited to **Dr. Marina Schopf**, **Barbara Tremmel**, **Dr. Carolin Gleißner** and **Dr. Anja Fux**, who were always around when I needed a distraction. Of course I am very thankful to my family, including my soon-to-be parents-in-law **Monika and Prof. Dr. Wolfgang Bibel**, my brother **Martin Wißmiller**, and, most importantly: to my parents **Christine and Wilfried Wißmiller** for always encouraging me and for investing all the time and love to make me the person I am today. Particularly well-deserved credit belongs to my shoulder to lean on, my fiancé **Hannes Bibel**, who had to suffer from failed experiments almost as much as I did. **Thank you all for supporting me!**

VI List of Publications

Katharina Wißmiller, Andras Franko, Stefan Z. Lutz, Sara Bilekova, Arnulf Stenzl, Martin Heni, Miriam Katsburg, Lucia Berti, Hans-Ulrich Häring and Heiko Lickert:

Inceptor correlates with markers of prostate cancer progression and modulates insulin/IGF1 signaling and cancer cell migration.

in revision

Ansarullah*, Chirag Jain*, Fataneh Fathi Far*, Sarah Homberg*, Katharina Wißmiller*, Felizitas Gräfin von Hahn*, Aurelia Raducanu, Silvia Schirge, Michael Sterr, Sara Bilekova, Johanna Siehler, Julius Wiener, Lena Oppenländer, Amir Morshedi, Aimee Bastidas-Ponce, Gustav Collden, Martin Irmeler, Johannes Beckers, Annette Feuchtinger, Michal Grzybek, Christin Ahlbrecht, Regina Feederle, Oliver Plettenburg, Timo D. Müller, Matthias Meier, Matthias H. Tschöp, Ünal Coskun and Heiko Lickert:

*These authors contributed equally to this work

Inceptor counteracts insulin signalling in β -cells to control glycaemia.

Nature, 2021

Andras Franko, Lucia Berti, Alke Guirguis, Jörg Hennenlotter, Robert Wagner, Marus O. Scharpf, Martin Hrabe de Angelis, Katharina Wißmiller, Heiko Lickert, Arnulf Stenzl, Andreas L. Birkenfeld, Andreas Peter, Hans-Ulrich Häring, Stefan Z. Lutz and Martin Heni:

Characterization of Hormone-Dependent Pathways in Six Human Prostate-Cancer Cell Lines: A Gene-Expression Study

Genes, 2020

Anna Blöching, Johanna Siehler, Katharina Wißmiller, Alireza Shahryari, Ingo Burtscher and Heiko Lickert:

Generation of an INSULIN-H2B-Cherry reporter human iPSC line.

Stem Cell Research, 2020

Margret Schottelius, Alexander Wurzer, Katharina Wißmiller, Roswitha Beck, Maximilian Koch, Dimitrios Gorpas, Johannes Notni, Tessa Buckle, Matthias N. van Oosterom, Katja Steiger, Vasilis Ntziachristos, Markus Schwaiger, Fijis W.B. van Leeuwen, and Hans-Jürgen Wester:

Synthesis and Preclinical Characterization of the PSMA-Targeted Hybrid Tracer PSMA-I&F for Nuclear and Fluorescence Imaging of Prostate Cancer.

Journal of Nuclear Med, 2019

Joanna Deek, Fabian Hecht, Leone Rossetti, Katharina Wißmiller, Andreas R. Bausch:

Mechanics of soft epithelial keratin networks depend on modular filament assembly kinetics.

Acta Biomaterialia, 2016